



# Crosstalk of Glucocorticoid Receptor and AMP-activated protein kinase in macrophages during skeletal muscle regeneration

Thibaut Desgeorges

## ► To cite this version:

Thibaut Desgeorges. Crosstalk of Glucocorticoid Receptor and AMP-activated protein kinase in macrophages during skeletal muscle regeneration. Cellular Biology. Université de Lyon, 2019. English. NNT : 2019LYSE1058 . tel-03613961

**HAL Id: tel-03613961**

**<https://theses.hal.science/tel-03613961>**

Submitted on 19 Mar 2022

**HAL** is a multi-disciplinary open access archive for the deposit and dissemination of scientific research documents, whether they are published or not. The documents may come from teaching and research institutions in France or abroad, or from public or private research centers.

L'archive ouverte pluridisciplinaire **HAL**, est destinée au dépôt et à la diffusion de documents scientifiques de niveau recherche, publiés ou non, émanant des établissements d'enseignement et de recherche français ou étrangers, des laboratoires publics ou privés.



N° d'ordre NNT : 2019LYSE1058

# **THESE de DOCTORAT DE L'UNIVERSITE DE LYON**

opérée au sein de  
**L'Université Claude Bernard Lyon 1**

**Ecole Doctorale N° 205**  
**ECOLE DOCTORALE INTERDISCIPLINAIRE SCIENCES-SANTE**  
**(EDISS)**

**Spécialité de doctorat : BIOLOGIE CELLULAIRE**

Soutenue publiquement le 22/05/2019, par :

**Thibaut DESGEORGES**

---

**Crosstalk of Glucocorticoid Receptor and AMP-activated protein kinase in macrophages during skeletal muscle regeneration**

---

Devant le jury composé de :

Freyssenet, Damien

PR Université de Saint Etienne

Président

Bertrand, Luc  
Libert, Claude  
Jospin, Maëlle

PR Université Catholique de Louvain  
PR Université de Ghent  
MCU-HDR Université Lyon 1

Rapporteur  
Rapporteur  
Examinatrice

Chazaud, Bénédicte  
Mounier, Rémi

DR INSERM  
CR CNRS

Co-Directrice de thèse  
Co-Directeur de thèse





*« La vie est comme un livre :  
ne jamais sauter aucun chapitre et continuer à tourner les pages,  
tôt ou tard on comprendra pourquoi chaque paragraphe était nécessaire. »*

*Bernard Werber*



## REMERCIEMENTS / ACKNOWLEDGMENTS

Je voudrais en tout premier lieu remercier chaleureusement la Docteure Bénédicte Chazaud et le Docteur Rémi Mounier pour m'avoir encadré tout au long de ces presque 5 années de Master 2 et de Doctorat. Rémi et Bénédicte sont pour moi un exemple de binôme scientifique qui fonctionne à merveille, chacun apportant ses compétences et son expertise pour essayer de résoudre les problèmes, interrogations, *etc.* rencontrés au cours de mon doctorat, bien qu'ils ne soient pas toujours d'accord l'un avec l'autre. Ce sont tous les 2 des scientifiques passionnés qui m'ont poussé tout au long de ces années à donner le maximum même dans les moments où ma motivation était quelque peu en berne. Ils m'ont enseigné la rigueur et m'ont appris à développer mon esprit critique. Je voudrais aussi les remercier pour leur disponibilité pour répondre à mes interrogations diverses et variées à n'importe quelles heures du jour sur la science en générale, le métier de chercheur, le management, le post-doc, comment bien présenter, les restaurants à essayer et j'en passe. Je tiens aussi à les remercier pour les opportunités qu'ils m'ont offertes, que ce soit pour la participation à des congrès ou des échanges scientifiques à l'étranger. Et enfin et surtout, un grand merci pour m'avoir fait profiter de votre culture à la fois cinématographique, musicale, littéraire et autres au cours de nos réunions scientifiques hebdomadaire (lorsque cela dérivait un peu). C'était pour moi très instructif et distrayant 😊

I would like to thanks the Professor Luc Bertrand and the Professor Claude Libert to accept to review my manuscript and to offer me the time to come in Lyon to evaluate my work during the defense. So, thank you very much for your participation.

Je souhaite remercier le Professeur Damien Freyssenet pour avoir accepté d'être examinateur lors de ma soutenance de thèse. C'est un réel plaisir pour moi car Damien était mon premier mentor en recherche. Il y a déjà quelques temps, Damien avait bien gentiment accepté de me prendre en stage dans son laboratoire lors de ma 3ème année de Licence et de mon Master 1. C'est sous sa supervision que j'ai découvert le milieu de la recherche sur le muscle qui a ensuite guidé la suite de mon parcours.

Je voudrais finalement remercier la Docteure Maëlle Jospin pour avoir accepté d'être Présidente de mon jury de thèse. Maëlle a d'abord été mon enseignante au cours de mon master. Elle a donc suivi mon parcours au fil des années. C'est un grand plaisir pour moi de l'avoir dans mon jury en tant que Présidente.

La recherche est un travail individuel qui s'effectue en équipe. A ce titre, je voudrais remercier sincèrement tous les membres de mon équipe pour m'avoir soutenu, aidé, supporté pendant ce doctorat.

Michèle Weiss-Gayet, pour tes nombreuses aides techniques, pour être un peu notre ange gardien qui veille à notre sécurité dans le laboratoire, pour ta gentillesse ainsi que pour ces quelques moments de franche camaraderie ;-)

Sabrina Ben Larbi, pour ton soutien autant technique que psychologique, pour nos conversions du vendredi soir en compagnie d'une bière, pour ta personnalité pétillante, voire quelques fois décoiffante, pour ton franc-parler. Je te souhaite beaucoup de bonheur avec ta petite Lina.

Peggy Del Carmine, pour m'avoir apporté ton expertise en matière d'expérimentation animale, pour ton aide lors des manip HFD où nous passions des après-midis entiers enfermés dans l'animalerie.

Gaëtan Juban, pour ton aide en matière de cytométrie, macrophages, biologie moléculaire. Je te souhaite de pouvoir continuer la science autant que tu le souhaites car tu es, selon moi, quelqu'un d'extrêmement compétent et tu le mérites.

Le doctorat permet de tisser des liens qui très sont particuliers entre les personnes qui vivent cette aventure au même moment. Plus que des collègues, je voudrais particulièrement remercier mes co-thésards et amis pour avoir partagé cette aventure avec moi.

Tout d'abord Linda Gsaier, nous avons commencé notre thèse au même moment. Nous avons tout partagé pendant presque 4 ans et surtout quelques délires que nous étions bien souvent seuls à comprendre. Tu as aujourd'hui choisi une autre voie. J'espère que celle-ci t'apportera tout ce que tu recherches autant professionnellement que personnellement. Gros bisous tête de mort !

Jessica Bouvière, pour avoir accepté (bien que tu n'aies en fait pas vraiment eu le choix) les multiples surnoms que je t'ai attribués, pour toutes ces discussions, ces danses endiablées le

vendredi soir au laboratoire, tous ces sushis (tu m'en dois toujours un d'ailleurs) et aussi m'avoir aidé lors de nombreuses expériences.

Jimmy Massennet, pour ton soutien en tant que seul autre personne du sexe masculin parmi toutes ces doctorantes et stagiaires. Pour toutes ces discussions passionnées sur tout et surtout sur rien car tu as toujours un point de vue intéressant, pour ces 10 mois de colocation mémorables, pour avoir souffert avec moi lors de nos séances de sport, pour ta gentillesse mimi et aussi parce que je sais que je suis ton préféré !

Laure Gallay (re), pour ta personnalité atypique (dans le bon sens du terme ;-), pour ta fraîcheur, ton optimisme, ta générosité, etc. Merci pour toutes ces petites gallayres qui m'ont beaucoup diverti, pour m'avoir ouvert au bienfait de l'art et pour avoir partagé ta culture sur des domaines aussi larges qu'intéressants. De manière un peu plus large, merci de m'avoir apporté ton soutien (logement, conférences en tous genres,...).

Dieu-Huong Hoang, la dernière venue dans l'équipe, pour m'avoir supporté les derniers mois de ma thèse car elle a été un peu la cible de mon humour (je pense qu'elle comprendra), à supporter mes vannes et autres remarques probablement un peu lourdes. Néanmoins, Huong possède une répartie des plus sympathiques. Bien que je sache que tu aies la flemme pour pas mal de chose, je te souhaite tout de même bonne chance pour la suite de ta thèse qui j'en suis sûr se déroulera à merveille.

Sophie Liot, j'ai vraiment apprécié de travailler avec toi même si cela n'aura été que pour une courte durée. Ces longs instants de FACS durant les manips HFD nous aurons permis de bien rigoler. Je te souhaite de t'épanouir là où tu es maintenant et te souhaite aussi le meilleur pour la suite.

Petite mention spéciale pour les anciens doctorants de l'équipe, Marine Théret, Emmeran Le Moal, Aurélie Trignol, merci à vous.

Merci aussi aux autres membres permanents de l'équipe, Guy Mouchiroud et Julien Gondin pour m'avoir aidé dans différents domaines, tant en analyse d'expression de gènes, en gestion d'animaux, ou pour toutes autres interrogations scientifiques.

Et enfin, je remercie aussi Eugénie Moulin et Anita Kneppers, nouvellement recrutées dans l'équipe, ainsi que les stagiaires avec qui j'ai eu la chance de travailler ou d'interagir, Roxane Cuzin, Emilie Charles, Cécile Fermon, et j'en oublie probablement.

I would like to thank the Professor Jan Tuckermann, Director of the Institute of Comparative Molecular Endocrinology with whom we collaborated for this project. Also, thank you to welcome me in your lab for 2 months during the 3<sup>rd</sup> year of my PhD. It was a very instructive experience, professionally and personally.

I would like to thank also Giorgio Caratti and Sabine Vettorazzi for your collaboration in this work.

Je voudrais aussi remercier tous les membres de l'association des jeunes chercheurs de l'INMG (YRIN) dans laquelle j'ai été amené à m'impliquer de manière plus ou moins active au cours d'un peu plus de 2 ans. Le bureau a été renouvelé il y a peu et la nouvelle équipe semble être très dynamique. Bon courage à eux pour la suite.

De manière plus générale merci à tous les gens dans l'institut avec qui j'ai pu interagir (Julien Courchet, Audrey Garcia, Vincent Gache, Emilie Christin, et bien d'autres).

Dans un autre ordre, au cours de mon doctorat et de mon année d'ATER, j'ai effectué des enseignements. Je voudrais remercier les membres des équipes pédagogique avec lesquelles j'ai pu travailler et principalement Dominique Baas, Olga Andrini, Maëlle Jospin, Christine Berthier, Valérie Pellier-Monnin, Caroline Romestaing et Karyn Julliard, pour m'avoir donné l'opportunité d'enseigner dans leur discipline respective, pour m'avoir formé, soutenu durant ces enseignements.

Dans un ordre plus personnel, je voudrais remercier mes amis d'enfance issus de ma campagne natale pour m'avoir supporté tout au long de cette thèse. Je m'excuse aussi pour les retards fréquents lors de nos rendez-vous la plupart du temps à cause des manips. Ils ont su aussi me soutenir et surtout me changer les idées lorsque cela était nécessaire. Ils représentent pour moi un ancrage solide qui m'apporte beaucoup.

Je remercie aussi mes amis lyonnais, Ange-Lyne, Guéna, Candice, Rémi, Mario, Marine, Kévin pour ces instants passés ensemble qui sont tellement rafraichissants, pour nos petits weekends. A quand le prochain d'ailleurs ???

Un petit merci spécialement pour Candice Kutchukian avec qui j'ai habité en coloc pendant 3 ans et Félicitations pour ce nouveau post-doc aux États-Unis. C'est une nouvelle aventure qui commence pour toi, je te souhaite bonne chance.

Et enfin, un immense merci à ma famille qui m'a toujours poussé à donner le meilleur de moi-même, qui était toujours présente pour moi quand j'en avais besoin. Juste merci ne suffit pas à exprimer ma gratitude envers vous. Je vous aime.

Merci à tous, sans vous tout ceci n'aurait pas pu être possible.





## ABSTRACT

### **Crosstalk of Glucocorticoid Receptor and AMP-activated protein kinase in macrophages during skeletal muscle regeneration.**

Skeletal muscle regenerates *ad integrum* after a sterile acute injury thanks to satellite cells (muscle stem cells). Inflammation, and notably macrophages, plays important roles during this process. Just after injury, monocytes infiltrate the tissue from the blood and convert into pro-inflammatory damaged associated macrophages. Macrophages phagocyte muscle debris and promote the proliferation of muscle stem cells. Then, macrophages switch their phenotype toward an anti-inflammatory restorative profile and promote muscle stem differentiation, fusion and myofiber growth. This sequence of macrophage profile is essential for an efficient skeletal muscle regeneration. The lab has shown that this phenotype switch is dependent of AMP kinase (AMPK) $\alpha$ 1, a major energetic sensor in the cell controlling cellular metabolism. Besides, glucocorticoids have been used for decades for their anti-inflammatory effects on inflammation. Their actions are mediated by the Glucocorticoid Receptor which induces or represses gene expression by direct or indirect binding to DNA. As AMPK $\alpha$ 1 and glucocorticoids induce similar anti-inflammatory effects on macrophages, we hypothesized that these 2 pathways could be interconnected in macrophages to allow the resolution of inflammation and muscle repair. Data from an *in vitro* model of skeletal muscle injury using bone marrow derived macrophages showed that: i) glucocorticoids induced AMPK $\alpha$ 1 phosphorylation; ii) AMPK $\alpha$ 1 was required for the functional acquisition of the anti-inflammatory phenotype induced by glucocorticoids. Indeed, AMPK $\alpha$ 1-deficient macrophages did not switch their phenotype and did not sustain myogenesis. *In vivo* experiments using LysM<sup>Cre/+</sup>;AMPK $\alpha$ 1<sup>fl/fl</sup> mice in which AMPK $\alpha$ 1 is depleted only in myeloid cells, showed that macrophagic AMPK $\alpha$ 1 drove the beneficial effects of glucocorticoids during skeletal muscle regeneration. Inversely, in the absence of AMPK $\alpha$ 1 in macrophages, glucocorticoids induced a delayed muscle regeneration and modifications in myofiber maturation, assessed by the alteration of the expression of myosin heavy chain isoforms. Altogether, these data show that AMPK $\alpha$ 1 is required in macrophages for the glucocorticoid-induced resolution of inflammation and an efficient skeletal muscle regeneration.

## RÉSUMÉ

### **Interactions entre le Récepteur aux Glucocorticoïdes et l'AMP-activated protein kinase dans les macrophages au cours de la régénération du muscle strié squelettique.**

Le muscle strié squelettique régénère *ad integrum* après une lésion aigüe stérile grâce aux cellules satellites qui sont les cellules souches du muscle strié squelettique. L'inflammation, et notamment les macrophages, joue un rôle important durant ce processus. En effet, après une lésion, les monocytes sanguins infiltrent le tissu et deviennent des macrophages avec un phénotype pro-inflammatoire associé à la lésion. Ces macrophages phagocytent les débris cellulaires et promeuvent la prolifération des cellules souches musculaires. Ensuite, les macrophages changent leur phénotype vers un phénotype anti-inflammatoire associé à la restauration du tissu. Ils promeuvent la différenciation, puis la fusion des cellules souches musculaires et la croissance des myofibres. Cette séquence de phénotypes inflammatoires est essentielle pour une régénération musculaire efficace. Le laboratoire a montré que ce changement de phénotype est dépendant d'un senseur énergétique majeur de la cellule qui contrôle le métabolisme cellulaire, l'AMP kinase (AMPK) $\alpha$ 1. Par ailleurs, les glucocorticoïdes sont utilisés depuis des décennies pour leurs effets anti-inflammatoires sur l'inflammation. Leur action est médiée par le Récepteur aux Glucocorticoïdes qui induit ou réprime l'expression de gènes par interaction directe ou indirecte à l'ADN. Comme l'AMPK $\alpha$ 1 et les glucocorticoïdes induisent des effets anti-inflammatoires similaires sur les macrophages, nous avons posé l'hypothèse que ces 2 voies de signalisation pourraient être interconnectées dans les macrophages afin de permettre leur changement de phénotype et la régénération musculaire. Les données issues d'un modèle *in vitro* de lésion musculaire utilisant des macrophages dérivés de la moelle osseuse de souris ont montré que : i) les glucocorticoïdes induisaient la phosphorylation de l'AMPK $\alpha$ 1 ; ii) l'AMPK $\alpha$ 1 était requise pour l'acquisition fonctionnelle du statut anti-inflammatoire des macrophages induit par les glucocorticoïdes puisque des macrophages déficients pour l'AMPK $\alpha$ 1 ne modifiaient pas leur phénotype et ne stimulaient pas la myogenèse. Les expériences *in vivo* utilisant des souris  $\text{LysM}^{\text{Cre/+}};\text{AMPK}\alpha 1^{\text{fl/fl}}$  dans lesquelles l'AMPK $\alpha$ 1 est invalidée uniquement dans les cellules myéloïdes ont montré que l'AMPK $\alpha$ 1 dans les macrophages régulait les effets bénéfiques des glucocorticoïdes au cours de la régénération du muscle strié squelettique. En effet, en absence d'AMPK $\alpha$ 1 dans

les macrophages, les glucocorticoïdes induisaient un retard de régénération et une modification de la maturation des fibres attestée par une modification de l'expression des isoformes des chaînes lourdes de myosines. En conclusion, ces données montrent que l'AMPK $\alpha$ 1 est requise pour le changement de phénotype des macrophages induit par les glucocorticoïdes et une régénération musculaire efficace.



# SUMMARY

<b>ABBREVIATIONS .....</b>	<b>- 17 -</b>
<b>GENERAL CONTEXT .....</b>	<b>- 19 -</b>
<b>INTRODUCTION .....</b>	<b>- 23 -</b>
<b>I. Skeletal muscle tissue .....</b>	<b>- 25 -</b>
I.1 Skeletal muscle functions.....	- 25 -
I.2 Skeletal muscle composition .....	- 26 -
I.3 Skeletal muscle plasticity: composition and phenotype of myofibers .....	- 29 -
<b>II. Skeletal muscle regeneration .....</b>	<b>- 33 -</b>
II.1 Adult muscle stem cell: the satellite cell.....	- 33 -
II.1.1. Muscle stem cell characterization .....	- 33 -
II.1.2 Functions of muscle stem cells.....	- 36 -
II.2 Myogenesis and myogenic regulators .....	- 37 -
II.2.1 Activation and proliferation .....	- 38 -
II.2.1 Differentiation and fusion .....	- 40 -
<b>III. Macrophages .....</b>	<b>- 43 -</b>
III.1 Origin of macrophages .....	- 43 -
III.2 Bone marrow-derived macrophages .....	- 45 -
III.3 Resident macrophages.....	- 46 -
<b>IV. Glucocorticoids and Macrophages .....</b>	<b>- 49 -</b>
IV.1 Macrophages and tissue repair – example of skeletal muscle regeneration .....	- 50 -
IV.1.1 Similar macrophage subtypes are found in various tissues during repair .....	- 50 -
IV.1.2 Skeletal muscle regeneration.....	- 51 -
IV.1.3 The inflammatory phase .....	- 52 -
IV.1.4 Macrophage phagocytosis and the resolution of inflammation .....	- 53 -
IV.1.5 Time and space orchestration of the inflammatory response .....	- 54 -
IV.2 Glucocorticoids .....	- 54 -
IV.2.1 Origins of GCs .....	- 54 -
IV.2.2 The GC Receptor .....	- 55 -
IV.2.3. Side effects .....	- 58 -
IV.2.4. GC resistance.....	- 58 -
IV.3. Glucocorticoids, macrophages and tissue repair .....	- 59 -
IV.4. GCs and macrophages – cellular aspects.....	- 60 -
IV.4.1. GCs regulate survival, migration and proliferation of macrophages .....	- 60 -
IV.4.2. GCs and phagocytosis .....	- 60 -
IV.5. GCs and gene expression in macrophages – molecular aspects.....	- 62 -
IV.5.1. Anti-inflammatory effects on macrophages .....	- 62 -
IV.5.2. The GC effector Gilz in macrophages .....	- 63 -
IV.5.3. New high throughput analyses .....	- 63 -
<b>V. AMP-activated protein kinase .....</b>	<b>- 66 -</b>
III.1. Structure and functions.....	- 66 -
III.2. AMPK and cellular metabolism .....	- 67 -

III.3. AMPK, macrophages and skeletal muscle.....	- 69 -
<b>SPECIFIC AIMS OF THE STUDY.....</b>	<b>- 73 -</b>
<b>STUDY #1 .....</b>	<b>- 77 -</b>
MATERIAL AND METHODS.....	- 80 -
RESULTS.....	- 85 -
DISCUSSION.....	- 102 -
<b>STUDY #2 .....</b>	<b>- 109 -</b>
<b>STUDY #3 .....</b>	<b>- 145 -</b>
<b>PERSPECTIVES .....</b>	<b>- 165 -</b>
AMPK and GR crosstalk: involvement of other molecular partners? .....	- 167 -
AMPK and GC crosstalk: metabolic regulation?.....	- 169 -
Regulation of gene expression .....	- 170 -
AMPK and GR crosstalk: on the GR side .....	- 170 -
<b>SCIENTIFIC PUBLICATIONS AND COMMUNICATIONS .....</b>	<b>- 173 -</b>
<b>REFERENCES .....</b>	<b>- 179 -</b>

## ABBREVIATIONS

AICAR: 5-Aminoimidazole-4-carboxamide ribonucleotide

ACC: Acetyl CoA Carboxylase

ADP: Adenosine di-phosphate

AMP: Adenosine mono-phosphate

AMPK: AMP- activated Kinase

ATP: Adenosine tri-phosphate

BSA: Bovine serum albumine

CAMKK: Calcium/Calmodulin-dependent protein Kinase Kinase

C/EBP $\beta$ : CCAAT/enhancer-binding protein

CCL: C-C motif ligand

CCR: C-C chemokine receptor

CDK9: Cyclin-Dependent Kinase 9

CD163: Cluster of differentiation 163 = scavenger receptor for hemoglobin-haptoglobin

CD206: Cluster of differentiation 206 = mannose receptor

CRE: cre recombinase

CX3CR1: chemokine (C-X3-C motif) receptor 1

DAMPs: Damaged associated molecular patterns

DEX: Dexamethasone

DT: Diphtheria Toxin

DTR: Diphtheria Toxin Receptor

ECM: extra-cellular matrix

EDL: *Extensor digitorum longus*

ERK: Extracellular signal-regulated kinase

FAP: Fibro-Adipogenic precursor

FGF: Fibroblast growth Factor

FRP: Formyl peptide Receptor

GC: Glucocorticoid

GILZ: Glucocorticoid-Induced Leucin Zipper

GR: Glucocorticoid Receptor

GRE: Glucocorticoid Response Element



GRIP1: Glutamate receptor-interacting protein 1

HMG-CoA: 3-hydroxy-3-methyl-glutaryl-coenzyme A

IFN: Interferon

iNOS: inducible Nitric Oxide Synthase

KO: Knock out

IL: Interleukine

LPS: Lipopolysaccharide

LXR: Liver X receptor

LysMA: LysM<sup>cre/+</sup>;AMPK $\alpha$ 1<sup>fl/fl</sup>

Ly6C: Lymphocyte antigen 6 complex

MCP-1: Monocyte chemoattractant protein 1 (=CCL2)

MerTK: Mer tyrosine kinase

MHC: Myosin heavy chain

MKP1: Mitogen-activated protein kinase phosphatase-1

MRF: Myogenic Regulatory Factor

MuSCs: Muscle stem cells

NFEL: Negative elongation factor

NF $\kappa$ B: Nuclear factor kappa-light-chain-enhancer of activated B cells

Pax: Homeodomain paired box

PPAR: Peroxisome proliferator-activated Receptor

RXR $\alpha$ : Retinoid X receptor  $\alpha$

Ser: Serine

TA: *Tibialis anterior*

TAK1: Transforming growth factor- $\beta$ -activated kinase 1

TGF: Transforming growth factor

Thr: Threonine

TNF $\alpha$ : Tumor necrosis factor  $\alpha$

TLR: Toll like receptor

VEGF: Vascular endothelial growth factor

WT: Wild Type

## **GENERAL CONTEXT**



Inflammation is a very important process that is activated after injury or infection, in order to contain the damage/infection, cleanse the tissue debris and return to homeostasis. This complex process can be divided in 2 main steps which are the mounting of the inflammation and the resolution of inflammation. This last step is crucial to stop the inflammatory process, so the tissue/organ is not further damaged by inflammation. When the inflammatory response cannot be resolved, chronic inflammation is observed associated with tissue damage. This process is driven by immune cells including lymphocytes, neutrophils or macrophages. In most tissues, macrophages are shown to orchestrate tissue repair thanks to their phagocytic activity (to clean debris) and their ability to stimulate regeneration and healing of the tissue. Thus, macrophages participate to both the mounting of the inflammatory response and the resolution of inflammation that allows tissue repair. The molecular mechanisms that drive the resolution of inflammation by macrophages are not completely understood.

Post-injury skeletal muscle regeneration provides a good model to study the inflammatory response. This is a model of sterile inflammation without immune challenge allowing to analyze the role of innate immunity and especially the role of macrophages. During skeletal muscle regeneration, macrophages have several sequential roles and interact with various cell types to drive regeneration. After the injury, monocytes infiltrate the tissue and become pro-inflammatory macrophages that phagocyte cell debris, which makes them to switch their phenotype toward an anti-inflammatory status. In this context, the lab demonstrated that a main metabolic regulator of the cell, AMPK, is required for macrophage phenotype switch and is therefore necessary for skeletal muscle regeneration. Functionally, AMPK is required in macrophages so they stimulate myogenesis. In a previous study, the lab used glucocorticoids to induce an anti-inflammatory profile in macrophages, and showed that similarly, they induce a stimulating phenotype on *in vitro* myogenesis.

That was the situation when I arrived in the lab. My project was to decipher the interactions between AMPK and glucocorticoids pathways in macrophages in an *in vitro* model of inflammation, then, *in vivo*. My thesis work is therefore focused on several topics including macrophages in the resolution of inflammation, glucocorticoids in macrophages, AMPK activation and inflammation, and skeletal muscle regeneration.



# **INTRODUCTION**



# I. Skeletal muscle tissue

## I.1 Skeletal muscle functions

The word “*muscle*” comes from the latin word “*musculus*” meaning “little mouse” that refers to the movement of muscle during contraction that is similar to a mouse moving under a fabric. One of the first descriptions of skeletal muscle is the organ allowing locomotion, that refers to the contractile property of the tissue. Muscles are joint attached to the bones by tendons and allow the movement by contraction.

Skeletal muscle tissue is one of the three muscle tissues including cardiac and smooth muscles (Figure 1A). Skeletal muscle is present in all parts of the body and can represent more than 50% of the total body mass in Human (Figure 1B). The main function of skeletal muscle is to transform chemical energy into mechanical energy and to confer to the organism the capacity to move and to interact with the environment. However, skeletal muscle is more than a contracting tissue. Indeed, skeletal muscle is sensitive to metabolic signals in the body and actively participates to homeostasis. By shaking when it is cold, muscle products warmth to keep the body temperature stable. Skeletal muscle also exerts an important role in the control of the global metabolic status of the body. Muscle is used by the body to control glycemia. This is the only tissue with liver that can store glucose as glycogen. Moreover, skeletal muscle is the organ of the human body that consumes the most glucose (Homsher and Kean, 1978).



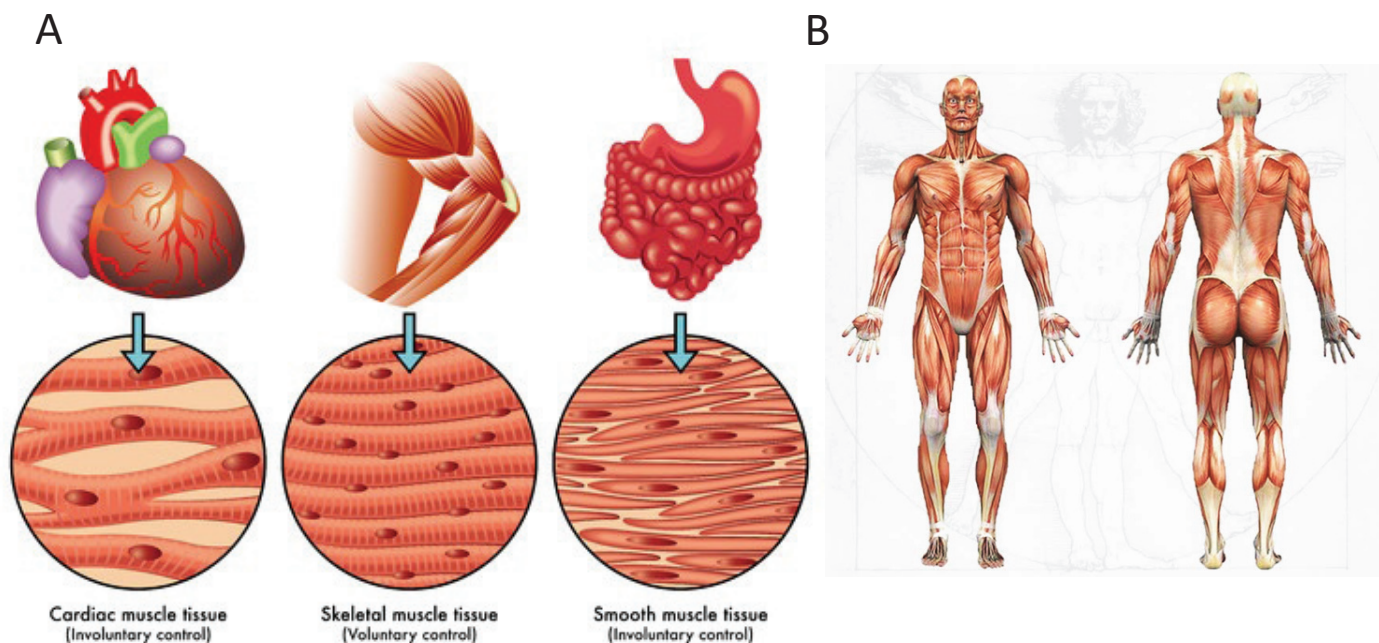


**Figure 1. The muscle tissues**

**(A)** The 3 types of muscles. Cardiac muscle tissue (left) is only found in heart. It is composed of cardiomyocytes, which contract simultaneously to allow blood circulation. Skeletal muscle tissue is the most abundant muscle tissue in the body (middle). It is composed of myofibers, which contract to allow the movement by voluntary control. Smooth muscle tissue (right) is associated with involuntary contraction in a lot of tissues (intestine, skin, vessels...). (www.biology101.com) **(B)** The anatomy of whole-body skeletal muscle tissue in Human. (www.anatomy.asktrainer.com).

## 1.2 Skeletal muscle composition

Skeletal muscle is a very well-organized tissue (Figure 2). Each muscle is attached at both ends to the bones by tendons. Muscle has several levels of architecture. The organ is itself enveloped in a connective tissue called epimysium. Muscle is composed of fascicles that are enveloped in perimysium and the fascicles are themselves composed of a set of muscle cells, the myofibers. Each myofiber is surrounded by a connective tissue, which is the endomysium. Myofibers may be among the biggest cells of the body, up to dozens of centimeters. These cells are syncytia containing hundreds of nuclei. The contractile apparatus occupies the main part of the myofiber cytoplasm and is composed of an arrangement of myofilaments organized in sarcomeres, the structural units allowing contraction (Figure 2). Contraction is under the control of a motoneuron. Each myofiber is innervated by a motoneuron and forms a specific synapse called the neuromuscular junction. This cholinergic

synapse induces the depolarization of the myofiber plasma membrane and therefore, the contraction of the sarcomere.

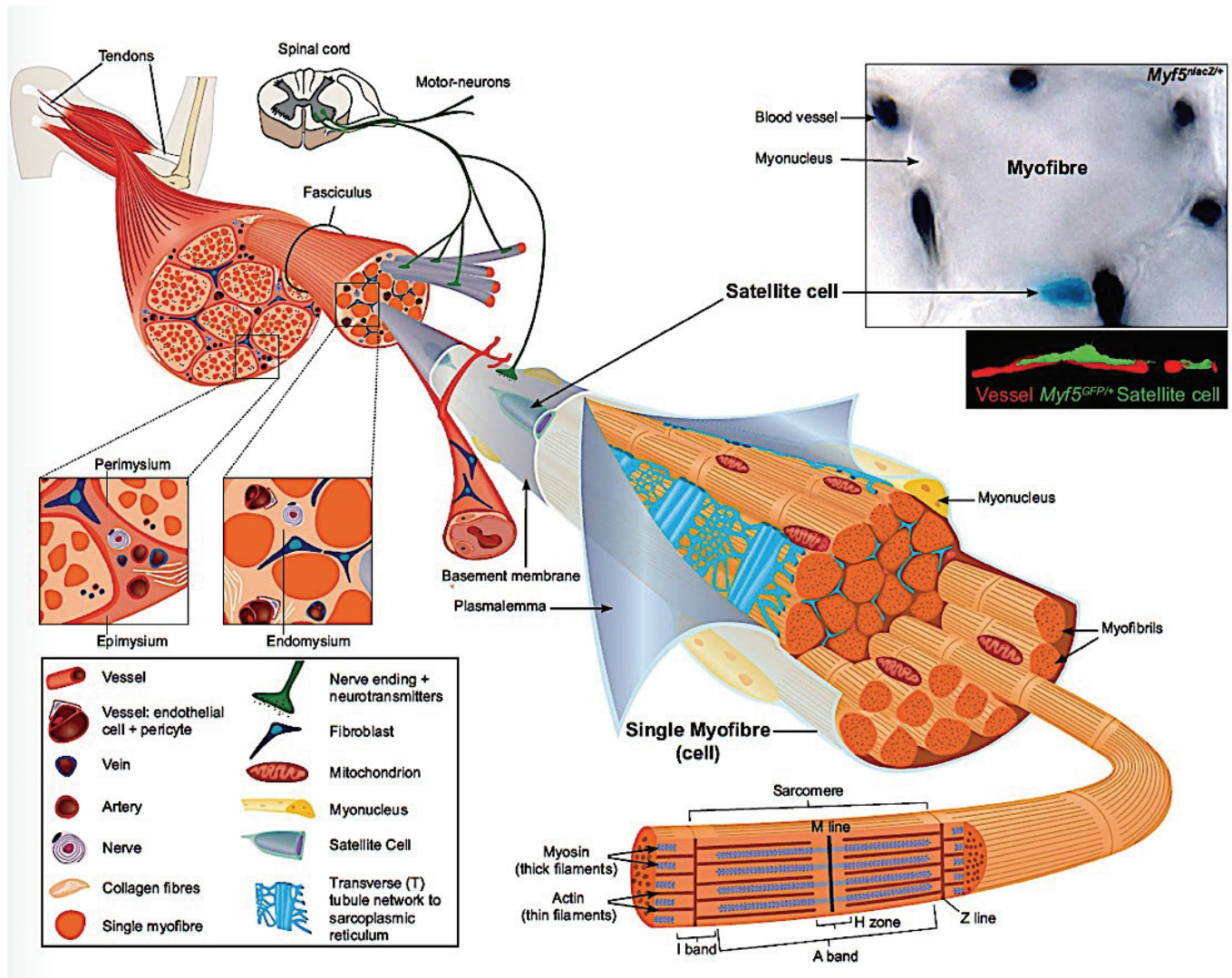


**Figure 2. Skeletal muscle tissue composition**

Skeletal muscle tissue is composed of fascicles and myofibers. Myofibers contain the contractile apparatus, which is composed of sarcomeres. The contraction of each myofiber is under the control of the motoneuron. Skeletal muscle tissue is also composed of other cells and especially satellite cells, the muscle stem cells, which are around the myofibers under the basal lamina surrounding the myofibers (Tajbakhsh, 2009).

Because all skeletal muscle structures are delineated by connective tissue, fibroblasts have an important role in muscle homeostasis although their role has been poorly investigated. The precursors of fibroblasts in skeletal muscle are the Fibro-Adipogenic Precursors (FAPs) (Joe et al., 2010). Muscle fibroblasts secrete molecules which compose the extra-cellular matrix (ECM). ECM in muscle is composed of a large number of molecules including collagens (IV and VI), dystroglycans, laminin, *etc.* ECM forms a scaffold for myofibers and it is essential for muscle contraction to produce force (Chapman et al., 2016). In degenerative myopathies, proteins belonging to the Dystro Glycan Complex (DGC) are mutated. DGC allows the link between cytoskeleton and ECM, its disruption leading to myofiber fragilization and damage (Parsons et al., 2002; Ibraghimov-Beskrovnaya et al., 1992). These diseases show that the link between myofibers and ECM is crucial for muscle function.

Myofibers also require another cell partner to work properly: endothelial cells that compose the vessels in association with other cell types such as pericytes. Vascularization is crucial for skeletal muscle function since it ensures metabolite exchanges. There are at least 5 to 10 blood capillaries for 3-4 myofibers (Latroche et al., 2015).

Thus, skeletal muscle is composed of various cell types beside myofibers ([Figure 3](#)). These cells interact, communicate and exchange molecules to allow movement, posture and adaptation of the body to its environment and to maintain homeostasis of the tissue and the body.

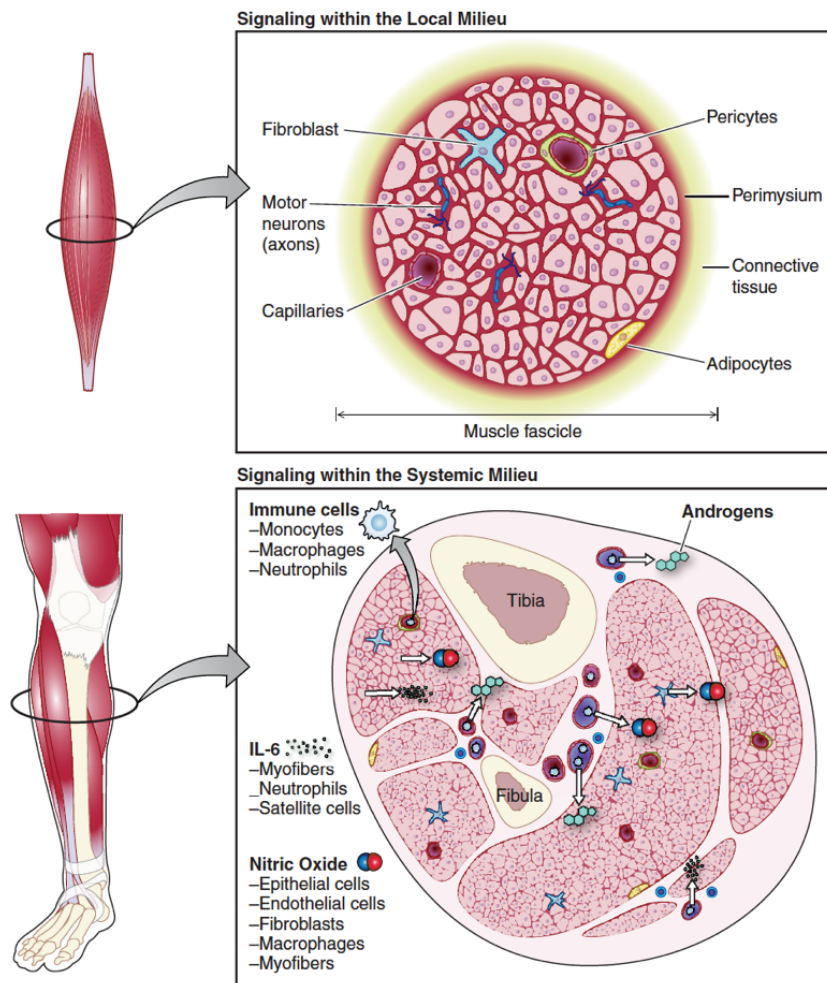


**Figure 3. Various cell types in the muscle tissue**

Skeletal muscle is composed of endothelial cells, fibroblasts and immune cells such as monocytes/macrophages or neutrophils. Endothelial cells form the vessels necessary for metabolic exchanges with blood. Fibroblasts secrete ECM essential for muscle contraction. Immune cells control the maintenance of the tissue integrity (Yin et al., 2013).

### 1.3 Skeletal muscle plasticity: composition and phenotype of myofibers

Myofiber cytoplasm contains the contractile apparatus. This structure is complex and composed of repetitions of the structural unit, which is the sarcomere. Sarcomere is mainly composed of 2 types of filaments: thin actin filaments and thick myosin filaments. Actin filaments measure about 7 nm length and contain tropomyosin and troponin. Thick filaments are composed of myosin, including myosin heavy chain and myosin light chain. Myosin heavy chain is the structure able to bind the actin filament to induce the contraction. The incoming signaling that induces the contraction comes from the motoneuron. One motoneuron can innervate several myofibers and the bunch of myofibers innervated by the same motoneuron is



called the motor unit. Motoneuron induces membrane depolarization thanks to the cholinergic synapse. Depolarization induces calcium release in the cytoplasm of the myofiber *via* the sarcoplasmic reticulum (a specific endoplasmic reticulum in the myofiber). Calcium binds to troponin, inducing the rotation of tropomyosin and the release of the binding site on actin filament. Then, myosin binds to actin. Myosin also contains an ATP binding site. When myosin and actin are bound, myosin releases ADP+P<sub>i</sub>, which induces the slide of the 2 filaments to allow the shortening of the sarcomere and the contraction of the myofiber (Figure 4). Later, calcium is pumped back to the sarcoplasmic reticulum and ATP binding to myosin induces the relaxation of the sarcomere and of the myofiber.

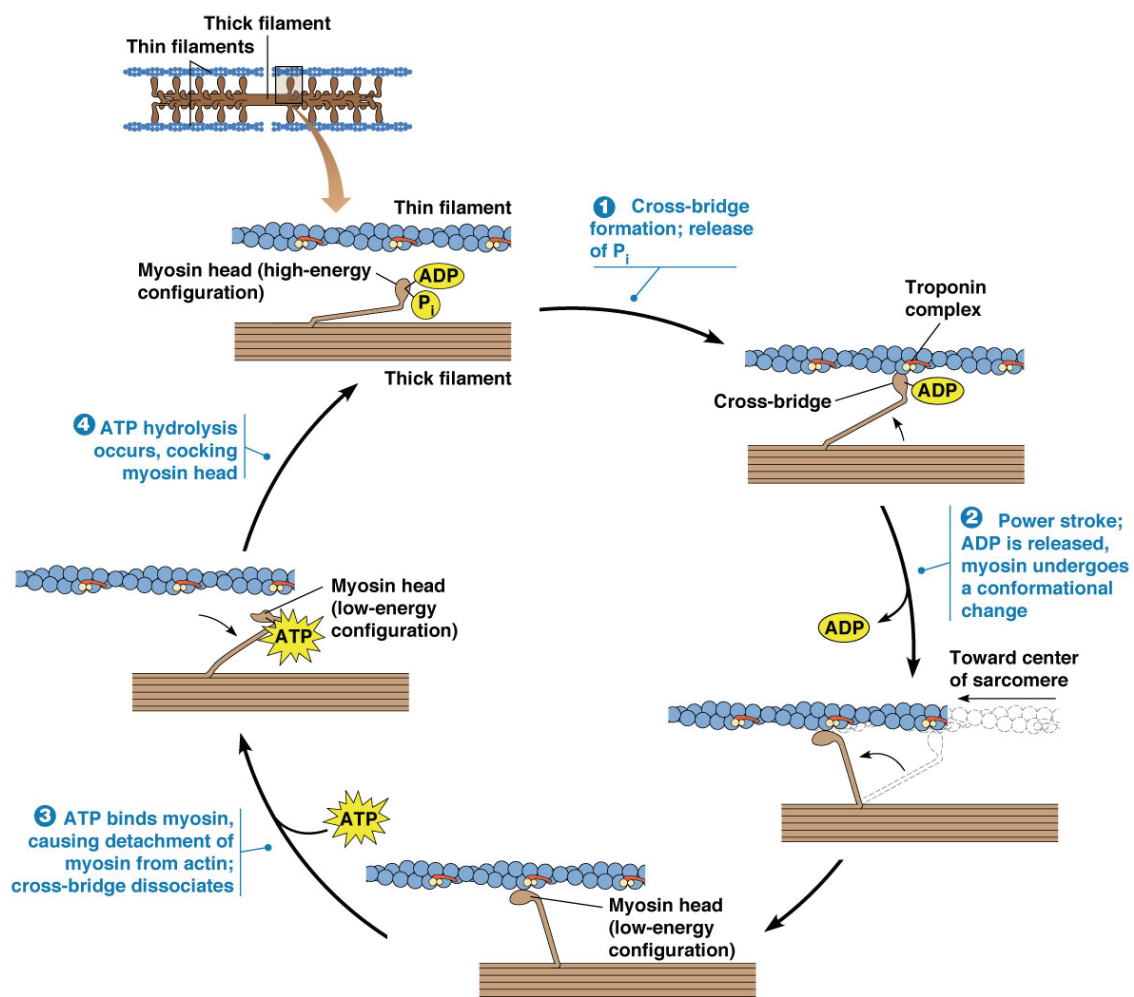


**Figure 4. Molecular aspects of muscle contraction**

Contraction of sarcomere requires ATP. ADP and P<sub>i</sub> are bound to the myosin head. The release of P<sub>i</sub> induces the cross-bridge formation between actin and myosin. The release of ADP by the myosin head induces a conformational change of myosin and sliding of the 2 filaments, leading to contraction. ATP binding on myosin head leads to the detachment of actin and myosin myofilaments that induces the relaxation of the sarcomere and of the muscle (www.mun.ca).

Another level of complexity exists in skeletal muscle as various types of myofibers are present. Myofiber type is associated with the myosin heavy chain (MHC) content, actin content being not different. In 1962, Engel proposed a classification based on the ATPase staining and Henneman proposed the following nomenclature for the adult MHC:

- Myosin Heavy Chain Type I (MHCI) enriched myofibers are slow-twitch myofibers, have a high content of mitochondria and a very oxidative metabolism. A higher number of vessels is observed nearby the myofibers. Slow-twitch myofibers do not develop high level of strength but they are resistant to fatigue that is required for endurance exercise.

- Myosin Heavy Chain Type IIB (MHCIIB) enriched myofibers are fast-twitch myofibers. They have a glycolytic metabolism with a low number of mitochondria. These fibers are able to develop high level of strength but are rapidly fatigable. This myofiber type is not found in Human.

- Myosin Heavy Chain Type IIA (MHCIIA) enriched myofibers are fast-twitch myofibers. They have a higher number of mitochondria than MHCIIB myofibers. These fibers exhibit a mixed phenotype between MHCI and MHCIIB myofibers. MHCIIA fibers produce energy using oxidative metabolism thanks to mitochondria. They develop strength (less than MHCIIB but more than MHCI) and resist more to fatigue (less than MHCI but more than MHCIIB).

- Myosin Heavy Chain Type IIX (MHCIIX) enriched myofibers are also fast-twitch myofibers. These myofibers have a poor content of mitochondria. They produce ATP by the glycolytic pathway and are rapidly fatigable. Like MHCIIB, these cells develop high level of strength.

MHC composition ([Figure 5A](#)) is specific for each muscle and is different between species.

During development, another type of MHC is observed, *i.e.*, embryonic Myosin Heavy Chain. This embryonic MHC is not found in adult muscle except during the regeneration process where it is the first one to be expressed in newly formed myofibers before being replaced by the adult MHC at the end of the regeneration process ([Figure 5B](#)).

Although myofibers may exhibit various types, they are all derived from the same cells in adult muscle, the satellite cells, which are the muscle stem cells.

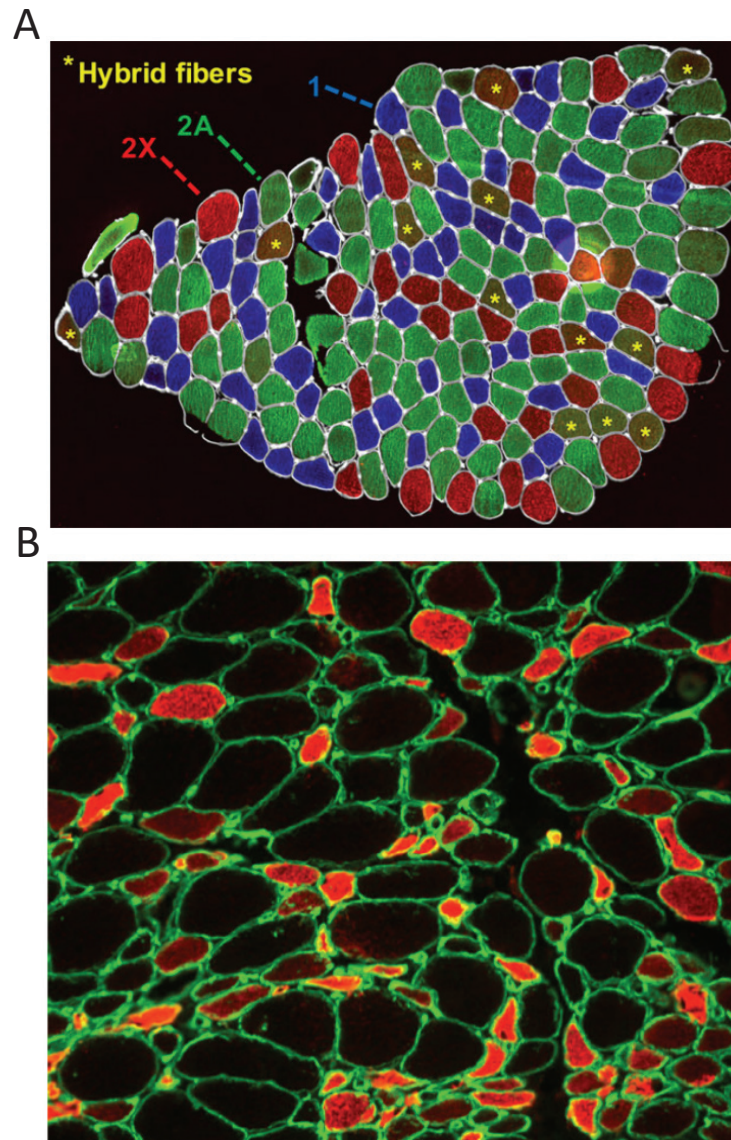


**Figure 5. Myofiber types in skeletal muscle**

**(A)** Immunofluorescent analysis of human *Vastus Lateralis* muscle shows that the muscle is composed of myofibers expressing MHCI (blue), MHCIIA (green) and MHCIIIX (red). **(B)** Embryonic MHC expression analyzed by immunofluorescence of a human muscle biopsy with muscle disease. The presence of embryonic myosin in adult muscle is a hallmark of myofiber regeneration (Schiaffino, 2018).

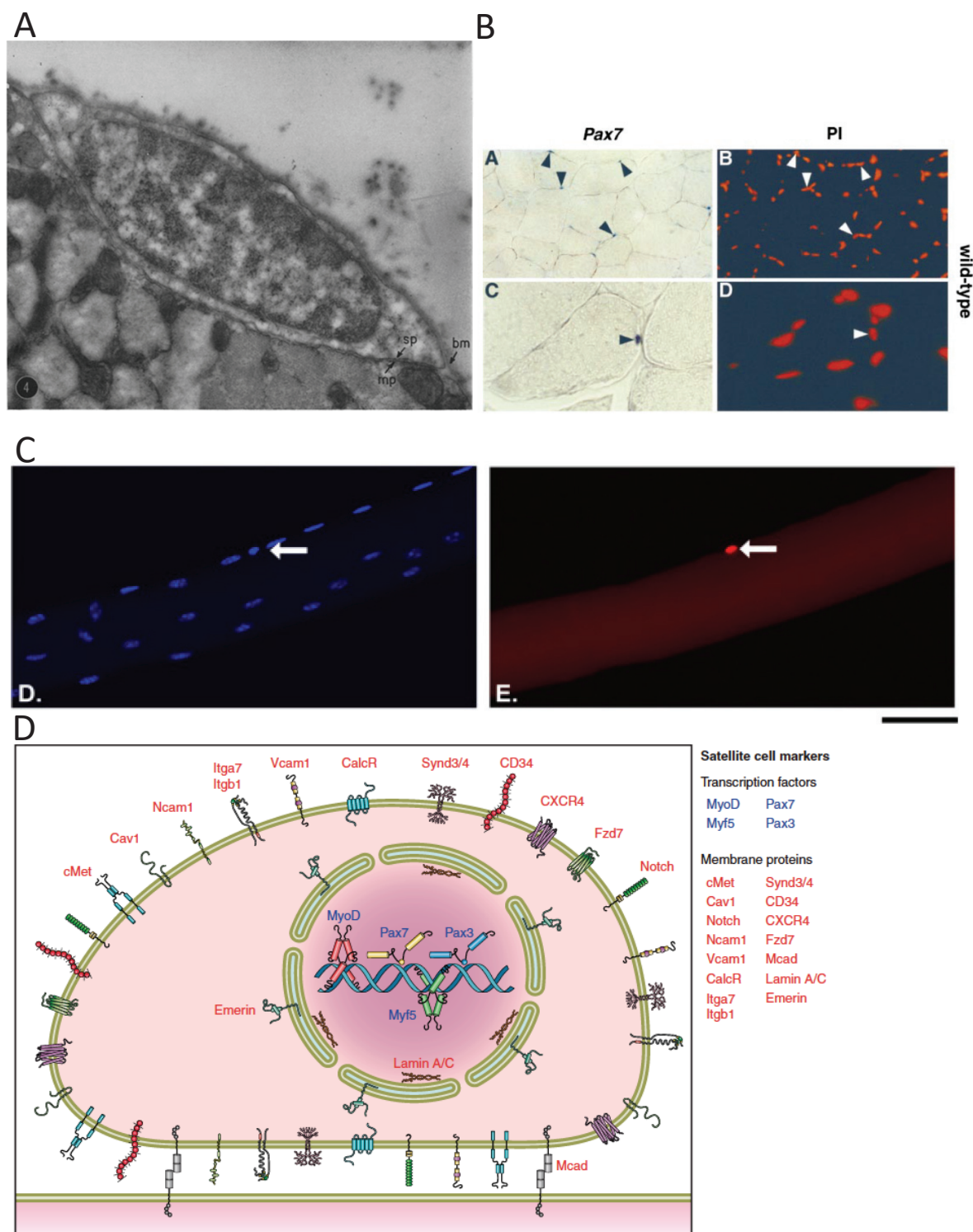
## II. Skeletal muscle regeneration

### II.1 Adult muscle stem cell: the satellite cell

#### *II.1.1. Muscle stem cell characterization*

Skeletal muscle stem cells were highlighted in 1961 thanks to the development of electronic microscopy. Alexander Mauro found in frog and rat muscles that small cells were located very close to the adult myofiber. Actually, these cells are between the plasma membrane of the myofiber and the basal lamina. They were named “satellite cells” because of their position around the myofiber ([Figure 6A](#)) (Mauro, 1961). At this time, they were suggested to be “dormant myoblasts” that can be activated after a trauma to repair myofibers. In the next half century, satellite cells were better characterized. They were first isolated by enzyme dissociation in 1974 (Bischoff, 1974). More recently, isolation of satellite cells and histological analyses allowed the discovery of the marker Pax7 (homeodomain Paired box 7), which is highly specific of satellite cells in muscle (Seale et al., 2000). Pax7 belongs to the family of homeodomain paired box transcription factors that are involved in development. In constitutive Pax7 null mice, satellite cells completely disappear and muscles show several defects (Seale et al., 2000). Thus, the expression of Pax7 is crucial for the establishment of satellite cell population in muscle ([Figures 6B, 6C](#)). Pax7 is often used to identify satellite cells. However, other markers are expressed by satellite cells such as CD34, CXCR4, syndecan4, Vcam1 and  $\beta$ 1-integrin,  $\alpha$ 7-integrin ([Figure 6D](#)) (Beauchamp et al. 2000; Seale et al.; 2000, Kuang and Rudnicki, 2008).





In resting condition, satellite cells are located around the myofibers in the so-called *satellite cell niche* (Figure 7). Although not well-characterized yet, this structure is essential for the maintenance of satellite cell quiescence. Indeed, protein interactions between the muscle fiber and satellite cells were identified to maintain satellite cells in quiescent state such as M-cadherin and Notch pathway (Kuang and Rudnicki 2008; Bjornson et al., 2012; Mourikis et al., 2012; Baghdadi et al., 2018; Evano and Tajbakhsh 2018). Interactions between satellite cells and ECM, which composes the basal lamina, also participate to maintain satellite cells quiescent thanks to integrins (Labarge et Blau 2002; Evano and Tajbakhsh, 2018). Other cell types participate to the homeostasis of the satellite cell niche. Endothelial cells are found to be very close to satellite cells in resting condition (Christov et al., 2007). After an injury, satellite cell niche alteration is critical for satellite cell activation (Yin et al, 2013).

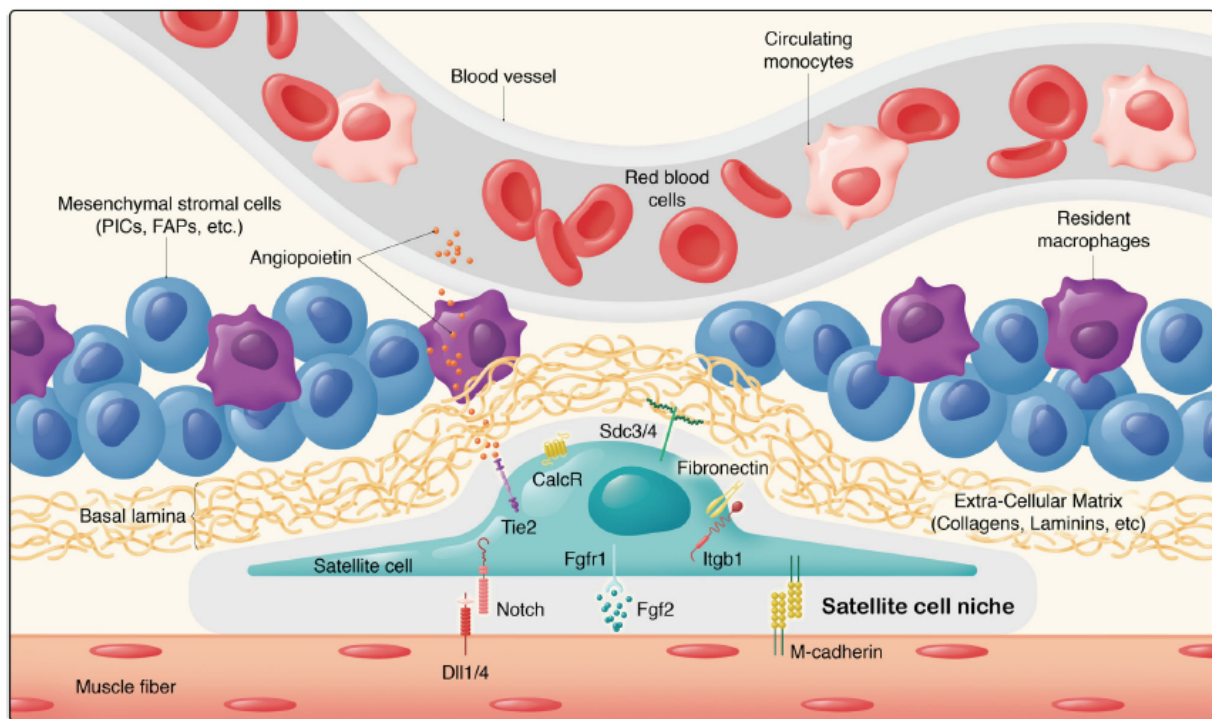


**Figure 7. The satellite cell niche**

In resting muscle, quiescent satellite cells are located in a niche. Myofiber itself is involved in the maintenance of the quiescence by Notch and cadherin signaling. Other factors are implicated in the maintenance of the quiescence such as angiopoietin or Fgf2. Macrophages, mesenchymal stromal cells and endothelial cells are close neighbors of the niche (Evano and Tajbakhsh, 2018).

### *II.1.2 Functions of muscle stem cells*

In 1975, regeneration of a single myofiber was analyzed *in vitro* for the first time (Bischoff, 1975). By contrast microscopy, it was possible to see *in vitro* the proliferation of cells at the surface of the isolated myofiber. In 1977, a first analysis done by electron microscopy of the satellite cells during muscle regeneration showed that satellite cells are activated and differentiate into myoblasts to repair the myofiber (Sakai, 1977). More recently, Pax7 marker was highlighted thanks to an inducible cre-lox system. When Pax7-positive cells (satellite cells) are depleted, skeletal muscle regeneration is impaired (Figure 8) (Sambasivan et al., 2011; Lepper et al., 2011; Murphy et al., 2011; Von Maltzahn et al., 2013). These results show the essential role of satellite cells during adult muscle regeneration.

Moreover, few weeks after injury, satellite cells are present in the muscle, back to their location under the basal lamina, indicating that cells do participate to skeletal muscle regeneration, as well as return to quiescence in order to reform the pool of stem cells (Sacco et al., 2008; Montarras et al., 2005; Collins and Partridge, 2005). This phenomenon of self-renewal is essential for the long-term maintenance of muscle homeostasis.

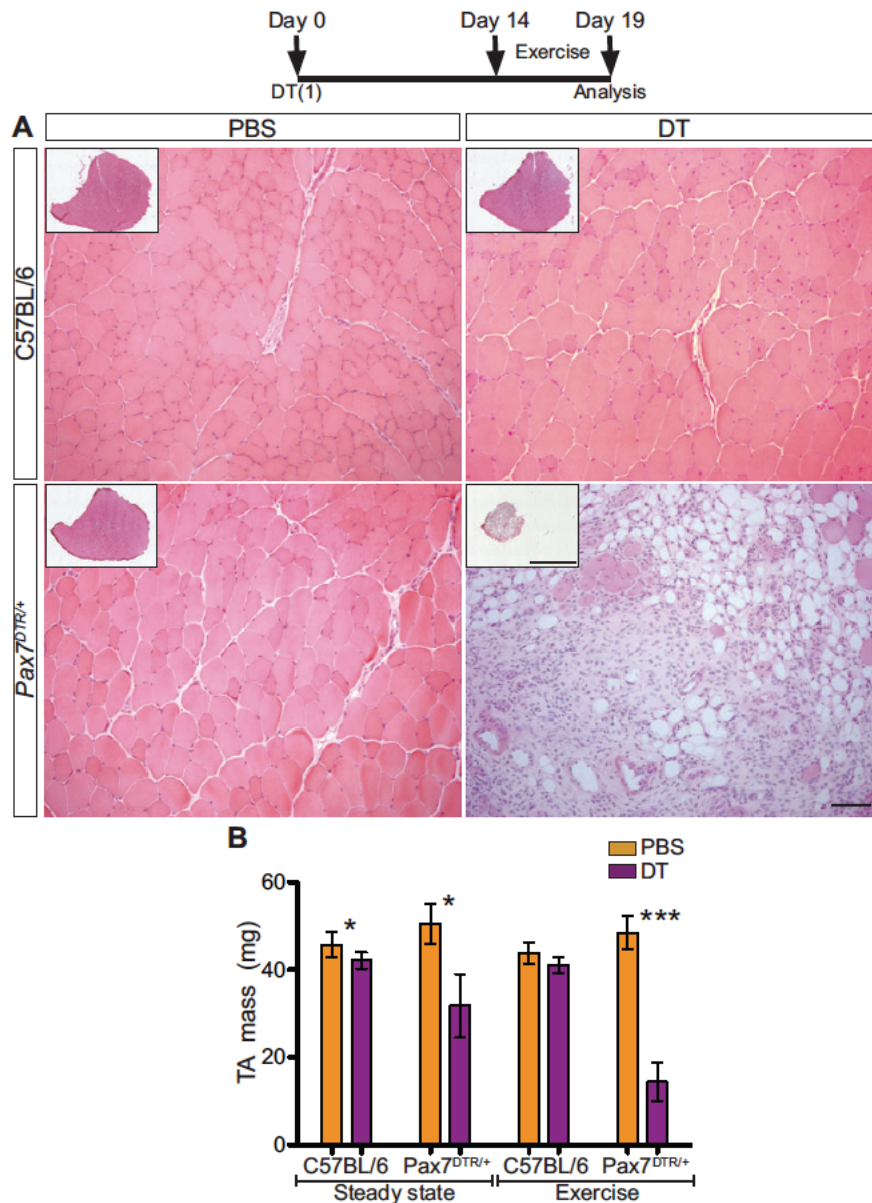


**Figure 8. Pax7<sup>pos</sup> satellite cells are required for skeletal muscle regeneration**  
**(A)** Skeletal muscle regeneration is dependent of Pax7<sup>pos</sup> cells. In a Pax7<sup>DTR/+</sup> mouse model in which cells expressing Pax7 are depleted after injection of diphtheria toxin (DT), skeletal muscle regeneration is completely altered after exercise induced injury as shown by Hematoxylin and Eosin staining. Moreover, muscle mass of the *tibialis anterior* muscle was drastically decreased in exercised mice injected with DT **(B)**. Scale bars 150  $\mu$ m in main panels; 1 mm in insets. These results indicate that satellite cells are essential for skeletal muscle regeneration (Sambasivan et al., 2011).

## II.2 Myogenesis and myogenic regulators

Myogenesis is the process that allows the formation of muscle fibers during embryonic development or during adult regeneration. We here focus only on adult myogenesis. This process starts from the activation of satellite cells toward the complete reformation of



myofibers (Figure 9). Each step of the process is tightly controlled by intrinsic and extrinsic myogenic regulators. Myogenesis is mainly driven by the family of the Myogenic Regulatory Factors (MRFs). This family is composed of 3 main factors: Myf5, MyoD and myogenin. These markers are differentially expressed during myogenesis (Figure 10).

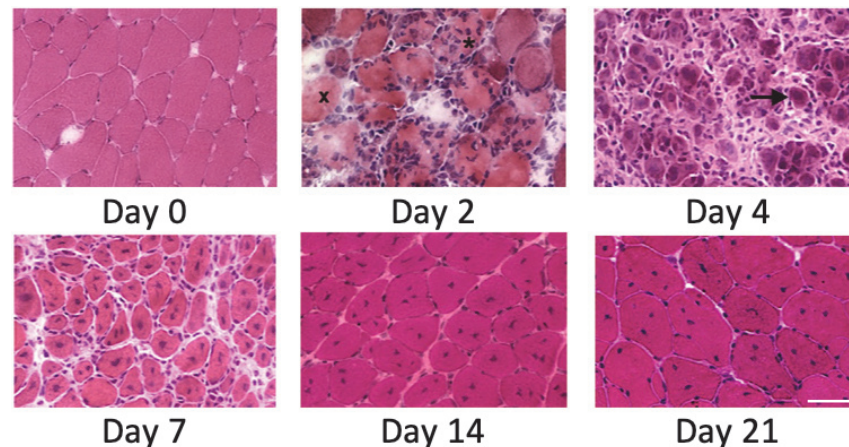


**Figure 9. Skeletal muscle regeneration**

Skeletal muscle regenerates *at integrum* after an injury thanks to satellite cells. Before injury (day 0), all the myofibers present peripheral nuclei and no inflammation is observed. At day 2, after cardiotoxin injury, Hematoxylin and eosin staining shows myofiber necrosis and infiltration of immune cells in the tissue. At day 4 after cardiotoxin injury, a large number of immune cells are still present in muscle and newly formed myofibers appear (arrow). At Day 7 after injury, few immune cells are present in the muscle and a lot of regenerating myofibers are observed. These myofibers exhibit centrally located nuclei. At day 14 and day 21, immune cells are barely observable and regenerating myofibers are growing. They still present centrally located nuclei (pictures from Mounier et al., 2013). Scale bar: 50  $\mu$ m.

### *II.2.1 Activation and proliferation*

In resting muscle, muscle stem cells are quiescent. The cell cycle is arrested in G<sub>0</sub> phase. This quiescent state is maintained by the niche. When the niche is altered by muscle injury, muscle stem cells emerge from quiescence to activate (Yin et al, 2013) and give rise to myoblasts or myogenic precursor cells. An intermediate state between the quiescent state and the activated state was recently described and called the G<sub>alert</sub>, in non-injured muscles of a mouse that was injured in a remote muscle. Muscle stem cells in G<sub>alert</sub> state activate faster than G<sub>0</sub> state after an injury (Rodgers et al., 2014). Activated muscle stem cells expressed Pax7. Quickly after activation, they also express the MRF *Myf5* (Figure 10). *Myf5* was shown to be expressed by quiescent stem cells but the mRNA is sequestered in a structure called

messenger ribonucleoprotein granules. During activation state, these granules are dissociated and allow the rapid translation of the *Myf5* mRNA (Crist et al., 2012). *Myf5* is required for proliferation of myoblasts. Indeed, in the *myf5*<sup>-/-</sup> mouse model, the rate of myoblast proliferation is decreased (Ustanina et al., 2007). *Myf5* is a transcription factor that controls gene expression that is required for proper myogenesis (Conerly et al., 2016). The MRF MyoD is also expressed by proliferating cells and this factor is important for the differentiation step. Moreover, other signaling pathways are required for proliferation of muscle stem cells such as Notch signaling pathway (Conboy and Rando, 2002). At the end of the proliferation/expansion phase, muscle stem cells differentiate. However, not all the cells differentiate. Indeed, a subset returns to quiescence in order to replenish the muscle stem cell pool (Yin et al., 2013; Sacco et al., 2008; Montarras et al., 2005; Collins and Partridge, 2005). This phenomenon, called self-renewal, is partly mediated by AMPKα1 (Théret et al., 2017).

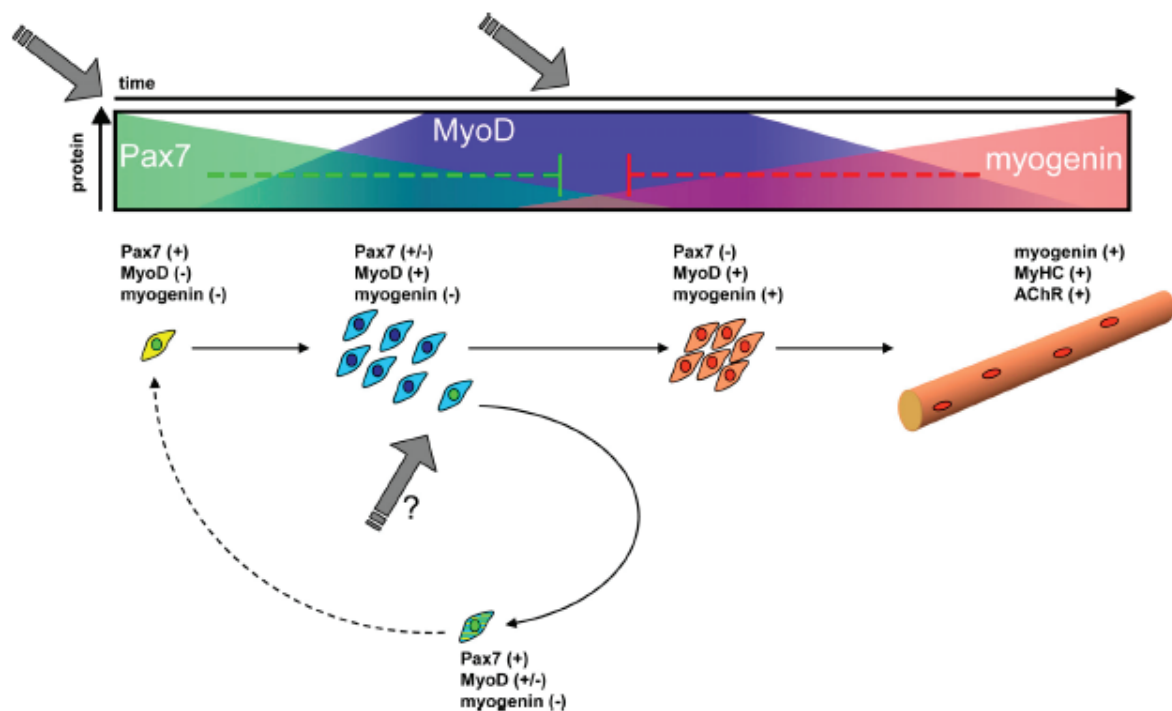


**Figure 10. MRF expression during myogenesis**

During myogenesis, several myogenic regulated factors are expressed by myogenic cells. Quiescent cells expressed Pax7. Activated satellite cells expressed Pax7 and MyoD. Differentiated myoblasts express myogenin. MRFs are sequentially expressed and regulate specific gene expression at each step of adult myogenesis (Olguin et al., 2007).

### *II.2.1 Differentiation and fusion*

The end of proliferation is marked by differentiation of myogenic cells ([Figure 11](#)). Differentiating cells shutdown the expression of Pax7. Cells start to express the MRF MyoD during proliferation and continue to express it during differentiation (Tedesco et al., 2010). Actually, a ratio between Pax7 and MyoD was implicated for the induction of the differentiation (Olguin et al., 2007). A low Pax7/MyoD ratio was suggested to induce the commitment of proliferating cells to differentiation (Olguin et al., 2007). Studies have shown that satellite cells deficient for MyoD do not differentiate properly (Yablonka-Reuveni et al., 1999; Wood et al., 2013; Yamamoto et al., 2018) showing the essential role of this transcription factor in myogenic cell differentiation. While MyoD appears to be necessary for the early state of differentiation, the MRF myogenin is expressed at the end of the differentiation process, when cells definitively escape from cell cycle, to specifically trigger the expression of myogenic genes (Bentzinger et al., 2012). Myogenin was originally discovered in 1989 to allow the expression of myogenic markers in mesenchymal cells after transfection (Wright et al., 1989). Moreover, myogenin null-mice show a defect in embryonic myogenesis showing the importance of this factor for myogenesis (Hasty et al., 1993). The sequential expression of the myogenic regulators is primordial for muscle stem cell differentiation and skeletal muscle regeneration.

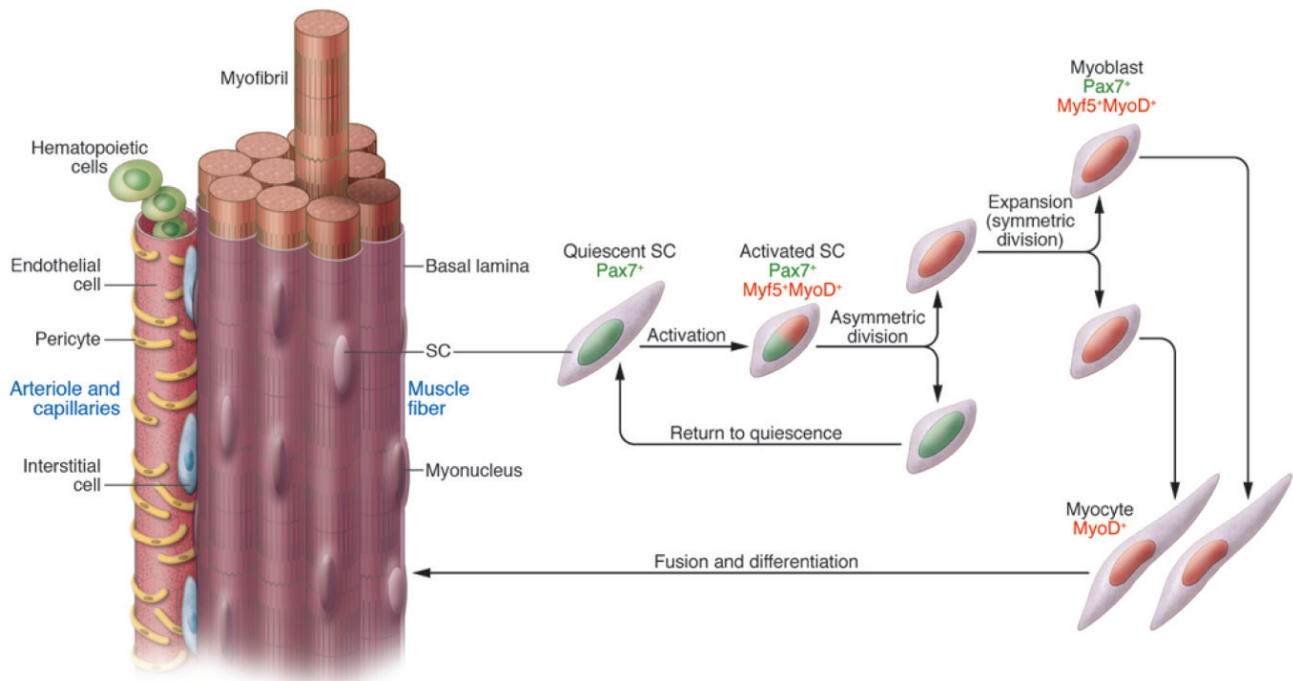


**Figure 11. Differentiation of muscle stem cells**

After an injury, Pax7<sup>pos</sup> quiescent cells (green cells) are activated. These activated cells express *Myf5* and *MyoD* (green and red cells). After proliferation, cells differentiate into myocytes and stop to express Pax7 (red cells). Then, they fuse to repair myofibers. A proportion of myogenic proliferating cells (green and red cells) returns to quiescence in order to replenish the pool of muscle stem cells (back to green cells) (Tedesco et al., 2010).

Once differentiated, myogenic cells (or myocytes) fuse with each other to form new multinucleated myofibers. To fuse, cells first move and contact each other. The recognition of partner to fuse is highly specific since myogenic cells fuse only with myogenic cells. Moreover, fusion events induce cytoskeletal reorganization and implicate the regulation of the plasma membrane tension between the two-fusing partner-cells depending on actin and myosin (Figure 12) (Kim et al., 2015). Membrane protein content is important to allow fusion. Integrins and cadherins are essential in this process (Schwander et al., 2003; Chargé and Rudnicki, 2004). Recently, a master protein involved in fusion was identified, myomaker. Myogenic cells depleted for myomaker are not able to fuse and in myomaker null mice, embryos die perinatally due to absence of muscle fusion (Millay et al., 2013).

Finally, the myogenesis process is well-orchestrated to induce proliferation of muscle stem cells in order to obtain a substantial pool of cells able to further differentiate and fuse to



form new myofibers. Each step of this process is tightly regulated. If one step is altered, the whole myogenesis is compromised and leads to skeletal muscle regeneration defects.

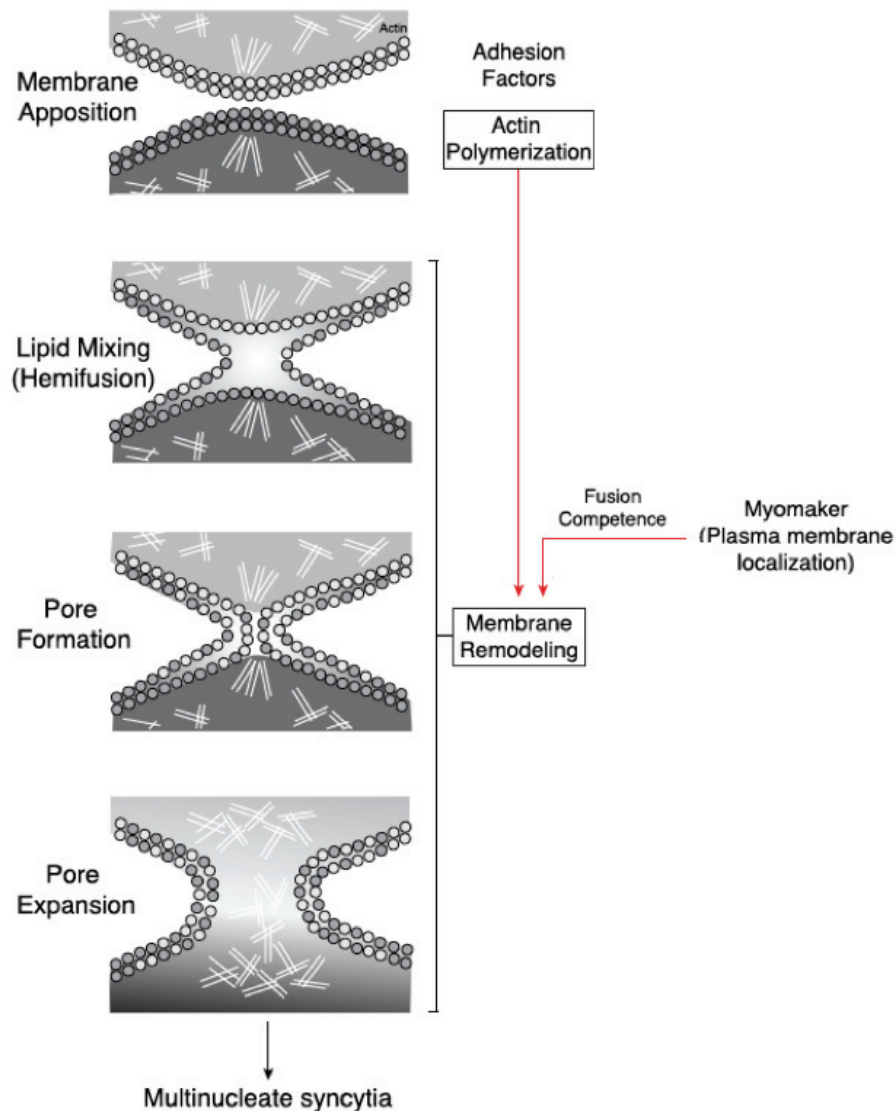


**Figure 12. Mechanism of myoblast fusion**

The fusion of differentiated myoblasts is essential to form new myofiber syncytia or to fuse with existing myofibers. Fusion requires specific apposition of the cells. Reorganization of the cytoskeleton is essential. Moreover, specific proteins are crucial for myoblast fusion, such as myomaker, a transmembrane protein (Sampath et al., 2018).

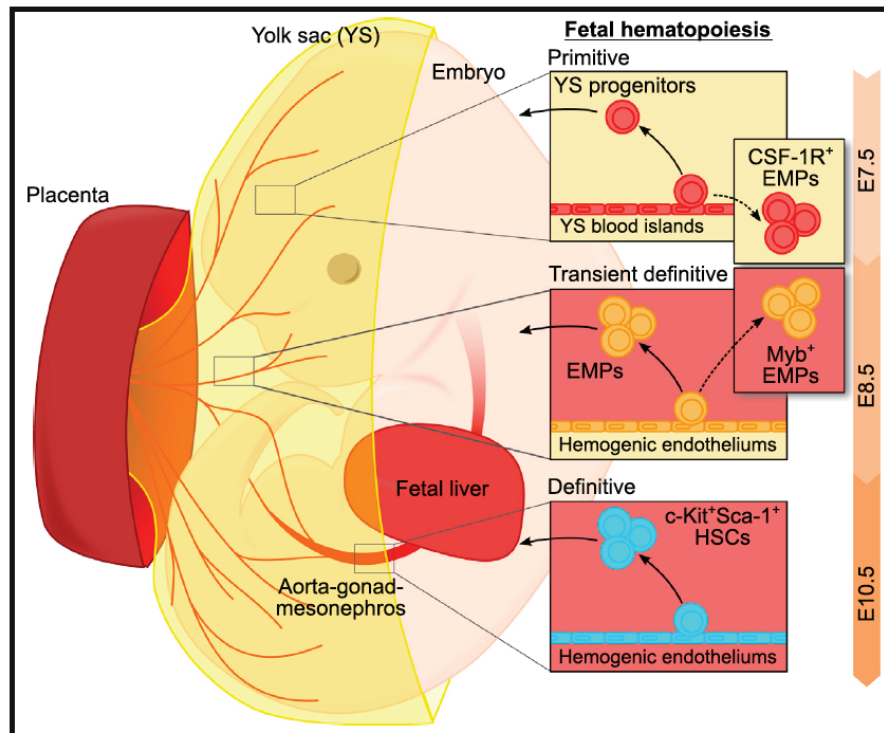
### III. Macrophages

#### III.1 Origin of macrophages

Macrophages were first discovered in the late 19<sup>th</sup> by Elie Metchnikoff. They were originally identified by their phagocytic activity of bacteria. In the next century, scientists tried to identify more precisely this cell population. In the 1960's, "mononuclear phagocytes" were defined as "cells which are able to adhere to glass and phagocyte". At this time, two main populations of mononuclear phagocytes were known, circulating monocytes in blood and tissue macrophages in organs. But the origin of these cells was still unknown. First evidence was given in 1968. Ralph van Furth and Zanvil Cohn used macrophage labelling by thymidine-<sup>3</sup>H, irradiated mice and cell culture experiments to show that the major population of circulating monocytes derives from the bone marrow. They identified a progenitor cell in the bone marrow called the promonocyte (van Furth and Cohn, 1968). Furthermore, they showed that the major population of tissue macrophages observed during inflammation derives from blood circulating monocytes (van Furth and Cohn, 1968). Thus, bone marrow progenitors give rise to blood circulating monocytes that in turn give rise to tissue macrophages. In 1972, a classification of the "mononuclear phagocyte system" was proposed by van Furth and colleagues. This classification was more restrictive than the previous one and included only monocyte/macrophages and their progenitors (van Furth et al., 1972). Moreover, a new hierarchy of the mononuclear phagocyte system was proposed (van Furth et al., 1972). Although well accepted for decades, the model of mononuclear phagocyte system was recently questioned because it appeared to be an oversimplification of the origin of all macrophages. Indeed, the persistence of macrophages in many tissues at steady state in the adulthood questioned their origin. To understand the origin of macrophages, it is necessary to look at the embryonic development. Actually, macrophages were described during early vertebrate embryo development, even before the blood circulating system appears. These macrophages are generated during the primitive phase of hematopoiesis in the yolk sac (Rieger and Schroeder, 2012; Orkin and Zon, 2008). At E10.5 in the mouse, definitive hematopoiesis takes place in the aorta-gonad-mesonephros of the embryo, before to move to fetal liver. Finally, hematopoiesis moves definitively to the bone marrow between E14.5 and E18.5 where it still occurs in the adulthood ([Figure 13A, 13B](#)) (Rieger and Schroeder, 2012;

Orkin and Zon, 2008). In adulthood, two main types of macrophages are found, resident macrophages which are persistent macrophages residing in tissues at steady state and macrophages derived from circulating blood monocytes. These two macrophage subsets do not have the same origin and do not have exactly the same functions.

A



B

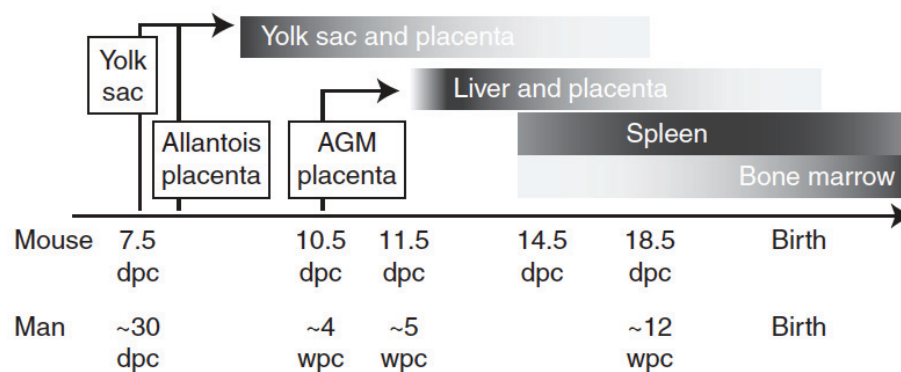


**Figure 13. Origins of monocytes/macrophages**

**(A)** Macrophages are observed at the beginning of the life span in the embryo, where they derived first from the yolk sac that corresponds to the primitive hematopoiesis. Then the definitive hematopoiesis moves to the aorta-gonad-mesonephros and to the fetal liver. EMP: erythro-myeloid precursor; CSF: Colony Stimulating Factor (Ginhoux and Guilliams, 2016). **(B)** Macrophages sequentially derive from the yolk sac to fetal liver in embryo and to bone marrow in adulthood. The graph shows the time line of hematopoiesis location in human and mice. d/wpc: days/weeks post conception (Rieger and Schroeder, 2012).

### III.2 Bone marrow-derived macrophages

As proposed in 1972 with the mononuclear phagocyte system, macrophages derive from circulating monocytes, themselves deriving from the hematopoietic stem cells in the bone marrow (Fogg et al., 2006). Blood circulating monocytes present two main subpopulations in mouse: Ly6C<sup>pos</sup>CX3CR1<sup>low</sup> and Ly6C<sup>neg</sup>CX3CR1<sup>high</sup>. Ly6C (Lymphocyte antigen 6 complex) is expressed by monocytes giving rise to pro-inflammatory macrophages whereas CX3CR1 (CX3C receptor 1) is higher expressed by anti-inflammatory macrophage-derived monocytes. These two subpopulations of monocytes derive from the myeloid precursor in the bone marrow (Figure 14). Ly6C<sup>pos</sup> monocytes are able to give rise to Ly6C<sup>neg</sup> monocytes (Geissmann et al., 2010). These two subtypes of monocytes present different functions. Ly6C<sup>pos</sup> monocytes infiltrate injured tissues, in all the tissues studied so far. For example, Ly6C<sup>pos</sup> monocytes are the only one infiltrating the muscle after injury, and they give rise to pro-inflammatory macrophages (Varga et al., 2016; Varga et al., 2013; Arnold et al., 2007). Within the tissue, Ly6C<sup>pos</sup> macrophages change their phenotype to become anti-inflammatory macrophages, that lose the expression of Ly6C. Tracing studies showed that Ly6C<sup>neg</sup> are never recruited in regenerating muscle (Arnold et al., 2007) as in other tissues (Chazaud, 2016). This was confirmed in a genetic model lacking circulating Ly6C<sup>neg</sup> monocytes (*nur77* KO) that shows a completely normal inflammatory response and muscle regeneration (Varga et al., 2013). Ly6C<sup>neg</sup> monocytes do not infiltrate damaged tissues. They have a patrolling function in vessels. In resting tissue, they control endothelium integrity by crawling thanks to specific adhesion molecules which are CX3CR1 and integrins (Auffray et al., 2007). They are involved in endothelium repair, together with neutrophils by replacing damaged endothelial cells (Carlin et al., 2013). Thus, the two subpopulations of circulating monocytes have specific roles, Ly6C<sup>neg</sup> patrolling in vessels and Ly6C<sup>pos</sup> monocytes infiltrating the damaged tissues.

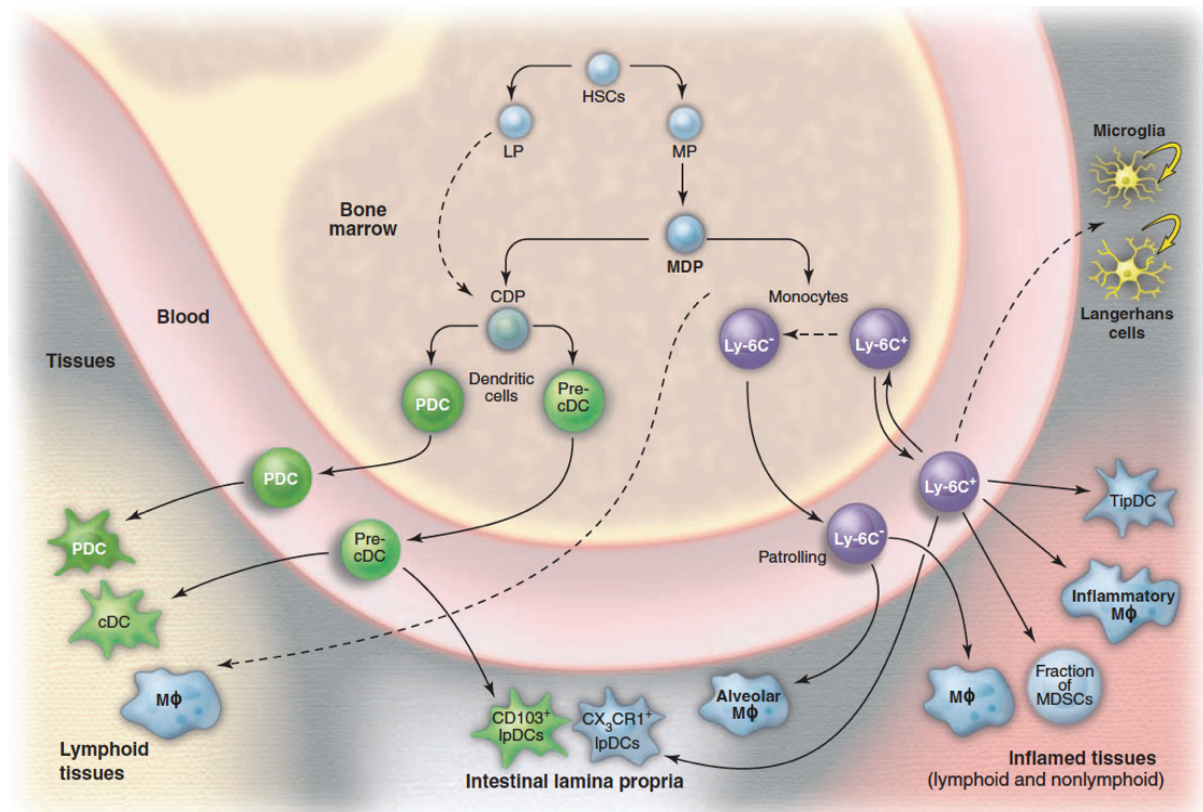


**Figure 14. Different subtypes of circulating monocytes**

Two monocyte subpopulations derive from monocyte progenitors, issued from hematopoietic stem cells: Ly6C<sup>pos</sup> monocytes and Ly6C<sup>neg</sup> monocytes. Ly6C<sup>pos</sup> monocytes are involved in the inflammation process whereas Ly6C<sup>neg</sup> monocytes present a patrolling behavior in vessels. Abbreviations: HSC: Hematopoietic Stem Cell; MP: Myeloid Progenitor; LP: Lymphoid Precursor; MDP: Monocyte/Macrophage and Dendritic Cell Precursor; TipDC: TNF and iNOS-producing Dendritic Cell; Mφ: Macrophage; MDSCs: Myeloid-Derived Suppressor Cell; CDP: Common Dendritic cell Precursor; cDC: classical Dendritic Cell; PDC: Plasmacytoid Dendritic Cell. Dashed arrow: susceptible to give rise (Geissmann et al., 2010).

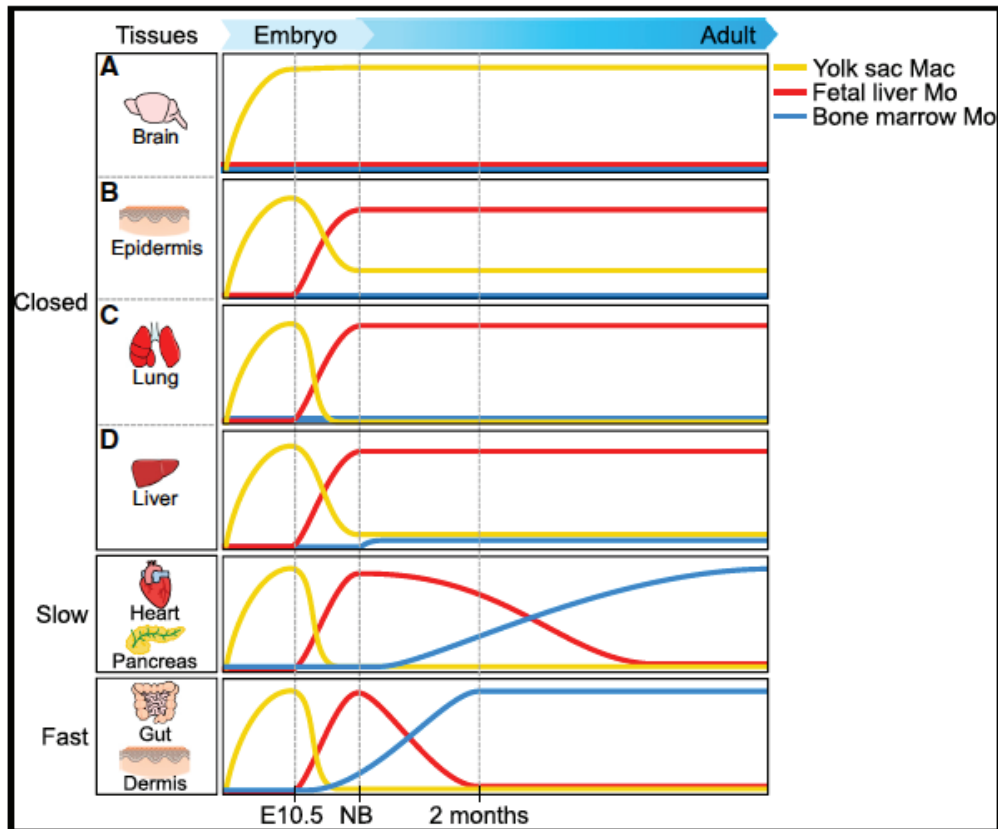
### III.3 Resident macrophages

Resident macrophages are present within the tissues at steady state. They are found in almost all tissues, for instance in liver as Kupffer cells, in lung as alveolar macrophages, in bone as osteoclasts, in central nervous system as microglia, in skin as Langerhans cells (Figure 15A). Resident macrophages are associated with specific functions of their tissue (Figure 15B) (Davies et al., 2013). After birth, resident macrophages are coming from embryogenesis as described above and depending on the tissue, they come from yolk sac or fetal liver. Then, after birth, they are more or less replaced by circulating monocyte-derived cells. The extent of embryo-derived tissue macrophages by monocyte-derived macrophages depends on the tissue. Two paradigmatic situations are the central nervous system, where 100% of microglia

comes from embryo-derived macrophages and the gut, where these cells are quickly replaced by circulating monocytes that constitute 100% of residing macrophages (Ginhoux and Guillemins, 2016). Considering the M1-M2 paradigm, resident macrophages are classified as “M2-like” macrophages (Davies et al., 2013). While specific roles of resident macrophages are reported in several tissues, only few information is available on these cells in skeletal muscle. In resting muscle, macrophages reside mainly in the epimysium (the conjunctive tissue surrounding the whole muscle) and perimysium (conjunctive tissue surrounding each muscle fascicle) (Brigitte et al., 2010; Saclier et al., 2013b). They exhibit a F4/80<sup>pos</sup>Ly6C<sup>neg</sup>CX3CR1<sup>low</sup> phenotype. Concerning their function, it was suggested that resident macrophages have a role after muscle injury by attracting neutrophils and monocytes. When resident macrophages are depleted (using chimeric CD11b-DTR mice transplanted with WT bone-marrow), muscle inflammation after injury is strongly reduced (Brigitte et al., 2010). Highly severe phenotypes are observed in C-C chemokine receptor 2 (CCR2) KO mice (receptor required for monocyte infiltration), where an almost total inhibition of macrophage entry into the regenerating tissue is observed, associated with strongly impaired muscle regeneration (Shireman et al., 2007; Ochoa et al., 2007). This indicates that skeletal muscle regeneration after a toxic injury is mainly driven by monocyte-derived macrophages that bear CCR2 (on the contrary to resident macrophages).



A



B

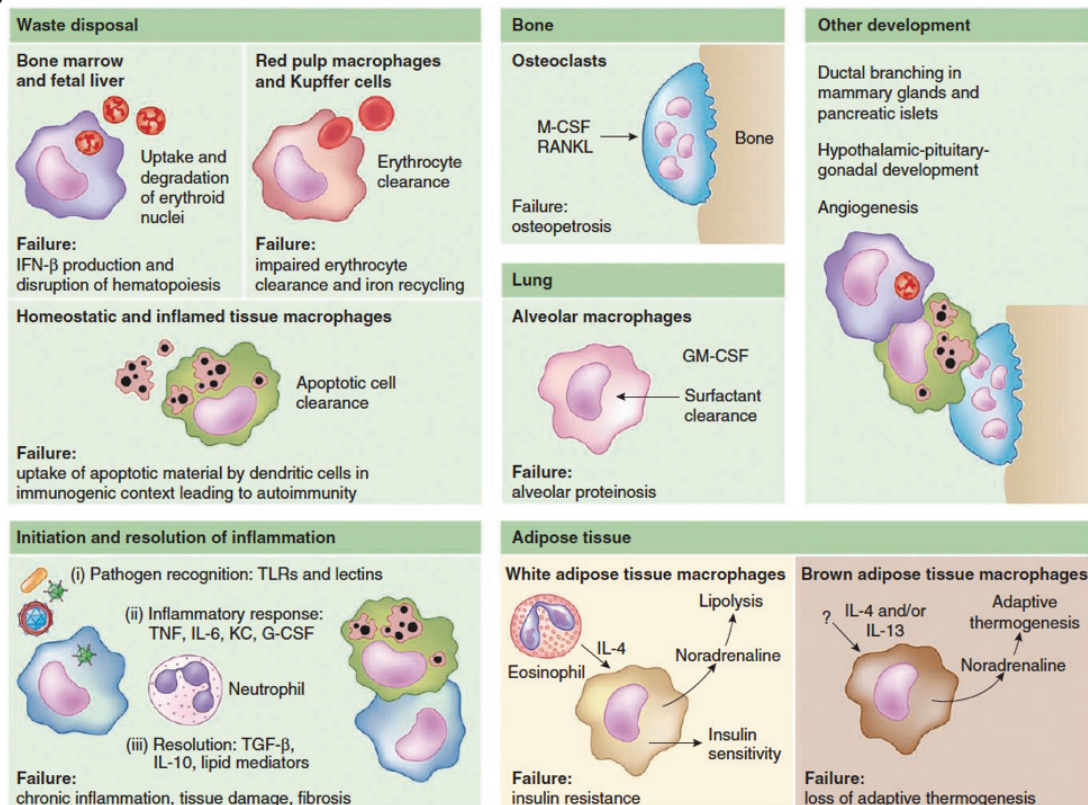


**Figure 15. Origin and function of resident macrophages.**

(A) Resident macrophages come from different origins depending on the tissue (Ginhoux and Guillemin, 2016). (B) In each tissue, macrophages display specific functions (Davies et al., 2013)

## IV. Glucocorticoids and Macrophages

This section IV will be part of a review entitled “Glucocorticoids shape macrophage phenotype for tissue repair” submitted in *Frontiers in Immunology*.

Inflammation is a complex process which is conserved among species. Inflammation is required to face abnormal situations (injury, infection, cancer, ...) and to allow the maintenance of the tissue/organ integrity. Excessive inflammation is associated with numerous diseases; thus, it is often considered as a negative event that has to be fought. Anti-inflammatory drugs were therefore developed to switch inflammation off. However, the inflammatory process may be beneficial for the organism, such as the inflammatory response that occurs after a sterile tissue injury. Inflammation can be divided in several sequences. The first step is the mounting of the inflammatory response itself. This stage is characterized by the presence of pro-inflammatory cytokines and the infiltration of immune cells into the injured area. The second step is the resolution of inflammation which is characterized by the switch of the phenotype of immune cells toward an anti-inflammatory status and the decrease of the secretion of pro-inflammatory cytokines. The last stage consists of the regeneration process to rebuild the tissue. Innate immune cells are major actors of the inflammatory response where macrophages take an important role. Macrophages are highly sensitive to a large number of stimuli coming from their environment. They can adapt their phenotype and their function on demand and are involved in all steps of post-damage tissue repair.

Because of their central role in inflammation, macrophages appear to be an ideal target of anti-inflammatory drugs. Glucocorticoids (GCs) are the most used anti-inflammatory drugs in the world. GCs have been used for decades to treat a variety of diseases such as rheumatoid arthritis, skin irritation or pulmonary diseases. Since the first GC therapies during the 50's, various synthetic GCs have been developed to optimize their action and new molecules are still under development to modulate therapeutic effects *versus* the adverse effects of these drugs (see below). Surprisingly, given the importance of macrophages in the inflammatory response, the direct effects of GCs on macrophages are less-well documented. The present review aims at recapitulating the knowledge on macrophage functions during the



post-injury inflammatory response, on GC signaling pathways operative in macrophages and finally on the specific action of GCs on macrophages.

#### IV.1 Macrophages and tissue repair – example of skeletal muscle regeneration

##### *IV.1.1 Similar macrophage subtypes are found in various tissues during repair*

Macrophages are cells of innate immunity. In the late XIX<sup>th</sup> century, Metchnikoff originally described and named these cells as phagocytes, meaning *big “macro” eaters “phage”*. During the next century, scientists have found that macrophages are not only phagocytic cells. Indeed, they secrete a large number of factors and play diverse roles in various systems. Different macrophage subtypes were described, first in *in vitro* experiments. Based on the main cytokinic activation of lymphocytes, they were called “classically activated” macrophages when stimulated by the Th1 cytokine IFN $\gamma$  and “alternatively activated” macrophages when stimulated by the Th2 cytokine IL-4 (Gordon, 2003). These two activation states were also called M1 (or pro-inflammatory macrophages) and M2 (or anti-inflammatory macrophages), respectively. It was demonstrated that beside the paradigmatic M1/M2 status, macrophages adopt a very large panel of phenotypes depending on the inflammatory cues they encounter, even *in vitro* (Mosser and Edwards, 2008; Sica and Montovani, 2012; Martinez et al., 2009; Xue et al., 2014). *In vivo*, the situation is more complex and the terms M1 and M2, although widely used, are not appropriated to describe specific and dynamic inflammatory status (Murray et al., 2014; Varga et al., 2016). Thanks to the Ly6C (Lymphocyte antigen 6 complex is a membrane protein expressed by monocytes and macrophages) and CX3CR1 (chemokine (C-X3-C motif) receptor 1 is a transmembrane protein involved in the adhesion and migration of leukocytes) antigens, one can observe pro-inflammatory and anti-inflammatory macrophages in the context of post-injury inflammatory response. During sterile inflammation, it was described in various tissues that Ly6C<sup>pos</sup>CX3CR1<sup>neg</sup> cells (that are also CCR2<sup>pos</sup> F4/80<sup>low</sup> CD64<sup>pos</sup>) infiltrate the injured tissue, and exhibit a pro-inflammatory status. Then, these cells switch their phenotype toward a Ly6C<sup>neg</sup>CX3CR1<sup>pos</sup> (CCR2<sup>low/neg</sup> F4/80<sup>high</sup> CD64<sup>pos</sup>) status, corresponding to the anti-inflammatory status (Juban and Chazaud, 2017; Saclier et al., 2013b). This sequence of events from the infiltration of pro-inflammatory macrophages to the phenotype switch toward an anti-inflammatory phenotype appears to be universal since it was described after injury in heart (Nahrendorf et al., 2010), central nervous

system (Michelucci et al., 2009; Fumagalli et al., 2011), liver (Pellicoro et al., 2014), kidney (Ricardo et al., 2008; Rogers et al., 2014) and skeletal muscle (Arnold et al., 2007; Saclier et al., 2013, Mounier et al., 2013).

#### *IV.1.2 Skeletal muscle regeneration*

Skeletal muscle tissue is composed of myofibers, which are multinucleated cells. Skeletal muscle has a high regenerative capacity. Indeed, after injury, muscle regenerates *ad integrum* thanks to the satellite cells, which are the muscle stem cells (MuSCs). Therefore, skeletal muscle regeneration represents an ideal paradigm to study the biological events sustaining tissue repair/regeneration, notably thanks to highly reproducible experimental models in mouse (Hardy et al., 2016). Satellite cells are localized under the basal lamina surrounding each myofiber, in a quiescent state. After an injury, damaged myofibers undergo necrosis that triggers alteration of the satellite cell niche, which leads to their activation (Yin et al., 2013). Activated MuSCs proliferate, in order to produce a critical pool of cells necessary to repair muscle. After the expansion phase, MuSCs differentiate into myocytes, that eventually fuse to form new myofibers. While myogenesis takes place, other biological processes occur during muscle regeneration. Angiogenesis is required for efficient muscle regeneration. Endothelial cells and MuSCs communicate through secreted factors to mutually induce myogenesis and angiogenesis (Latroche et al., 2015). Also, extracellular matrix remodeling is observed during muscle regeneration, controlled by the number and activation of Fibro-Adipogenic Precursors (FAPs) (Joe et al., 2010; Lemos et al., 2015). Thus, muscle regeneration is a complex process where multiple cell types interact in a coordinate way to reconstruct the tissue (Figure 16).

Each step of muscle regeneration is linked to the inflammatory response, which is mainly mediated by macrophages. They were shown to modulate myogenesis driven by MuSCs, as well as angiogenesis and matrix remodeling that occur concomitantly. Although macrophages represent more than 75% of leukocytes in regenerating muscle, other immune cells are present in lower numbers (Mounier et al., 2013) and their role was analyzed during the early steps of muscle regeneration. Neutrophils are transiently present during the very first days after injury and their role in muscle regeneration has not been deciphered yet. Eosinophils are involved through the secretion of IL-4 that acts on FAPs (Heredia et al., 2013)

and TReg lymphocytes through the secretion of amphiregulin that also acts on FAP biology (Burzyn et al., 2013).

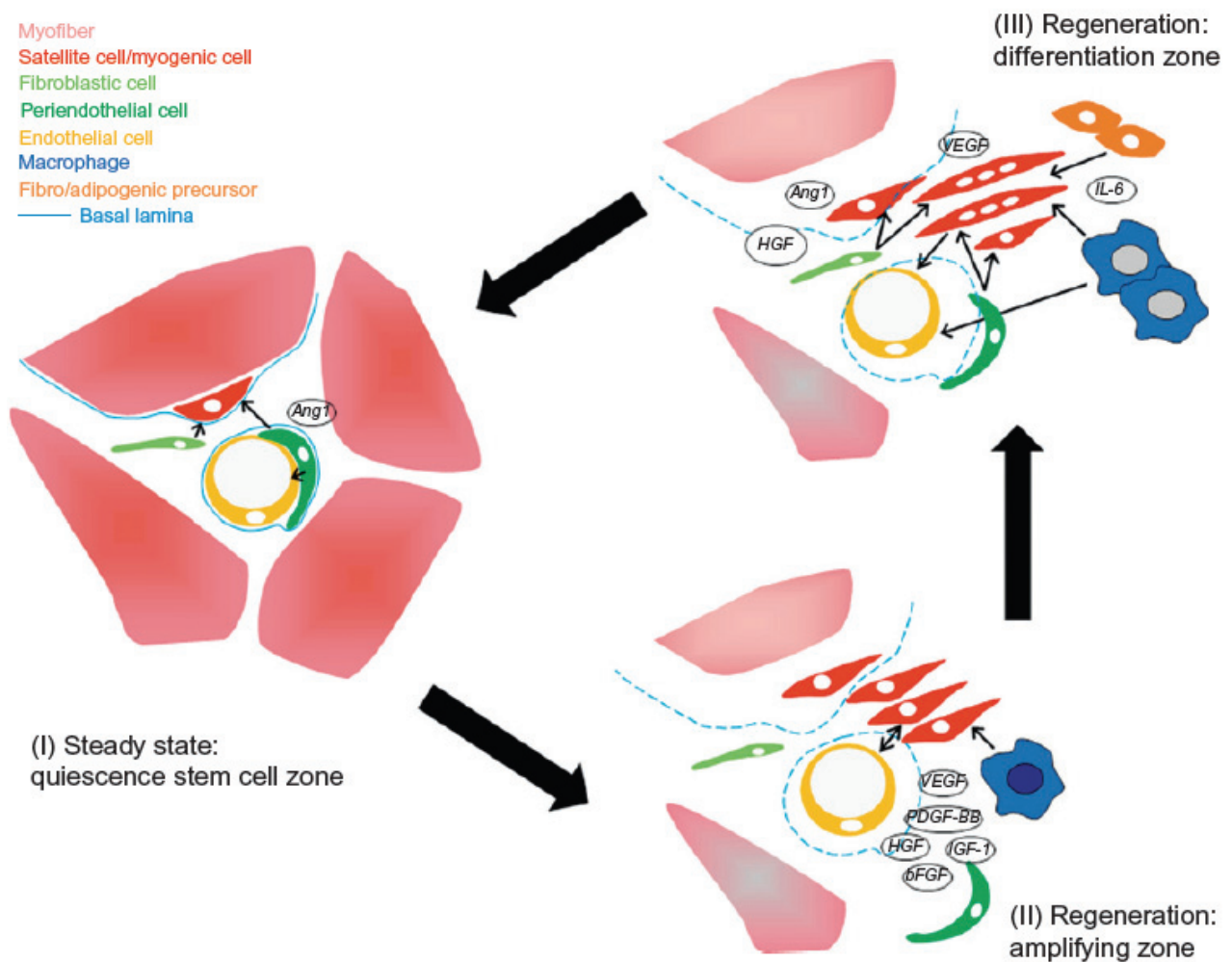


**Figure 16. Interactions between cell types involved in myogenesis**

Macrophages, satellite cells, fibroblasts, endothelial cells and others interact with each other to sustain myogenesis in order to reconstruct the tissue (Mounier et al., 2011).

#### IV.1.3 The inflammatory phase

Tissue injury triggers the release of chemoattractant molecules in the bloodstream, that recruit circulating leukocytes. The main axis of monocyte entry into the injured muscle is the chemokine CCL2 (MCP1)/CCR2 axis. In models depleted for either CCR2 or CCL2, muscle regeneration is severely altered (Shireman et al., 2007; Sun et al., 2009). Circulating Ly6C<sup>pos</sup> monocytes, that bear CCR2, are the only monocytes to be recruited (Arnold et al., 2007; Varga et al., 2013; Varga et al., 2016). Indeed, CCR2<sup>neg</sup>Ly6C<sup>neg</sup> monocytes are not recruited in injured

muscle and their absence (in the *nur77*KO mouse) does not alter muscle regeneration (Varga et al., 2013; Arnold et al. 2007). Once in the tissue, monocytes become pro-inflammatory macrophages. Their functions are very specific. First, macrophages allow the clearance of debris by phagocytosis. They also induce survival and growth of MuSCs by establishing direct cell-cell contacts (Chazaud et al., 2003, Sonnet et al., 2006). Moreover, pro-inflammatory macrophages secrete factors such as IL-6, IL-1 $\beta$  or VEGF that stimulate MuSCs proliferation (Arnold et al., 2007; Saclier et al., 2013). Finally, pro-inflammatory macrophages induce FAP and fibroblast apoptosis to avoid excess of matrix deposition (Lemos et al., 2015; Juban et al., 2018).

#### *IV.1.4 Macrophage phagocytosis and the resolution of inflammation*

At the time of resolution of inflammation, pro-inflammatory macrophages shift their inflammatory status toward an anti-inflammatory phenotype. Signaling pathways involved in this switch start to be documented. For now, 3 main intracellular pathways have been described: AMPK, p38/MKP1, CREB-C/EBP $\beta$  (see below). While the activation of these pathways is required, the upstream cues are not known. However, it was shown that phagocytosis is essential for the acquisition of an anti-inflammatory phenotype. The expression of pro-inflammatory markers is reduced and the expression of anti-inflammatory markers is increased in macrophages that have ingested apoptotic cells (Fadok et al., 1998; Freire-de-Lima et al., 2006; Weigert et al., 2006). Anti-inflammatory macrophages exert various roles on several cell types in regenerating skeletal muscle. They induce both differentiation and fusion of MuSCs as well as growth of the newly regenerated myofibers (Arnold et al. 2007; Saclier et al., 2013; Mounier et al., 2013). Anti-inflammatory macrophages promote extracellular matrix remodeling by inducing fibroblast survival and collagen production through the secretion of TGF- $\beta$  (Juban et al., 2018). They also induce angiogenesis: *in vitro* experiments showed that anti-inflammatory macrophages induce endothelial cell sprouting and differentiation, triggering to vessel formation concomitantly to myogenesis, through the delivery of specific effectors, such as Oncostatin M (Latroche et al., 2017). Accordingly, CCR2 KO mice exhibit defect of vascularization in regenerating muscle (Ochoa et al, 2007). Thus, anti-inflammatory macrophages act on various cell types by promoting simultaneously growth of newly formed muscle cells, remodeling of extracellular matrix and revascularization in order to obtain a complete functional recovery of the muscle tissue.

#### *IV.1.5 Time and space orchestration of the inflammatory response*

The inflammatory response needs to be tightly orchestrated to be efficient. Modulation of the macrophage inflammatory status is highly time-dependent. It was shown that the time, more than the subtype of macrophages (Ly6C<sup>pos</sup> or Ly6C<sup>neg</sup>) is the driving force controlling the expression of inflammatory genes in macrophages during skeletal muscle regeneration (Varga et al., 2016). Resolution of inflammation is a key step in that process, that must occur timely. Indeed, when the pro-inflammatory phase is blunted by the inhibition of the expression of the pro-inflammatory cytokine IFN $\gamma$  (Cheng et al., 2008) or reduced by the early administration of anti-inflammatory cytokine IL-10 (Perdiguero et al., 2011), muscle regeneration is altered, with the formation of smaller myofibers. Moreover, blunting the inflammatory phase by administering anti-inflammatory drug or icing to prevent entry of monocytes into the injured area is detrimental for muscle regeneration (review in Chazaud, 2016). Therefore, the regulation of the macrophage phenotype switch is crucial for an efficient muscle regeneration. AMP-activated protein kinase (a key metabolic regulator in the cell) is an important regulator of the macrophage phenotype switch. AMPK activation is required for the acquisition of an anti-inflammatory status that is necessary for muscle regeneration (Mounier et al., 2013). Similarly, p38/MKP1 pathway (MAP kinase pathway) modulates the phenotype switch of macrophages. Inhibition of MKP1 induces an early activation of AKT, leading to a too early acquisition of the anti-inflammatory status, triggering impairment of muscle regeneration (Perdiguero et al., 2011). Finally, blocking the CREB-C/EBP $\beta$  cascade prevents the acquisition of the anti-inflammatory phenotype of macrophages, that also impairs muscle regeneration (Ruffell et al., 2009). Given the importance of the process of the resolution of inflammation for tissue homeostasis, it is likely that other pathways are also involved in the switch of the inflammatory status of macrophages.

### IV.2 Glucocorticoids

#### *IV.2.1 Origins of GCs*

The hypothalamic-pituitary-adrenal axis is very important in the body as it is involved in the control of a variety of biological processes: stress, feeding, circadian rhythms, growth and reproduction... GCs are under the control of this axis (Figure 17). Under the control of the nervous system and circulating hormones, hypothalamus secretes the corticotropin release

hormone (CRH). CRH acts on the pituitary gland to induce the secretion of the Adreno Cortico Trophic Hormone (ACTH) into the bloodstream. ACTH binds to cells within the adrenal cortex to induce secretion of diverse hormones and especially GCs. GCs are synthesized from the cholesterol molecule in a specific area of the adrenal gland cortex called zona fasciculata. The natural GCs observed in Human is cortisol or hydro-cortisone (corticosterone in the mouse). Investigations on GCs started in the 30's by Philip Hanch, Edward Kendall and Tadeus Reichstein, who showed the large potential of these molecules as anti-inflammatory drugs and received the Nobel prize for their work in 1950. From that point, GC therapies spread all around the world and are still used today to counter inflammation.

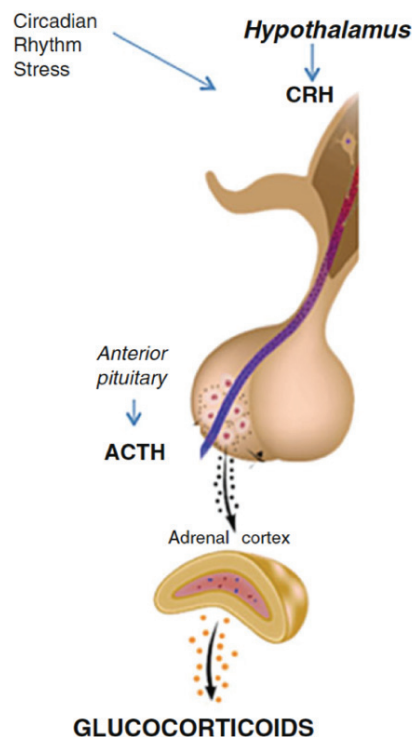


**Figure 17. The Hypothalamic-Pituitary-Adrenal axis**

Glucocorticoids are synthesized by the adrenal gland under the control of the Hypothalamus and the Pituitary gland (adapted from Spadaro et al., 2017).

#### *IV.2.2 The GC Receptor*

GCs act on target cells through the Glucocorticoid Receptor (GR). The human GR, cloned in 1985, was found to be a member of the nuclear receptor superfamily (Hollenberg et al., 1985). The gene encoding GR is located on the locus 5q31.3 in the human genome and

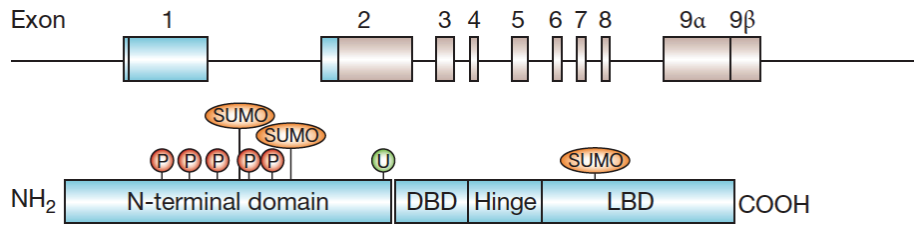
comprises 9 exons. GR expression gives rise to the expression of 2 isoforms: GR $\alpha$  (777 amino acids) and GR $\beta$  (742 amino acids). The 2 isoforms are similar between amino acid 1 and amino acid 727 (Hollenberg et al., 1985). GR $\alpha$  is the active isoform that directly binds GCs and that regulates target gene expression. GR $\beta$  isoform acts as a dominant negative regulator of the  $\alpha$  isoform (Leung et al., 1997; Caratti et al., 2015). The 3D structure of GR shows several domains: the N-terminal domain, the DNA Binding Domain (DBD), the Hinge, the Ligand Binding Domain (LBD) and the C-terminal domain (Figure 18A) (Kumar and Thompson, 1999; McMaster and Ray, 2008; Nicolaides et al., 2010; Baschant et al., 2011). GR regulates gene expression by 2 main mechanisms (Figure 18B, 18C):

- Transactivation: after GC binding in the cytoplasm, GR homodimerizes, translocates to the nucleus and directly binds specific palindromic regions on DNA called Glucocorticoid Response Elements (GRE). GRE are present in the promoter of target genes (such as *giz* and *dusp1*) and binding of GR dimer induces the transcription of these genes (positive GRE). Transactivation can also be induced by a tethering mechanism. GR associates with other transcription factors that positively drive gene expression. Transcription can also be induced by monomeric GR that binds DNA to a half-site motif.
- Transrepression: transrepression is the mechanism that represses transcription of genes by GR. It can be induced by several mechanisms. GR can directly act as a monomer in association with other transcription factors such as NF $\kappa$ B (Ray and Prefontaine, 1994) or AP-1 (Miner and Yamamoto, 1992) to repress gene expression by a tethering mechanism. GR monomer sequesters transcription factors to prevent their binding to promoters and so to prevent transcription. Moreover, GR dimer can directly bind GRE to repress gene expression (negative GRE).

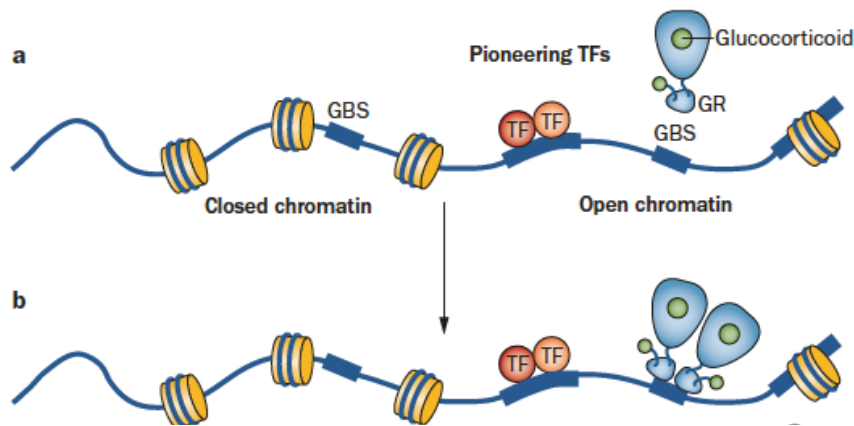
Thus, GR is a transcription factor that regulates gene expression through several pathways (reviewed in Scheschowitsch et al., 2017; Xavier et al., 2016; Caratti et al., 2015; McMaster and Ray, 2008) and in a tissue dependent manner (Whirledge and DeFranco, 2018). Non-genomic effects of GCs have been described in several tissues and that were very recently reviewed in (Panettieri et al., 2019).



A



B



C

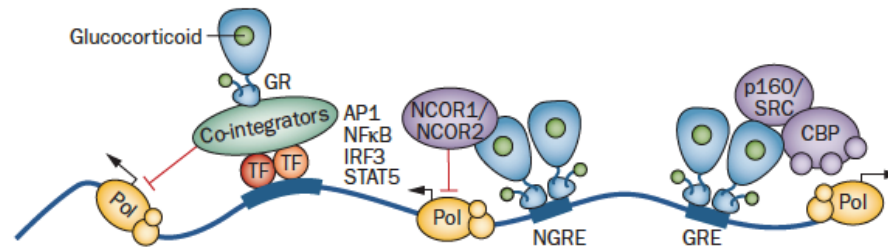


**Figure 18. The glucocorticoid receptor (GR)**

**(A)** The gene encoded the GR comprises 9 exons. The structure of the GR protein is divided in several domains: N-terminal domain, the DNA Binding Domain (DBD), the Hinge, the Ligand Binding Domain (LBD) and the C-terminal domain (McMaster and Ray, 2008). **(B)** After binding with Glucocorticoid (GC), GR translocate to the nucleus to induce (transactivation) or repress (transrepression) gene expression by several mechanisms: as a monomer (a) or as a dimer (b) (Baschant et al., 2012). **(C)** GR monomer bound to GC is able to bind other pro-inflammatory transcription factors to inhibit their activity (left). GR dimer can bind Negative Glucocorticoid Response Element (NGRE) in association with corepressors (*e.g.* NCOR1/2) (middle) or GRE (in association with cofactors) to induce gene expression (right) (Baschant et al., 2012). TF: transcription factor; GBS: glucocorticoid receptor binding site.



#### *IV.2.3. Side effects*

During the 60's, studies showed that GC exposure induces side effects. In 1970, David and colleagues reviewed 20 years of GC utilization (David et al., 1970). They discussed side effects that were observed in almost all tissues of the body. In 1970, it was already known that long exposure to GCs was responsible for several metabolic disturbances such as diabetes (due to increased gluconeogenesis, decreased insulin sensitivity and decreased glucose consumption), skin thinning, muscle atrophy and bone mass reduction (both due to induction of catabolism and/or reduction of anabolism). Moreover, free fatty acids are increased in the bloodstream and abnormal lipid deposition are observed (well-known in Cushing's syndrome), mainly localized in the face, trunk and neck. Although literature concerning GC side effects is very abundant, the molecular mechanisms involved in their regulation are not completely elucidated.

Because GR monomer can be associated with the pro-inflammatory molecule NF $\kappa$ B to downregulate the expression of pro-inflammatory cytokines, anti-inflammatory effects of GCs were historically associated with the monomer form of GR and the adverse effects were assigned to the GR dimer. However, thanks to the use of a model in which GR dimerization is impaired (GR<sup>dim</sup>), several laboratories showed that GR dimerization is also required for the anti-inflammatory properties of GCs in several contexts, such as rheumatoid arthritis (Baschant et al., 2011), septic shock (Kleiman et al., 2012) or inflammatory bowel disease (Ballegeer et al., 2018). Therefore, both anti-inflammatory and side effects of GCs may be driven by the two GR isoforms depending on the cell type, the tissue and the pathology considered.

#### *IV.2.4. GC resistance*

Beside side effects, another problem which could be encountered when treating patients with GC is GC resistance. GC resistance is characterized by a loss of efficiency of GC therapies. As mentioned above, two main isoforms of GR exist, GR $\alpha$  and GR $\beta$ . GR $\alpha$  is known to be the functional isoform of GR with transcriptional activity. GR $\beta$  isoform is reported to be associated with GC resistance. Indeed, GR $\beta$  can bind to GR $\alpha$  into the nucleus to modulate GR $\alpha$  transcriptional activity, as a negative dominant (Caratti et al., 2015; Lewis-Tuffin and Cidlowski, 2006; Leung et al., 1997). Moreover, it was reported that cytokines such as TNF $\alpha$

or IFN $\gamma$  can affect GC responsiveness by modulating the expression of GR $\beta$  isoform in smooth muscle cells (Tliba et al., 2005). Other cytokines such as IL-17 or IL-23 can also modulate GR $\beta$  expression and GC sensitivity (Vazquez-Tello et al., 2012). However, the exact mechanism of GC resistance is not completely understood.

#### IV.3. Glucocorticoids, macrophages and tissue repair

First investigations on the action of GCs on macrophages during tissue repair started a few decades ago. One of the side-effects of GCs is loss of bone mass (osteopenia). Bone resorption is more efficient when macrophages are in direct contact with the bone. Macrophages treated with cortisol are more adherent to bone, which enhances the bone resorption process (Bar-Shavit et al., 1984) and release more calcium useable for bone resorption (Teitelbaum et al., 1981). More recently, a mouse model based on the cre/lox system was designed to specifically deplete GR in the myeloid lineage where the *cre* recombinase gene is located at the Lysozyme M locus. Thus, LysM<sup>cre</sup>;GR<sup>fl/fl</sup> mice show GR deletion in macrophages and neutrophils. In a mouse model of contact hypersensitivity, anti-inflammatory effects of GCs are shown to be operated through GR in macrophages and involve the repression of the cytokines IL1- $\beta$ , MCP1, MIP2 and IP10. In addition, GR<sup>dim</sup> mice are not sensitive to GCs, indicating that GR dimerization is required in this context (Tuckermann et al., 2007). In a model of myocardial infarction, LysM<sup>cre</sup>;GR<sup>fl/fl</sup> mice dye earlier after infarction than non-depleted animals, probably due to the persistence of Ly6C<sup>pos</sup> macrophages into the infarcted area that leads to a deregulation of the resolution of inflammation and a defect in wound healing. Consequences are alteration of angiogenesis, abnormal production of TGF $\beta$ , decreased production of IL-1 $\alpha$  and finally deregulation of myofibroblast differentiation leading to scar formation (Galuppo et al., 2017). Moreover, in a mouse model of inflammatory bowel disease, macrophages from LysM<sup>cre</sup>;GR<sup>fl/fl</sup> animals show a defect in the acquisition of anti-inflammatory status. After 10 days, IL-1 $\beta$  and IL-6 expression is not repressed and expression of anti-inflammatory genes (CD163, CD206 and IL-10) is not induced, triggering a defect in tissue repair (Meers et al., 2018). On the contrary, no effect of the GC beclomethasone is observed in the migratory capacity of macrophages towards the wounding area in an amputation model in zebrafish (Chatzopoulou et al., 2016). Thus, in most tissue injuries, GC-GR axis appears to be a central pathway in macrophages to regulate the resolution of inflammation and to proceed to tissue repair after injury.

#### IV.4. GCs and macrophages – cellular aspects

##### *IV.4.1. GCs regulate survival, migration and proliferation of macrophages*

Maintenance of living immune cells in appropriate number is essential to modulate the inflammatory response, where GCs appear to play several roles. GCs exert anti-apoptotic effects on macrophages: macrophages treated with dexamethasone are more resistant to lipopolysaccharide (LPS)-induced apoptosis (Luedke and Cerami, 1990). Similar results were obtained with other apoptotic stimuli (staurosporine, actinomycinD or cyclohexine) where GC effects are mediated through ERK1/2 phosphorylation in an adenosine receptor A3-dependent-manner (Barczyk et al., 2010; Ehrchen et al., 2007). Moreover, macrophages treated with dexamethasone are smaller with less cytoplasmic extensions (Norton et Munck, 1980), that could be related to altered migratory capacity. The capacity of macrophages to move towards the injured area also shapes the inflammatory response. Macrophages treated with hydrocortisone (cortisol) show a decreased capacity to migrate *in vitro* (Balow and Rosenthal, 1973; Prokic and Vilic, 1983). *In vivo*, a similar effect was observed in a model of lung injury induced by bleomycin. GCs inhibited macrophage infiltration in the lung (Khalil et al., 1993). GCs also decrease proliferation of macrophages *in vitro* (Miller et Melnykovych, 1982; Shezen et al., 1985), adding another anti-inflammatory property. Thus, GCs decrease motility and proliferation of macrophages and promote their survival in order to switch off inflammation and to sustain late phase of healing. In the following decades, studies have focused on the understanding of the molecular aspects of GC signaling pathways.

##### *IV.4.2. GCs and phagocytosis*

During inflammation, damaged tissue produces cell debris and release cytoplasmic proteins in the environment due to cell lysis. Before tissue repair can start, debris must be clean up. Cleansing is mainly operated by macrophages through phagocytosis. Since phagocytosis is a major function of macrophages and is an essential trigger of their inflammatory switch (see above), the action of anti-inflammatory treatments on this process is of importance. GCs were detected very early to have an impact on phagocytic activity of macrophages (Spain et al., 1950). Later on, studies showed in *in vitro* models using a variety of particles (zymosan, heat-kill yeast, apoptotic neutrophils, latex beads, bacteria) that

dexamethasone induces the phagocytic activity of monocytes/macrophages (Lombardi et al., 1978; Shezen et al., 1985; Liu et al., 1999; van der Goes et al., 2000; Giles et al., 2001; Heasman et al., 2003; Heasman et al., 2004; Gratchev et al., 2005; Ehrchen et al., 2007; Michlewska et al., 2009). Some of these studies have also shown, using a GR antagonist (RU486), that GC-induced phagocytosis is GR dependent (Liu et al., 1999; van der Goes et al., 2000). The increased macrophage phagocytic activity by dexamethasone is annexin 1-FRP1 dependent. Annexin 1 is a member of annexin protein superfamily. They are proteins which bind acidic phospholipids in presence of  $\text{Ca}^{2+}$  (Gerke and al., 2005) and annexin A1 is described to be pro-resolving molecules during inflammation (Perretti and D'Acquisto, 2009). Indeed, when FRP (annexin receptor) is antagonized by the Boc1 compound or in annexin 1-null macrophages, dexamethasone loses its effect on phagocytosis (Maderna et al., 2005).

On closer examination of the phagocytic process, it was shown that dexamethasone induces the up-regulation of several membrane receptors such as the scavenger receptor CD163, required to detect and bind haptoglobin, a product from hemoglobin degradation, (Schaer et al., 2002; Giles et al., 2001; Heasman et al., 2004; Gratchev et al., 2005). The mannose receptor CD206, required for the detection of specific oligosaccharides on the bacterial wall, is also upregulated in macrophages treated by GCs (Shepherd et al., 1985). Moreover, dexamethasone induces the upregulation of the membrane receptor Mer tyrosine kinase (MerTK) (Zahuczky et al., 2011), in a C/EBP $\beta$  dependent-manner (Garabuczi et al., 2015). When *mertk* is silenced, dexamethasone-induced phagocytosis is reduced (Zahuczky et al., 2011). MerTK belongs to the Tyro3, Axl, Mer (TAM) family of tyrosine kinase receptor. It binds to phosphatidyl serine exposed on the surface of apoptotic cells (Zahuczky et al., 2011; Garabuczi et al., 2015; Roszer, 2017). MerTK is also responsible for the phagocytosis of protein S-opsonized apoptotic neutrophils by dexamethasone-treated macrophages (McColl et al., 2009). Finally, dexamethasone induces the C/EBP $\beta$ -dependent expression of the nuclear receptors (liver X receptor [LXR], retinoid X receptor  $\alpha$  [RXR $\alpha$ ] and peroxisome proliferator-activated receptor  $\delta$  [PPAR $\delta$ ]), which are required for prolonged phagocytosis of macrophages (Garabuczi et al., 2015). Thus, GCs act on several steps of phagocytosis and their effects on this process are regulated by various signaling pathways.

#### IV.5. GCs and gene expression in macrophages – molecular aspects

##### *IV.5.1. Anti-inflammatory effects on macrophages*

Although the first effects of GCs on macrophages were reported in 1950, the literature about their specific effects on this cell type is not abundant. In 1950, Dougherty and colleagues showed in a model of local inflammation in mice that cortisone treatment induces a reduction of macrophage number in the inflamed area (Dougherty and Schneebeil, 1950). In another model of skin inflammation induced by injection of turpentine, Spain and colleagues showed that cortisone inhibits the formation of granulation in the inflamed area (granulations corresponding to macrophages according to the authors) and a decrease of carbon particle phagocytosis when administrated early during the inflammatory response (Spain et al., 1950). However, the experiments done by Gell and Hinde on intraperitoneal macrophages exposed to bacteria showed that cortisone does not alter either the number of macrophages or their phagocytic capacity (Gell and Hinde, 1953). In another aspect, it is well-known that macrophages exert their various functions by secretion of factors. Because of their high versatility, they may secrete pro-inflammatory, anti-inflammatory or other factors necessary at each step of the inflammatory response. For instance, dexamethasone induces in macrophages a decrease of the secretion of the pro-inflammatory cytokines  $\text{TNF}\alpha$  (Luedke and Cerami, 1990; Franchimont et al., 1999), IL-1, IL-6 that are induced by  $\text{IFN}\gamma$  exposure (Heasman et al., 2004; Khalil et al., 1993). Accordingly, monocytes treated with dexamethasone express high level of the anti-inflammatory markers CD206 (Shepherd et al., 1985), CD163 (Schaer et al., 2002; Giles et al., 2001; Heasman et al., 2004; Gratchev et al., 2005; Ehrchen et al., 2007; Van de Garde et al., 2014) and other markers such as CD16, CD169, CXCR4 or IL-10 (Franco et al., 2019; Heideveld et al., 2018; Ehrchen et al., 2007). GC anti-inflammatory effects are partly mediated by Mitogen-activated protein kinase phosphatase-1 (MKP-1) in macrophages, such as the inhibition of IL-6 expression (Pemmari et al., 2018). GCs may act on either GR monomer or GR dimer functions, depending on the gene considered. For example, in dermatitis, GR dimerization is required to shut down the expression of the pro-inflammatory cytokines IL-1 $\beta$  or MCP-1 whereas  $\text{TNF}\alpha$  downregulation induced by GCs does not require GR dimerization (Tuckermann et al., 2007). Another mechanism could be also involved in gene regulation by GCs in macrophages. Indeed, GCs modulate chromatin

compaction where GR binds to DNA, allowing chromatin reorganization for transcription of the target genes, although chromatin decompaction is observed even if no increase of transcriptional activity was observed (Jubb et al., 2017). Furthermore, macrophages exposed to GC secrete molecules having direct functions on the extracellular matrix and participate to matrix remodeling during the inflammatory response. The production of elastase, collagenase and plasminogen activator (which secretion is elevated in pro-inflammatory macrophages and which are required to degrade extracellular matrix) is reduced in macrophages treated with dexamethasone (Werb, 1978a; Werb et al., 1978b). On the contrary, macrophages exhibiting an alternatively activated status (*i.e.*, IL-4 driven) secrete more fibronectin when treated with dexamethasone (Gratchev et al., 2001; Armbrust et al., 2004; Gratchev et al., 2005).

#### *IV.5.2. The GC effector Gilz in macrophages*

GC-mediated anti-inflammatory effects are known to be partly mediated through the regulation of the expression of specific proteins that in turn modulate the activity or expression of pro- or anti-inflammatory effectors. A very well-studied protein is the Glucocorticoid-Induced Leucin Zipper (Gilz). Originally found expressed in lymphoid tissues (thymocyte, spleen, lymph nodes) treated by dexamethasone (D'Adamio et al., 1997), Gilz is a major regulator of GC effects in a variety of cells. Gilz was also found to be expressed by macrophages in liver and lung treated by dexamethasone. In the THP-1 macrophage cell line, dexamethasone induces the expression of Gilz only after 30 min of treatment. Gilz binds p65 on NF $\kappa$ B to shut down its activity. Gilz also inhibits the expression of the Toll like receptor 2 (TLR2), which is used for the recognition of bacterial components (Berrebi et al., 2003). Furthermore, GC-induced Gilz expression is annexin A1-dependent. In annexin A1 KO macrophages, dexamethasone-induced Gilz expression is reduced, preventing the downregulation of the pro-inflammatory cytokines IL-1, IL-6, and TNF $\alpha$  (Yang et al., 2009; Hoppstädter and Kiemer, 2015). This regulation is not dependent of the annexin receptor FRP (Yang et al., 2009), thus, the exact mechanism by which annexin regulates *gilz* expression remains to be elucidated.

#### *IV.5.3. New high throughput analyses*

Recent technological advances allow the analysis of the modulation of gene expression in macrophages by GCs/GR. First experiments were CHIP-seq analyses. It was shown that

depending on the activation state of macrophages, GCs do not regulate the same set of genes. Indeed, more than 10,000 genomic GR binding sites are induced by dexamethasone in resting macrophages with more than 5,400 known GR target genes. In LPS-stimulated macrophages, dexamethasone induces more than 13,000 binding sites with more than 6,400 GR target genes (Uhlenhaut et al., 2013). Furthermore, GCs do not regulate similar set of genes in macrophages activated with LPS or IFN $\gamma$  indicating that GC target genes are related to the inflammatory stimulus (Van de Garde et al., 2014). To go further, GR was shown to bind DNA with less efficiency without LPS stimulation indicating that pro-inflammatory stimulation potentializes GC effects (Oh et al., 2017). LPS stimulation induces NF $\kappa$ B signaling, which is inhibited by GCs whether given before or after LPS stimulation (Oh et al., 2017). These results confirm other studies showing that the regulation of genes by GCs is cell type- and context-dependent. Indeed, 9 primary human cell types (B cells, CD4 $^{+}$  T cells, monocytes, neutrophils, endothelial cells, osteoblasts, myoblasts, fibroblasts and preadipocytes) were shown to have a specific response to GCs. Genes with same baseline of expression are differentially regulated by GCs (Franco et al., 2019). Moreover, other studies showed that GR regulates gene expression in combination with several other partners. Transcriptomic and CHIP-seq approaches identified an increase of the expression of the KLF transcription factors (which are known to inhibit NF $\kappa$ B) in LPS-stimulated macrophages treated with dexamethasone (Chinenov et al., 2014). Other genes encoding for transcription factors such as *ATF3*, *EGR1*, *CEBP $\beta$*  or *IRF* are also up regulated by dexamethasone in macrophages (Chinenov et al., 2014). Interestingly, some promoters present a PPAR $\gamma$  binding site near the GR binding site, indicating that these 2 transcription factors could be associated to regulate the expression of a set of genes (Chinenov et al., 2014). Another genome wide analysis in macrophages showed the role of the factor NFEL (negative elongation factor) in GR-mediated decreased expression of pro-inflammatory factors such as NF $\kappa$ B (Sacta et al., 2018). Furthermore, another GR partner, the Glutamate receptor-interacting protein (GRIP) 1 (a protein that mediates trafficking of proteins and membrane organizations of proteins), is required for the acquisition of the anti-inflammatory phenotype of macrophages (Coppo et al., 2016). GRIP1 and GR colocalize at the promoter of FKBP5, PER1, DUSP1, KLF9 genes. GRIP1 can be phosphorylated by Cyclin-Dependent Kinase 9 (CDK9) in a GR dependent-manner. Phosphorylated GRIP1, in association with GR, binds GRE to induce expression of the above anti-inflammatory genes. On the contrary, phosphorylated GRIP1 is never observed in co-repressing sites such as of *IL1 $\alpha$*  or *IL1 $\beta$*  sites, indicating that



phosphorylated GRIP1 only acts on positive transcription of anti-inflammatory genes (Rollins et al., 2017). The authors suggested that the phosphorylated state of GRIP1 could modulate GR transcriptional activity (Rollins et al., 2017). As GC-GR signaling in macrophages is more and more investigated, studies reveal a high degree of complexity, mainly due to the involvement of different coregulators according to the context and inflammatory status of macrophages. Moreover, even inducing an anti-inflammatory phenotype in both species, GCs modulate the expression of a different set of genes in mouse and human (Jubb et al., 2016), adding another level of complexity.

## **CONCLUSION**

GCs induce numerous processes in macrophages that lead to the acquisition of the anti-inflammatory status. GCs regulate the secretion of a plethora of molecules by macrophages such as cytokines and enzymes. GCs enhance macrophage phagocytosis by regulating the expression of genes involved in the recognition of molecules harbored by cells or bacteria that have to be eliminated. GCs act in association with several partners including other transcription factors (C/EBP $\beta$ , PPARs, NF $\kappa$ B) or proteins that modulate its activity (GRIP1). Finally, GCs regulate the expression of a huge number of genes that are essential to relay their anti-inflammatory properties such as *gilz* and *annexin a1*. Because GCs differently regulate the expression of thousands of genes according to the context of inflammation, further investigations are necessary to decipher, for each situation, how GCs operate to regulate gene expression in macrophages, and therefore their functions.



## V. AMP-activated protein kinase

### III.1. Structure and functions

Originally, it was suggested in 1973 by 2 groups that a sensitive-enzyme to the ATP level could regulate the activity of the rat liver Acetyl-CoA Carboxylase (ACC) (Carlson and Kim, 1973) and the 3-hydroxy-3-methylglutaryl (HMG)-CoA reductase (Beg et al., 1973) by phosphorylation. But, the evidence of the existence of AMP-activated protein kinase (AMPK) was done in 1986 by Hardie and colleagues. They showed *in vitro* that a protein with a kinase activity regulates ACC after stimulation with  $\text{Ca}^{2+}$  (Hardie et al., 1986). In the same time, it was also shown that the same kinase regulates HMG-CoA reductase activity (Carling et al., 1987). Finally, it was assumed that AMPK is an important metabolic regulator of the cell metabolism (Hardie et al., 1986).

AMPK is the main metabolic sensor of the cell (Hardie, 2008). This protein is very conserved between species as it is also present in yeast (Townley and Shapiro, 2007). AMPK is composed of 3 subunits: the catalytic  $\alpha$ -subunit, the scaffolding  $\beta$ -subunit and the regulatory  $\gamma$ -subunit (Figure 19). These subunits present several isoforms  $\alpha 1$ ,  $\alpha 2$ ,  $\beta 1$ ,  $\beta 2$ ,  $\gamma 1$ ,  $\gamma 2$  and  $\gamma 3$ , each encoded by a different gene (Figure 19). The various combinations of these isoforms enable the formation of 12 heterotrimers (Mounier et al., 2015). AMPK is mainly activated by phosphorylation at the Threonine (Thr) 172 residue present in the  $\alpha$  subunit. The  $\beta$  subunit can be glycosylated at several sites and binding to carbohydrates inhibits AMPK activity (McBride et al., 2009). AMPK is sensitive to the energy status of the cell and especially to the rate of AMP in the cytoplasm, which can bind directly to the  $\gamma$  subunit. The AMPK subunit composition is different between cell types and confers various levels of sensitivity to AMP. The  $\gamma$  subunits have different sensitivity to AMP,  $\gamma 2$  is higher sensitive to AMP than  $\gamma 1$ , which is higher sensitive than  $\gamma 3$  (Cheung et al., 2000). Combined effects of phosphorylation and allosteric regulation by  $\gamma$ -subunit bound to AMP is responsible of a change of AMPK activity by 1000-fold (Suter et al., 2006). Thus, the presence of several combinations of AMPK allows the detection of small energy changes in the cell.

AMPK is activated by high AMP/ATP ratio when ATP store decreases due to high consumption. AMP induces conformational changes when it binds to  $\gamma$ -subunit, uncovering Thr172 for phosphorylation by upstream kinases (Cheung et al., 2000) and protecting it from

dephosphorylation (Davies *et al.*, 1995). Some kinases are known to phosphorylate AMPK such as Liver Kinase B1 (LKB1) (Hong *et al.*, 2003; Hawley *et al.*, 2003; Woods *et al.*, 2003; Shaw *et al.*, 2004) and the  $\text{Ca}^{2+}$ /Calmodulin-dependent protein kinase kinase (CaMKK)  $\beta$  (Hawley *et al.*, 2005; Woods *et al.*, 2005). Other kinases such as Transforming growth factor- $\beta$ -activated kinase 1 (TAK1) may activate AMPK (Neumann, 2018). When activated, AMPK phosphorylates target proteins to induce energy production (*i.e.*, catabolic pathways) and to inhibit anabolic pathways in order to maintain stable the energy status.

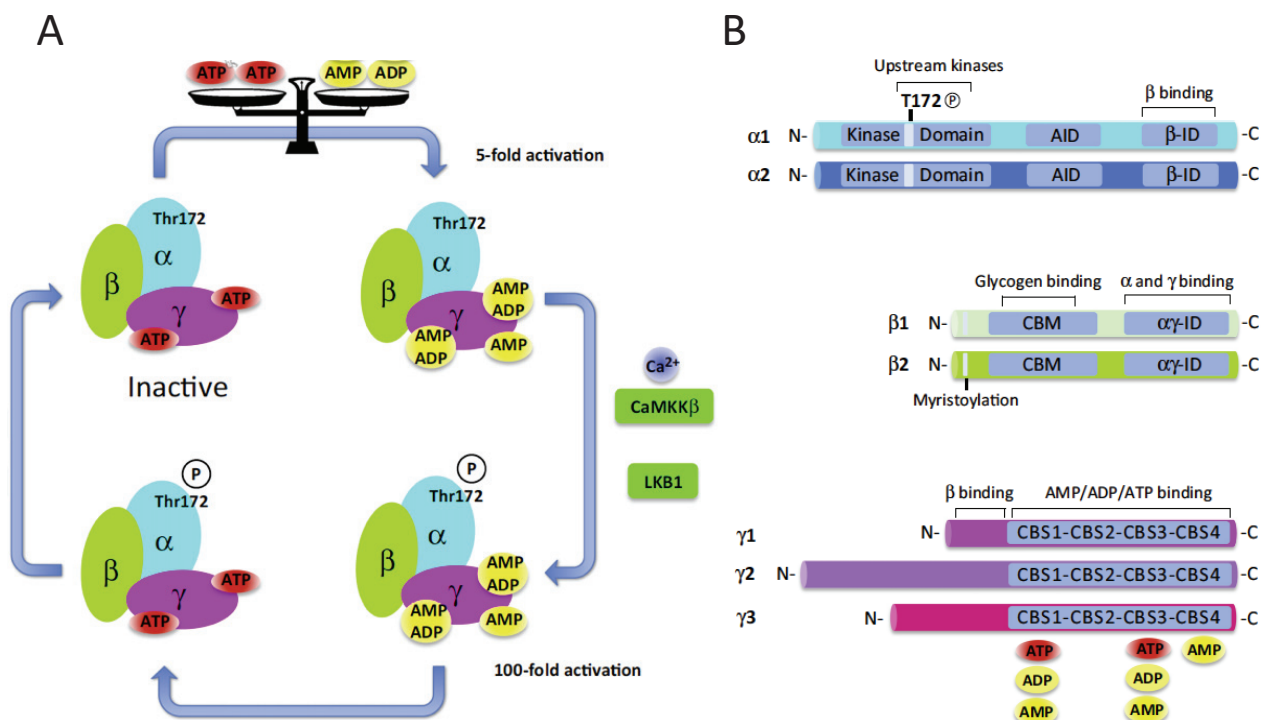


**Figure 19. AMPK**

**(A)** AMP activated protein kinase is composed of 3 subunits. AMPK is activated by phosphorylation and low energy ratio (binding of AMP). AMPK is activated by upstream kinases, such as CaMKK  $\beta$  and LKB1. **(B)** Each subunit is encoded by separate genes (Mounier *et al.*, 2015).

### III.2. AMPK and cellular metabolism

Metabolism can be defined as the entire biochemical modifications suffered by the components of an organism/organ/cell in order to maintain homeostasis by degradation (catabolism) and biosynthesis (anabolism) mechanism. The key cellular functions of metabolism are energy production, macromolecule synthesis such as lipids, elimination of

degraded macromolecules/organelles, substrate production and extraction, and renewal of cell components. AMPK acts on several pathways to modulate macromolecule synthesis. The first identified targets of AMPK are part of the lipid metabolism: ACC and HMG-CoA reductase (Carlson and Kim, 1973; Beg et al., 1973). ACC acts in lipid biosynthesis pathway, whereas HMG-CoA has a role in cholesterol biosynthesis. When ACC or HMG-CoA are phosphorylated by AMPK, they become inactive, inhibiting the formation of lipids and cholesterol, respectively, in order to spare energy (lipid synthesis or cholesterol synthesis are processes requiring energy). Moreover, AMPK directly acts on substrate extraction. For example, AMPK regulates glucose uptake. During skeletal muscle contraction, increase of glucose uptake induced by exercise is associated to AMPK (Jensen and Richter, 2012). AMPK induces the translocation of the glucose transporter GLUT-4 to the plasma membrane leading to an increase of glucose uptake (Jensen et al., 2014). Furthermore, regarding energy production, mitochondria play an important role, biogenesis and degradation of this organelle being well-regulated. AMPK is crucial for the regulation of biogenesis/degradation of mitochondria. In skeletal muscle, it was shown that AMPK can induce mitochondrial biogenesis through activation of the peroxisome proliferator-activated receptor  $\gamma$  coactivator 1 (PGC1)  $\alpha$  (Iwabu et al., 2010). On the other hand, AMPK can also regulate mitophagy. After endurance exercise, oxidative stress induces mitochondria damages. Damaged mitochondria have to be eliminated by the cell. For this purpose, AMPK regulates lysosome formation and fusion with mitochondria through Ulk1 phosphorylation (Laker et al., 2017). Whether AMPK or Ulk1 are absent, mitophagy does not occur properly (Laker et al., 2017). In a model of fasting, AMPK is shown to regulate metabolism of hepatocytes (Ratman et al., 2016). When hepatocytes are submitted to long-term fasting, phosphorylated AMPK is recruited on the promoter of genes that are co-controlled by the glucocorticoid receptor and PPAR $\alpha$ . These genes are implicated in the regulation of lipid metabolism in response to fasting (Ratman et al., 2016). Thus, AMPK is the main energy sensor of the cell that regulates metabolism and energy (Figure 20).

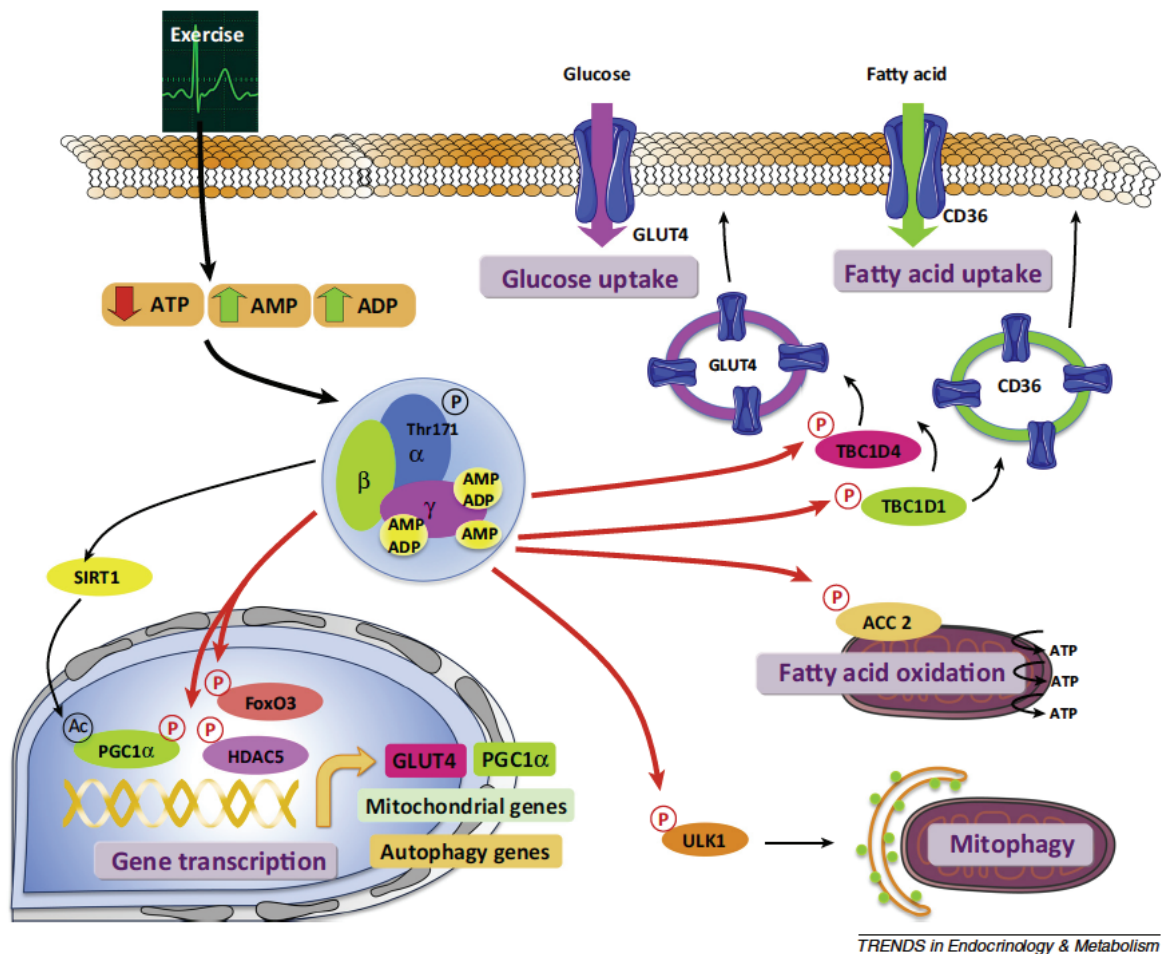


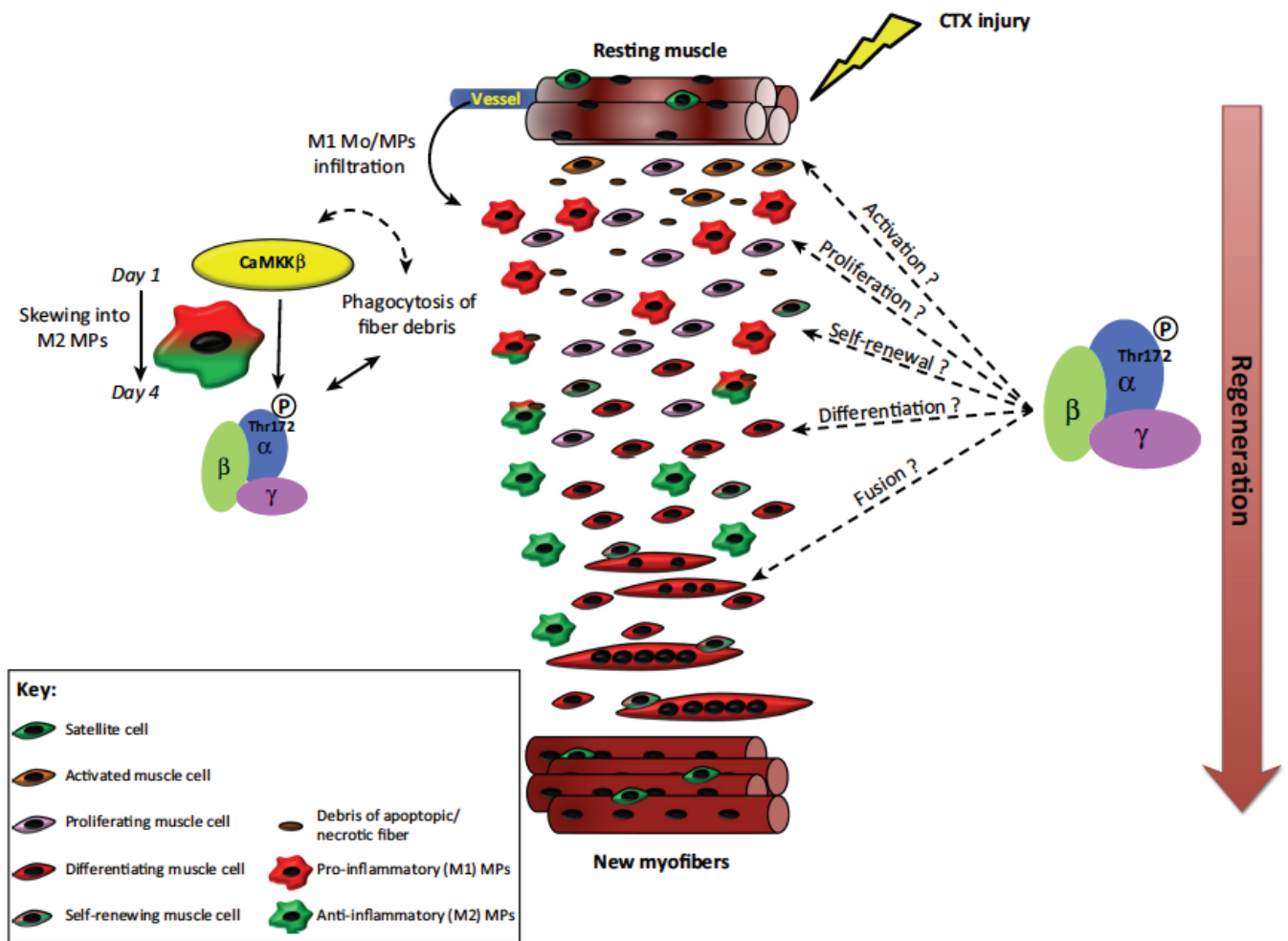
**Figure 20. AMPK regulates cellular metabolism**

AMPK is the main energy sensor of the cell. Once activated, AMPK is able to regulate various pathways. AMPK increases glucose uptake by increasing GLUT4 translocation. AMPK induces mitochondria biogenesis. AMPK acts also on lipid metabolism by inhibiting lipid synthesis and activation of fatty acid oxidation in order to produce more ATP and maintain cell homeostasis (Mounier et al., 2015).

### III.3. AMPK, macrophages and skeletal muscle

During skeletal muscle regeneration, several cell types are involved such as endothelial cells, fibroblasts or immune cells. Among immune cells, macrophages were shown to have a crucial role. Deletion of monocytes using the CD11b-DTR mouse impaired skeletal muscle regeneration (Arnold et al., 2007). Furthermore, after an injury, monocyte-derived pro-inflammatory macrophages phagocytose cell debris and induce myoblast proliferation and fibroblast apoptosis. Then, they switch their phenotype toward an anti-inflammatory phenotype to induce differentiation and fusion of myoblasts, ECM remodeling and

angiogenesis (Juban et al., 2018; Latroche et al., 2017; Mounier et al., 2013, Arnold et al., 2007). Because each macrophage inflammatory status is associated with specific functions, it appears that the phenotype switch of macrophages is an essential event during regeneration. Some pathways were shown to regulate the phenotype switch such as C/EBP $\beta$  (Ruffell et al., 2009) and p38/MKP1 (Perdiguero et al., 2011). Moreover, AMPK is shown to regulate macrophage function. AMPK activation by berberine (an antibacterial compound also used to treat metabolic disorders) downregulates the expression of pro-inflammatory cytokines in macrophages exposed to LPS (Jeong et al., 2009). Activation of AMPK by several compounds (AICAR and metformin) also increases the phagocytic activity of macrophages (Bae et al., 2011). On the other hand, when AMPK phosphorylation is prevented by deletion of the  $\beta$ 1 subunit in bone marrow, macrophages keep their pro-inflammatory profile in high fat diet mouse model (Galic et al., 2011). Furthermore, the lab showed few years ago that AMPK is required for the phenotype switch of macrophages after skeletal muscle injury (Mounier et al., 2013). Macrophages express only the  $\alpha$ 1 isoform of AMPK (Mounier et al., 2013; Sag et al., 2008). In AMPK $\alpha$ 1<sup>-/-</sup> global KO and in a tissue specific KO LysM<sup>+/cre</sup>;AMPK $\alpha$ 1<sup>fl/fl</sup> mice (AMPK $\alpha$ 1 is only deleted in myeloid lineage including macrophages), the phenotype switch from pro to anti-inflammatory status does not occur properly during skeletal muscle regeneration (Mounier et al., 2013). Moreover, AMPK $\alpha$ 1<sup>-/-</sup> macrophages do not sustain myogenesis *in vitro* (Mounier et al., 2013). This result is correlated by a delayed skeletal muscle regeneration observed *in vivo* (Mounier et al., 2013). Similar results are obtained in a mouse model of ischemia in which AMPK is demonstrated to drive polarization of macrophages toward an anti-inflammatory phenotype (Vaibhav et al., 2018). All these results give evidence for the central role of AMPK $\alpha$ 1 in the functional acquisition of the anti-inflammatory profile of macrophages (Figure 21).



*TRENDS in Endocrinology & Metabolism*

### Figure 21. AMPK activation induces phenotype switch of macrophages

AMPK activation is required for phenotype switch of macrophages during skeletal muscle regeneration. If AMPK is missing, macrophages do not acquire the anti-inflammatory status and skeletal muscle regeneration is altered (Mounier et al., 2015).



## **SPECIFIC AIMS OF THE STUDY**





Macrophages are crucial for skeletal muscle regeneration. Depletion of monocytes at the time of injury impairs regeneration and their depletion in the second phase of regeneration alters muscle repair. During this process, macrophages sequentially present two main phenotypes: a pro-inflammatory phenotype and then an anti-inflammatory phenotype. These two status are associated with specific functions. Pro-inflammatory macrophages are associated with myoblast proliferation whereas anti-inflammatory macrophages are associated with myoblast differentiation and fusion, angiogenesis and ECM remodeling. Thus, the phenotype switch of macrophage, that drives the resolution of inflammation, is crucial for skeletal muscle regeneration.

On one hand, the lab showed that AMPK activation (by AICAR compound) induced the anti-inflammatory status of macrophages, since AICAR-treated macrophages stimulated the fusion of myoblasts (Figure 22A). On the other hand, the lab showed that the GC dexamethasone (DEX) treatment induced the anti-inflammatory status of macrophages as the fusion of myoblasts was stimulated when cultured in conditioned medium from DEX-treated macrophages (Figure 22B).

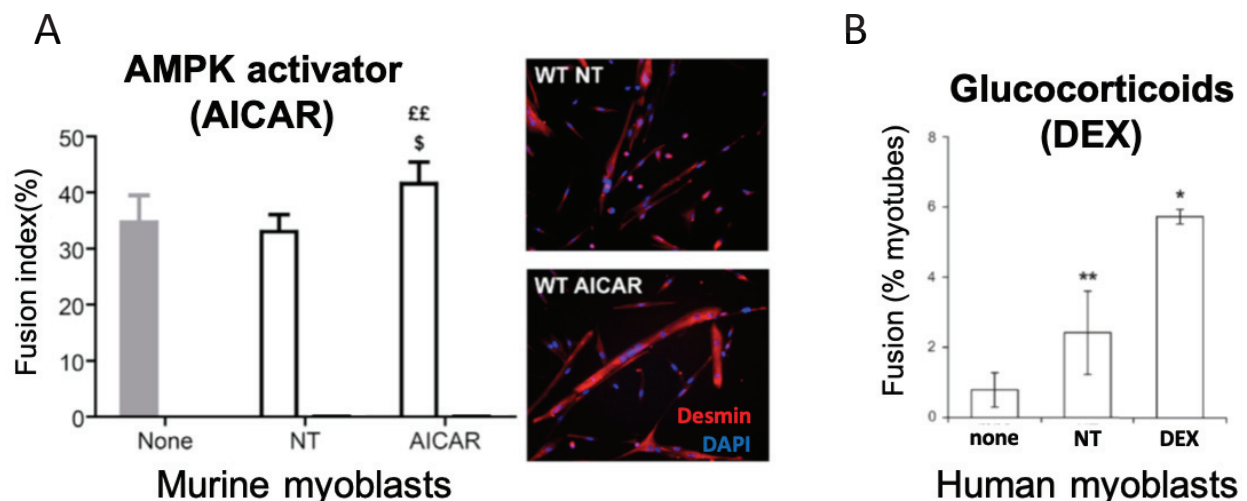


**Figure 22. AMPK activation and Glucocorticoids induce same anti-inflammatory effects on macrophages. (A)** Macrophages treated with AMPK activator induce the fusion of myoblasts (Mounier et al., 2013). **(B)** Macrophages treated with the glucocorticoid DEX induce the fusion of myoblasts (Arnold et al., 2007). *None*: control medium without macrophages. *NT*: conditioned medium from untreated macrophages. *AICAR/DEX*: conditioned medium from macrophages treated by AICAR/DEX.

Given that AMPK activation and GCs induce both the switch of macrophages toward an anti-inflammatory profile, we investigated the question whether these 2 pathways could be interconnected in macrophages to resolve inflammation. More specifically, we asked whether AMPK is required for driving the anti-inflammatory signaling pathways of GCs in macrophages. This question was addressed in the context of sterile inflammation provided by post-injury skeletal muscle regeneration. This work constitutes the first and main study of my thesis.

Meanwhile, we investigated the role of another factor, annexin A1, in the resolution of inflammation and especially its role in macrophage polarization during skeletal muscle regeneration. As annexin A1 and AMPK activation both induce the anti-inflammatory profile of macrophages, the purpose of this second study was to decipher whether annexin A1 and AMPK are linked to induce macrophage phenotype switch during skeletal muscle regeneration.

In both studies #1 and #2, measurement of the myofiber size was performed to evaluate the efficiency of skeletal muscle regeneration. However, myofiber size measurement is currently performed manually and it is time-consuming. In a third study, we developed and validated an ImageJ macro to semi-automatically measure myofiber size. This new tool was used for both studies #1 and #2.

## **STUDY #1**



## **Crosstalk of Glucocorticoid Receptor and AMP-activated protein kinase in macrophages during tissue repair**

Thibaut Desgeorges\*, Giorgio Caratti\*, Bénédicte Chazaud, Jan Tuckermann and Rémi Mounier

We hypothesized that AMPK $\alpha$ 1 and GR pathways are connected in macrophages to promote the shift from pro- to anti-inflammatory status. This work is done in collaboration with the group of Jan Tuckermann in Ulm, Germany. This project was co-funded by the French agency “Agence Nationale de la Recherche” (ANR, projets de recherche collaborative – International, PRCI) and German agency Deutsche Forschungsgemeinschaft (DFG).

To decipher whether these 2 molecular pathways are interconnected, we used 2 models of inflammation provided by each lab. We first deciphered AMPK-GR crosstalk in a model of sterile inflammation which is post-injury skeletal muscle regeneration. This part was developed by our team and constituted my main PhD project. The second model of inflammation is an acute lung inflammation induced by bacterial infection monitored by the German team. This will not be described here.

This work is still ongoing (see Perspectives section). We expect to submit the study, including both models, for publication during the next fall in a high rank journal since this work could be of interest to improve glucocorticoid therapy.

# MATERIAL AND METHODS

## Animal models

Experiments were performed on AMPK $\alpha$ 1<sup>-/-</sup> (Mounier et al., 2009), AMPK $\alpha$ 1<sup>fl/fl</sup> (Miller et al., 2011) and LysM<sup>cre/+</sup>;AMPK $\alpha$ 1<sup>fl/fl</sup> adult male mice (8 to 14-week-old), according to French legislation. For injury experiments, mice were anesthetized with isoflurane and *Tibialis Anterior* (TA) muscle was injected with cardiotoxin (Latoxan) at 12  $\mu$ M (50  $\mu$ l per muscle) as previously described (Mounier et al., 2013). Muscles were harvested at different time points after injury (8, 14 and 28 days post-injury).

Mouse treatment: mice were treated by intraperitoneal injection of either dexamethasone (0.05 or 0.1 mg/kg/day, D2915, Sigma-Aldrich) or vehicle at various time points after injury.

## Histological analysis and *in vivo* immunostaining

Once harvested, TA muscles were mounted on piece of cork and fixed with tragacanth gum before being frozen in isopentane cooled by liquid nitrogen. Muscles were stored at -80°C. TA muscles were sectioned with cryomicrotome (NX50, Microme) in 10  $\mu$ m thick sections and slides were kept at -80°C. Slides were first stain with Hematoxylin and Eosin to check cardiotoxin injection and immunofluorescence was performed only on muscles that showed at least 85% of their area with regenerating myofibers (*i.e.*, with central nuclei). For immunofluorescence experiments, slides were dried for 10 min at room temperature before encircling sections with a hydrophobic pen (Dako). They were incubated with Triton x100 0.5% for 10 min and then washed 3 times with PBS. They were incubated with bovine serum albumin (BSA) 2% for 1 h at room temperature and were incubated overnight with a rabbit anti-laminin antibody (1:200, L9393, Sigma-Aldrich), a mouse anti-embryonic myosin (1:100, sc-53091, Santa Cruz), a mouse anti-myosin I (1:100, BA-D5, DHSB), a mouse anti-myosin IIA (1:100, sc-71, DHSB) or a mouse anti-myosin IIB (1:100, BF-F3, DHSB). Slides were washed 3 times with PBS and incubated with secondary antibodies (see Table1). Sections were soaked for 10 s in Hoechst solution H 33342 (1:1000, B2261, Sigma-Aldrich) and washed once with PBS before mounting with antifading Fluoromount G medium (FP-483331, Interchim). Slides were stored at 4°C protected from light until picture acquisition. For adult myosin immunostaining, triton was not used and slides were blocked with Mouse on Mouse

(M.O.M™) Blocking Reagent (MKB-2213, Vector Laboratories). All samples of the same experiment were recorded in similar conditions (microscope, magnification, exposure time and binning). For whole section analysis, slides were automatically scanned at x10 or x20 of magnification using an Axio Observer.Z1 (Zeiss) connected to a CoolSNAP HQ2 CCD Camera (Photometrics) using Metavue software. The whole muscle section was automatically reconstituted by Metavue software. Cross sectional analysis was performed using Open-CSAM ImageJ macro (Desgeorges et al., 2019).

Myosin	Primary antibody	Secondary antibody (Jackson Immuno reseach)	
I	BA-D5	Alexa Fluor 405 anti-IgG2b	115-475-07
IIA	SC-71	Alexa Fluor 488 anti-IgG1	115-545-205
IIB	BF-F3	Rhodamine anti-IgM	115-295-020
embryonic	Sc-53091	Alexa Fluor 488 anti-IgG1	115-545-205

**Table 1. Antibodies used for immunostaining of myosins.**

### **Bone marrow-derived macrophage culture**

Macrophages were obtained from bone marrow precursors as previously described (Mounier et al. 2013). Total bone marrow was isolated from mice by flushing the femur and tibiae bone marrow with culture medium. Extracted bone marrow was cultured in DMEM high glucose high pyruvate (11995065, Gibco) containing 20% of FBS, 1% of peni/streptomycin, 1% of fungizone and 30% of L929 conditioned medium for 5 to 7 days. L929 secrete high levels of Macrophage Colony-Stimulating Factor (MCSF) that triggers macrophage differentiation. L929 conditioned medium was obtained after 7 days of L929 cells culture with DMEM containing 10% FBS.

### **DAMPs – Damaged associated molecular patterns from muscle**

DAMPs were obtained from injured muscles. Briefly, mice hindlimb underwent an ischemia for 2 h. After 20 h of reperfusion, all the muscles of the hindlimb were harvested. 3 mice were pooled for each substrate. Once harvested, muscles were digested with Mammalian cell lysis buffer (MCL1, Sigma-Aldrich). 2 tungsten beads were added in samples to homogenize the



muscle extract with a Tissue lyser. After centrifugation, samples were sonicated and supernatant was recovered, pooled, and stored at -80°C.

### **Macrophage polarization**

Macrophages were seeded at 54000 cells/cm<sup>2</sup> in DMEM containing 10% of FBS on glass coverslips in 12-well plates. Cells were treated with 0.1 mM of AICAR (Tocris), 1x10<sup>-8</sup> M of dexamethasone (DEX) (D4902, Sigma-Aldrich) or 1 µg/ml of muscle DAMPs. Cells were treated in DMEM 10 % FBS with muscle DAMPs for 24 h and then AICAR and/or DEX were directly added in the well for 6 h. After treatment, cells were fixed with PFA 4% for 10 min and washed. Then, they were permeabilized for 10 min with Triton x100 0.5% and washed. Cells were incubated for 1 h with BSA 4% before staining for CCL3 (1:50, sc-1383, Santa Cruz), iNOS (1:50, ab3523, Abcam), CD206 (1:50, sc-58987, Santa Cruz), CD163 (1:50, sc-33560, Santa Cruz), TGFβ1 (1:50, ab64715, Abcam). All samples of the same experiment were recorded in similar conditions (microscope, magnification, exposure time and binning). At least 10 pictures *per* condition were acquired at x20 magnification on an Axio Imager.Z1 microscope (Zeiss) connected to a CoolSNAP MYO CCD camera (photometrics) using MetaMorph Software. Quantification of macrophage markers was done by manual quantification on ImageJ software.

### **Muscle precursor cell (MPC) - macrophage coculture**

Macrophages were seeded at 54000 cells/cm<sup>2</sup> in 12-well plates in DMEM 10% FBS (Gibco, Thermofisher scientific). They were treated for 3 days with 1x10<sup>-7</sup> or 1x10<sup>-8</sup> M of dexamethasone (DEX) (Sigma-Aldrich). DMEM free serum was added for 24 h to obtain conditioned medium. MPCs were obtained from TA muscles and were cultured in DMEM/F12 containing 20% FBS and 2% ultrosorG (Pall Inc) as previously described (Mounier et al., 2013). For proliferation studies, MPCs were seeded at 10000 cells/cm<sup>2</sup> on Matrigel (1:10) and incubated for 1 day with macrophage-conditioned medium + 2.5% FBS. MPCs were then washed, fixed and incubated with anti-Ki67 antibody (1:100, 15580, Abcam) visualized using cy3-conjugated secondary antibody (Jackson Immunoresearch). For differentiation experiments, MPCs were seeded at 30000 cells/cm<sup>2</sup> on Matrigel (1:10) for 3 days with macrophage-conditioned medium containing 2% HS. Cells were washed, fixed and stained

with anti-desmin antibody (1:200, 32362, Abcam) and visualized by cy3-conjugated secondary antibody (Jackson immunoresearch)

### **Glucocorticoid receptor localization**

Macrophages were seeded at 54000 cells/cm<sup>2</sup> in DMEM containing 10% of FBS on glass coverslips in 12-well plates. Cells were treated with 0.1 mM of AICAR (Tocris) and/or 1x10<sup>-8</sup> M of dexamethasone (DEX) (Sigma-Aldrich). After treatment, cells were fixed with PFA 4% for 10 min and washed. Then, they were permeabilized for 10 min with Triton x100 0.5% and washed. Cells were incubated for 1 h with BSA 4% before staining for the Glucocorticoid Receptor (1:500, #3660, Cell Signaling) or Phalloidin-Atto 488 (49409, Signa-Aldrich). All samples of the same experiment were recorded in similar conditions (microscope, magnification, exposure time and binning). At least 10 pictures *per* condition were acquired at x40 magnification on an Axio Imager.Z1 microscope (Zeiss) connected to a CoolSNAP MYO CCD camera (photometrics) using MetaMorph Software. The quantification of GR localization was done using a home-made ImageJ macro and based on the ratio of the mean fluorescent intensity of the GR staining evaluated in the cytoplasm and in the nucleus.

### **Western blot**

Macrophages were seeded at 208000 cells/cm<sup>2</sup> for western blot experiments. Cells were treated with 0.1 mM of AICAR (Tocris), 1x10<sup>-7</sup> or 1x10<sup>-8</sup> M of dexamethasone (DEX) (Sigma-Aldrich), 1 mM of 991 (Spirochem). Cells were treated for 0.5 to 1 h in DMEM containing 10% of charcoal stripped serum (Gibco, Thermofisher scientific). Total protein extract was obtained in cell lysis buffer containing 50 mM Tris-HCL (pH 7.5), 1 mM EDTA, 1 mM EGTA, 0.27 M sucrose, 1% triton, 20 mM glycerol-2-phosphate disodium, 50 mM NaF, 0.5 mM PMSF, 1 mM benzamidine, 1 mM Na<sub>3</sub>VO<sub>4</sub> and 1% cocktail phosphatase inhibitor 3 (Sigma, P0044). Twenty micrograms of proteins were subjected to SDS-PAGE (100V) and transferred onto a nitrocellulose membrane overnight at 4°C, 30V. Blots were probed with antibodies against p-AMPKα (1:1000, Cell signaling, #2535), AMPKα (1:1000, Cell signaling, #2532), p-ACC (1:1000, Cell signaling, #3661), ACC (1:1000, Cell signaling, #3662), p-Raptor (1:1000, Cell signaling, #2283), Raptor (1:1000, Cell signaling, #2279) or β-actin for loading control (1:2000, Sigma-Aldrich, A5316).

### **Quantification of AMPK deletion**

Quantification of AMPK deletion in macrophages was done by PCR analysis after isolation of myeloid cells. Bone marrow was extracted from mice. After lysis of erythrocytes with ACK lysis buffer (Lonza), cells were stained with FcγRII/III (Miltenyi Biotec), then with biotin coupled-CD11b antibody. Cells were purified using anti-biotin magnetic beads (Miltenyi biotec). Genomic DNA from CD11b<sup>+</sup> cells was extracted using cell lysis buffer containing 100 mM Tris-HCl (pH 8), 5 mM EDTA, 200 mM NaCl, 0.2% SDS and 0.1 mg/ml proteinase K (Roche) for 2 h at 55°C. Extracted DNA was precipitated with isopropanol and glycogen. DNA was washed with ethanol 70% and finally dried and solubilized in water. PCR was performed using Phire Hot Start II DNA Polymerase (Thermofisher Scientific) as previously described (Mounier et al., 2013).

### **Statistical analysis**

All experiments were performed at least with three independent primary cultures (except for GR localization where two experiments were done). For *in vivo* experiments, at least 4 mice were analyzed from three independent experiments for each group. Statistic tests were performed with GraphPad Prism software. Normality was tested with Shapiro-Wilk test. Depending on the experiment and the normality, parametric (Student *t* test or ANOVA) or non-parametric (Mann-Whitney or Kruskal-Wallis) tests were used.  $P < 0.05$  was considered significant.

## RESULTS

### *GCs induce AMPK activation in resting macrophages*

AMPK is a kinase that is activated when the  $\alpha$ -subunit is phosphorylated on threonine (Thr) 172. Investigation of AMPK activation by GCs requires the analyze of the phosphorylation state of the Thr172 in  $\alpha$ 1-subunit, which is the only AMPK isoform expressed in macrophages (Mounier et al., 2013; Sag et al., 2008). First, resting WT macrophages were treated with AICAR at 0.1 mM and/or DEX at  $10^{-8}$  M or  $10^{-7}$  M for 30 or 60 min and AMPK phosphorylation was analyzed by western blot. At 30 min of treatment, no differences were observed on AMPK phosphorylation upon AICAR or DEX treatment (Figures 1A, 1B). As expected, at 60 min of treatment, AMPK phosphorylation was induced by AICAR (+111% as compared with untreated condition at 60 min,  $p<0.05$ ) (Figure 1B). DEX at  $10^{-8}$  M tended to induce AMPK phosphorylation (+45 %) whereas DEX at  $10^{-7}$  M significantly increased AMPK phosphorylation (+47 %,  $p<0.001$ ). Combined 60 min-treatment of AICAR and DEX induced AMPK phosphorylation in a higher rate than each compound did separately (+177 %,  $p<0.001$ ) (Figure 1B). These data showed that GCs induced AMPK phosphorylation.

AICAR being an AMP mimetic, it is not a specific activator of AMPK. We then decided to use the 991 compound, which is an allosteric activator of AMPK (Xiao et al., 2013). WT macrophages were treated with 991 compound (1  $\mu$ M) and/or DEX ( $10^{-8}$  M). As expected, AMPK phosphorylation was increased by 36 % ( $p<0.05$ ) in WT macrophages treated with 991 compound for 60 min (Figures 1C, 1D). As shown above, DEX induced a significant increase of AMPK phosphorylation (+86 %,  $p<0.01$ ). However, combined treatment of 991 and DEX did not show a synergistic effect on AMPK phosphorylation as compared with each compound used separately (+ 66 %,  $p<0.05$ ) (Figures 1C, 1D).

Because AMPK can be phosphorylated and dephosphorylated quickly (in few minutes), we checked if the increased phosphorylation observed upon DEX treatment also induced the phosphorylation of 2 AMPK targets: Acetyl-CoA Carboxylase (ACC) and Raptor. After 60 min of treatment, 991 induced ACC phosphorylation in macrophages (+123 %,  $p=0.079$ ), as expected (Figures 1C, 1D). Interestingly, DEX also increased ACC phosphorylation by 32 % ( $p<0.05$ ) (Figures 1C, 1D). Note that the second AMPK target, Raptor, was not responding to treatment, keeping similar level of phosphorylation rate as in untreated condition, even upon 991 compound treatment, suggesting that Raptor is not an AMPK target in resting macrophages

(Figures 1C, 1D). Altogether, these data showed that GCs induced AMPK $\alpha$ 1 phosphorylation and activation in macrophages.

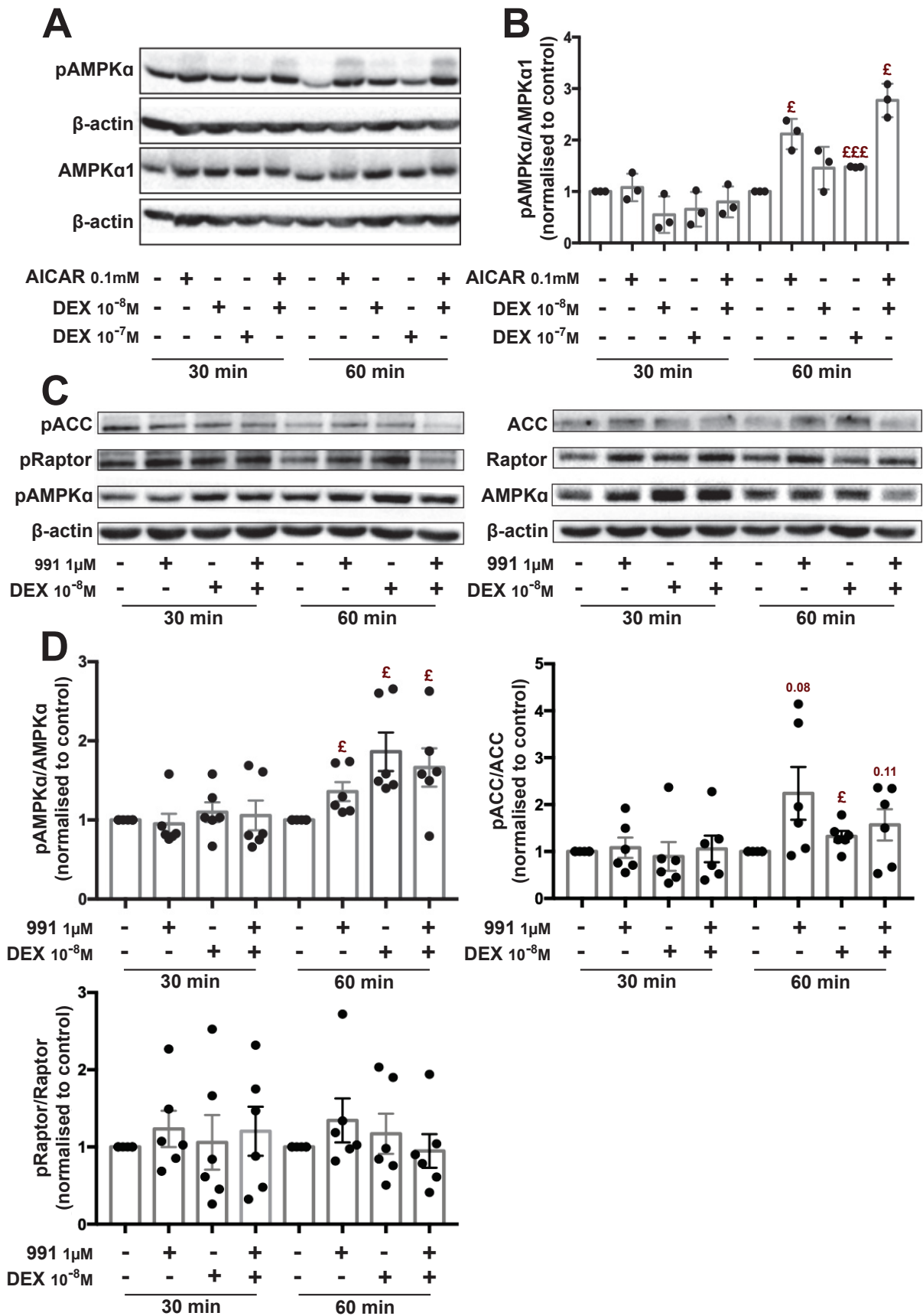


**Figure 1. GCs induce phosphorylation of AMPK $\alpha$ 1 in macrophages.** (A) Western blot experiments were performed on WT macrophages. Macrophages were treated with AICAR (a non-specific AMPK $\alpha$ 1 activator) and with the glucocorticoid (GC) dexamethasone (DEX) at 30 and 60 min. Phosphorylation of Thr172 of AMPK $\alpha$  was measured. (B) Quantification of western blot shown in (A). (C) AMPK $\alpha$ 1 phosphorylation in WT macrophages was measured after 991 (an allosteric activator of AMPK) and DEX treatment for 30 and 60 min. Phosphorylation of the AMPK target proteins Acetyl CoA Carboxylase (ACC) on Ser79 and Raptor on Ser792 was analyzed after 991 and DEX at 30 and 60 min of treatment. (D) Quantification of AMPK $\alpha$ 1 phosphorylation, ACC phosphorylation and Raptor phosphorylation. Quantification results show ratio between the phospho-protein on  $\beta$ -actin and total-protein on  $\beta$ -actin. £  $p < 0.05$ , £££  $p < 0.001$  versus the untreated condition of each time of treatment.

---

***AMPK $\alpha$ 1 is required for the GC-induced acquisition of an anti-inflammatory profile by resting macrophages***

It was previously shown that AMPK activation in macrophages leads to the acquisition of the anti-inflammatory status (Mounier et al., 2013). Because DEX induced AMPK phosphorylation (Figure 1), we analyzed whether AMPK is required for the acquisition of the anti-inflammatory status by macrophages upon DEX treatment. Bone marrow-derived macrophages isolated from WT and AMPK $\alpha$ 1<sup>-/-</sup> mice were treated for 6 h with AICAR and/or DEX. The expression of inflammatory markers was analyzed by immunolabelling as the lab showed few years ago that immunolabelling gave more accurate results than RT-qPCR (*e.g.*, the number of positive cells for Transforming Growth Factor  $\beta$  (TGF $\beta$ ) immunolabelling was increased after anti-inflammatory polarization whereas no effect was measured by RT-qPCR (Mounier et al., 2013). Inducible Nitric Oxide Synthase (iNOS) is a pro-inflammatory marker in macrophages. The number of cells expressing iNOS was not different in the several conditions tested in both WT and AMPK $\alpha$ 1<sup>-/-</sup> macrophages (Figure 2A). Then, cells expressing the anti-inflammatory markers mannose receptor (CD206) and TGF $\beta$  was quantified. As expected in WT macrophages, AICAR and DEX treatment increased the number of cells expressing both CD206 and TGF $\beta$  as compared with untreated condition (Figure 2B). The number of CD206 positive cells in WT macrophages treated by AICAR, DEX and AICAR+DEX increased by +26 % ( $p < 0.01$ ), +23 % ( $p < 0.05$ ) and +25 % ( $p < 0.01$ ), respectively (Figure 2B). Similarly, the number of TGF $\beta$  positive cells was increased in WT macrophages upon AICAR, DEX and AICAR+DEX treatment by +12.5 % ( $p < 0.01$ ), +13.7 % ( $p < 0.01$ ) and +15.6 % ( $p < 0.05$ ), respectively, as compared with untreated condition. No additional effect was measured in WT macrophages treated with both AICAR

and DEX (Figure 2B). On the contrary, AMPK $\alpha$ 1<sup>-/-</sup> macrophages treated with AICAR did not show a higher number of cells positive for either CD206 or TGF $\beta$  immunostaining. These results were expected as AICAR acts mainly through AMPK activation. Interestingly, DEX did not increase the number of positive cells for these 2 anti-inflammatory markers in AMPK $\alpha$ 1<sup>-/-</sup> macrophages (Figure 2B), suggesting that DEX treatment did not induce the expression of these markers in AMPK $\alpha$ 1<sup>-/-</sup> macrophages. These results indicate that AMPK $\alpha$ 1 was required for the acquisition of the anti-inflammatory profile of macrophages induced by GCs.

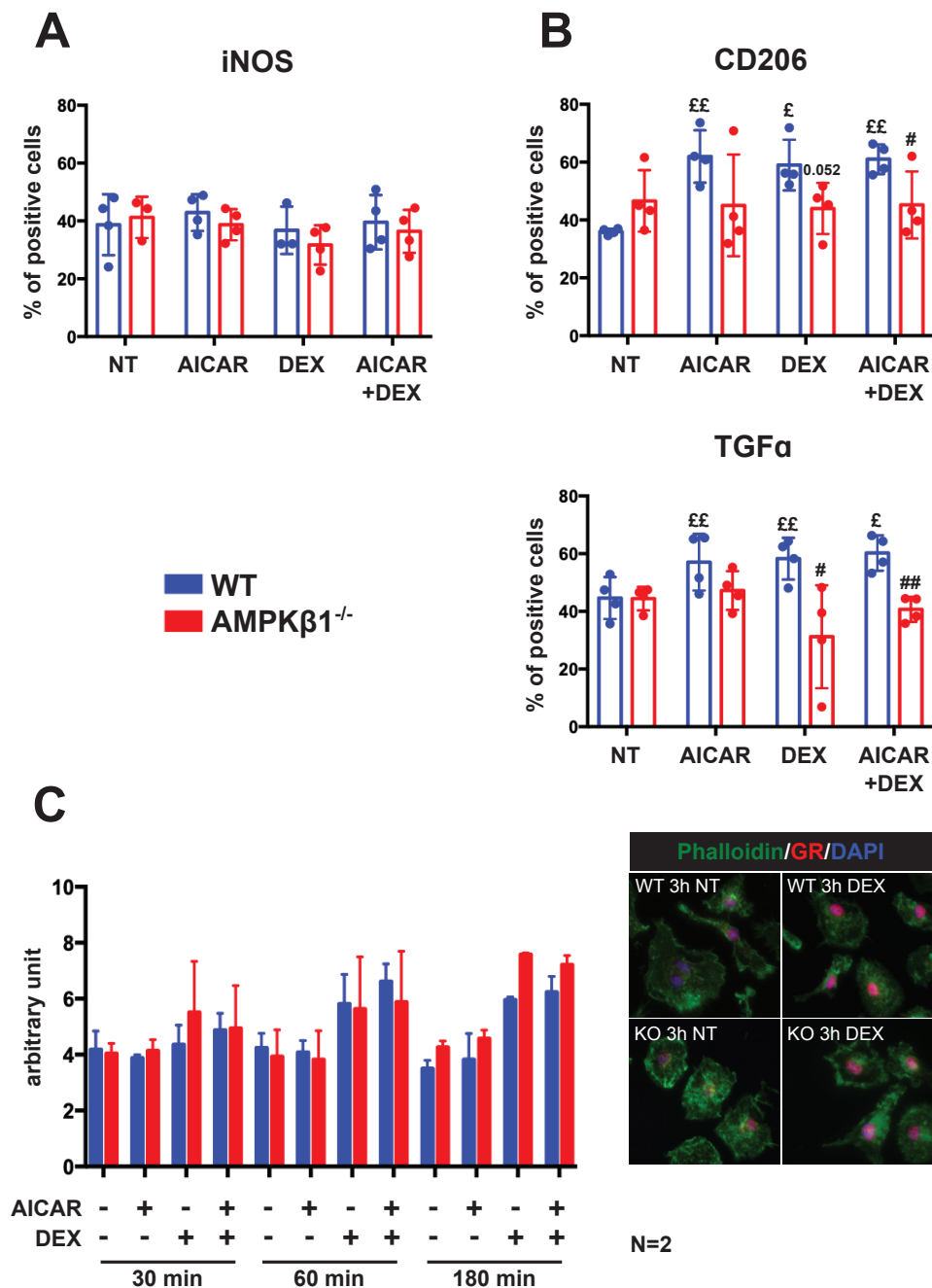
In a first attempt to understand how AMPK $\alpha$ 1 and GR could interact, we analyzed the subcellular localization of GR in WT and AMPK $\alpha$ 1<sup>-/-</sup> macrophages under AICAR and DEX treatments. Indeed, GR is localized in the cytoplasm and translocates into the nucleus when bound to GCs, to regulate gene expression. So, GR localization gives information about its potential transcriptional activity. GR localization was quantified using a home-made ImageJ macro that evaluated the mean fluorescence value of GR staining either in the cytoplasm or in the nucleus of macrophages. Results showed that only DEX induced the translocation of GR into the nucleus after 30 min (in a lesser extent) and after 60 or 180 min (in a larger extent), in a similar way in both WT and AMPK $\alpha$ 1<sup>-/-</sup> macrophages (Figure 2C, N=2). This result shows that GR translocation after GC binding was not dependent of AMPK $\alpha$ 1 in macrophages.

---

**Figure 2. GCs require AMPK $\alpha$ 1 to induce anti-inflammatory profile of resting macrophages.**

Immunofluorescence analysis of the expression of the pro-inflammatory marker iNOS (A) and the anti-inflammatory markers CD206 and TGF $\beta$  (B) after 6 h of treatment with AICAR [0.1 mM] and DEX [10<sup>-8</sup> M]. Graphs show the number of positive cells. (C) The sub-cellular localization of the GR was quantified after immunofluorescence experiment. ImageJ macro indicated the mean fluorescence intensity of GR staining either in cytoplasm or in nucleus of each cell. Graph indicates the ratio between intensity of GR staining between cytoplasm and nucleus after 30 min, 60 min or 180 min of treatment with AICAR and DEX. On the right, representative immunofluorescent pictures of GR staining (red), actin network stained by phalloidin (green) represents the cytoplasmic fraction of the cell and DAPI staining (blue) shows nucleus. Blue bars represent WT macrophages whereas red bars represent AMPK $\alpha$ 1<sup>-/-</sup> macrophages. £ p<0.05, ££ p<0.01 *versus* the untreated condition. # p<0.05, ## p<0.01 *versus* AMPK $\alpha$ 1<sup>-/-</sup> macrophages in each condition of treatment.





### ***AMPK $\alpha$ 1 is required for the GC-induced acquisition of an anti-inflammatory profile by pro-inflammatory macrophages***

To better mimic sterile inflammation of skeletal muscle *in vitro*, a model was developed using muscle Damaged Associated Molecular Patterns (DAMPs) to activate macrophages. Muscle-DAMPs are protein lysate extracted from early ischemia/reperfusion injured muscle. We validated this model by analyzing the number of macrophages expressing inflammatory markers after muscle-DAMPs treatment of WT macrophages. As shown in [Figure 3A](#), macrophages expressing the pro-inflammatory marker iNOS were more numerous after muscle-DAMPs treatment (+13 %,  $p < 0.001$ ). Similarly, the number of macrophages expressing

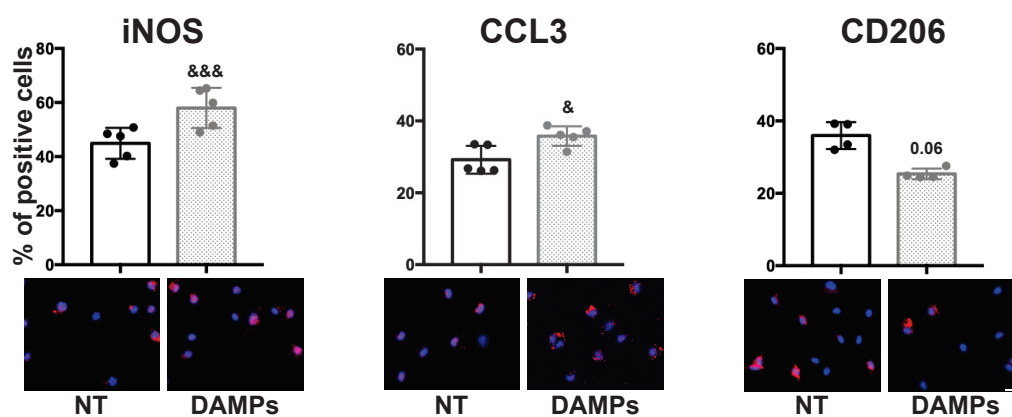


another pro-inflammatory marker, C-C motif chemokine ligand 3 (CCL3), was increased by muscle-DAMPs treatment (+6,5 %,  $p<0.05$ ) (Figure 3A). Conversely, the number of macrophages expressing the anti-inflammatory marker CD206 was decreased by muscle-DAMPs (-10.5%,  $p<0.06$ ) (Figure 3A).

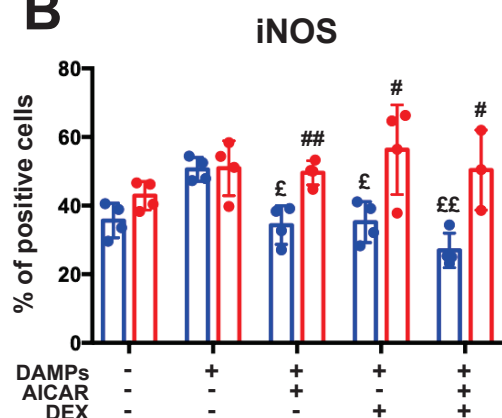
Then, in this context of pro-inflammatory activated macrophages, the acquisition of an anti-inflammatory status of WT and AMPK $\alpha$ 1<sup>-/-</sup> macrophages was assessed as in Figure 2. Macrophages were treated with AICAR and/or DEX after muscle-DAMPs exposition for 24 h. iNOS and CCL3-expressing macrophages were increased by muscle-DAMPs treatment in both WT and AMPK $\alpha$ 1<sup>-/-</sup> macrophages (Figure 3B). As expected, AICAR and DEX treatment in WT macrophages significantly decreased the number of macrophages expressing iNOS (AICAR: -16 %,  $p<0.05$ ; DEX: -15 %,  $p<0.05$ ; AICAR+DEX: -23 %,  $p<0.01$  as compared with WT DAMPs condition) and CCL3 (AICAR: -19 %,  $p<0.05$ ; DEX: -19.5 %,  $p<0.05$ ; AICAR+DEX: -18.5 %,  $p<0.05$ ) (Figure 3B). On the contrary, in AMPK $\alpha$ 1<sup>-/-</sup> macrophages, AICAR and DEX treatment induced no effect on the expression of iNOS and CCL3, that remained high (Figure 3B). AICAR and DEX treatment in WT macrophages significantly increased the number of macrophages expressing the anti-inflammatory markers CD206 (AICAR: +13.8 %,  $p<0.01$ ; DEX: 25.6 %,  $p<0.05$ ; AICAR+DEX: 24.4 %,  $p<0.05$  as compared with WT DAMPs condition), TGF $\beta$  (AICAR: +17 %,  $p<0.05$ ; DEX: 25 %,  $p<0.05$ ; AICAR+DEX: 20.3 %,  $p<0.001$  as compared with WT DAMPs condition) and CD163 (AICAR: +16.1 %,  $p<0.01$ ; DEX: 19.9 %,  $p<0.001$ ; AICAR+DEX: 17.6 %,  $p<0.05$  as compared with WT DAMPs condition) (Figure 3C). In AMPK $\alpha$ 1<sup>-/-</sup> macrophages, the expression of these 3 markers was not changed by AICAR and DEX treatments and remained low (Figure 3C). Altogether, these data show that AMPK $\alpha$ 1 was required in pro-inflammatory activated macrophages for GC signaling in the acquisition of the anti-inflammatory status.

**Figure 3. GCs require AMPK $\alpha$ 1 to induce anti-inflammatory profile of activated macrophages.** To mimic sterile inflammation, macrophages were first activated by muscle Damaged Associated Molecular Patterns (DAMPs) for 24 h. **(A)** Number of cells expressing the pro-inflammatory markers iNOS and CCL3 and the anti-inflammatory markers CD206 was measured by immunofluorescence experiments. Untreated condition (black bars) and DAMPs treated condition (grey bars). The number of cells expressing the pro-inflammatory markers iNOS and CCL3 **(B)** and the anti-inflammatory markers CD206, TGF $\beta$  and CD163 **(C)** was analyzed by immunofluorescence on DAMPs-activated macrophages after AICAR and DEX treatment for 6 h. Graphs show the number of positive cells. Blue bars represent WT macrophages, red bars represent AMPK $\alpha$ 1<sup>-/-</sup> macrophages. &  $p<0.05$ , &&&  $p<0.001$  versus NT. £  $p<0.05$ , ££  $p<0.01$  and £££  $p<0.001$  versus DAMPs condition. #  $p<0.05$ , ##  $p<0.01$  and ###  $p<0.001$  versus AMPK $\alpha$ 1<sup>-/-</sup> macrophages for each condition. The scale bar represents 10  $\mu$ m.

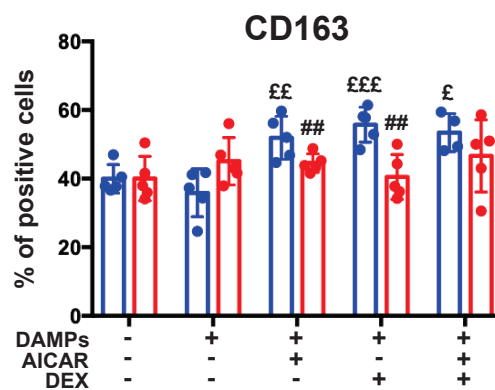
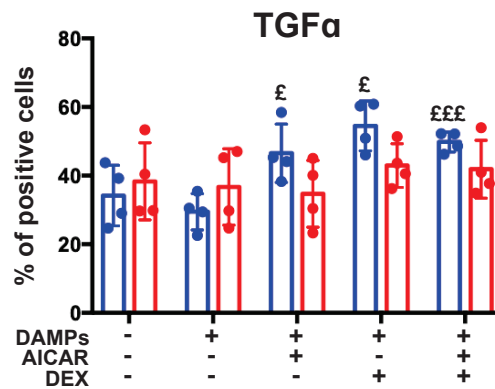
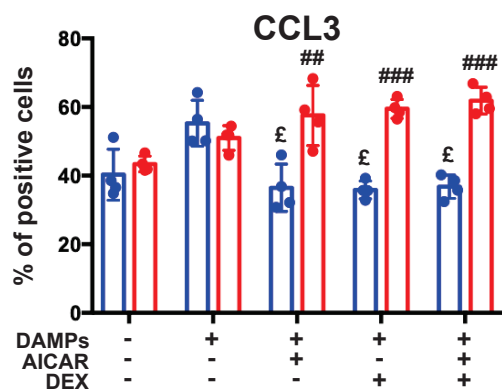
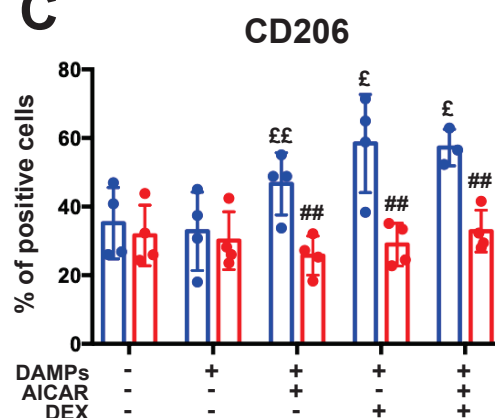
**A**



**B**



**C**



■ WT  
■ AMPK $\beta$ <sup>-/-</sup>

### ***AMPK $\alpha$ 1 is required for the GC-induced acquisition of functional anti-inflammatory status by macrophages***

The inflammatory status of macrophages is associated with specific functions during skeletal muscle regeneration (Varga et al., 2016; Mounier et al., 2013; Saclier et al., 2013; Arnold et al., 2007). Pro-inflammatory macrophages promote myoblast proliferation whereas anti-inflammatory macrophages stimulate myoblast differentiation and fusion into myotubes. Using co-culture experiment, we addressed the functional properties of WT and AMPK $\alpha$ 1<sup>-/-</sup> macrophages on myogenesis upon DEX treatment (Figure 4).

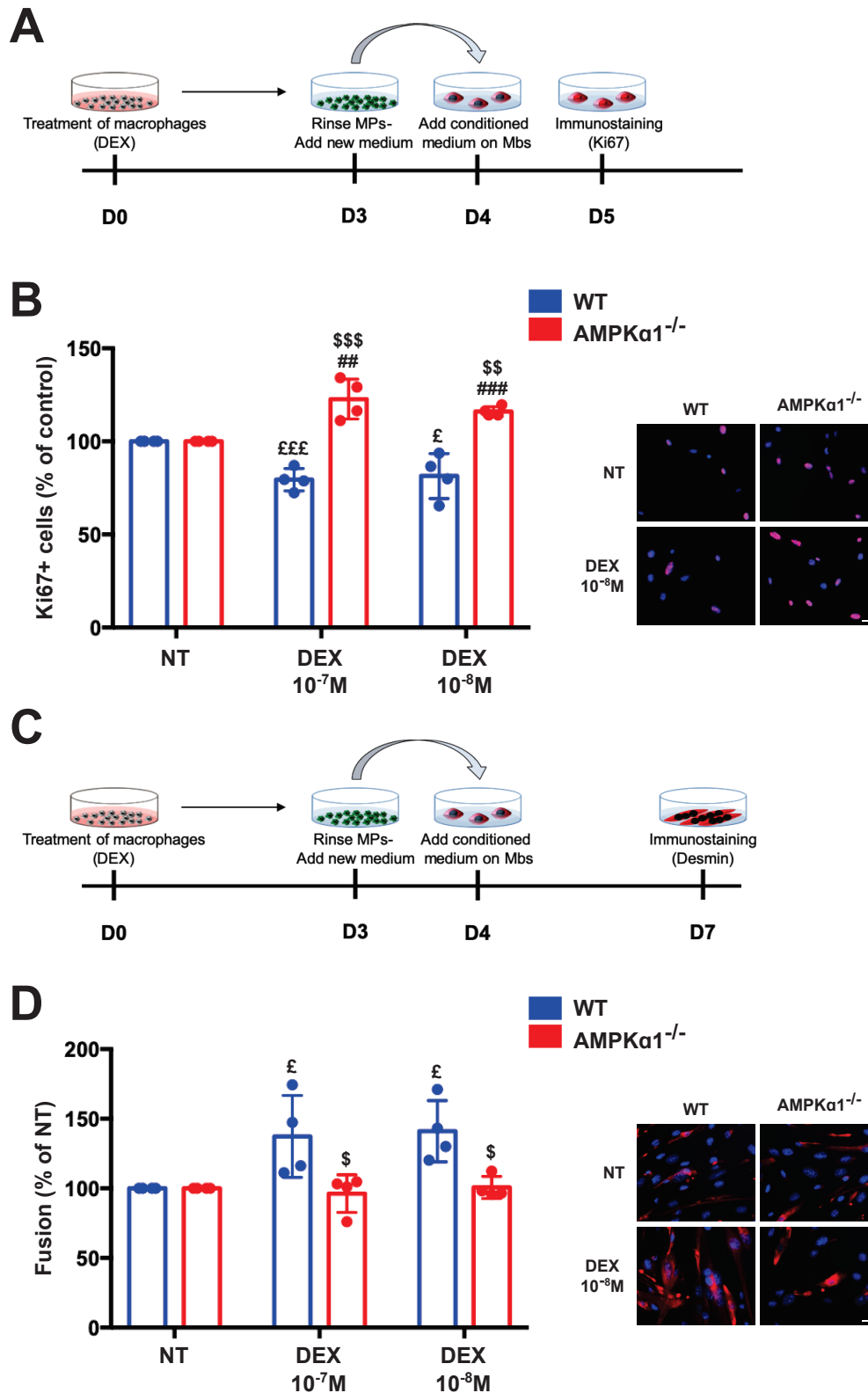
Myoblast proliferation was measured by Ki67 immunostaining using conditioned medium from WT and AMPK $\alpha$ 1<sup>-/-</sup> macrophages previously treated by DEX at 10<sup>-7</sup> M or 10<sup>-8</sup> M (Figure 4A). Conditioned-medium from DEX-treated WT macrophages decreased the number of Ki67 positive (cycling) myoblasts as compared with conditioned-medium from untreated WT macrophages, by 20 % ( $p < 0.001$ ) and 18.6 % ( $p < 0.05$ ) for 10<sup>-7</sup> M or 10<sup>-8</sup> M concentrations, respectively (Figure 4B). Conversely, DEX-treated AMPK $\alpha$ 1<sup>-/-</sup> macrophages increased the number of Ki67 positive myoblasts by +22 % ( $p < 0.01$ ) and +16 % ( $p < 0.001$ ) for 10<sup>-7</sup> M or 10<sup>-8</sup> M concentrations, respectively. Myoblast differentiation was evaluated using similar co-culture experiments (Figure 4C). Myoblasts cultured with conditioned medium from WT macrophages previously treated with DEX showed an increased number of myotubes (by 37 % ( $p < 0.05$ ) and 41 % ( $p < 0.05$ ) at 10<sup>-7</sup> M or 10<sup>-8</sup> M, respectively). However, myoblasts cultured with conditioned medium from DEX-treated AMPK $\alpha$ 1<sup>-/-</sup> macrophages did not show modification of myogenesis as compared with myoblasts treated with conditioned medium from untreated AMPK $\alpha$ 1<sup>-/-</sup> macrophages (Figure 4D).

Thus, these data indicate that AMPK $\alpha$ 1<sup>-/-</sup> macrophages treated by DEX did not acquire the functional phenotype of anti-inflammatory macrophages that sustain myogenesis.

---

**Figure 4. Functional acquisition of macrophage anti-inflammatory status induced by GCs requires AMPK $\alpha$ 1.** (A) Experimental procedure used to analyze the effects of macrophage-conditioned medium on myoblast proliferation (Ki67 staining). (B) Quantification of proliferating myoblasts (Ki67 positive cells) exposed to conditioned medium from WT and AMPK $\alpha$ 1<sup>-/-</sup> macrophages treated with DEX at 10<sup>-7</sup> M or 10<sup>-8</sup> M. Graph represents the number of Ki67<sup>+</sup> myoblasts normalized to untreated condition. (C) Experimental procedure used to analyze the effects of macrophage-conditioned medium on myoblast differentiation (desmin staining and DAPI to count multinucleated cells). (D) Quantification of myotubes exposed to conditioned medium from WT and AMPK $\alpha$ 1<sup>-/-</sup> macrophages treated with DEX at 10<sup>-7</sup> M or 10<sup>-8</sup> M. Graph represents the percentage of myotubes normalized to untreated condition. Blue

bars represent myoblasts exposed to conditioned medium from WT macrophages, red bars represent myoblasts exposed to conditioned medium from AMPK $\alpha$ 1<sup>-/-</sup> macrophages. £ p<0.05 and £££ p<0.010 *versus* the WT NT condition. ## p<0.01 and ### p<0.001 *versus* AMPK $\alpha$ 1<sup>-/-</sup> NT condition. \$ p<0.01, \$\$ p<0.01 and \$\$\$ p<0.001 *versus* AMPK $\alpha$ 1<sup>-/-</sup> macrophages for each condition. The scale bar represents 10  $\mu$ m.



### ***GC treatment timing has to be tightly controlled during skeletal muscle regeneration***

After skeletal muscle injury, anti-inflammatory molecules are often prescribed for accelerating tissue repair. In order to analyze muscle regeneration upon GC treatment, we used the model of cardiotoxin injury as previously described (Mounier et al. 2013). Cardiotoxin is a snake venom that is injected in the *Tibialis Anterior* (TA) muscle of mice to cause myofiber necrosis due to depolarization and contraction of myofibers (Hardy et al., 2016). Muscles are then collected at different time points for histological analysis. In a first series of experiment, DEX was administrated by intra-peritoneal injection from various time points after injury until day 7 and skeletal muscle regeneration was analyzed at day 8. When DEX was administrated at the time of injury, skeletal muscle regeneration was strongly impaired with the persistence of necrotic myofibers as shown by Hematoxylin & Eosin staining, as compared with vehicle (Figure 5A). When DEX was administrated 1 day after injury, skeletal muscle regeneration was still impaired but in a lesser extent since small regenerating myofibers were observed with presence of inflammatory cells (Figure 5A). When DEX was administrated at day 2 after injury, skeletal muscle regeneration was also impaired with the appearance of small myofibers (Figure 5A). These results indicate that too early DEX injection after injury was deleterious for skeletal muscle regeneration.

Macrophage phenotype switch occurs between day 2 and day 3 *in vivo* after cardiotoxin injury (Mounier et al., 2013). Thus, we decided to treat mice from day 3 after injury until day 7 (Figure 5B) in an attempt to reinforce the anti-inflammatory status of macrophages until the drop of macrophage number in the regenerating muscle at day 8 (Arnold et al., 2007; Mounier et al., 2013). Moreover, to understand the role of AMPK $\alpha$ 1 in GC signaling in macrophages, we investigated muscle regeneration in LysM<sup>cre/+</sup>;AMPK $\alpha$ 1<sup>fl/fl</sup> (LysMA) mouse model where AMPK $\alpha$ 1 is specifically depleted in the myeloid lineage, including macrophages (Mounier et al., 2013). Skeletal muscle regeneration was analyzed at day 14 (middle time point) and day 28 (late time point) after cardiotoxin injury which allowed us to analyze newly formed myofibers (day 14) and the maturation of myofibers (day 28). No differences were observed in TA muscle mass at day 14 or day 28 between PBS-treated and DEX-treated WT mice (Figure 5C). However, at day 14, muscle mass was decreased in DEX-treated LysMA mice when compared with PBS-treated WT (-11%;  $p < 0.05$ ) and LysMA (-10%;  $p < 0.05$ ) mice. Cross sectional area (CSA) was measured since it is a reliable output of skeletal muscle regeneration. At day 14, mean CSA tended to decrease in WT DEX and LysMA PBS groups as compared with

WT PBS group (by  $-600\ \mu\text{m}^2$  and  $-600\ \mu\text{m}^2$  respectively) (Figure 5E). The mean CSA decrease was even more important in LysMA DEX group as compared with WT PBS group ( $-940\ \mu\text{m}^2$ ,  $p<0.01$ ) (Figure 5E). Myofiber size distribution indicated a significant increase of small myofiber number ( $<200\ \mu\text{m}^2$ ) between WT PBS and LysMA PBS confirming, the results showed by Mounier et al. in 2013 (Figure 5G). Moreover, an increased number of smaller myofibers was observed both in WT DEX and LysMA DEX groups as compared with PBS condition (Figure 5G). Day 28 after cardiotoxin injection, no significant differences were observed between the groups concerning the mean CSA (Figure 5F). However, DEX treatment significantly increased the number of smaller myofibers in both WT and LysMA groups. Furthermore, the amount of small myofibers was drastically increased in LysMA DEX-treated group as compared with WT DEX (Figure 5H). Moreover, DEX treatment also decreased the number of bigger myofibers in LysMA group as compared with the WT DEX condition ( $p<0.01$ ) (Figure 5H).

Thus, DEX treatment in WT mice impaired skeletal muscle regeneration if administrated too early after the injury. Moreover, 5 days of treatment in WT mice seemed to delay skeletal muscle regeneration as the size of myofibers was decreased at day 14. Altogether, these results show that DEX treatment for 5 days delayed skeletal muscle regeneration in both in WT and in LysMA groups but in a more significant way in LysMA mice. This may be explained by the combined effect of AMPK deficiency in macrophages and an effect of GCs on myofiber size, long-term GC treatment inducing myofiber atrophy (Schakman et al., 2013).

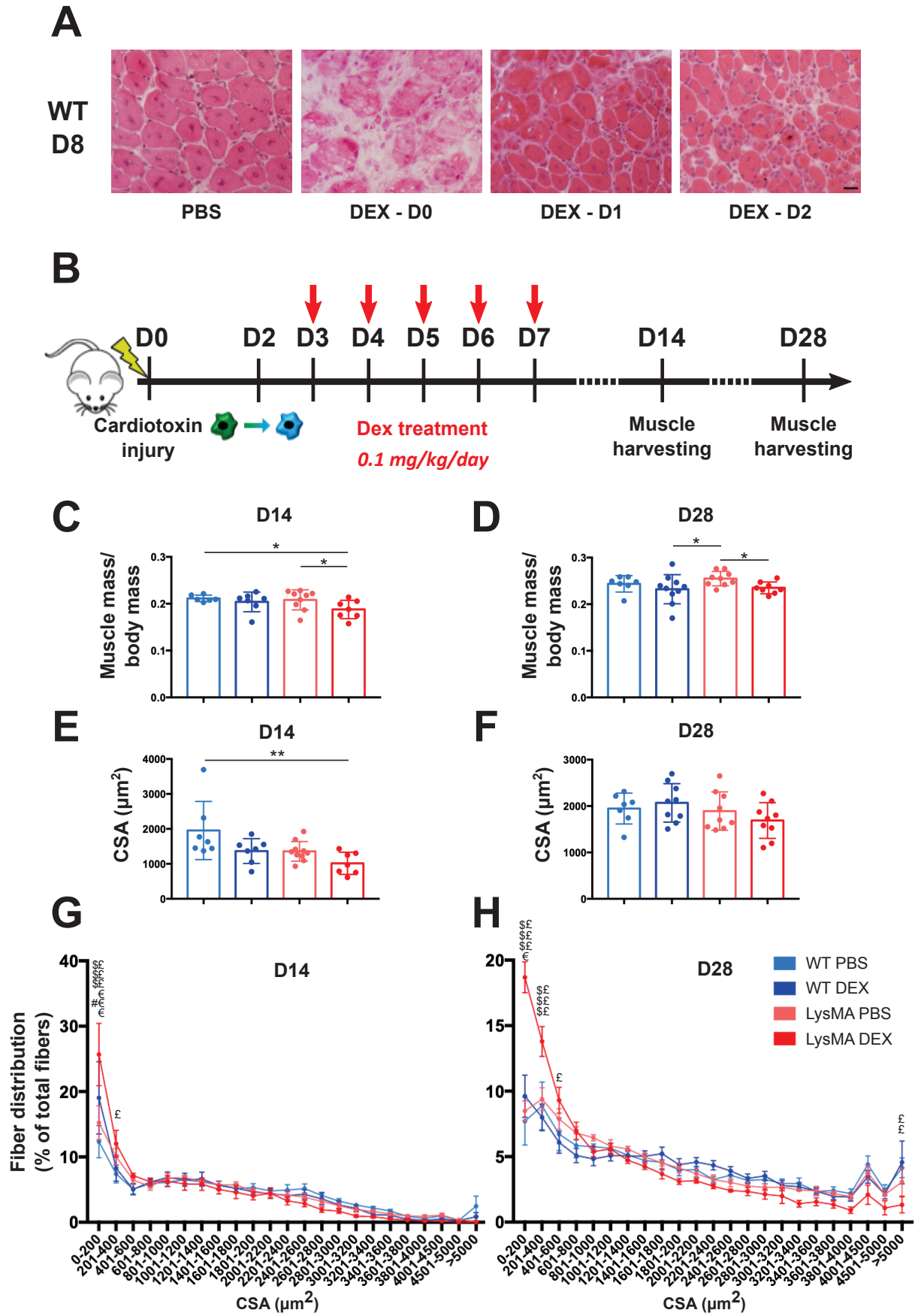




**Figure 5. Timing of GC treatment has to be tightly controlled during skeletal muscle regeneration.** (A) Hematoxylin and eosin staining of *Tibialis Anterior* (TA) from mice treated with DEX from day 0, day 1 and day 2 after cardiotoxin injury until day 7. Muscles were harvested at day 8 after cardiotoxin injury. (B) Experimental procedure of mice treatment with DEX. After cardiotoxin, mice were treated with PBS (control) or DEX for 5 days at day 3, day 4, day 5, day 6 and day 7. Muscles were harvested at day 14 and day 28. (C, D) Muscle mass of mice at day 14 (C) and day 28 (D) after cardiotoxin injury. Graphs represent ratio of muscle mass on the total mass of mouse body. (E, F) Mean cross sectional area (CSA) of myofibers from AMPK $\alpha$ 1<sup>fl/fl</sup> (WT) and LysM<sup>cre/+</sup>;AMPK $\alpha$ 1<sup>fl/fl</sup> (LysMA) mice treated either with PBS or DEX at day 14 (E) and day 28 (F) after cardiotoxin injury. (G, H) Graphs represent the distribution of myofiber size at day 14 (G) and day 28 (H). \* p<0.05, \*\* p<0.01, \*\*\* p<0.001. WT PBS versus WT DEX (€ p<0.05, €€ p<0.01, €€€ p<0.001); WT PBS versus LysMA PBS (# p<0.05, ## p<0.01, ### p<0.001); LysMA PBS versus LysMA DEX (\$ p<0.05, \$\$ p<0.01, \$\$\$ p<0.001); WT DEX versus LysMA DEX (£ p<0.05, ££ p<0.01, £££ p<0.001). The scale bar represents 10  $\mu$ m.

---

#### ***GC treatment delays muscle regeneration in the absence of AMPK $\alpha$ 1 in macrophages***

It was recently shown that a single weekly DEX treatment was enough to induce an anti-inflammatory effect and to avoid adverse effects on muscle wasting in a dystrophic mouse model, when compared with a daily administration of GCs (Quattrocchi et al, 2017). We therefore investigated the impact of a single injection of DEX at day 3 in skeletal muscle regeneration, once the macrophage switch is operated, in both WT and LysMA mice (Figure 6A). No differences were observed for muscle weight at day 8 between each group (Figure 6B). At day 14, muscle mass from DEX-treated LysMA mice decreased as compared with DEX-treated WT mice (-7%,  $p<0.07$ ). Accordingly, CSA in DEX-treated LysMA mice was significantly lower than in all the other groups (Figure 6C). This result was confirmed by the myofiber size distribution indicating that the number of smaller myofibers was increased in DEX-treated LysMA mice (Figure 6D). At day 28, muscle mass was decreased in PBS-treated LysMA mice as compared with both PBS- and DEX-treated WT groups (vs WT PBS: -9.5%,  $p<0.05$ ; vs WT DEX: -11.8%,  $p<0.01$ ) indicating that the impairment of muscle regeneration in LysMA mice observed in 2013 by Mounier et al. at day 14 was persistent at later time point (Figure 6B). No differences were observed between each group for the mean CSA at D28 (Figure 6E, 6F). Thus, in the absence of AMPK $\alpha$ 1 in macrophages, DEX treatment seemed to delay skeletal muscle regeneration *in vivo*.



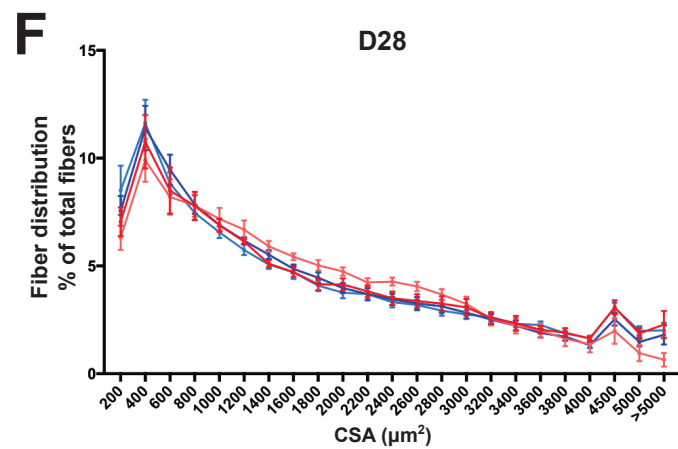
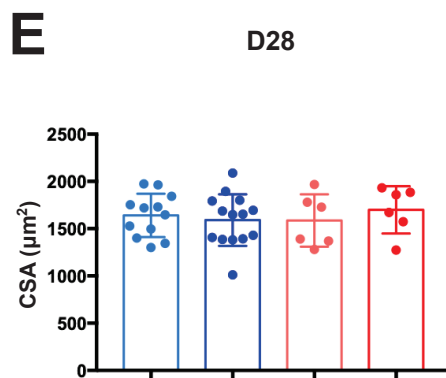
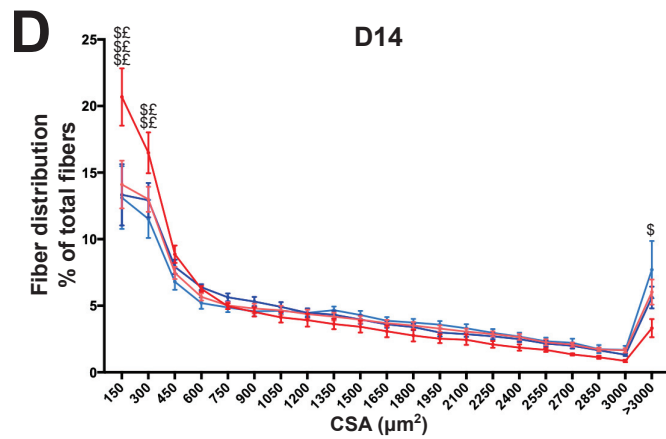
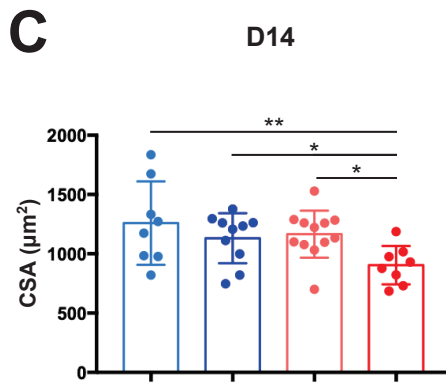
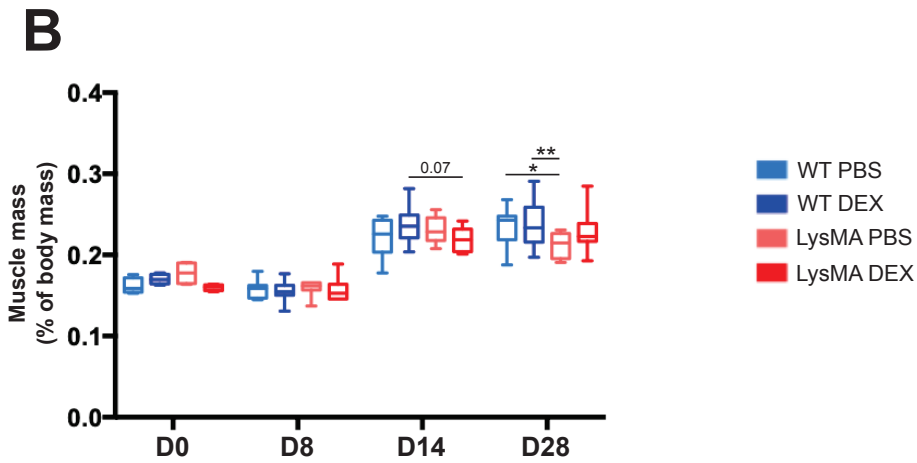
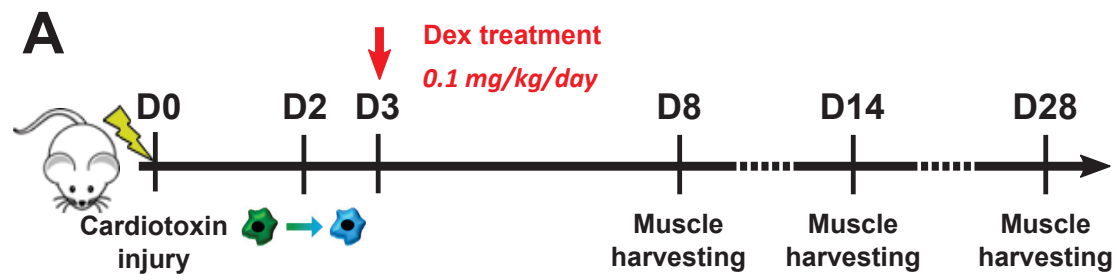


**Figure 6. GCs treatment delays skeletal muscle regeneration in the absence of AMPK $\alpha$ 1 in macrophages.** (A) Experimental procedure of mice treatment with DEX. After cardiotoxin, mice were treated with PBS (control) or DEX at day 3. *Tibialis anterior* muscles were harvested at day 8, day 14 and day 28. (B) Muscle mass of mice at day 0, day 8, day 14 and day 28 after cardiotoxin injury. Graphs represent ratio of muscle mass on the total mass of mouse body. (C) Mean cross sectional area (CSA) of myofibers from AMPK $\alpha$ 1<sup>fl/fl</sup> (WT) and LysM<sup>cre/+</sup>;AMPK $\alpha$ 1<sup>fl/fl</sup> (LysMA) mice treated either with PBS or DEX at day 14 after cardiotoxin injury. (D) Graph represents myofiber distribution at day 14. (E) CSA of muscles from WT and LysMA mice treated either with PBS or DEX at day 28 after cardiotoxin injury. (F) Graph represents myofiber distribution at day 28. \*  $p < 0.05$ , \*\*  $p < 0.01$ , \*\*\*  $p < 0.001$ . LysMA PBS versus LysMA DEX (\$  $p < 0.05$ , \$\$  $p < 0.01$ , \$\$\$  $p < 0.001$ ); WT DEX versus LysMA DEX (£  $p < 0.05$ , ££  $p < 0.01$ , £££  $p < 0.001$ ).

---

### ***GC treatment impacts the maturation of myofibers by modulating the expression of Myosin Heavy Chains in a macrophage-AMPK $\alpha$ 1 way***

One valuable indicator to analyze the efficiency of skeletal muscle regeneration is to measure the number of necrotic myofibers. Usually, a persistence of necrotic myofibers is a hallmark of an impaired regeneration. No differences in the number of necrotic myofibers were observed at day 8 between the groups. However, the number of necrotic myofibers was increased by 3-fold in PBS-treated LysMA mice as compared with PBS-treated WT mice at day 14 after injury ( $p < 0.05$ ) (Figure 7A), confirming the results of Mounier et al. in 2013.

Sarcoplasm contains myosin heavy chains (MHC), which compose the contractile apparatus. During skeletal muscle regeneration, the first MHC expressed in new regenerating myofibers is the embryonic MHC, an immature form of MHC (embMHC). embMHC is replaced later by mature forms of MHCs such as MHCI (slow-twitch, oxidative), MHCIIa (fast-twitch, oxidative), MHCIIb (fast-twitch, glycolytic) and MHCIIx (fast-twitch, glycolytic), which are associated with muscle function (Schiaffino, 2018). We first measured the number of myofibers expressing embMHC. While no differences were found at day 8 between LysMA PBS-treated group as compared with WT PBS-treated group, at day 14, a 2-fold increase of embMHC<sup>pos</sup> myofibers was measured as compared with WT PBS ( $p = 0.058$ ) indicating that maturation of myofibers was slower in LysMA PBS animals. This result confirmed data from Mounier et al. in 2013 showing that regeneration is delayed in LysMA mice. At day 8 after injury, the number of embMHC<sup>pos</sup> myofibers was decreased by DEX treatment in WT mice (-13%,  $p < 0.01$ ), while at day 14 no differences were observed between WT PBS and WT DEX (Figure 7B), suggesting that DEX may have accelerated myofiber maturation. In LysMA, we did not find a decrease of

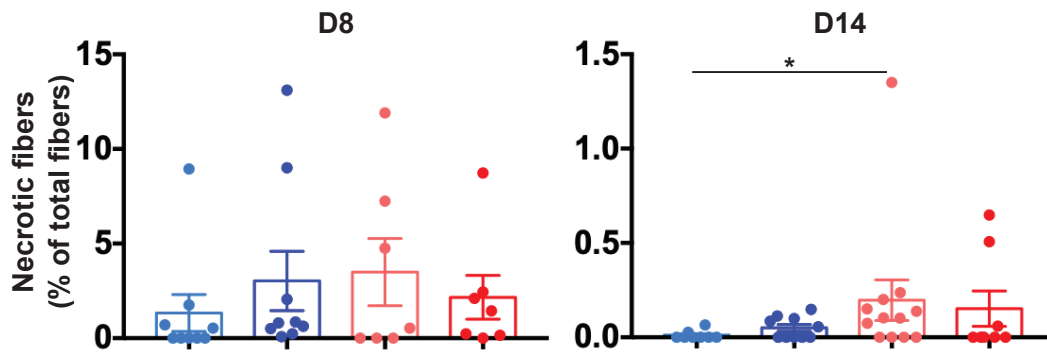
embMHC<sup>pos</sup> myofibers between LysMA PBS and LysMA DEX groups (Figure 7B), suggesting that DEX had no effect on myofiber maturation when AMPK $\alpha$ 1 is absent in macrophages. At day 14, the number of embMHC<sup>pos</sup> myofibers was higher in LysMA DEX as compared with WT PBS-treated group (+10%,  $p<0.05$ ) and WT-DEX treated group (+8.5%,  $p<0.05$ ), indicative of higher number of immature myofibers. These data show that a single DEX injection induced the maturation of muscle fibers during skeletal muscle regeneration in a macrophage AMPK $\alpha$ 1-dependent manner. At day 28, embMHC<sup>pos</sup> myofibers were barely detectable in all groups (Figure 7B).

Then, we investigated the distribution of adult myosins in TA muscle at day 28 after injury (Figure 7C). MHCIIa, MHCIIb and MHCIIX were detected in TA muscle in each group whereas almost no MHCI myofiber was observed. No effect of DEX treatment was observed on WT mice. A decrease of the expression of MHCIIa (-5 %,  $p<0.05$ ) and an increase of MHCIIb (+9 %,  $p<0.001$ ) was observed in LysMA mice as compared with WT (Figure 7C). DEX treatment reversed the phenotype and triggered an increase of the expression of MHCIIa (+11 %,  $p<0.001$ ) and a decrease of the expression of MHCIIb (-12 %,  $p<0.001$ ) in LysMA mice (Figure 7C). These results suggest that DEX treatment modulated maturation of myofibers *via* AMPK $\alpha$ 1 in macrophages.

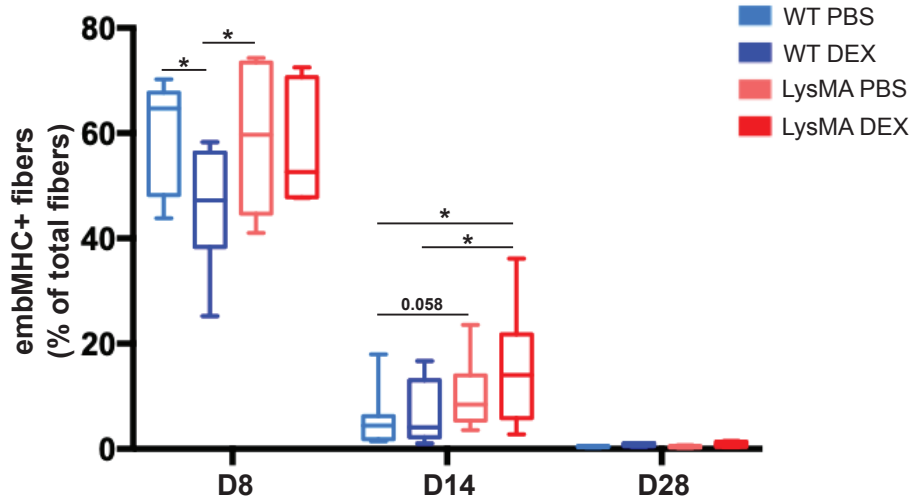
---

**Figure 7. GC treatment modulates the maturation of myofibers by altering the expression of myosins through AMPK $\alpha$ 1 in macrophages. (A)** Percentage of necrotic myofibers at day 8 and day 14 after cardiotoxin in *Tibialis Anterior* (TA) muscles assessed by immunofluorescence. **(B)** Percentage of myofibers expressing embryonic myosin heavy chain (embMHC) at day 8, day 14 and day 28 after cardiotoxin injection in TA muscle. **(C)** Percentage of myofibers expressing the adult MHCI, MHCIIa, MHCIIb or MHCIIX in section of TA muscles at day 28 after cardiotoxin injection. \*  $p<0.05$ , \*\*  $p<0.01$ , \*\*\*  $p<0.001$

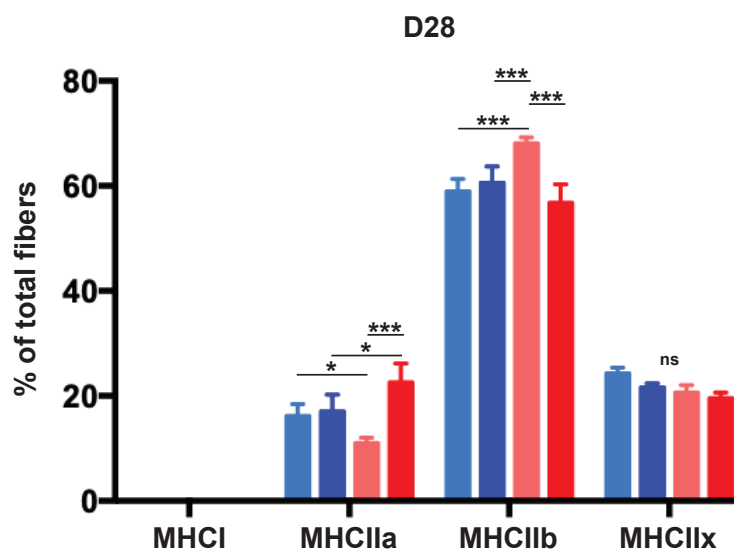
**A**



**B**



**C**



## DISCUSSION

In this study, the results showed that AMPK $\alpha$ 1 was required to induce the phenotype switch of macrophages from the pro-inflammatory status toward the anti-inflammatory status induced by GCs. AMPK $\alpha$ 1<sup>-/-</sup> macrophages exposed to GCs did not acquire the anti-inflammatory profile *in vitro*. Moreover, AMPK $\alpha$ 1 was required in macrophages to drive GC signaling *in vivo*. Mice lacking AMPK $\alpha$ 1 in macrophages treated with DEX presented an increased number of small myofibers with modifications of myosin heavy chain composition indicating an altered skeletal muscle regeneration ([Figure 9](#)).

AMPK $\alpha$ 1 activation is essential for the macrophage transition phenotype (Mounier et al., 2013). We first demonstrated in this study that GCs induced AMPK $\alpha$ 1 phosphorylation, which is a *sine qua non* requirement for AMPK $\alpha$ 1 activation and, for a part, the phenotype transition of macrophages. While activation of AMPK $\alpha$ 1 by GCs was shown for the first time in macrophages at the cellular level, our results are in accordance with other studies reporting a similar effect of GCs in tissues. Indeed, GC exposure induces AMPK $\alpha$ 1 phosphorylation in tissues such as hypothalamus (Liu et al., 2014; Christ-Crain et al., 2008), liver (Christ-Crain et al., 2008), arcuate nucleus (Shimizu et al., 2008) and skeletal muscle (Liu et al., 2016). However, our results did not give evidence about the mechanism by which GCs induced AMPK activation. AICAR treatment suggested a synergistic mechanism with DEX but we were not able to confirm this synergistic mechanism by cotreating the cells with 991 (specific AMPK activator) and DEX. Moreover, immunofluorescence experiments of the inflammatory status of macrophages did not show any synergistic effects of AICAR and DEX. AICAR is not a specific activator of AMPK. It is an AMP mimetic, which simulates an increase of AMP level in cell. Because 991 and AICAR do not act by the same mechanisms, it could explain the different results obtained with these 2 compounds. For immunofluorescence experiments of the inflammatory status of macrophages, several hypotheses can explain the absence of synergy. The phenotype characterization of macrophages by immunofluorescence is a robust method to characterize the number of macrophages expressing inflammatory markers but with a poor sensibility. Only the positive cells were counted, therefore excluding cells expressing markers to a lesser extent, *i.e.*, under the threshold of detection. If the number of cells expressing markers at a low level was increased but not that of the highly positive cells, this technic could miss variations of expression between AICAR or DEX alone and AICAR+DEX conditions. On the

other hand, the absence of synergy between AICAR and DEX is also a possibility. These 2 pathways could be involved in the same final common pathway that regulates the phenotype switch. In this way, the activation of this common signaling pathway by one or the other compound would be sufficient to trigger the switch and no additive effects are therefore observed. Furthermore, it was suggested in muscle cells that GCs induce ATP deprivation after several hours, which consequently activates AMPK (Liu et al., 2016). However, the Liu study did not present experiments using shorter time points (*e.g.*, 1 h). So, deeper investigations are required to explain the mechanistic pathway.

We demonstrated that AMPK activation and GCs both induced the phenotype switch of macrophages toward an anti-inflammatory phenotype in resting macrophages. WT macrophages treated either with DEX or 991 increased the expression of the anti-inflammatory markers CD206 and TGF $\beta$  (Figure 2). However, to mimic physiological conditions *in vitro*, we developed the model of muscle-DAMPs. Muscle-DAMPs are protein lysates from ischemia/reperfusion injured muscle before the massive infiltration of immune cells. While the exact composition of muscle-DAMPs is not known, one can suggest that alarmins molecules are present in this lysate. Indeed, molecules released from damaged cells are known to activate macrophages such as HMGB1 (Su et al., 2016). We confirmed by immunofluorescence analysis of inflammatory markers that muscle-DAMPs acted as a pro-inflammatory signal on macrophages. In this model of sterile inflammation, our study demonstrated that the acquisition of the anti-inflammatory phenotype of macrophages induced by DEX was regulated by AMPK $\alpha$ 1 (Figures 2, 3). Furthermore, the function of macrophages was also affected. We showed that the functional acquisition of the anti-inflammatory properties of macrophages treated by DEX was also AMPK $\alpha$ 1-dependent as AMPK $\alpha$ 1<sup>-/-</sup> macrophages treated with DEX did not sustain myogenesis. Moreover, we can also note that AMPK $\alpha$ 1<sup>-/-</sup> macrophages treated with DEX induced myoblast proliferation as compared with untreated condition, revealing not a partial failure but a complete incapacity of AMPK $\alpha$ 1<sup>-/-</sup> macrophages to switch into anti-inflammatory macrophages upon DEX treatment. Thus, these data on functional role of macrophages treated with DEX are in accordance with the phenotypic analysis of macrophages. In the absence of AMPK $\alpha$ 1, macrophages were not able to switch their phenotype upon DEX stimulation and did not acquire their functional properties. These results showed a central role of AMPK $\alpha$ 1 in GC signaling pathway in macrophages.

We can note that GR localization was not affected by the absence of AMPK $\alpha$ 1 in macrophages treated with DEX. The translocation of GR into the nucleus is necessary for transcriptional activity of this receptor/transcription factor. However, this is not the only requirement for its transcriptional activity. GR can be phosphorylated on several residues by several kinases and the phosphorylation state can modulate its activity and its target genes (Kino, 2018). Jan Tuckermann's lab investigated the phosphorylation of GR in WT and AMPK $\alpha$ 1<sup>-/-</sup> macrophages upon DEX treatment. They showed that phosphorylation of GR on Ser211 upon DEX treatment was reduced in AMPK $\alpha$ 1<sup>-/-</sup> macrophages (Figure 8). Thus, even if GR translocated to the nucleus in AMPK $\alpha$ 1<sup>-/-</sup> macrophages, its phosphorylation state was affected by the absence of AMPK $\alpha$ 1 suggesting that its transcriptional activity could be modified. To confirm this hypothesis, RNAseq experiments are ongoing to analyze the genes expressed by WT and AMPK $\alpha$ 1<sup>-/-</sup> macrophages upon 991 and DEX treatment. These experiments should give us more information about GR transcriptional activity in AMPK $\alpha$ 1<sup>-/-</sup> macrophages.

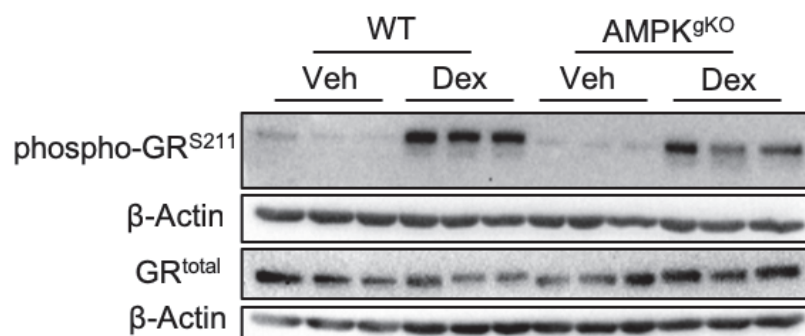


**Figure 8. AMPK $\alpha$ 1 is required for GR phosphorylation on Ser211 induced by DEX in macrophages.** AMPK $\alpha$ 1<sup>-/-</sup> macrophages (=AMPK<sup>gKO</sup>) were less sensitive to DEX-induced phosphorylation on Ser211. Experiment performed by Giorgio Caratti from Jan Tuckermann's lab (Ulm, Germany).

We focused on the role of GCs in sterile inflammation, *i.e.*, during skeletal muscle regeneration. Cardiotoxin injury provides an excellent model to study inflammation as it is well-characterized and reproducible (Hardy et al., 2016). In this model, the phenotype switch of macrophages occurs mainly between day 2 and 3 after injury. We demonstrated that DEX treatment administrated before day 3 after cardiotoxin injury was deleterious for skeletal muscle regeneration. These results are in accordance with previous studies showing that blunting the pro-inflammatory phase impairs skeletal muscle regeneration (Perdiguero et al.,

2011; Cheng et al., 2008). At day 3, most macrophages have switched toward an anti-inflammatory status. We decided to treat the mice from this time point to avoid blunting the pro-inflammatory phase and to sustain the resolution of inflammation. Mice were treated for 5 days until the end of the inflammatory phase, *i.e.*, at day 8. We confirmed that regeneration was delayed in LysMA PBS group as compared with WT PBS (Mounier et al., 2013). Moreover, the results indicated that daily DEX treatment delayed skeletal muscle regeneration, associated with a decreased in muscle mass and an increase of the number of small myofibers. GC long exposure is known to induce muscle atrophy by a direct effect on myofibers (Schakman et al., 2013). For example, GCs inhibit anabolism by inhibition of Pi3K/AKT/mTOR pathway and induce catabolism by induction of FOXO1, 3a transcription factors, which stimulate the expression of atrogenes (such as Murf1) in muscle cells (Schakman et al., 2013). A recent study also showed that GC treatment administrated during regeneration impairs skeletal muscle regeneration (Otrocka-Domagala et al., 2019). We suggest that GC treatment as short as 5 days directly impact muscle cells. Interestingly, LysMA mice treated with DEX presented a higher number of small fibers than other groups even at D28 suggesting additional effects of AMPK $\alpha$ 1 deficiency in macrophages and DEX-driven atrophy of myofibers. Thus, 5 days-DEX treatment drastically impaired skeletal muscle regeneration in absence of AMPK $\alpha$ 1 in macrophages.

Therefore, in order to push the phenotypic switch of macrophages while avoiding adverse effects of GCs on myofibers, we treated the mice with a single injection of GCs at day 3 after injury. A recent study showed in dystrophic mice that single weekly dose of DEX was sufficient to keep anti-inflammatory properties of GCs and to avoid GC side effects when compared with daily GC administration (Quatrocelli et al, 2017). First, at day 28, muscle mass of LysMA PBS-treated animals was significantly lower than WT confirming the results of Mounier et al. in 2013. Muscle mass was decreased in LysMA DEX-treated animals with a higher number of small myofibers indicating that DEX induced deleterious effects on LysMA mice. Second, we questioned other parameters than CSA as indicators of muscle fiber regeneration and maturation. We investigated the expression of embMHC in muscle, which reflects the number of immature regenerating myofibers. The number of embMHC<sup>POS</sup> myofibers was higher in LysMA PBS mice as compared with WT PBS as well as the number of necrotic myofibers confirming the results of Mounier et al. in 2013 indicating an impairment of regeneration. The number of embMHC<sup>POS</sup> was decreased in WT mice treated with DEX at day 8, suggesting that



regeneration was improved by DEX treatment. A decreased number of embMHC<sup>pos</sup> myofibers at day 8 was an evidence of accelerated regeneration with DEX in WT mice as the number of “immature” myofibers was decreased. Kinetics of embMHC expression was different in LysMA mice treated with DEX. The decreased number of embMHC<sup>pos</sup> myofibers was not observed in LysMA treated by DEX at day 8, and higher embMHC<sup>pos</sup> myofibers were observed at day 14. These results indicate that GCs improved regeneration in a macrophagic AMPK $\alpha$ 1 dependent manner.

Finally, we found that macrophages modulated the expression of adult myosin heavy chain (MHC) in TA muscle after muscle injury in an AMPK $\alpha$ 1-dependent manner. Moreover, DEX-treated macrophages differentially regulate the expression of MHC through AMPK $\alpha$ 1. To our knowledge, there is no report in the literature indicating that macrophages are able to regulate myosin expression in skeletal muscle, directly or indirectly. Few molecules were shown to trigger changes of the composition of MHCs in skeletal muscle. For example, injection of TGF $\beta$  in the slow-twitch *soleus* muscle during regeneration upregulates the expression of MHCIIa and decreases the expression of MHCI (Noirez et al., 2005). However, in the fast-twitch *extensor digitorum longus* (EDL) muscle, inhibition of TGF $\beta$  induced similar effects by increasing the number of MHCIIa myofibers (Noirez et al., 2005). Thus, depending on which muscle type is considered, either injection or inhibition of TGF $\beta$  modulate MHC expression, but the mechanism by which TGF $\beta$  acts remains to be elucidated. It is to note that TGF $\beta$  expression was not modified by DEX treatment in our *in vitro* experiments in AMPK $\alpha$ 1<sup>-/-</sup> macrophages (Figures 2, 3) indicating that TGF $\beta$  may not be the candidate to explain the difference in MHC expression in LysMA regenerating muscle. Supplemented food with arginine was also found to modulate myosin expression in normal muscle toward a slow twitch phenotype (Chen et al., 2018). But, to our knowledge, no study demonstrated that macrophages secrete arginine during regeneration. More generally, the literature about the regulation of myosin expression is scant, and concerns only the MHCI *versus* the MHCII balance and not MHCIIa *versus* MHCIIb. The main difference between MHCIIa and MHCIIb myofibers is their metabolism. MHCIIa myofibers have a more oxidative metabolism whereas MHCIIb myofibers have a glycolytic metabolism. We were not able to find a study reporting balanced or unbalanced expression between MHCIIb and MHCIIa in skeletal muscle. Finally, expression of adult myosins being modulated by the motoneuron which innervates each myofiber (Schiaffino and Reggiani, 2011), another hypothesis could be that macrophages

differently modulate re-innervation of the myofiber by acting directly on motoneurons. One study shows that macrophages are found close to neuro-muscular junction in amyotrophic lateral sclerosis and could play a role in motoneuron survival (Van Dyke et al., 2016). Also, in peripheral nerve repair, several macrophages profiles were described (pro- and anti-inflammatory) associated with secretion of specific factors required for nerve repair (Tomlinson et al., 2016). Macrophages could play a role in re-innervation of myofibers after injury, which could modulate myosin expression in the myofiber. However, here again, there is no study showing a role of macrophages on the re-innervation during skeletal muscle regeneration. Thus, further investigations are required to explain the link between macrophage inflammatory status and MHC expression by the myofiber.

To conclude, our *in vitro* results clearly demonstrated that AMPK $\alpha$ 1 was required in macrophages for anti-inflammatory signaling induced by GCs for the acquisition of both the anti-inflammatory phenotype and function towards myogenesis. We have also shown that DEX induced adverse effects in the regenerating skeletal muscle in the absence of AMPK $\alpha$ 1 in macrophages, as reported by myofiber alteration. While our study demonstrates the requirement of AMPK $\alpha$ 1 for GC-induced effects in macrophages, the molecular mechanisms linking the 2 pathways are still unresolved. We are currently investigating several hypotheses (see Perspectives section). Nevertheless, a link between GCs and AMPK $\alpha$ 1 for the resolution of inflammation during tissue repair is of interest for muscle physiopathology. Our study indicates that GC treatment must be operated at a specific time after injury to be beneficial. Also, both GC treatment (Quattrocelli et al., 2017) and AMPK activation (Juban et al., 2018) are beneficial for muscle dystrophies, though reduction of chronic inflammation. This suggests the possibility of combining the 2 treatments in order to reduce GC dosage, and then side effects.

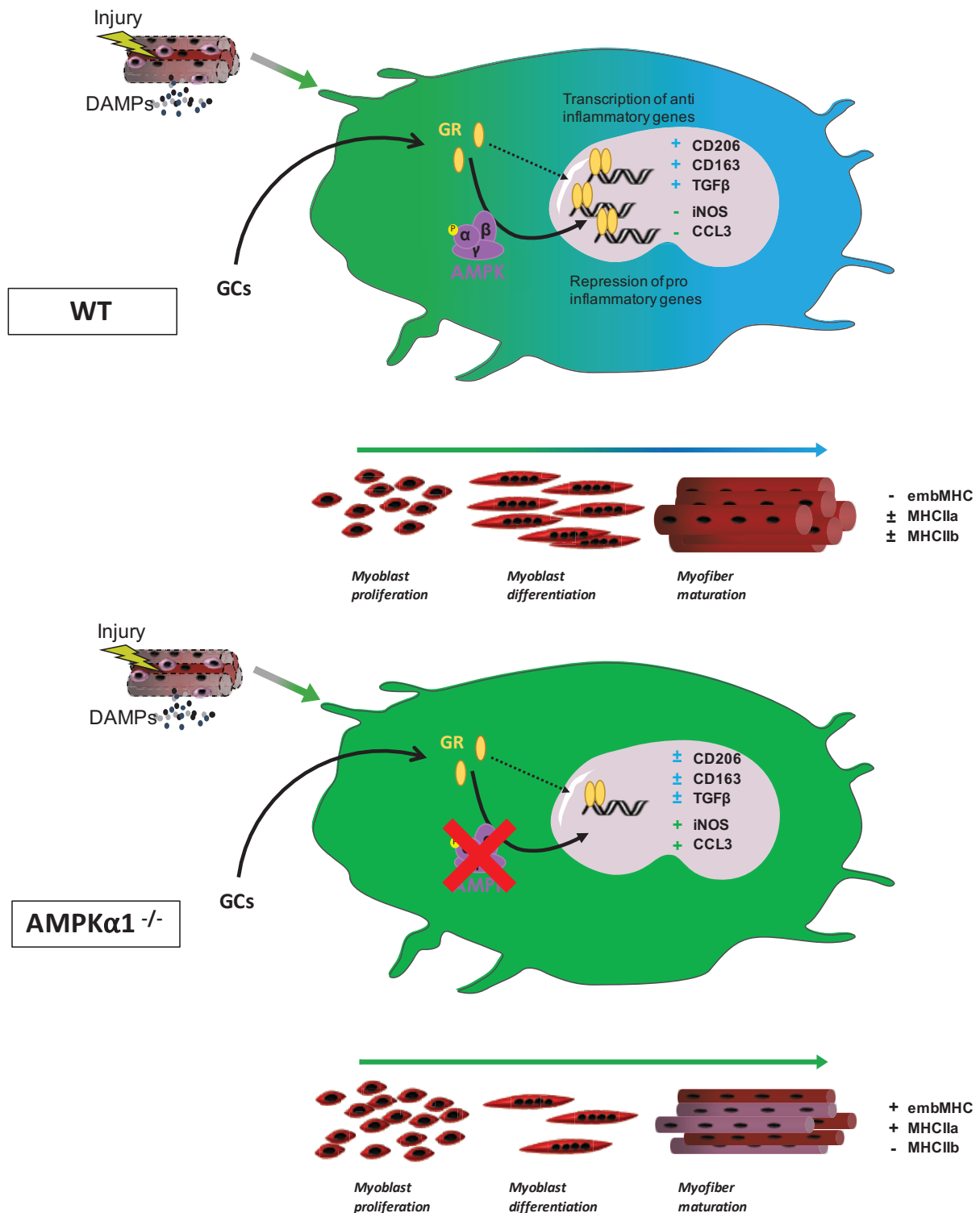


**Figure 9. AMPK $\alpha$ 1 is required for anti-inflammatory glucocorticoid (GC) signaling in macrophages during skeletal muscle regeneration.** GC treatment on WT macrophages induce the anti-inflammatory status which increase myoblast differentiation and maturation of myofiber (e.g. decrease embMHC expression). Conversely, GC does not induce the anti-inflammatory status of AMPK $\alpha$ 1<sup>-/-</sup> macrophages. Myoblast fusion is not induced and maturation of myofiber is altered.

## **STUDY #2**



## **Annexin A1 drives macrophage skewing towards a resolving phenotype to accelerate the regeneration of muscle injury through AMPK activation**

Simon McArthur<sup>1,#</sup>, Thomas Gobbetti<sup>2,#</sup>, Gaëtan Juban<sup>3,#</sup>, Thibaut Desgeorges<sup>3</sup>, Marine Theret<sup>3</sup>, Julien Gondin<sup>3</sup>, Juliana E Toller-Kawahisa<sup>4</sup>, Mauro Perretti<sup>2,5\*</sup> and Rémi Mounier<sup>3\*</sup>

During my PhD, we developed other aspects of macrophage phenotype skewing. The group of Mauro Perretti showed few years ago that annexin A1 is important for macrophage polarization (Perretti and D'Acquisto, 2009). Few years later, our lab highlighted the role of AMPK $\alpha$ 1 in the phenotype switch of macrophages (Mounier et al., 2013). Because annexin A1 and AMPK activation both induce the anti-inflammatory status of macrophages, it was hypothesized that annexin A1 and AMPK could be linked to induce the phenotype switch of macrophages. I was involved in this project to perform: i) immunofluorescence on macrophages to analyze their phenotype after annexin A1 treatment; ii) co-culture experiments to analyze the effect of molecules secreted by macrophages after annexin A1 treatment on myogenesis; and iii) *in vivo* experiments of muscle injury in the Mauro Perretti's lab in London. Interestingly, the promoter of annexin A1 gene contains a Glucocorticoid Response Element site and so, the expression of this gene can be regulated by Glucocorticoids (see Perspectives section).

# **Annexin A1 drives macrophage skewing towards a resolving phenotype to accelerate the regeneration of muscle injury through AMPK activation**

Simon McArthur<sup>1,2,#</sup>, Thomas Gobbetti<sup>2,#</sup>, Gaëtan Juban<sup>3,#</sup>, Thibaut Desgeorges<sup>3</sup>, Marine Theret<sup>3</sup>, Julien Gondin<sup>3</sup>, Juliana E Toller-Kawahisa<sup>2,4</sup>, Christopher P Reutelingsperger<sup>5</sup>, Mauro Perretti<sup>2,6\*</sup> and Rémi Mounier<sup>3\*</sup>

<sup>1</sup>Institute of Dentistry, Barts & the London School of Medicine & Dentistry, Queen Mary, University of London, Blizard Institute, Newark Street, London E1 2AT, United Kingdom

<sup>2</sup>William Harvey Research Institute, Barts & the London School of Medicine & Dentistry, Queen Mary, University of London, Charterhouse Square, London EC1M 6BQ, United Kingdom

<sup>3</sup>Institut Neuromyogène, CNRS UMR5310, INSERM U1217, Université Claude Bernard Lyon1, France

<sup>4</sup>Department of Biochemistry & Immunology, Ribeirao Preto Medical School, University of Sao Paulo, Avenida Banderiantes, 3900, Ribeirao Preto, Sao Paulo 14049-900, Brazil

<sup>5</sup>Department of Biochemistry, Maastricht University, Cardiovascular Research Institute Maastricht, Maastricht, The Netherlands

<sup>6</sup>Centre for Inflammation and Therapeutic Innovation, Queen Mary, University of London

#share first authorship

\* share senior authorship

Correspondence: s.mcarthur@qmul.ac.uk, m.perretti@qmul.ac.uk and remi.mounier@univ-lyon1.fr

## Summary

Understanding the circuits that promote an efficient resolution of inflammation is crucial to deciphering the molecular and cellular processes required to promote tissue repair. Macrophages play a central role in the regulation of inflammation, resolution and repair/regeneration. Using a model of skeletal muscle injury and repair, herein we identify Annexin A1 (AnxA1) as the extracellular trigger of macrophage skewing towards a pro-reparative phenotype. Brought into the injured tissue initially by migrated neutrophils, and then over-expressed in infiltrating macrophages, AnxA1 activates FPR2/ALX receptors and the downstream AMPK signalling cascade leading to macrophage skewing, dampening of inflammation and regeneration of muscle fibres. Mice lacking AnxA1 in all cells or in myeloid cells only display a defect in this reparative process. *In vitro* experiments recapitulated these properties, with AMPK null macrophages lacking AnxA1-mediated polarization. Collectively, these data identify the AnxA1/FPR2/AMPK axis as a novel pathway in skeletal muscle injury regeneration.

**Keywords:** macrophage switch, resolution of inflammation, skeletal muscle homeostasis



## Introduction

An efficient inflammatory response is a necessary component of the reaction to injury or infection, but it is equally critical for this inflammatory response to be terminated in a timely and appropriate manner, enabling the restoration of tissue homeostasis (Perretti et al., 2017; Serhan, 2014). Indeed, chronic inflammation that results from failure of resolution represents a major contributing factor to a multitude of pathologies, from arthritis to sepsis to dementia (Perretti et al., 2015; Tabas and Glass, 2013).

An inflammatory reaction consists of the co-ordinated activity of numerous cells and soluble mediators, but a central role is played by macrophages. These cells, whether resident in the tissue or recruited from circulating monocyte populations, are amongst the first responders to pathogen- or damage-associated molecular patterns, initiating endothelial activation and neutrophil recruitment (Davies and Taylor, 2015). Beyond their roles as sentinels, macrophages are important drivers of the progression of an inflammatory response, acting to clear pathogens, effete cells and debris by phagocytosis (Mantovani et al., 2013), serving as antigen presenting cells to recruit the adaptive arm of the immune response (Motwani and Gilroy, 2015), and ultimately enabling processes of tissue repair and resolution (Lucas et al., 2010; Troidl et al., 2009). That one cell type is able to achieve this diverse array of functions is due in large part to their remarkable degree of phenotypic plasticity, with macrophages existing in a wide variety of forms along a spectrum running from a largely pro-inflammatory state, often indicated as M1, to a primarily non-phlogistic and pro-resolving phenotype, termed M2 (Murray et al., 2014).

A number of factors promoting this phenotypic transformation have been studied including exposure to anti-inflammatory cytokines such as interleukin (IL)-10 and IL-4, and the phagocytic removal of cell debris, although a complete description of the underlying mechanisms is lacking (Martinez and Gordon, 2014). We and others have identified a key role for the intracellular signalling pathway governed by AMP-activated protein kinase (AMPK) (Chan et al., 2015; Mounier et al., 2013; Park et al., 2017). Activation of this pathway is required for efficient conversion of pro- to anti-inflammatory-type macrophages, and inhibition of such a response significantly attenuated recovery in a model of inflammatory skeletal muscle injury (Mounier et al., 2013). Whilst AMPK is undoubtedly important in the phenotypic conversion of macrophages during the course of an inflammatory reaction, the nature of the extracellular trigger(s) for its stimulation remain unclear.

The protein annexin A1 (ANXA1) (Lim and Pervaiz, 2007; Perretti and D'Acquisto, 2009), is a major driver of inflammatory resolution, promoting neutrophil apoptosis (Solito et al., 2003), non-phlogistic monocyte recruitment (McArthur et al., 2015) and macrophage efferocytosis (Dalli et al., 2012; Scannell et al., 2007). We have recently reported that endogenous ANXA1 is critical for the time-dependent regulation of macrophage phenotype in a murine model of fatty liver disease (Locatelli et al., 2014): animals lacking ANXA1 expression exhibited enhanced liver inflammation and fibrosis, associated with prolonged macrophage pro-inflammatory phenotype. Similarly, ANXA1 promotes an anti-inflammatory macrophage phenotype in an *in vitro* model of tumour growth (Moraes et al., 2017).

Against this background, we applied a well-characterised model of skeletal muscle injury (Arnold et al., 2007; Varga et al., 2013; Varga et al., 2016a) to test the hypothesis that ANXA1 and its receptor FPR2/ALX could be the upstream trigger of AMPK activation, and hence be a major driver of the pro-to anti-inflammatory macrophage phenotype shift, promoting inflammatory resolution and the restoration of skeletal muscle tissue homeostasis.

## Results

### *Annexin A1 and Fpr2/3 null mice show impaired recovery from skeletal muscle injury*

To investigate the role of ANXA1 and its receptor FPR2/ALX (in humans, or the orthologue Fpr2/3 in mice) in the control of macrophage phenotype we first utilised the murine model of cardiotoxin-induced *Tibialis Anterior* (TA) injury, a model characterised by necrotic tissue damage and extensive macrophage activity (d'Albis et al., 1988; Mounier et al., 2013). Analysis of immune cell infiltration in lesioned wild-type mice revealed a typical inflammatory profile, dominated by Ly6G<sup>+</sup> neutrophils for the initial post-lesioning period, supplanted by F4/80<sup>+</sup> macrophages from day 2 onwards (Suppl Fig 1A-B). Monitoring ANXA1 expression in the tissue revealed that while absent in uninjured tissue, the protein was primarily restricted to immune cells until day 2 post-lesioning, with regenerating muscle fibres displaying weak immunostaining from Day 7 (Suppl Fig 1A-B), as reported previously (Bizzarro et al., 2012). Whilst F4/80<sup>+</sup> murine macrophages expressed AnxA1 at all time-points examined (Suppl Fig 1B-C), the proportion of macrophages expressing its primary receptor, Fpr2/3, decreased over time, from approximately 95% at day 2 to 70% at day 7 and just 5% two weeks post-lesioning, even though significant numbers of macrophages were still detected in the tissue (Suppl Fig 2A-B). Importantly, expression of Fpr2/3 on muscle fibers was not apparent at any time-point examined (Suppl Fig 2A).

Whilst uninjured TA muscle weights were comparable between wild-type, AnxA1<sup>-/-</sup> and Fpr2/3<sup>-/-</sup> mice (Fig 1A-B, Suppl Fig 3A), recovery of muscle mass following administration of cardiotoxin was significantly reduced in AnxA1<sup>-/-</sup> and Fpr2/3<sup>-/-</sup> mice than in wild-type animals (Fig 1B). Histological analysis of muscles 28 days post-injury revealed significantly reduced myofiber cross-sectional area (CSA) and myonuclei *per fiber* (*i.e.* the result of differentiation and fusion of muscle stem cells) in AnxA1<sup>-/-</sup> and Fpr2/3<sup>-/-</sup> animals (Fig 1C-E). These outcomes are suggestive of impaired skeletal muscle regeneration, a notion confirmed by marked lipid accumulation in AnxA1<sup>-/-</sup> mice (Fig 1F). Analysis of immune cell infiltration by flow cytometry revealed that 2 days following cardiotoxin administration, approximately 60% of macrophages expressed a pro-resolving, anti-inflammatory phenotype (CD45<sup>+</sup>Ly6C/G<sup>neg</sup>F4/80<sup>hi</sup>) in wild-type mice, whilst AnxA1<sup>-/-</sup> and Fpr2/3<sup>-/-</sup> animals showed comparable levels of pro- (CD45<sup>+</sup>Ly6C/G<sup>hi</sup>F4/80<sup>low</sup>) and anti-inflammatory (CD45<sup>+</sup>Ly6C/G<sup>low</sup>F4/80<sup>hi</sup>) cells (Fig 1G, Suppl Fig 3B). Consequently, the resolution index (ratio of anti- to pro-inflammatory macrophages) of AnxA1<sup>-/-</sup> and Fpr2/3<sup>-/-</sup> mice was significantly lower than that of wild-type animals, indicative of a prolonged inflammatory response (Fig 1H). These results indicate that a proportion of pro-

inflammatory macrophages fail to convert to an anti-inflammatory phenotype at the time of resolution in the absence of AnxA1 or Fpr2/3.

#### *Macrophages are the major source of AnxA1 in lesion recovery*

The more pronounced effects of cardiotoxin in AnxA1<sup>-/-</sup> and Fpr2/3<sup>-/-</sup> mice indicate the existence of important regulatory functions for this pathway in skeletal muscle injury. However, while Fpr2/3 expression appears restricted to immune cells infiltrating the TA muscle (Suppl Fig 2), AnxA1 is expressed markedly by immune cells and to a lower extent by regenerating muscle fibres (Suppl Fig 1). As such, we deemed it important to define the primary cell source of this mediator in the repair process, a question we addressed using chimeric mice bearing wild-type muscle but AnxA1<sup>-/-</sup> bone marrow-derived leukocytes. Therefore, CX3CR1-GFP mice, which harbour GFP-expressing monocytes/macrophages were irradiated and transplanted with wild-type or AnxA1<sup>-/-</sup> derived bone marrow cells, prior to injection of cardiotoxin in the TA muscle (Fig 2A). Analysis of bone marrow populations at the time of euthanasia showed less than 1% of monocytes (CD115<sup>pos</sup> cells) expressed GFP, suggesting >99% engraftment efficiency with either wild-type or AnxA1<sup>-/-</sup> bone marrow (Fig 2B-C). Weight recovery was similar after wild-type or AnxA1<sup>-/-</sup> transplant (Suppl Fig 3C), but histological analysis of TA muscles 28-days post-CTX injury revealed that animals receiving AnxA1<sup>-/-</sup> bone marrow cells displayed a significantly reduced myofiber cross-sectional area than animals receiving wild-type bone marrow cells (Fig 2D-E). These data indicate that the defective regeneration quantified in AnxA1<sup>-/-</sup> muscle is a consequence of an intrinsic defect in myeloid, rather than stromal, cells.

#### *Exogenous ANXA1 can induce human macrophage phenotype conversion in vitro*

As our murine analyses indicate a potential role for AnxA1 in the polarization of macrophages from a pro-inflammatory to a pro-resolving/reparative phenotype, we investigated these effects *in vitro* using human PBMC-derived macrophages. An M1-like macrophage phenotype was induced by 24 h incubation with bacterial lipopolysaccharide (LPS) and  $\gamma$ -interferon (IFN $\gamma$ ), prior to addition of human recombinant ANXA1 (hrANXA1). Following hrANXA1 treatment, analysis of cell surface markers revealed a significant reduction in expression of the M1 marker protein major histocompatibility complex II (MHCII) (Fig 3A), accompanied by a significant increase in expression of the M2 marker protein CD206 (Fig 3B). These surface marker changes were mirrored by changes at the transcriptional level, with hrANXA1 treatment inducing a reduction in mRNA expression for the pro-inflammatory species *Tnfa* and *Nos2* paired with increased message of *Il-10* (Fig. 3C-E). No significant changes in *Tgfb1* expression were quantified (Fig. 3F). Together, these *in vitro* data support our *in*

*vivo* findings, providing evidence that ANXA1 application favours a pro-resolving macrophage phenotype.

The specificity of hrANXA1 action through its human receptor FPR2/ALX was then determined, to complement the *in vivo* observations made with *Fpr2/3<sup>-/-</sup>* mice lacking the orthologue of the human FPR2/ALX (Dufton et al., 2010). Intriguingly, we observed significant FPR2/ALX surface expression both in unstimulated human PBMC-derived macrophages and M1-phenotype cells, yet cell surface expression of the receptor was lost on cells stimulated towards an M2 phenotype with IL-4 (Suppl Fig. 4). These data are in agreement with the *in vivo* observation that *Fpr2/3<sup>-/-</sup>* is absent from macrophages that have infiltrated the injured muscle at Day 7 and beyond, that is, when a reparative cell phenotype has been acquired (Suppl Fig 2B-C). The functional engagement of FPR2/ALX was then confirmed through use of the selective antagonist WRW<sub>4</sub>. The modulatory effects of hrANXA1 on pro-inflammatory PBMC-derived macrophages (*i.e.* reduced surface MHCII expression and augmented surface CD206 expression) were lost in the presence of WRW<sub>4</sub> (Fig. 3G-H).

Together these experiments represent a clear *in vitro* counterpart to the effects observed in the muscle injury model, showing the key role of ANXA1 acting through FPR2/ALX to drive a shift in macrophage phenotype towards a pro-resolving and reparative polarization.

#### *Exogenous ANXA1 treatment stimulates AMPK activation through FPR2/ALX*

The enzyme 5'-adenosine monophosphate-activated protein kinase, AMPK, plays a critical role in macrophage phenotype skewing and is necessary for efficient regeneration after skeletal muscle damage (Mounier et al., 2013). We queried whether this signalling pathway would underlie the effects of hrANXA1 upon human macrophage phenotype and indeed muscle repair *in vivo*.

Exposure of human PBMC-derived macrophages to hrANXA1 activated a number of components of the AMPK signalling pathway, promoting phosphorylation of Ca<sup>2+</sup>/calmodulin-dependent protein kinase II, AMPKα1 itself and its downstream effector acetyl-CoA carboxylase (Fig 4A-B). Interestingly, the phosphorylation of these proteins in macrophages only occurred to an appreciable degree following exposure to hrANXA1 for 30-60 min (Fig 4B-D), in contrast to early MAP kinase signalling previously reported in human monocytes (McArthur et al., 2015). That activation of AMPKα1 depended upon binding of hrANXA1 to FPR2/ALX was confirmed through analysis of the effects of the antagonist WRW<sub>4</sub>, which abrogated hrANXA1-evoked AMPKα1 phosphorylation in human

macrophages (Fig 4E). Analyses of murine bone marrow-derived macrophages from wild-type and *Fpr2/3<sup>-/-</sup>* animals confirmed the pivotal role of this receptor: whilst treatment with hrANXA1 induced phosphorylation of AMPK $\alpha$ 1 in wild-type cells, this response was absent in macrophages from *Fpr2/3<sup>-/-</sup>* mice (Fig 4F).

#### *AMPK activation is required for macrophage phenotype conversion induced by ANXA1*

We investigated the relationship between FPR2/ALX-mediated AMPK activation and the shift in macrophage phenotype induced by hrANXA1 treatment through analyses in primary bone marrow-derived macrophages taken from wild-type mice and animals lacking the key catalytic  $\alpha$ <sub>1</sub> subunit of AMPK (Jorgensen et al., 2005). Whilst treatment of wild-type macrophages with hrANXA1 (10nM, 24h) reduced the percentage of macrophages positive for the pro-inflammatory markers iNOS and CCL3, this response was notably absent in cells from AMPK $\alpha$ 1<sup>-/-</sup> mice (Fig 5A). Correspondingly, hrANXA1 treatment augmented the proportion of wild type cells expressing the anti-inflammatory markers TGF $\beta$ 1 (notably at variance from human macrophages), CD163 and CD206, but this did not occur in cells lacking AMPK $\alpha$ 1 (Fig 5B). Together, these data indicate activation of AMPK $\alpha$ 1 as a key step in the macrophage phenotype shift induced by ANXA1.

To confirm these findings in human cells, we employed an RNA interference approach, transfecting primary PBMC-derived macrophages with three distinct siRNA constructs targeting the AMPK $\alpha$ 1 subunit (Fig. 5C). Treatment of M1-like pro-inflammatory macrophages for 6 h with 10 nM ANXA1 reduced expression of MHCII and augmented CD206 in mock transfected cells and in cells bearing a non-targeting siRNA construct; this effect was absent in cells transfected with any of three different siRNA constructs targeting human AMPK $\alpha$ 1 (Fig. 5D-E).

#### *Adult myogenesis is ANXA1-AMPK signalling dependent in vitro*

Together, these data from human and mouse macrophages make a compelling case that macrophage phenotype shifting can be induced through an ANXA1/FPR2/AMPK cascade. To investigate whether this process underlies differences in recovery from cardiotoxin-induced muscle lesions seen between wild-type and *Anx1<sup>-/-</sup>* and *Fpr2/3<sup>-/-</sup>* mice, we made use of an established model of *in vitro* muscle repair (Mounier et al., 2013; Varga et al., 2016b).

We employed an *in vitro* model of adult myogenesis in which conditioned medium from primary bone marrow-derived macrophages was used to stimulate primary murine myoblasts for 72h, quantifying the proportion of multinucleated myotubes (Fig. 5F). As such this *in vitro* setting

recapitulates the processes of adult myogenesis (activation, differentiation, migration and fusion of muscle cells) that occur during skeletal muscle regeneration (Mounier et al., 2013; Varga et al., 2016b). Conditioned medium from ANXA1-treated wild-type macrophages induced an increase in myotube fusion index (Fig 5G-I). This response was absent when myotubes were treated with conditioned medium from ANXA1-treated AMPK $\alpha$ 1<sup>-/-</sup> macrophages (Fig 5G-I).

## Discussion

The timely resolution of inflammation is a fundamental requirement for restoring homeostasis following infection or damage, with its failure being a significant contributory factor to numerous chronic inflammatory pathologies. Macrophages are key players in this process, given their ability to transition from generally pro-inflammatory to anti-inflammatory phenotypes (Motwani and Gilroy, 2015). Substantial effort has gone into deciphering the complex signals underpinning macrophage plasticity, with numerous soluble mediators having been implicated (Martinez and Gordon, 2014), but the mechanistic link between these factors and changes in phenotype remains poorly understood especially when investigated in specific tissue-restricted settings. In the current study, we have employed a well-characterised model of muscular injury and recovery (Mounier et al., 2013) to identify the ability of myeloid cell-derived ANXA1 to promote an anti-inflammatory macrophage phenotype, promoting resolution and tissue repair. Moreover, we show the actions of this protein to be mediated through the cell surface receptor FPR2/ALX and consequent activation of the intracellular signalling molecule AMPK, mechanistically linking external and intracellular pro-resolving signals governing macrophage phenotype.

These data reinforce the status of the ANXA1-FPR2/ALX pair as a major endogenous driver of inflammatory resolution, and add to its known roles in regulating neutrophil apoptosis (Solito et al., 2003), efferocytosis (Maderna et al., 2005; Scannell et al., 2007), and the recruitment of monocytes to inflammatory sites (Gobbetti et al., 2014; McArthur et al., 2015). Notably, despite muscle tissue itself beginning to express ANXA1 during tissue repair, as noted previously (Bizzarro et al., 2012), experiments with chimeric mice confirmed that the most important source of the protein to enable muscle repair remains the myeloid cells themselves. While the current studies do not permit conclusive determination of whether neutrophils or macrophages are the primary source of endogenous ANXA1 in the injured tissue, neutrophils contain substantial quantities of ANXA1 (Francis et al., 1992), which we have previously shown to be a major monocyte chemoattractant (McArthur et al., 2015) suggesting that the protein - produced at an early stage by and released from infiltrating neutrophils (Damazo et al., 2006) - may act to both recruit monocytes and promote a pro-resolving phenotype in resulting macrophages. Whatever the ultimate cellular source of ANXA1 however, the dependency upon the presence of ANXA1-expressing leukocytes for efficient macrophage phenotypic conversion is another example of how “the beginning programs the end” in resolution (Serhan and Savill, 2005), emphasising the finely tuned nature of the acute inflammatory response and its ability to encode its own termination.



Besides highlighting the role of ANXA1 as a regulator of inflammatory resolution (Leoni and Nusrat, 2016), these new data add further weight to the importance of its principal receptor FPR2/ALX in this process, identifying it as a conduit for induction of a pro-resolving macrophage phenotype through AMPK activation. It is notable that macrophage FPR2/ALX expression declined during the course of the response to muscular injury in our study; similarly, FPR2/ALX expression was significantly lower on M2 when compared with M1 phenotype cells *in vitro*. This change in receptor expression may reflect a strategy whereby once the macrophage is polarised towards a reparative phenotype, the utility of the FPR2/ALX signalling is then limited or unnecessary.

There is considerable redundancy in the mediators known to induce the conversion of macrophage phenotypes, as is perhaps to be expected given the importance of this process to the restoration of homeostasis after infection or damage, including immune complexes, apoptotic cells and a number of cytokines (Amici et al., 2017). Notably however, a significant proportion of the soluble pro-resolving mediators so far identified derive from the adaptive arm of the immune response, particularly from T<sub>H</sub>2 lymphocytes (Martinez and Gordon, 2014). Our data however, highlight the ability of signalling components derived from the innate side of the immune system to promote resolution in the absence of significant activation of adaptive mechanisms. Moreover, these results support the concept of how it is crucial to decipher which mediator and signal(s) are operative in specific tissues and organs to control macrophage polarization and the overall process of resolution and repair.

Our data are the first to associate activation of FPR2/ALX and the major regulator of cellular metabolism, AMPK, showing the central involvement of FPR2/ALX-stimulated AMPK activation in the induction of a pro-resolving macrophage phenotype. The precise mechanism linking AMPK activation with a change in phenotype is as yet unclear, but there is increasing evidence that changes in the metabolic status of immune cells can affect their inflammatory activity (O'Neill et al., 2016; Pearce and Pearce, 2013). Pro-inflammatory dendritic cells and T lymphocytes are characterised by high levels of glycolysis, akin to the Warburg shift described in cancer (Rodriguez-Prados et al., 2010), whereas immune cells with an anti-inflammatory or pro-resolving profile tend to exhibit greater mitochondrial respiration (Jha et al., 2015; Mounier et al., 2013; Tannahill et al., 2013). The mechanistic details of how such changes in metabolic phenotype relate to immune function, and indeed whether these differences reflect or drive immunophenotype is unclear (Van den Bossche et al., 2017), but it is notable that AMPK is a significant promoter of mitochondrial respiration and a regulator of glycolysis through the modulation of lactate dehydrogenase activity (Theret et al.,

2017), driven by its ability to respond to energy debt and an increased AMP:ATP ratio (Mounier et al., 2015). Activation of this pathway would therefore seem ideally placed to induce the metabolic phenotype most closely associated with anti-inflammatory macrophage activation, but this hypothesis requires further investigation.

AMPK is involved in different cellular mechanisms that regulate skeletal muscle homeostasis (Kjobsted et al., 2018). Our previous findings highlight the importance of crosstalk between AMPK and the mTOR signaling pathway for the control of muscle cell size in the adaptive response of skeletal muscle (Lantier et al., 2014; Lantier et al., 2010; Mounier et al., 2011; Mounier et al., 2009). Moreover, we have recently shown that AMPK $\alpha$ 1, activated following phagocytosis, is crucial for macrophage skewing from a pro- to an anti-inflammatory phenotype during resolution (Mounier et al., 2013), demonstrating that the CAMKKII/AMPK $\alpha$ 1 pathway within macrophages is required for proper and complete skeletal muscle regeneration. Anti-inflammatory macrophages promote myogenic differentiation and fusion (Saclier et al., 2013a; Saclier et al., 2013b; Varga et al., 2016b), a finding of importance for skeletal muscle regeneration where a sequential presence of pro- then anti-inflammatory cells is necessary for efficient regeneration process (Arnold et al., 2007; Varga et al., 2013). Therefore, the pro-resolving effect of ANXA1-AMPK signalling in macrophages is likely to be beneficial for skeletal muscle regeneration, as suggested by the positive effect of conditioned medium from ANXA1-treated macrophages on adult myogenesis *in vitro*.

In summary, we present here a novel mechanism governing the conversion of pro-inflammatory macrophages to a pro-resolving phenotype, linking leukocyte-derived ANXA1, FPR2/ALX and intracellular AMPK activation. This finding reinforces the position of the ANXA1-FPR2/ALX pathway as a pivotal regulator of inflammatory resolution, and suggests that it may represent a suitable target for therapeutic exploitation for the innovative treatment of pathologies characterised by chronic, non-resolving inflammation.

## **Acknowledgments**

This work was supported by CNRS, French Society of Myology and Wellcome Trust Programme Grant 086867/Z/08/Z. GJ was supported by Fondation pour la Recherche Medicale (Equipe FRM DEQ20140329495).

## **Author Contributions**

SM, TG, GJ, JG, MT & RM performed TA lesion and analysis, GJ & RM produced and analyzed chimeric mice, SM, TG and JETK performed analysis of human macrophages, GJ, JG, MT & RM performed analysis of AMPK $\alpha$ 1 null mice, TD & RM performed murine macrophages and myoblast fusion analysis, CPR produced and provided human recombinant ANXA1, SM, MP & RM conceived and designed the study, all authors contributed to the drafting of the paper.

## **Declaration of Interests**

## Figure Legends

### Figure 1. Non-redundant role of ANXA1 in cardiotoxin-induced muscle injury and repair.

(A) Experimental set-up. Acute injury was induced by cardiotoxin (CTX) injection in the *Tibialis Anterior* (TA) of Wild-Type, *Anx1<sup>-/-</sup>* and *Fpr2/3<sup>-/-</sup>* mice. Muscles were analysed 0, 7 and 28 days after injury. (B) TA mass normalised to mouse body weight. (C) Hematoxylin-eosin (HE) staining of muscles 28 days after injury. White bar = 50  $\mu$ m. (D-E) Myofiber cross-sectional area (D), number of nuclei *per* myofiber (E) and lipid accumulation (F) in muscles 28 days post-CTX injury. (G-H) Macrophage subtypes analysis 2 days post-CTX injury. Shown are the percentage of pro- and anti-inflammatory macrophages within the *F4/80<sup>+</sup>* population (G) and the resolution index (H). Results are mean  $\pm$  SEM of at least three animals. \**p*<0.05, \*\**p*<0.01 and \*\*\**p*<0.001 *versus* Wild-Type.

### Figure 2. Infiltrating myeloid cell-derived ANXA1 controls muscle repair.

(A) Experimental set-up. CX3CR1-GFP mice were irradiated and then transplanted with bone marrow cells isolated from Wild-Type or *Anx1<sup>-/-</sup>* mice. Bone marrow engraftment was checked on a blood sample after around 5 weeks. Then animals were injured in their *Tibialis Anterior* by cardiotoxin (CTX) injection and muscles analysed 0 or 28 days later. Engraftment was confirmed on the bone marrow of each animal on the day of sacrifice. (B-C) Representative FACS plots (B) and quantification (C) of the GFP<sup>+</sup> monocytes in the bone marrow of the sacrificed animals. (D-E) HE staining (D) and myofiber cross-sectional area (E) of TA muscles 28 days post-CTX injury. White bar = 50  $\mu$ m. Results are mean  $\pm$  SEM of at least four muscles. \**p*<0.05 *versus* Wild-Type.

### Figure 3. Exogenous hrANXA1 controls human and mouse macrophage polarization *in vitro*.

Human PBMC-derived macrophages were incubated for 24 hours with LPS+IFN $\gamma$  to promote an M1-like phenotype, prior to addition of human recombinant ANXA1 (hrANXA1, 10nM) for further 6 hours. (A-B) Mean Fluorescent Intensity (MFI) units measured by flow cytometry of MHCII pro-inflammatory (A) and CD206 anti-inflammatory (B) markers. Shown are MFI quantification (left panel) and representative FACS plots (right panel). (C-F) RT-qPCR analysis of *Tnfa* (C) and *Nos-2* (D) pro-inflammatory genes, and *Il-10* (E) and *Tgfb1* (F) anti-inflammatory genes. (G-H) MFI units as measured by flow cytometry of MHCII pro-inflammatory (G) and CD206 anti-inflammatory (H) markers after treatment by hrANXA1 in the presence or absence of the FPR2/ALX antagonist WRW<sub>4</sub> (10  $\mu$ M). Results are mean  $\pm$  SEM of at least three independent experiments. \**p*<0.05 *versus* Vehicle. #*p*<0.05 *versus* Control.

**Figure 4. The ANXA1/FPR2/ALX pathway activates the AMPK signalling cascade in human and murine macrophages.**

(A) Schematic representation of the ANXA1/FPR2/ALX signalling cascade. (B-D) Western blot analysis of pCaMK, pAMPK $\alpha$ 1 and pACC in human PBMC-derived macrophages treated with hrANXA1. Shown are representative blots (B) and quantification of pAMPK $\alpha$ 1 to AMPK $\alpha$ 1 (C) and pACC to ACC (D) ratios. (E) Representative western blot (top panel) and quantification (bottom panel) of pAMPK $\alpha$ 1 to AMPK $\alpha$ 1 ratio in human PBMC-derived macrophages treated by hrANXA1 in the presence or absence of 10  $\mu$ M WRW<sub>4</sub>. (F) Representative western blot (top panel) and quantification (bottom panel) of pAMPK $\alpha$ 1 to AMPK $\alpha$ 1 ratio in Wild-Type or Fpr2/3<sup>-/-</sup> murine bone marrow derived macrophages treated with hrANXA1. Results are means  $\pm$  SEM of at least three independent experiments. \*p<0.05, \*\*p<0.01 versus Vehicle.

**Figure 5. Null or reduced AMPK expression affects ANXA1-mediated macrophage polarization.**

(A-B) Primary macrophages derived from Wild-Type or AMPK $\alpha$ 1<sup>-/-</sup> mice were treated with 10nM hrANXA1 and the percentage of cells expressing the pro-inflammatory markers iNOS and CCL3 (A) and the anti-inflammatory markers TGFB1, CD163 and CD206 (B) was determined by immunofluorescence. (C-E) Human PBMC-derived macrophages were transfected by a non-targeting or three different AMPK $\alpha$ 1-targeting siRNAs and treated with 10 nM hrANXA1 for 24 h. AMPK $\alpha$ 1 protein level was determined by western blot (C) and the MFI units of the pro-inflammatory MHCII (D) and anti-inflammatory CD206 (E) markers were measured by flow cytometry. (F-I) Conditioned medium produced by murine macrophages was transferred onto murine primary myoblasts and their fusion was measured by immunofluorescence. (F) Experimental set-up. (G) Representative images of desmin (red) and Hoechst (blue) labelling of myoblast cultures. White bar = 50  $\mu$ m. (H-I) Fusion index calculated after desmin labelling. Shown are the means  $\pm$  SEM of the independent experiments (H) and the results of each individual replicate (I). Results are mean  $\pm$  SEM of at least three independent experiments. \*p<0.05 versus Mock or Control. <sup>##</sup>p<0.01 versus Wild-Type.

**Suppl Fig 1. Related to Figure 1. Immune cell recruitment and pattern of AnxA1 expression in cardiotoxin-induced muscle injury and repair.**

Immunofluorescence analysis of ANXA1 protein in *Tibialis Anterior* muscle after cardiotoxin injury. Images show co-localisation of ANXA1 protein with Ly6G<sup>+</sup> (A) and F4/80<sup>+</sup> (B) cells. White bar = 50  $\mu$ m. (C) Quantification of F4/80<sup>+</sup> ANXA1<sup>+</sup> cells in *Tibialis Anterior* (TA) muscle after cardiotoxin (CTX) injury.

**Suppl Fig 2. Related to Figure 1. Immune cell recruitment and Fpr2/3 expression in cardiotoxin-induced muscle injury and repair.**

Quantification of F4/80<sup>+</sup> ANXA1<sup>+</sup> cells in *Tibialis Anterior* (TA) muscle after cardiotoxin (CTX) injury (A), representative immunofluorescence analysis of Fpr2/3 protein in TA muscle after cardiotoxin (CTX) injury (B) and quantification of the percentage of F4/80<sup>+</sup> cells expressing Fpr2/3 (C). White bar = 50  $\mu$ m. Results are means  $\pm$  SEM of three animals. \*p<0.05 and \*\*\*p<0.001 *versus* Day 0.

**Suppl Fig 3. Related to Figure 1 and 2.**

(A) HE staining of non-injured Wild-Type and AnxA1<sup>-/-</sup> *Tibialis Anterior* (TA) muscles. White bar = 50  $\mu$ m. (B) Representative FACS plots of F4/80 and Ly6C/G markers in TA of Wild-Type, AnxA1<sup>-/-</sup> and Fpr2/3<sup>-/-</sup> mice 2 days post-cardiotoxin injury. (C) Weight follow-up, represented as percentage of Day 0, of mice after irradiation and bone marrow transplantation. Results are means  $\pm$  SEM of at least six animals. \*p<0.05 *versus* Day 0

**Suppl Fig 4. Related to Figure 3. FPR2/ALX expression varies following human macrophage polarization.**

Human primary macrophages were polarised into M1 or M2 macrophages with IFN $\gamma$  and IL-4, respectively (A-C) Flow cytometry analysis of FPR2/ALX expression. Shown are representative FACS plots (A), percentage of cells expressing FPR2/ALX (B) and FPR2/ALX MFI (C). (D) RT-qPCR analysis of FPR2/ALX mRNA level. Results are means  $\pm$  SEM of at least four independent experiments. \*p < 0.05 *versus* M0 (non-activated).

## STAR Methods

### Animals

All procedures were performed under the UK Animals (Scientific Procedures) Act, 1986 in the UK or in compliance with European legislation in France. Animal facilities are fully licensed by relevant national authorities and protocols have been validated by ethical committee. Male C57Bl/6 mice, male *alx/fpr2/3<sup>GFP/GFP</sup>* mice (referred to as *Fpr2/3<sup>-/-</sup>*) bearing a knocked-in green fluorescent protein (Dufton et al., 2010) and male *anxA1<sup>-/-</sup>* mice (Hannon et al., 2003), aged 10 weeks were used for *in vivo* experiments. Both transgenic strains were fully backcrossed onto a C57Bl/6 genetic background.

### Production of Recombinant Human Annexin A1

Human recombinant annexin A1 (hrANXA1) was produced by a prokaryotic expression system and purified essentially as described previously (Kusters *et al*, 2015). Briefly, cDNA for human ANXA1 was inserted into the expression vector pQE30Xa (Qiagen) and transfected into E.coli (#SG13009 pREP4, Novagen) which were then grown in Luria-Bertani broth medium supplemented with ampicillin (50 µg/ml, Roche), kanamycin (30 µg/ml, Thermofisher) and 0.5% glycerol. Protein overexpression was initiated by addition of 5mM isopropyl β-D-1-thiogalactopyranoside (Eurogentec) and proteins were purified by IMAC. Purity and homogeneity were assessed by SDS-PAGE, western blotting and MALDI-TOF/TOF analysis. Endotoxin was determined with the Endosafe-PTS (FDA-licensed LAL cartridge from Charles-River) according to the manufacturer's protocol. HrANXA1 contained < 0.2 unit endotoxin *per* mg hrANXA1 protein.

### Skeletal Muscle Injury

Skeletal muscle injury was caused by intramuscular injection of cardiotoxin (Latoxan) in the *Tibialis Anterior* (TA) muscle of male animals, as described previously (Mounier et al., 2013). Left TA muscles were injected with cardiotoxin (50 µl *per* TA, 12 µM); 1, 2, 7, 14 or 28 days post-lesioning animals were killed by exposure to CO<sub>2</sub>. TA were isolated and snap-frozen in liquid nitrogen-cooled isopentane for storage and later analysis.

### Murine Bone Marrow-Derived Macrophages

Bone marrow-derived macrophages (BMDMs) were prepared from adult male wild-type sv129/C57Bl6 and *Prkaa1<sup>-/-</sup>* mice (referred to as AMPKα1<sup>-/-</sup> (Jorgensen et al., 2005)). Mice were killed by cervical dislocation under isofluorane anaesthesia, and marrow was flushed from tibiae and femurs. Cells were plated, washed and grown for 6-7 days in DMEM High Glucose High Pyruvate, 20% heat inactivated fetal calf serum (ThermoFisher), 30% L929-cell conditioned medium, 1%

Amphotericin B (2.5 µg/ml, ThermoFisher) and 100 µg/ml streptomycin (ThermoFisher). For phenotypic characterisation, BMDMs were fixed for 10 minutes in 4% formaldehyde, permeabilized for 10 minutes in PBS with 0.5 % Triton X-100 and blocked for 1 hour in PBS with 4 % BSA. They were then labeled overnight at 4°C with anti-NOS2 (#ab15323, Abcam), anti-CCL3 (#ab32609, Abcam), anti-TGFβ1 (#ab64715, Abcam), anti-CD163 (#sc-20066, Santa-Cruz) and anti-CD206 (#sc-58987, Santa-Cruz), followed by incubation for 1 hour at 37°C with FITC- or Cy3-conjugated secondary antibodies (Jackson ImmunoResearch Inc). Cells were stained with Hoechst (Sigma) and mounted in Fluoromount (Interchim) and pictures were taken on an Axio Imager.Z1 (Zeiss) at 20X of magnification connected to a CoolSNAP MYO CCD Camera (Photometrics).

### ***In vitro* model of adult myogenesis**

Macrophages were obtained from bone marrow (BM) precursor cells that were cultured in DMEM containing 20% FBS and 30% conditioned medium of L929 cell line (enriched in CSF-1) for 7 days. Macrophages were activated with human recombinant annexin A1 for 3 days (10 nM) in DMEM containing 10% FBS. After the washing steps, serum-free DMEM was added for 24 hr to obtain macrophage-conditioned medium. Murine myogenic precursor cells (MPCs) were obtained from TA muscle and cultured using standard conditions in DMEM/F12 medium (Gibco Life Technologies) containing 20% heat inactivated Foetal Bovine Serum (FBS) and 2% G/Ultrosor (Pall Inc). MPCs were seeded at 30,000 cell/cm<sup>2</sup> on Matrigel (diluted 1:10) and incubated for 3 days with conditioned medium containing 2% heat inactivated horse serum. Cells were then incubated with an anti-desmin antibody (#ab32362, Abcam), followed by a Cy3-conjugated secondary antibody (Jackson ImmunoResearch Inc) (Mounier *et al*, 2013; Varga *et al*, 2016). Cells were stained with Hoechst (Sigma) and mounted in Fluoromount (Interchim) and pictures were taken on Axio Observer.Z1 (Zeiss) at 20X of magnification connected to a CoolSNAP HQ2 CCD Camera (Photometrics).

### **Bone Marrow Transplantation**

Total bone marrow cells were isolated by flushing the tibiae and femurs of 8- to 20-week-old donor mice (wild-type or AnxA1<sup>-/-</sup> males) with RPMI-1640 / 10% FBS. They were transplanted into 8- to 12-week-old recipient CX3CR1-GFP<sup>+/+</sup> males (monocytes/macrophages expressing GFP) previously lethally irradiated for 10 min with a dose of 0.85 Gy/min in an X-RAD 320 (Precision X-Ray). Total bone marrow cells were injected (10<sup>7</sup> cells diluted in 100 µL of RPMI-1640 / 50 % mouse serum) into the retro-orbital vein of recipient mice. After transplantation, mice were fed with ciprofloxacin (10 mg/kg/day) in the drinking water for 3-weeks. Engraftment efficiency was determined on peripheral blood 5 weeks after the transplantation and on bone marrow when mice were sacrificed by FACS



analysis. Briefly, red cells were lysed with ACK buffer and leukocytes were incubated with FcR Blocking Reagent (Miltenyi Biotec) for 20 min at 4°C. Finally, cells were labeled with an APC-conjugated anti-CD115 antibody for 30 min at 4°C and analysed on a BD FACS Canto II (BD Biosciences). DAPI was used as viability marker. Engraftment was determined as the percentage of monocytes not expressing GFP.

### **Human Peripheral Blood-Derived Macrophages**

Human cells were prepared according to an approved protocol (East London & the City Local Research Ethics Committee; no. 06/Q605/40; P/00/029). Peripheral blood was collected from healthy volunteers by intravenous withdrawal in 3.2% sodium citrate solution (1:10). Peripheral blood mononuclear cells were isolated by density centrifugation on a Histopaque-1077 gradient (Sigma) according to the manufacturer's instructions, and were plated in RPMI 1640 for 1 hour. Cells were washed three times with ice-cold PBS without  $\text{Ca}^{2+}$ / $\text{Mg}^{2+}$  to remove lymphocytes, and adherent cells were incubated in RPMI 1640 containing 20% heat inactivated fetal calf serum for 14 days.

### **Histological and Immunohistochemical Analysis**

For histological analysis, muscles were harvested, snap frozen in liquid nitrogen-chilled isopentane and kept at -80°C until use. Cryosections (10µm) were prepared for hematoxylin-eosin (HE) or Sudan Black staining. Fluorescence immunohistochemical analysis was performed according to standard procedures. Briefly, transverse muscle cryosections (10 µm) were post-fixed by incubation for 15 minutes in 4% formaldehyde, blocked and immunostained using primary antibodies directed against Ly6G (1:100; #127602, Biolegend), F4/80 (1:200, #123102, Biolegend) ANXA1 (1:1,000; #71-3400, ThermoFisher) or Fpr2/3 (1:100, #sc-18191-R, SantaCruz). Secondary antibodies were Alexa Fluor 488- or 594-conjugated goat anti-rabbit or anti-rat IgG (1:300; Invitrogen). Sections were counterstained with DAPI, mounted and examined using a TCS SP5 confocal laser scanning microscope (Leica Microsystems) fitted with 405 nm, 488 nm and 594 nm lasers, and attached to a Leica DMI6000CS inverted microscope fitted with a 40× objective lens (NA 0.75 mm; working distance, 0.66 mm). Images were captured with Leica LAS AF 2.6.1 software and analysed using ImageJ 1.51w software (National Institutes of Health).

### ***In vivo* Macrophage Phenotype Analysis**

Macrophage phenotype was analyzed as previously described (Mounier et al., 2013). Briefly, CD45<sup>+</sup> cells were isolated from regenerating muscle TA using magnetic beads conjugated to anti-CD45 antibody (Milteny Biotec) and then incubated with Fc-block (Milteny Biotec) for 30 min at 4°C.

Finally, CD45<sup>+</sup> cells were stained with antibody against Ly-6C/G (#17-5931-82, eBioscience) and against F4/80 (#12-4801-82, eBioscience). Percentages of Ly-6C/G<sup>hi</sup>F4/80<sup>low</sup> and Ly-6C/G<sup>neg</sup>F4/80<sup>hi</sup> cells were calculated among total F4/80<sup>pos</sup> cells following analysis by flow cytometry with a FACSCalibur instrument (Becton Dickinson, UK) and FlowJo v.9.2 analysis software as described below.

### **AMPKα1 siRNA**

Primary human PBMC-derived macrophages were transfected with one of three different commercial siRNA sequences designed to target AMPKα1 or an Allstars negative control siRNA sequence using Hiperfect transfection reagent according to the manufacturer's instructions (final concentration 2 nM; all Qiagen GmbH, Hilden, Germany), alongside mock transfected cells. After 48 hours, cells were analysed for phenotypic conversion following hrANXA1 treatment (6 hours, 10 nM). A proportion of cells were analysed for AMPKα1 expression by western blot using a rabbit polyclonal antibody raised against human the AMPKα1 subunit (1:1,000, #2795, Cell Signalling Technology) and for β-actin expression using a mouse monoclonal antibody (1:10,000; #A5316, Sigma).

### **Human Macrophage Flow Cytometry Analysis**

Primary human PBMC-derived macrophages were labelled with FITC-conjugated mouse monoclonal anti-MHCII (#11-9956-42, Thermofisher) and APC-conjugated mouse monoclonal anti-CD206 (#17-2069-42, Thermofisher) or isotype controls (all Thermofisher) according to manufacturer's protocols. In all cases, 20,000 events were acquired using a FACSCalibur flow cytometer (Becton Dickinson), and analysed using FlowJo analysis software (Version 9.2, Treestar Inc). In some cases, macrophages were analysed for surface expression of FPR2/ALX; surface FcγR were blocked by incubation for 20 minutes at 4°C with IgG block (ThermoFisher Scientific, UK), followed by incubation for 30 minutes at 4°C with mouse monoclonal anti-FPR2/ALX (1μg/106 cells; GM1D6, Aldevron, Freiburg, Germany) then incubation for 30 minutes at 4°C with secondary antibody (AF488-conjugated goat anti-mouse 1:300; ThermoFisher Scientific, UK).

### **Western Blot Analysis**

Samples boiled in 6× Laemmli buffer were subjected to standard SDS-PAGE (10%) and electrophoretically blotted onto Immobilon-P polyvinylidene difluoride membranes (Millipore, Watford, UK). Membranes were incubated with antibodies raised against human phospho-Ca<sup>2+</sup>/calmodulin-dependent kinase (#12716, Cell Signalling Technology), phospho-AMPKα1 (#2531,

Cell Signalling Technology), AMPK $\alpha$ 1 (#2795, Cell Signalling Technology), phospho-acetyl-CoA carboxylase (#3661, Cell Signalling Technology), acetyl-CoA carboxylase (#3662, Cell Signalling Technology, all 1:1000) or  $\beta$ -actin (1:10,000; #A5316, Sigma) in Tris-buffer saline solution containing 0.1 % Tween-20 and 5 % (w/v) non-fat dry milk overnight at 4 °C. Membranes were washed for 30 minutes with Tris-buffer saline solution containing 0.1 % Tween-20, with the solution being changed at 10 minute intervals; membranes were then incubated with secondary antibody (horseradish peroxidase–conjugated goat anti-mouse 1:5000; ThermoFisher), for 2 hours at room temperature. Proteins were then detected using the enhanced chemiluminescence detection kit and visualized on Hyperfilm (Amersham Biosciences). Films were digitised and analysed using ImageJ 1.51w software (National Institutes of Health).

### Quantitative RT-PCR

Total RNA was prepared from primary human PBMC-derived macrophages using TRIzol reagent (Life Technologies Ltd), and then reverse transcribed with superscript III reverse transcriptase (Life Technologies Ltd) according to the manufacturer's protocols. Resultant cDNA was then analysed by real-time PCR in duplicate, using the Quantitect primer system (Primer sets: FPR2/ALX QT00204295, IL-10 QT00041685, NOS-2 QT00068740, TNF- $\alpha$  QT00029162 and TGF $\beta$ 1 QT00000728; all Qiagen Ltd.) and Power SYBR Green PCR Master Mix (Applied Biosystems). Reactions were performed in 384 well-format using the ABI Prism 7900HT Sequence Detection System. The PCR conditions consisted of 95 °C 15 min, [95 °C 15 s – 55 °C 30 s – 72 °C 30 s]  $\times$  40, with a dissociation step [95 °C 15 s/60 °C 15 s/95 °C 15 s] included after the PCR reaction to confirm the absence of non-specific products. Data was acquired and analyzed with SDS 2.3 (Applied Biosystems); fold change was calculated as  $2^{-\Delta\Delta Ct}$ .

### Statistical Analysis

All quantified *in vitro* data are derived from at least three independent donors, with experiments performed in triplicate, and are expressed as mean  $\pm$  SEM. Murine *in vivo* experiments were performed with a group size of n=6, sufficient to identify a 20% effect size with a power of 0.8, and are expressed as mean  $\pm$  SEM. Data were analyzed by one- or two-way ANOVA as appropriate, with *post hoc* comparison using Tukey's HSD test. For murine *in vitro* experiments, at least 3 independent experiments were performed and statistical significance was determined using Student's t test. In all cases, a  $P < 0.05$  was taken as indicating statistical significance.

## References

- Amici, S.A., Dong, J., and Guerau-de-Arellano, M. (2017). Molecular Mechanisms Modulating the Phenotype of Macrophages and Microglia. *Front Immunol* 8, 1520.
- Arnold, L., Henry, A., Poron, F., Baba-Amer, Y., van Rooijen, N., Plonquet, A., Gherardi, R.K., and Chazaud, B. (2007). Inflammatory monocytes recruited after skeletal muscle injury switch into antiinflammatory macrophages to support myogenesis. *The Journal of experimental medicine* 204, 1057-1069.
- Bizzarro, V., Belvedere, R., Dal Piaz, F., Parente, L., and Petrella, A. (2012). Annexin A1 induces skeletal muscle cell migration acting through formyl peptide receptors. *PLoS One* 7, e48246.
- Chan, K.L., Pilon, N.J., Sivaloganathan, D.M., Costford, S.R., Liu, Z., Theret, M., Chazaud, B., and Klip, A. (2015). Palmitoleate Reverses High Fat-induced Proinflammatory Macrophage Polarization via AMP-activated Protein Kinase (AMPK). *The Journal of biological chemistry* 290, 16979-16988.
- d'Albis, A., Couteaux, R., Janmot, C., Roulet, A., and Mira, J.C. (1988). Regeneration after cardiotoxin injury of innervated and denervated slow and fast muscles of mammals. Myosin isoform analysis. *Eur J Biochem* 174, 103-110.
- Dalli, J., Jones, C.P., Cavalcanti, D.M., Farsky, S.H., Perretti, M., and Rankin, S.M. (2012). Annexin A1 regulates neutrophil clearance by macrophages in the mouse bone marrow. *FASEB J* 26, 387-396.
- Damazo, A.S., Yona, S., Flower, R.J., Perretti, M., and Olini, S.M. (2006). Spatial and temporal profiles for anti-inflammatory gene expression in leukocytes during a resolving model of peritonitis. *J Immunol* 176, 4410-4418.
- Davies, L.C., and Taylor, P.R. (2015). Tissue-resident macrophages: then and now. *Immunology* 144, 541-548.
- Dufton, N., Hannon, R., Brancaleone, V., Dalli, J., Patel, H.B., Gray, M., D'Acquisto, F., Buckingham, J.C., Perretti, M., and Flower, R.J. (2010). Anti-inflammatory role of the murine formyl-peptide receptor 2: ligand-specific effects on leukocyte responses and experimental inflammation. *J Immunol* 184, 2611-2619.
- Francis, J.W., Balazovich, K.J., Smolen, J.E., Margolis, D.I., and Boxer, L.A. (1992). Human neutrophil annexin I promotes granule aggregation and modulates Ca(2+)-dependent membrane fusion. *J Clin Invest* 90, 537-544.
- Gobbetti, T., Coldewey, S.M., Chen, J., McArthur, S., le Faouder, P., Cenac, N., Flower, R.J., Thiernemann, C., and Perretti, M. (2014). Nonredundant protective properties of FPR2/ALX in polymicrobial murine sepsis. *Proceedings of the National Academy of Sciences of the United States of America* 111, 18685-18690.
- Hannon, R., Croxtall, J.D., Getting, S.J., Roviezzo, F., Yona, S., Paul-Clark, M.J., Gavins, F.N., Perretti, M., Morris, J.F., Buckingham, J.C., *et al.* (2003). Aberrant inflammation and resistance to glucocorticoids in annexin 1-/- mouse. *FASEB J* 17, 253-255.
- Jha, A.K., Huang, S.C., Sergushichev, A., Lampropoulou, V., Ivanova, Y., Loginicheva, E., Chmielewski, K., Stewart, K.M., Ashall, J., Everts, B., *et al.* (2015). Network integration of parallel metabolic and transcriptional data reveals metabolic modules that regulate macrophage polarization. *Immunity* 42, 419-430.
- Jorgensen, S.B., Wojtaszewski, J.F., Viollet, B., Andreelli, F., Birk, J.B., Hellsten, Y., Schjerling, P., Vaulont, S., Neufer, P.D., Richter, E.A., *et al.* (2005). Effects of alpha-AMPK knockout on exercise-induced gene activation in mouse skeletal muscle. *FASEB J* 19, 1146-1148.
- Kjobsted, R., Hingst, J.R., Fentz, J., Foretz, M., Sanz, M.N., Pehmoller, C., Shum, M., Marette, A., Mounier, R., Treebak, J.T., *et al.* (2018). AMPK in skeletal muscle function and metabolism. *FASEB J* 32, 1741-1777.
- Lantier, L., Fentz, J., Mounier, R., Leclerc, J., Treebak, J.T., Pehmoller, C., Sanz, N., Sakakibara, I., Saint-Amand, E., Rimbaud, S., *et al.* (2014). AMPK controls exercise endurance, mitochondrial

- oxidative capacity, and skeletal muscle integrity. *FASEB journal : official publication of the Federation of American Societies for Experimental Biology*.
- Lantier, L., Mounier, R., Leclerc, J., Pende, M., Foretz, M., and Viollet, B. (2010). Coordinated maintenance of muscle cell size control by AMP-activated protein kinase. *FASEB journal : official publication of the Federation of American Societies for Experimental Biology* 24, 3555-3561.
- Leoni, G., and Nusrat, A. (2016). Annexin A1: shifting the balance towards resolution and repair. *Biol Chem* 397, 971-979.
- Lim, L.H., and Pervaiz, S. (2007). Annexin 1: the new face of an old molecule. *FASEB J* 21, 968-975.
- Locatelli, I., Sutti, S., Jindal, A., Vacchiano, M., Bozzola, C., Reutelingsperger, C., Kusters, D., Bena, S., Parola, M., Paternostro, C., *et al.* (2014). Endogenous annexin A1 is a novel protective determinant in nonalcoholic steatohepatitis in mice. *Hepatology* 60, 531-544.
- Lucas, T., Waisman, A., Ranjan, R., Roes, J., Krieg, T., Muller, W., Roers, A., and Eming, S.A. (2010). Differential roles of macrophages in diverse phases of skin repair. *J Immunol* 184, 3964-3977.
- Maderna, P., Yona, S., Perretti, M., and Godson, C. (2005). Modulation of phagocytosis of apoptotic neutrophils by supernatant from dexamethasone-treated macrophages and annexin-derived peptide Ac(2-26). *J Immunol* 174, 3727-3733.
- Mantovani, A., Biswas, S.K., Galdiero, M.R., Sica, A., and Locati, M. (2013). Macrophage plasticity and polarization in tissue repair and remodelling. *J Pathol* 229, 176-185.
- Martinez, F.O., and Gordon, S. (2014). The M1 and M2 paradigm of macrophage activation: time for reassessment. *F1000Prime Rep* 6, 13.
- McArthur, S., Gobetti, T., Kusters, D.H., Reutelingsperger, C.P., Flower, R.J., and Perretti, M. (2015). Definition of a Novel Pathway Centered on Lysophosphatidic Acid To Recruit Monocytes during the Resolution Phase of Tissue Inflammation. *J Immunol* 195, 1139-1151.
- Moraes, L.A., Kar, S., Foo, S.L., Gu, T., Toh, Y.Q., Ampomah, P.B., Sachaphibulkij, K., Yap, G., Zharkova, O., Lukman, H.M., *et al.* (2017). Annexin-A1 enhances breast cancer growth and migration by promoting alternative macrophage polarization in the tumour microenvironment. *Sci Rep* 7, 17925.
- Motwani, M.P., and Gilroy, D.W. (2015). Macrophage development and polarization in chronic inflammation. *Semin Immunol* 27, 257-266.
- Mounier, R., Lantier, L., Leclerc, J., Sotiropoulos, A., Foretz, M., and Viollet, B. (2011). Antagonistic control of muscle cell size by AMPK and mTORC1. *Cell cycle (Georgetown, Tex)* 10, 2640-2646.
- Mounier, R., Lantier, L., Leclerc, J., Sotiropoulos, A., Pende, M., Daegelen, D., Sakamoto, K., Foretz, M., and Viollet, B. (2009). Important role for AMPKalpha1 in limiting skeletal muscle cell hypertrophy. *FASEB journal : official publication of the Federation of American Societies for Experimental Biology* 23, 2264-2273.
- Mounier, R., Theret, M., Arnold, L., Cuvellier, S., Bultot, L., Goransson, O., Sanz, N., Ferry, A., Sakamoto, K., Foretz, M., *et al.* (2013). AMPKalpha1 Regulates Macrophage Skewing at the Time of Resolution of Inflammation during Skeletal Muscle Regeneration. *Cell metabolism* 18, 251-264.
- Mounier, R., Theret, M., Lantier, L., Foretz, M., and Viollet, B. (2015). Expanding roles for AMPK in skeletal muscle plasticity. *Trends Endocrinol Metab* 26, 275-286.
- Murray, P.J., Allen, J.E., Biswas, S.K., Fisher, E.A., Gilroy, D.W., Goerdt, S., Gordon, S., Hamilton, J.A., Ivashkiv, L.B., Lawrence, T., *et al.* (2014). Macrophage activation and polarization: nomenclature and experimental guidelines. *Immunity* 41, 14-20.
- O'Neill, L.A., Kishton, R.J., and Rathmell, J. (2016). A guide to immunometabolism for immunologists. *Nat Rev Immunol* 16, 553-565.
- Park, S.Y., Lee, S.W., Lee, S.Y., Hong, K.W., Bae, S.S., Kim, K., and Kim, C.D. (2017). SIRT1/Adenosine Monophosphate-Activated Protein Kinase alpha Signaling Enhances Macrophage Polarization to an Anti-inflammatory Phenotype in Rheumatoid Arthritis. *Front Immunol* 8, 1135.
- Pearce, E.L., and Pearce, E.J. (2013). Metabolic pathways in immune cell activation and quiescence. *Immunity* 38, 633-643.

- Perretti, M., Cooper, D., Dalli, J., and Norling, L.V. (2017). Immune resolution mechanisms in inflammatory arthritis. *Nat Rev Rheumatol* 13, 87-99.
- Perretti, M., and D'Acquisto, F. (2009). Annexin A1 and glucocorticoids as effectors of the resolution of inflammation. *Nat Rev Immunol* 9, 62-70.
- Perretti, M., Leroy, X., Bland, E.J., and Montero-Melendez, T. (2015). Resolution Pharmacology: Opportunities for Therapeutic Innovation in Inflammation. *Trends Pharmacol Sci* 36, 737-755.
- Rodriguez-Prados, J.C., Traves, P.G., Cuenca, J., Rico, D., Aragones, J., Martin-Sanz, P., Cascante, M., and Bosca, L. (2010). Substrate fate in activated macrophages: a comparison between innate, classic, and alternative activation. *J Immunol* 185, 605-614.
- Saclier, M., Cuvellier, S., Magnan, M., Mounier, R., and Chazaud, B. (2013a). Monocyte/macrophage interactions with myogenic precursor cells during skeletal muscle regeneration. *The FEBS journal* 280, 4118-4130.
- Saclier, M., Yacoub-Youssef, H., Mackey, A.L., Arnold, L., Ardjoune, H., Magnan, M., Sailhan, F., Chelly, J., Pavlath, G.K., Mounier, R., *et al.* (2013b). Differentially activated macrophages orchestrate myogenic precursor cell fate during human skeletal muscle regeneration. *Stem Cells* 31, 384-396.
- Scannell, M., Flanagan, M.B., deStefani, A., Wynne, K.J., Cagney, G., Godson, C., and Maderna, P. (2007). Annexin-1 and peptide derivatives are released by apoptotic cells and stimulate phagocytosis of apoptotic neutrophils by macrophages. *J Immunol* 178, 4595-4605.
- Serhan, C.N. (2014). Pro-resolving lipid mediators are leads for resolution physiology. *Nature* 510, 92-101.
- Serhan, C.N., and Savill, J. (2005). Resolution of inflammation: the beginning programs the end. *Nat Immunol* 6, 1191-1197.
- Solito, E., Kamal, A., Russo-Marie, F., Buckingham, J.C., Marullo, S., and Perretti, M. (2003). A novel calcium-dependent proapoptotic effect of annexin 1 on human neutrophils. *FASEB J* 17, 1544-1546.
- Tabas, I., and Glass, C.K. (2013). Anti-inflammatory therapy in chronic disease: challenges and opportunities. *Science* 339, 166-172.
- Tannahill, G.M., Curtis, A.M., Adamik, J., Palsson-McDermott, E.M., McGettrick, A.F., Goel, G., Frezza, C., Bernard, N.J., Kelly, B., Foley, N.H., *et al.* (2013). Succinate is an inflammatory signal that induces IL-1 $\beta$  through HIF-1 $\alpha$ . *Nature* 496, 238-242.
- Theret, M., Gsaier, L., Schaffer, B., Juban, G., Ben Larbi, S., Weiss-Gayet, M., Bultot, L., Collodet, C., Foretz, M., Desplanches, D., *et al.* (2017). AMPK $\alpha$ 1-LDH pathway regulates muscle stem cell self-renewal by controlling metabolic homeostasis. *Embo J* 36, 1946-1962.
- Troidl, C., Mollmann, H., Nef, H., Masseli, F., Voss, S., Szardien, S., Willmer, M., Rolf, A., Rixe, J., Troidl, K., *et al.* (2009). Classically and alternatively activated macrophages contribute to tissue remodelling after myocardial infarction. *J Cell Mol Med* 13, 3485-3496.
- Van den Bossche, J., O'Neill, L.A., and Menon, D. (2017). Macrophage Immunometabolism: Where Are We (Going)? *Trends Immunol* 38, 395-406.
- Varga, T., Mounier, R., Gogolak, P., Poliska, S., Chazaud, B., and Nagy, L. (2013). Tissue LyC6-macrophages are generated in the absence of circulating LyC6- monocytes and Nur77 in a model of muscle regeneration. *J Immunol* 191, 5695-5701.
- Varga, T., Mounier, R., Horvath, A., Cuvellier, S., Dumont, F., Poliska, S., Ardjoune, H., Juban, G., Nagy, L., and Chazaud, B. (2016a). Highly Dynamic Transcriptional Signature of Distinct Macrophage Subsets during Sterile Inflammation, Resolution, and Tissue Repair. *J Immunol* 196, 4771-4782.
- Varga, T., Mounier, R., Patsalos, A., Gogolak, P., Peloquin, M., Horvath, A., Pap, A., Daniel, B., Nagy, G., Pintye, E., *et al.* (2016b). Macrophage PPAR $\gamma$ , a Lipid Activated Transcription Factor Controls the Growth Factor GDF3 and Skeletal Muscle Regeneration. *Immunity* 45, 1038-1051.



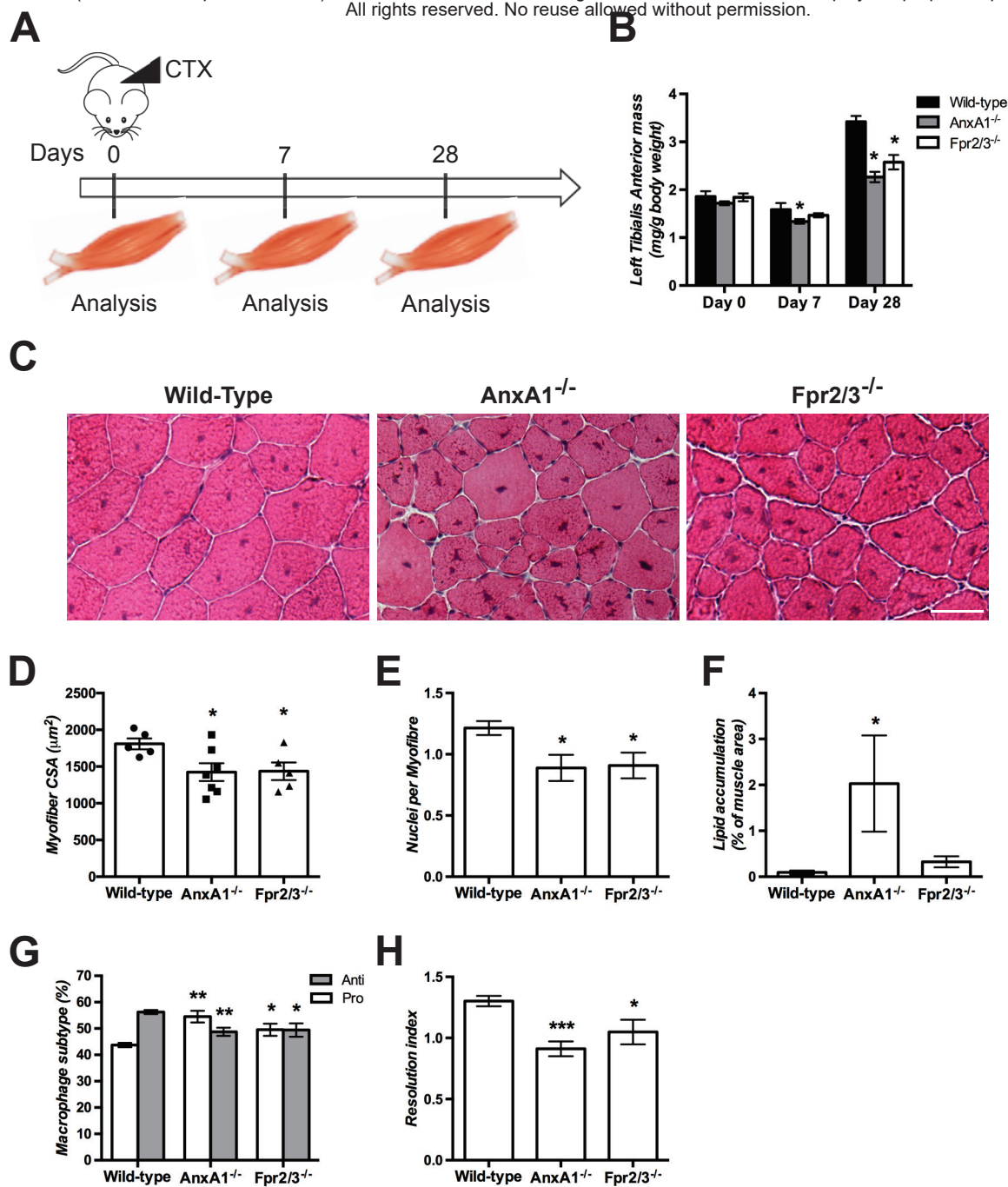
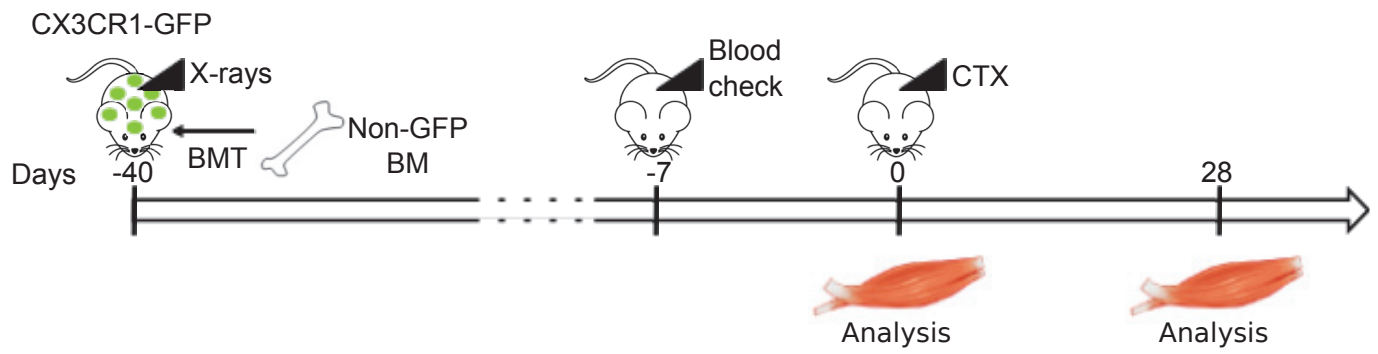
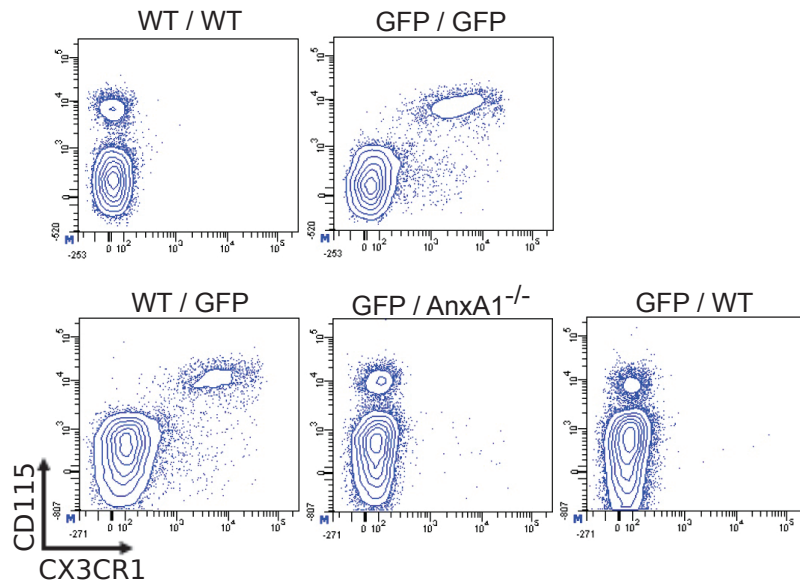


Figure 1

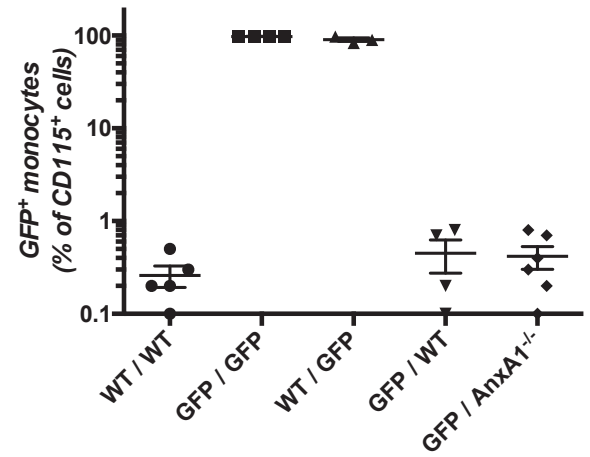
**A**



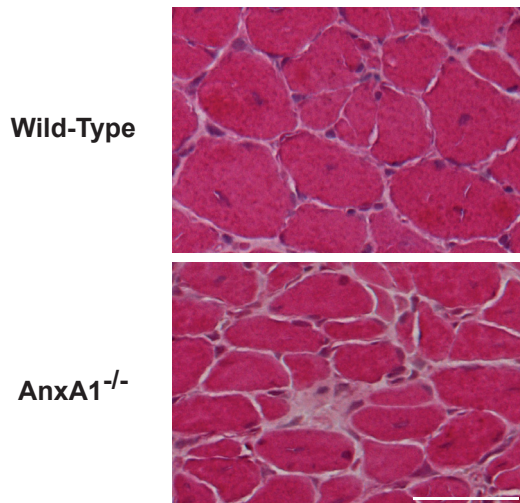
**B**



**C**



**D**



**E**

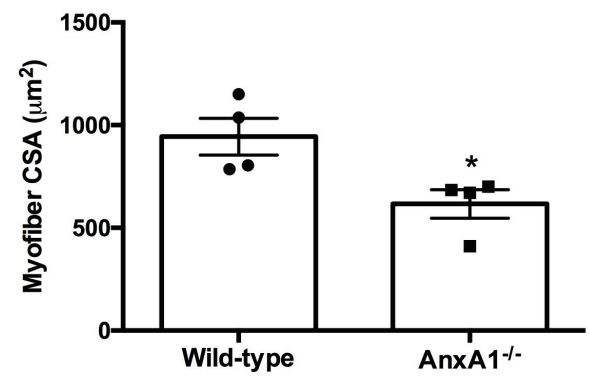


**Figure 2**



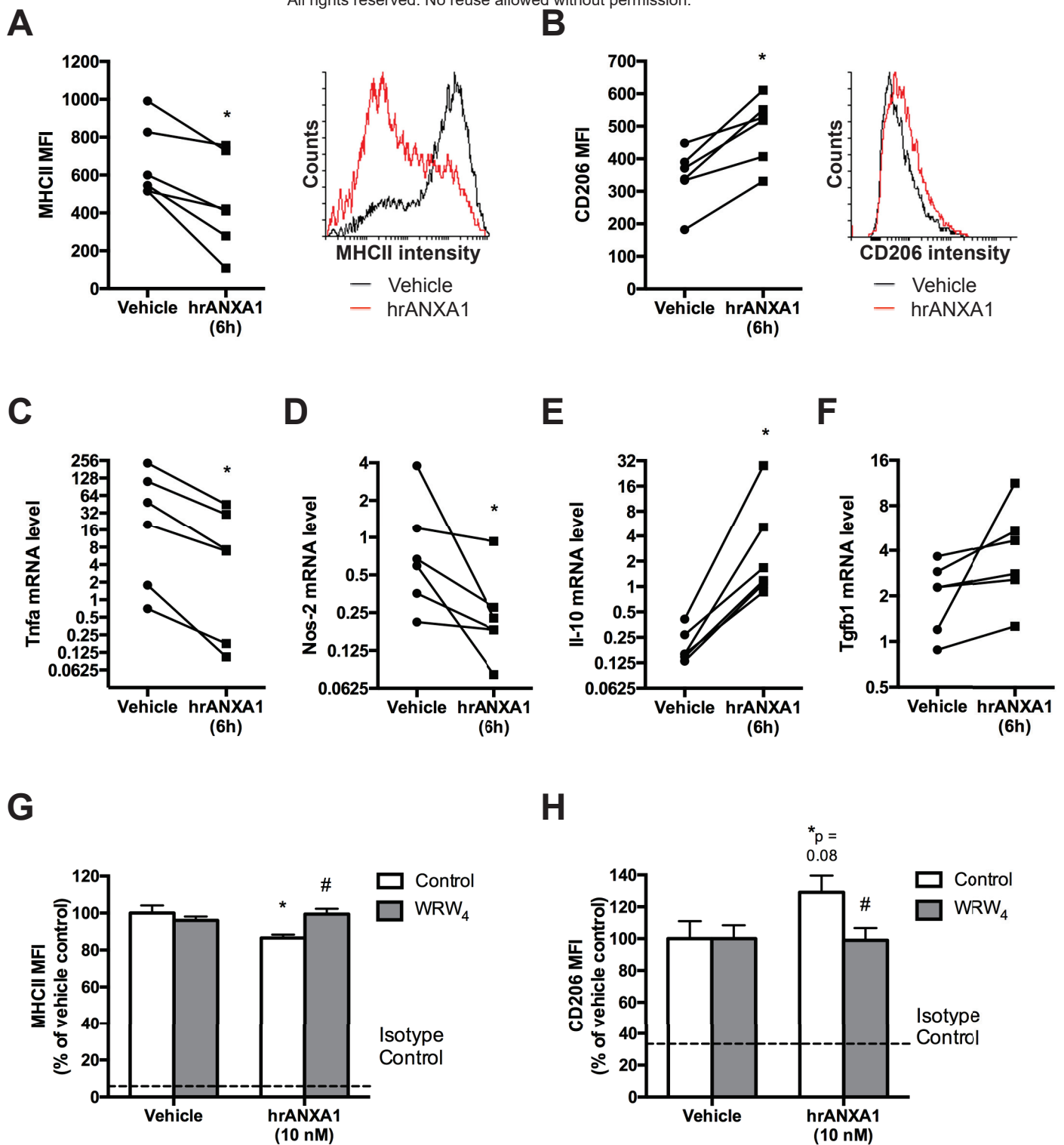
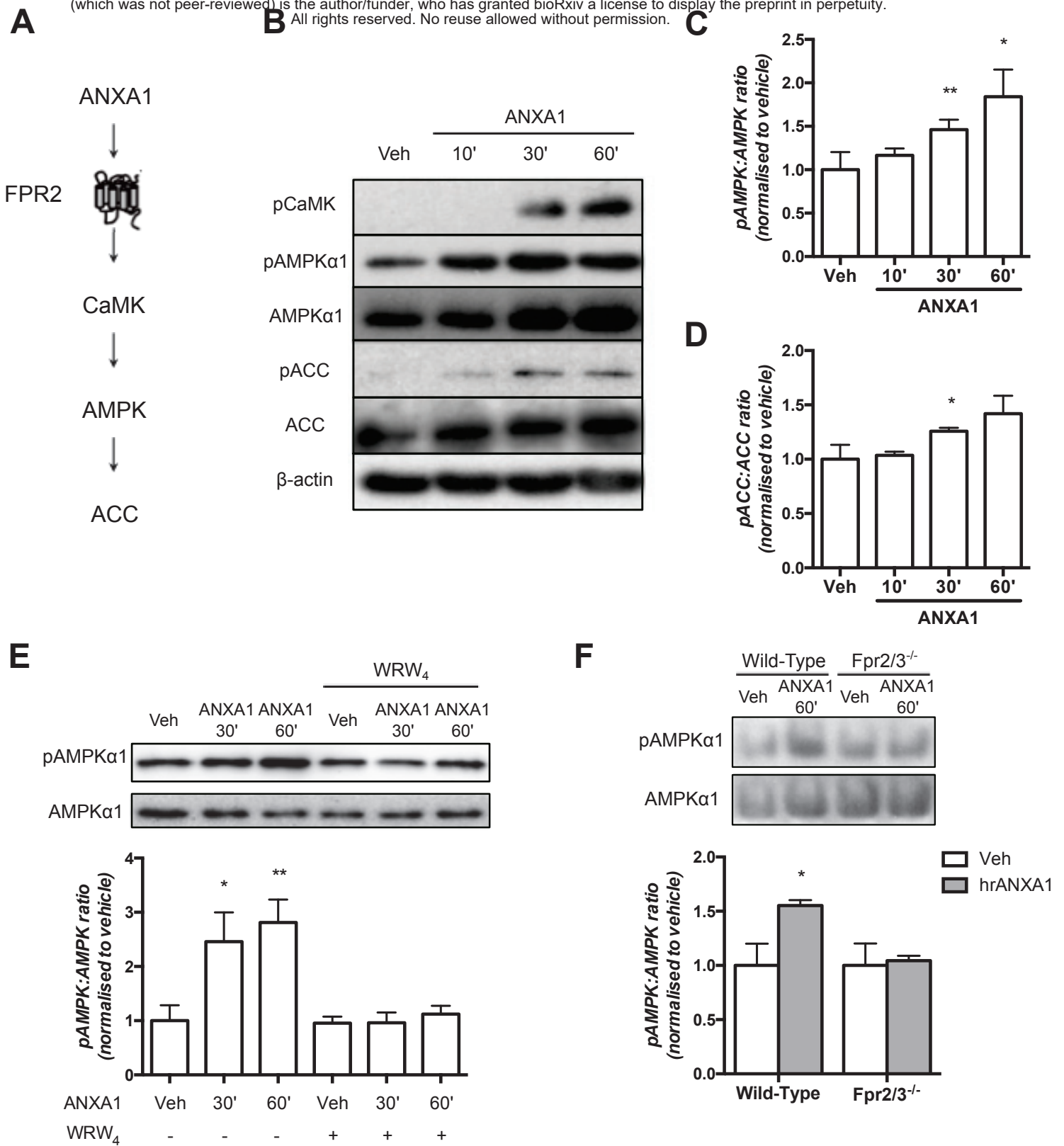
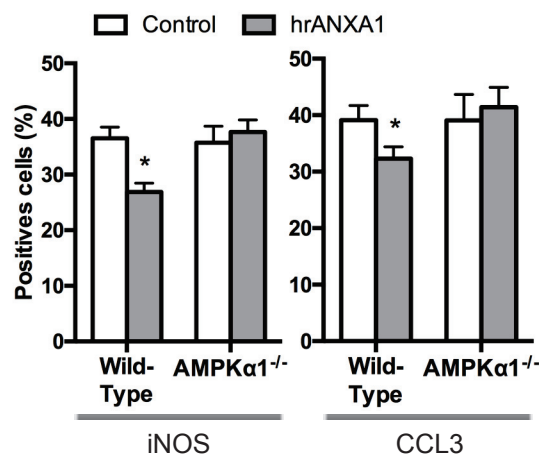


Figure 3

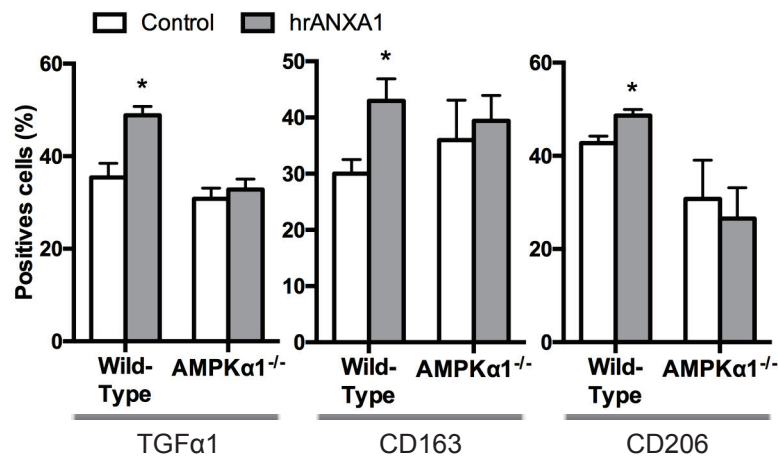


**Figure 4**

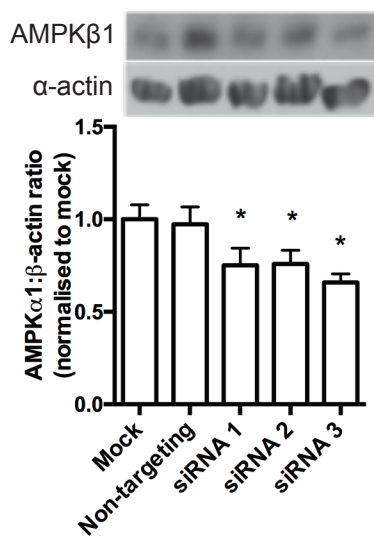
**A**



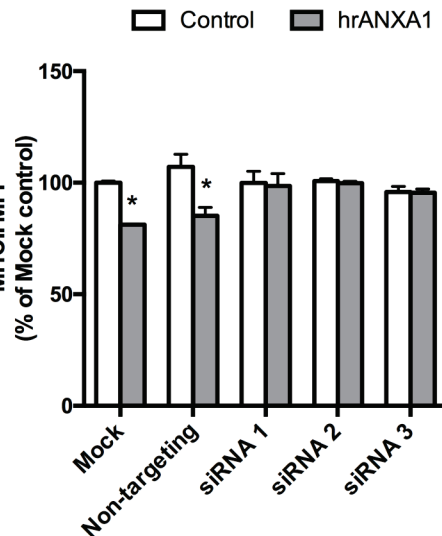
**B**



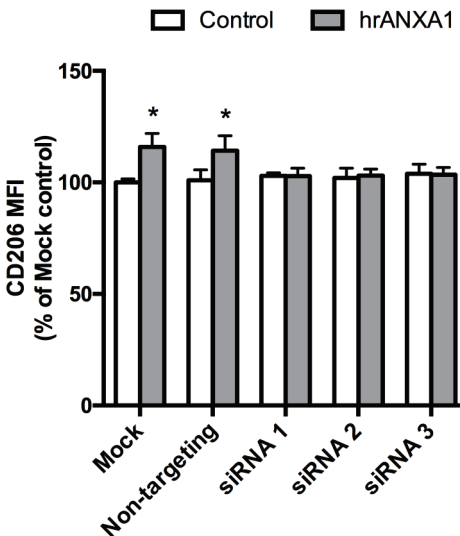
**C**



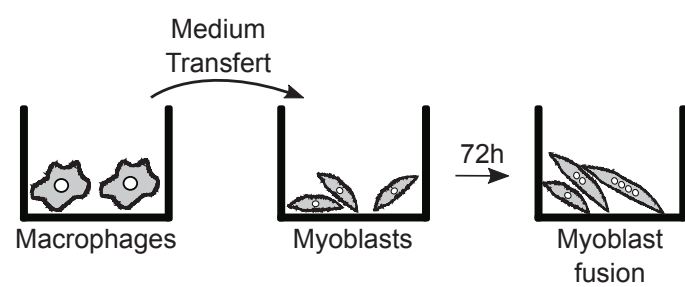
**D**



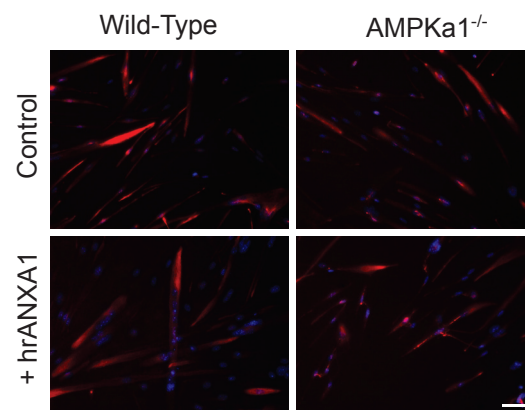
**E**



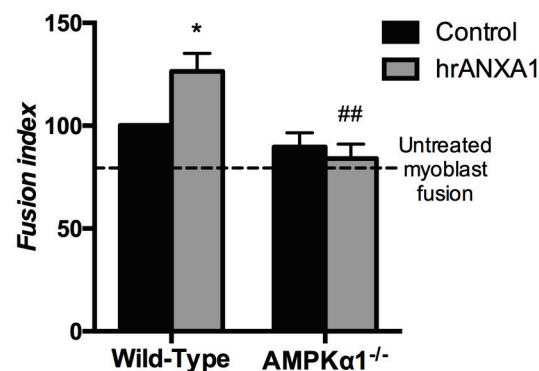
**F**



**G**



**H**



**I**

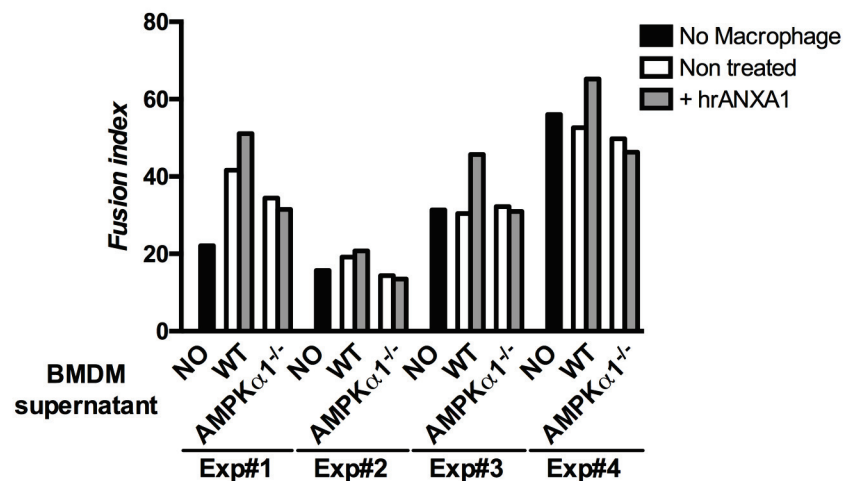
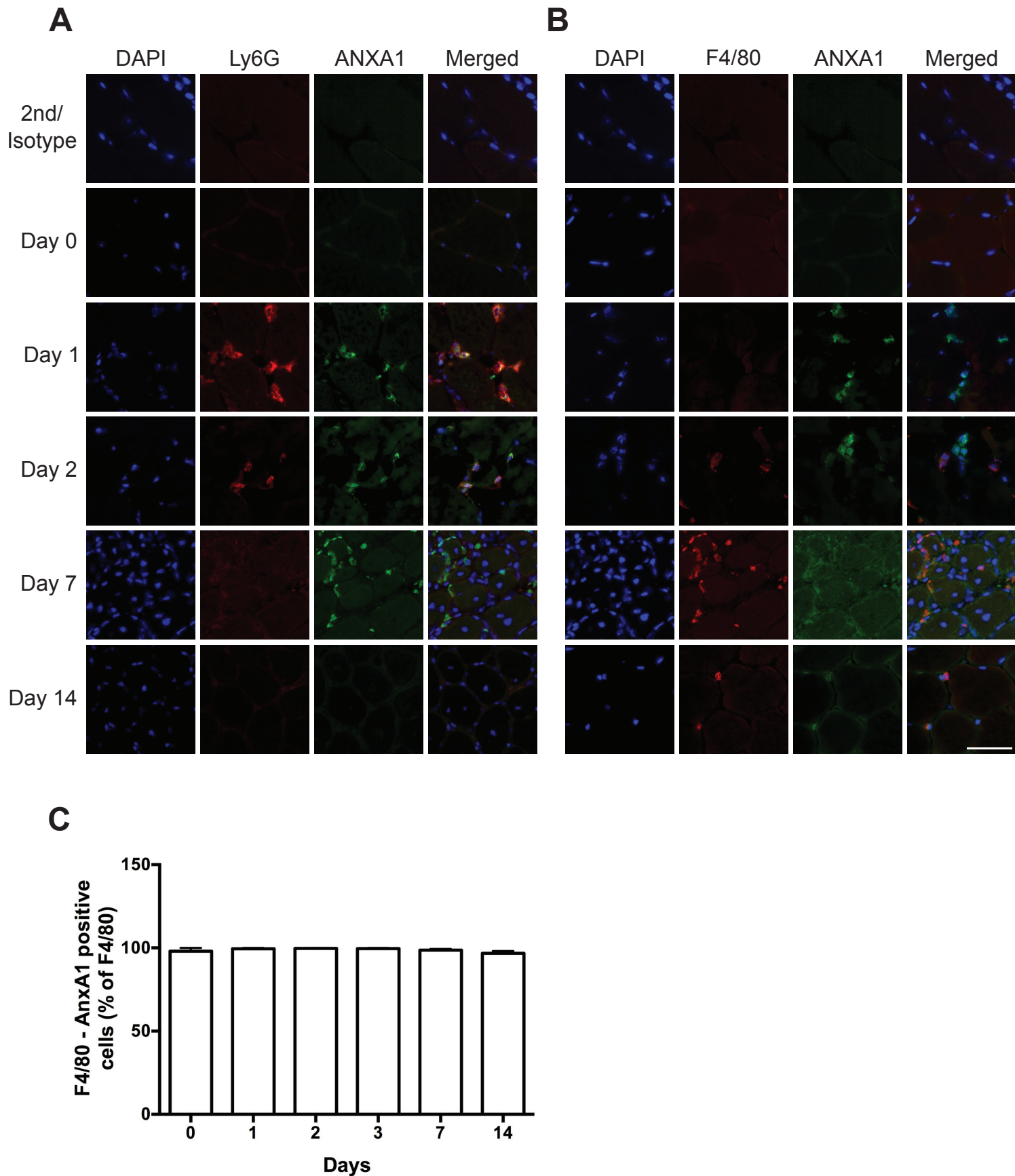
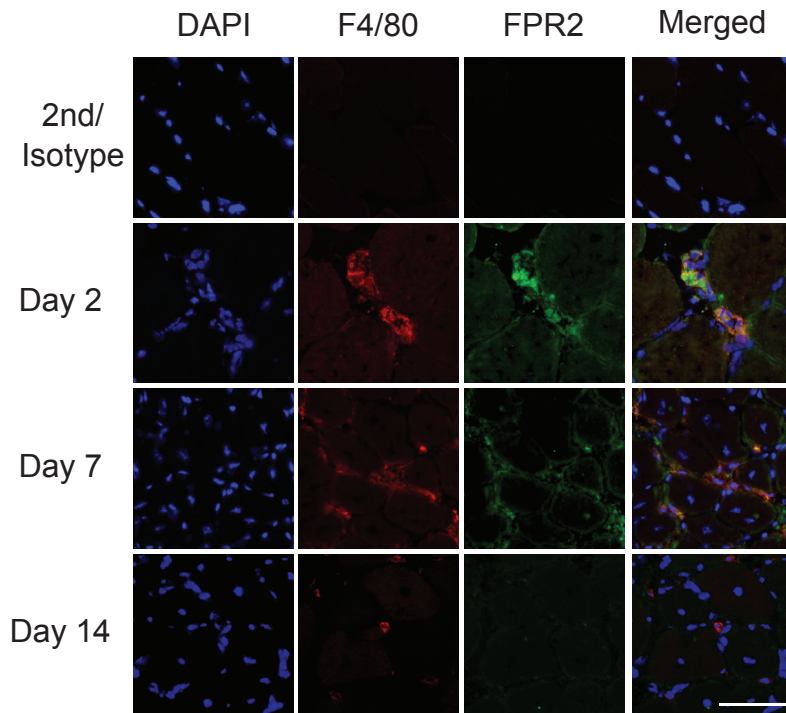


Figure 5

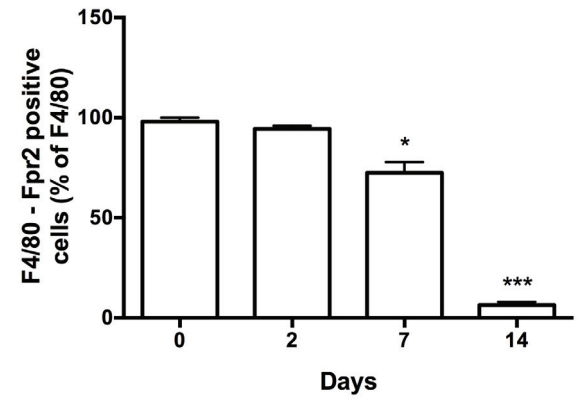


Supplementary Figure 1

**A**



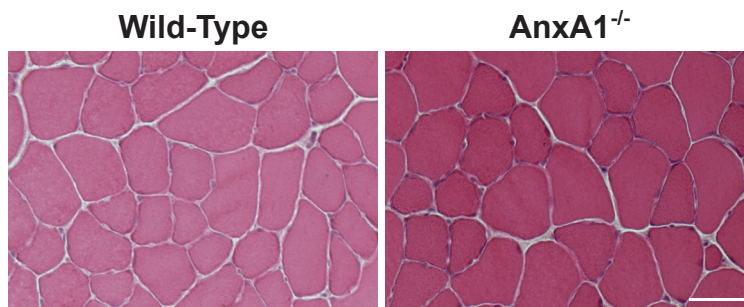
**B**



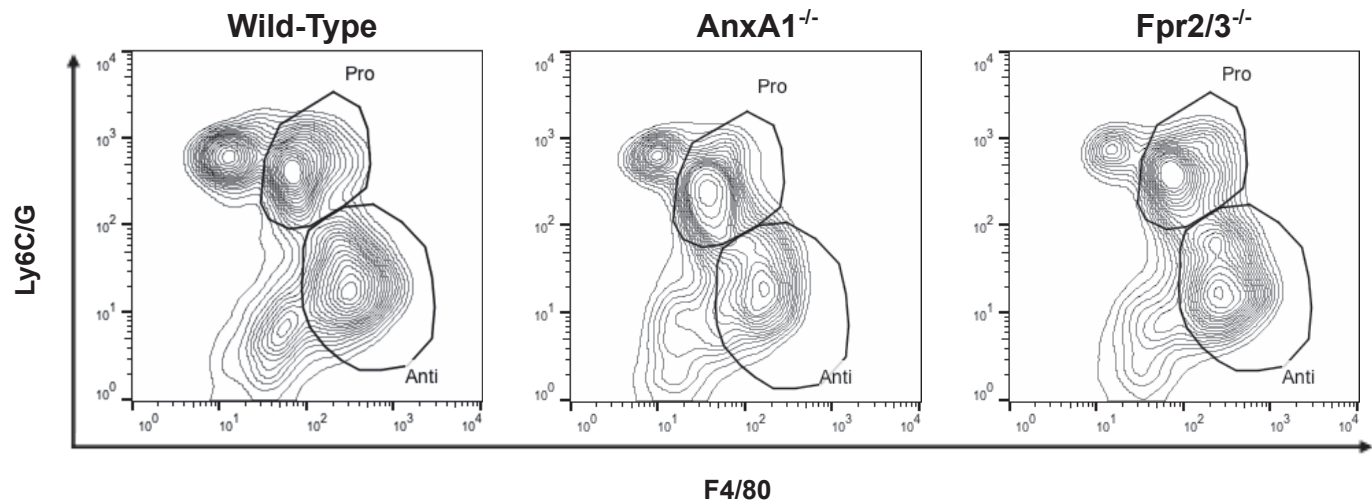
**Supplementary Figure 2**



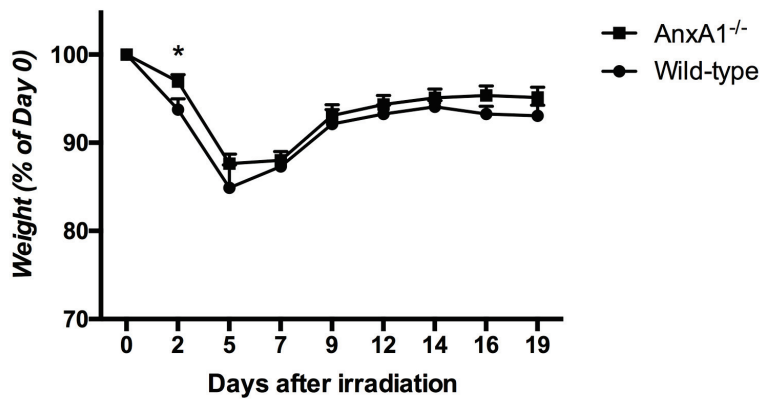
**A**



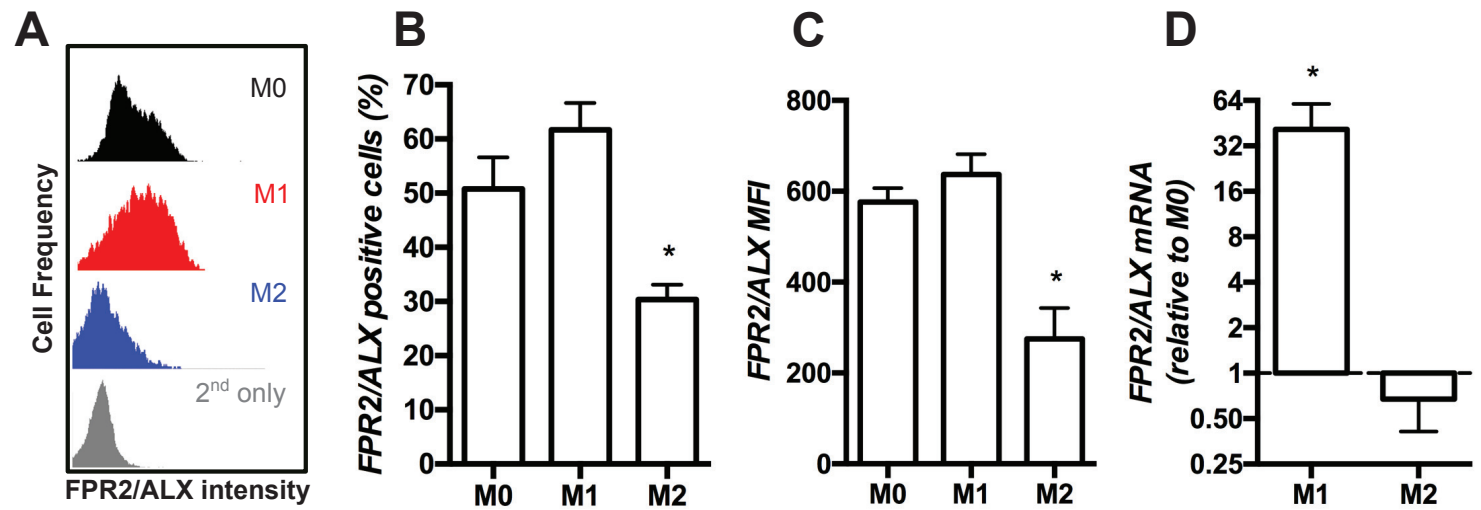
**B**



**C**



Supplementary Figure 3



Supplementary Figure 4

## **STUDY #3**





## **Open-CSAM, a new tool for semi-automated analysis of myofiber cross-sectional area in regenerating adult skeletal muscle**

Thibaut Desgeorges<sup>1</sup>, Sophie Liot<sup>1</sup>, Solene Lyon<sup>2</sup>, Jessica Bouvière<sup>1</sup>, Alix Kemmel<sup>1</sup>, Aurélie Trignol<sup>1</sup>, David Rousseau<sup>2</sup>, Bruno Chapuis<sup>3</sup>, Julien Gondin<sup>1</sup>, Rémi Mounier<sup>1</sup>, Bénédicte Chazaud<sup>1\*</sup> and Gaëtan Juban<sup>1\*</sup>

To analyze the efficiency of muscle regeneration, myofiber size is the main parameter studied as myofiber size is correlated with muscle force. For my PhD project, I had to measure myofiber size on muscle sections. This was usually done manually and was time-consuming, since no reliable software was available. Thus, I developed a program using ImageJ software to automatically analyze the size of myofibers in order to spare time. I also evaluated the accuracy, robustness and conditions of use of that program. The development of the ImageJ macro, published in *Skeletal muscle* journal, allowed the analyze of *in vivo* data of my thesis project, especially for Figures 6 and 7 of the Study #1 and Figures 1 and 2 of Study #2.

METHODOLOGY

Open Access



# Open-CSAM, a new tool for semi-automated analysis of myofiber cross-sectional area in regenerating adult skeletal muscle

Thibaut Desgeorges<sup>1</sup>, Sophie Liot<sup>1</sup>, Solene Lyon<sup>2</sup>, Jessica Bouvière<sup>1</sup>, Alix Kemmel<sup>1</sup>, Aurélie Trignol<sup>1</sup>, David Rousseau<sup>2</sup>, Bruno Chapuis<sup>3</sup>, Julien Gondin<sup>1</sup>, Rémi Mounier<sup>1</sup>, Bénédicte Chazaud<sup>1\*</sup>  and Gaëtan Juban<sup>1\*</sup>

## Abstract

Adult skeletal muscle is capable of complete regeneration after an acute injury. The main parameter studied to assess muscle regeneration efficacy is the cross-sectional area (CSA) of the myofibers as myofiber size correlates with muscle force. CSA analysis can be time-consuming and may trigger variability in the results when performed manually. This is why programs were developed to completely automate the analysis of the CSA, such as SMASH, MyoVision, or MuscleJ softwares. Although these softwares are efficient to measure CSA on normal or hypertrophic/atrophic muscle, they fail to efficiently measure CSA on regenerating muscles. We developed Open-CSAM, an ImageJ macro, to perform a high throughput semi-automated analysis of CSA on skeletal muscle from various experimental conditions. The macro allows the experimenter to adjust the analysis and correct the mistakes done by the automation, which is not possible with fully automated programs. We showed that Open-CSAM was more accurate to measure CSA in regenerating and dystrophic muscles as compared with SMASH, MyoVision, and MuscleJ softwares and that the inter-experimenter variability was negligible. We also showed that, to obtain a representative CSA measurement, it was necessary to analyze the whole muscle section and not randomly selected pictures, a process that was easily and accurately performed using Open-CSAM. To conclude, we show here an easy and experimenter-controlled tool to measure CSA in muscles from any experimental condition, including regenerating muscle.

## Background

Skeletal muscle is capable of complete regeneration after an acute injury [1]. Skeletal muscle integrity is usually assessed by histological analyses, consisting of staining and/or immunofluorescent labeling of various cellular or molecular structural components of the tissue. Among these analyses, myofiber cross-sectional area (CSA) is widely used because it reflects the regenerative capacity of the muscle, i.e., the formation of new myofibers from the activation, proliferation, differentiation, and fusion of muscle stem cells [1]. CSA measurement is usually performed after immunofluorescent staining of laminin, a

component of the basal lamina surrounding each myofiber, or of dystrophin that is located at the inside face of the sarcolemma.

Analysis methods range from manual quantification to programs showing various levels of automation. Manual quantification is potentially the most accurate method as the experimenter keeps total control over the myofibers being analyzed. However, the manual procedure is highly time-consuming and may present variability between experimenters. This is why automated programs were developed to limit the experimenter input and save time [2–7]. For example, SMASH [7] is a semi-automated open source MATLAB script allowing the assessment of several parameters, including CSA. MyoVision, a Windows program [2], was developed to fully automate the quantification process. This program combines several

\* Correspondence: benedicte.chazaud@inserm.fr; gaetan.juban@univ-lyon1.fr

<sup>1</sup>Institut NeuroMyoGène, Univ Lyon, Université Claude Bernard Lyon 1, CNRS UMR 5310, INSERM U1217, 8 Avenue Rockefeller, F-69008 Lyon, France  
Full list of author information is available at the end of the article



© The Author(s). 2019 **Open Access** This article is distributed under the terms of the Creative Commons Attribution 4.0 International License (<http://creativecommons.org/licenses/by/4.0/>), which permits unrestricted use, distribution, and reproduction in any medium, provided you give appropriate credit to the original author(s) and the source, provide a link to the Creative Commons license, and indicate if changes were made. The Creative Commons Public Domain Dedication waiver (<http://creativecommons.org/publicdomain/zero/1.0/>) applies to the data made available in this article, unless otherwise stated.

algorithms that were previously used separately in other programs, thus reducing the errors in the fiber identification and leading to a more accurate CSA measurement compared to SMASH on uninjured muscle [2]. Recently, MuscleJ, a fully automated plug-in in ImageJ described the fully automated quantification of various skeletal muscle parameters, including CSA [8].

Most of the automated softwares were tested on normal muscle or under conditions triggering atrophy/hypertrophy. In this context, the shape of the myofibers keeps polygonal and angular, myofibers keeping their contact with each other. On the contrary, regenerating muscle is characterized by the presence of round-shaped regenerating myofibers of highly variable size that, for the smallest ones, do not regularly contact surrounding fibers. Thus, variable myofiber shape, size, and extrafiber space characterize the regenerating muscle, rendering the automated quantification more difficult.

Here, we present a semi-automated CSA quantification method for skeletal muscle images applicable on any type of muscle and under any condition, including early and late regenerating muscle and dystrophic muscle. This method, named Open-CSAM (for Open [free]-Cross Sectional Area Measurement), is based on an ImageJ macro designed to automatically quantify CSA on immunofluorescent picture of the whole skeletal muscle section. It also includes some level of flexibility for the experimenter, allowing manual correction of the mistakes made by the automation. Moreover, it allows the analysis of the size of the myofibers on the whole muscle section, which we show here to be necessary to obtain an accurate measurement.

## Methods

### Animals and tissue preparation

C57BL/6 and mdx mice were used according to the French legislation. All experiments were performed on mice between 8- and 12-week-old, except for old mice, which were 2-year-old. In injury experiments, *Tibialis Anterior* (TA) muscles were injected with 50  $\mu$ l of cardiotoxin (Latoxan) at 12  $\mu$ M as previously described [9]. Fibrotic dystrophic mice (Fib-mdx) were generated as previously described [10] and mice were analyzed 1 week after the last injuries. TA muscles were mounted on pieces of cork and fixed with tragacanth gum. Then, they were frozen in isopentane cooled by liquid nitrogen and further stored at  $-80^{\circ}\text{C}$ . TA muscles were sectioned thanks to a cryomicrotome (CM3050s, Leica), and the thickness of cryosection was 8 to 10  $\mu\text{m}$ . The slides were then stored at  $-80^{\circ}\text{C}$  until immunostaining. TA muscles showing more than 15% of uninjured area (i.e., without centrally located nuclei), indicating that CTX did not spread into the entire muscle, were excluded from the study.

### Immunofluorescence

Slides were dried for 10 min at room temperature. Muscle cryosections were encircled with a hydrophobic pen (Dako) and were incubated with PBS containing Triton 0.5% for 10 min and then washed three times with PBS. They were incubated with BSA 2% for 1 h at room temperature and then incubated overnight with a rabbit anti-laminin antibody (1:200, L9393, Sigma-Aldrich) at  $4^{\circ}\text{C}$  in a moist chamber. Slides were washed three times with PBS and incubated with FITC-conjugated donkey anti-rabbit secondary antibody (1:200; 711-095-152, Jackson Laboratories) at  $37^{\circ}\text{C}$  for 45 min. Sections were soaked for 10 s in Hoechst solution H 33342 (1:1000, B2261, Sigma-Aldrich) and were washed once with PBS before mounting with antifading Fluoromount G medium (FP-483331, Interchim). Slides were stored at  $4^{\circ}\text{C}$  protected from light until picture acquisition.

### Image acquisition and quantification

As much as possible, the various conditions to be compared (e.g., WT vs. KO, normal vs. dystrophic muscle) should be recorded in similar conditions (microscope, magnification, exposure time, binning). For Open-CSAM validation and comparison with other softwares, at least 10 images were acquired manually at  $\times 20$  of magnification on an Axio Imager.Z1 microscope (Zeiss) connected to a CoolSNAP MYO CCD camera (photometrics) using MetaMorph Software (molecular devices). For whole cryosection analysis, slides were automatically scanned at  $\times 10$  of magnification using an Axio Observer.Z1 (Zeiss) connected to a CoolSNAP HQ2 CCD Camera (photometrics). The image of the whole cryosection was automatically reconstituted in MetaMorph Software. Open-CSAM was able to analyze images up to 110 Mo in 8 bit or 220 Mo in 16 bit. In case the final picture was too big to be analyzed at once because of limitation of ImageJ capacities, the picture was split into several parts (two to four) for the automated analysis. Between 2000 and 4000 fibers were analyzed in a few seconds. Open-CSAM workflow is presented in Fig. 1. The detailed macro code and explanations of the various functions are given in Additional file 1: Figure S1. If necessary, at the end of the automated measurement, manual correction is performed using ImageJ. The selection tools in the ROI Manager were used to remove “false” myofibers created by the automation, and the “Freehand selections” tool was used for hand-drawing “lacking” myofibers missed by the automation. These tools were used for full manual quantification. A tutorial is provided in Additional file 2: Figure S2.

MyoVision and MuscleJ analyses were performed as described [2, 8]. SMASH analysis was implemented with

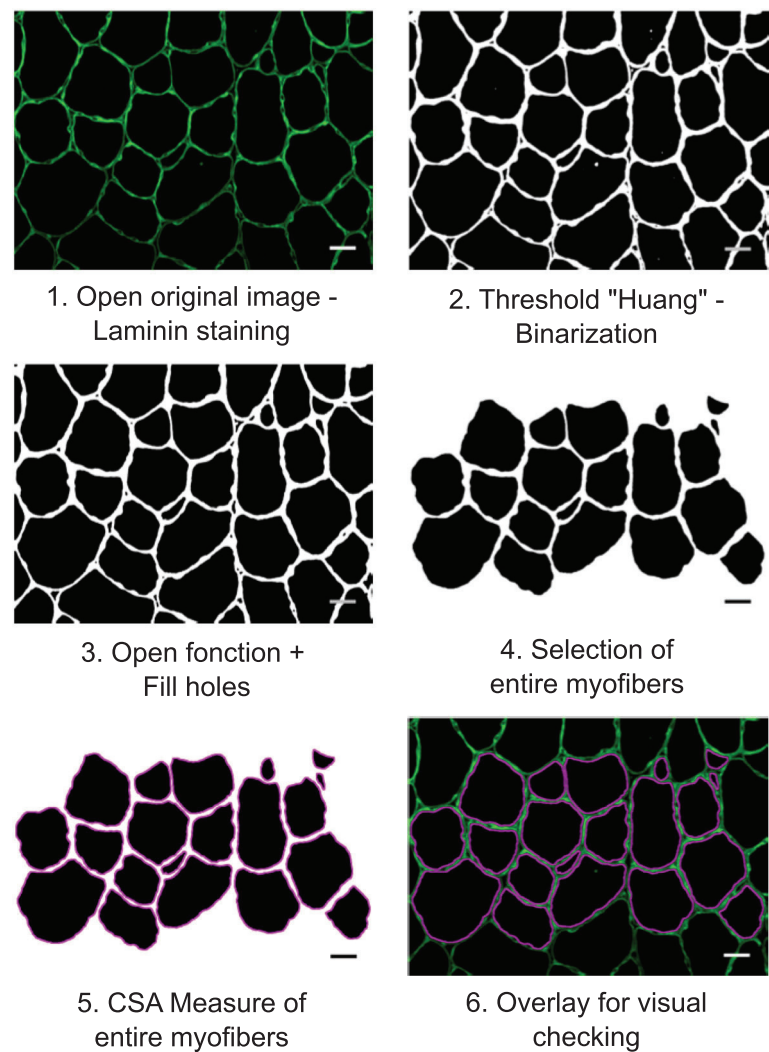


**Fig. 1** Open-CSAM workflow. Step 1: When the macro starts, a window automatically opens to select the image to be analyzed (here muscle cryosections immunostained for laminin). Step 2: Open-CSAM applies the ImageJ threshold "Huang" on the image. Huang threshold was chosen by empiric assays. Threshold application allows image binarization. Step 3: open function allows to adjust the myofiber contours. Myofibers are filled by the function "fill holes." Step 4: Only the entire myofibers are selected to be analyzed. Other selected parameters as circularity and the size are used to avoid the inclusion of too many false myofibers. Step 5: The area of the selected myofibers is measured. Step 6: At the end of the measurement, all the region of interests (ROI, here the myofibers) are automatically superimposed for visual checking. It is then possible to manually delete or add new myofibers. Bars = 25  $\mu\text{m}$

a segmentation filter set to 11 [7]. This was empirically determined by testing values between 5 and 12 and visually inspecting the results. For MuscleAnalyzer analysis, the TIFF pipeline was tested following recommendations provided in the tutorial video [11]. Several threshold values were tested from 1 to 0.955 with no difference on the results. In all analyses, the applied size filter was the same as the one used for Open-CSAM (Table 1).

Statistical analyses

All images were acquired from at least two independent TA muscles per experimental condition and at least five randomly selected images per muscle were analyzed.

**Table 1** Recommended size and circularity thresholds

Muscle type	Size threshold	Circularity threshold
D0 (young and old)	200 $\mu\text{m}^2$ *	0.4
D8	50 $\mu\text{m}^2$ then adjust*	0.4
D14	100 $\mu\text{m}^2$ then adjust*	0.4
D28 (young and old)	150 $\mu\text{m}^2$ then adjust*	0.4
Fib-mdx	50 $\mu\text{m}^2$	0.4

\*If too many small myofibers are missed, progressively decrease the size threshold by testing on 2–3 representative pictures

The Student *t* test, two-way ANOVA, or Spearman correlation test were used for statistical analyses.  $P < 0.05$  was considered significant.

## Results

### Open-CSAM is more accurate than previously described softwares

In order to test the accuracy of Open-CSAM, its performance was compared with a fully manual quantification, a semi-automated software (SMASH), as well as two fully automated softwares: MyoVision and MuscleJ (Fig. 2). We analyzed TA muscle from various conditions, including uninjured muscle, regenerating muscle at several time points after acute injury (D8 and D14) in young and old mice, and a model of fibrotic dystrophy (Fib-mdx). Quantification was performed on cryosections immunofluorescently labeled with anti-laminin antibody, which labels the myofiber basal lamina. Immunolabeling against dystrophin or sarcolemal proteins was not used as this precludes the analysis in dystrophies where these proteins are lacking or altered. As previously described [2], MyoVision produced significantly higher mean CSA values as compared with manual quantification (Fig. 2a, between 4.3 and 47.7% increase depending on the experimental condition). Mean CSA values obtained with MuscleJ were similar to the manual quantification for uninjured young as well as 14 and 28 days post-injury muscles. However, it gave higher mean CSA values in 8 days post-injury regenerating muscles, old muscles (uninjured and 28 days post-injury), and dystrophic muscles (Fig. 2a, between 3.2 and 19.4% increase). Mean CSA values obtained with SMASH were very close to the manual quantification in uninjured old and young 8- and 28-days post-injury muscles. However, SMASH produced higher mean CSA values in uninjured muscles (young and old) (+3 and +1%, respectively), and lower mean CSA values in 14 days post-injury muscles (−4%) (Fig. 2a). On the other hand, Open-CSAM without manual correction gave mean CSA values close to those obtained manually, with a slight underestimation (between 2 and 7.3% decrease as compared with manual quantification), except in Fib-mdx muscles where it was slightly overestimated (+4.4%) (Fig. 2a). This was explained by the fact that Open-CSAM measured the area inside the basal lamina staining, which corresponds to the true area of the myofiber. With manual quantification, the experimenter tends to draw the limits of the myofibers more on the laminin staining, thus including a small part of the basal lamina, therefore slightly overestimating the myofiber area (Fig. 2a). In the case of Fib-mdx muscle, the overestimation by

Open-CSAM was explained by an oversight of small myofibers (see below). During the revision process of this manuscript, MuscleAnalyzer, a customized pipeline within the CellProfiler program allowing fully automated CSA measurement, was released [11]. We tested this pipeline on the same samples as above (Additional file 3: Figure S3). As it strongly overestimated mean CSA as compared with manual quantification (between 38.4% and 254.8% increase depending on the condition), this software was not considered for further analysis.

Despite an increased CSA value obtained using MyoVision, the correlation between MyoVision and manual quantification for each picture was strong in uninjured muscles (young and old mice), as well as 14 and 28 days post-injury regenerating muscles (Fig. 2b and Additional file 4: Figure S4A,  $R^2 > 0.95$ ), suggesting that in these conditions, CSA overestimation by MyoVision was similar on all the pictures and did not introduce a specific bias. On the contrary, the correlation was much lower on muscles at 8 days post-injury, 28 days post-injury in old mice and in fibrotic muscles (Fig. 2b and Additional file 4: Figure S4A,  $R^2 < 0.89$ ), which represent conditions exhibiting smaller myofibers and/or defects in regeneration. Similarly, overall correlation between MuscleJ and manual quantification was very strong in uninjured muscles (young and old mice, Fig. 2b and Additional file 4: Figure S4A,  $R^2 > 0.97$ ). Although this correlation was lower on young 8 days and old 28 days post-injury as well as on fibrotic muscles, it was better than MyoVision. Finally, correlation was lower with MuscleJ than with MyoVision for the 14 and 28 days post-injury conditions. Correlation between SMASH and manual quantification was strong in uninjured young muscles (Fig. 2b,  $R^2 = 0.97$ ). However, correlation was less good when compared with MyoVision and MuscleJ in 28 days post-injury muscles (young and old mice, Additional file 4: Figure S4A,  $R^2 = 0.8352$  for young and 0.9278 for old). For all other conditions, SMASH accuracy compared with manual quantification was intermediate between that of MyoVision and of MuscleJ (Additional file 4: Figure S4A,  $0.8489 < R^2 < 0.9364$ ). These data indicate that the differences observed between manual quantification and MyoVision, MuscleJ, or SMASH are condition-dependent, thus introducing a bias. We then used Open-CSAM, first without applying any manual correction. The correlation between Open-CSAM and manual quantification was better or equivalent to that of MyoVision, MuscleJ, or SMASH in all the analyzed experimental conditions (Fig. 2b and Additional file 4: Figure S4A,  $R^2 > 0.9454$ ). This suggests that Open-CSAM performance was more consistent through the various experimental conditions.



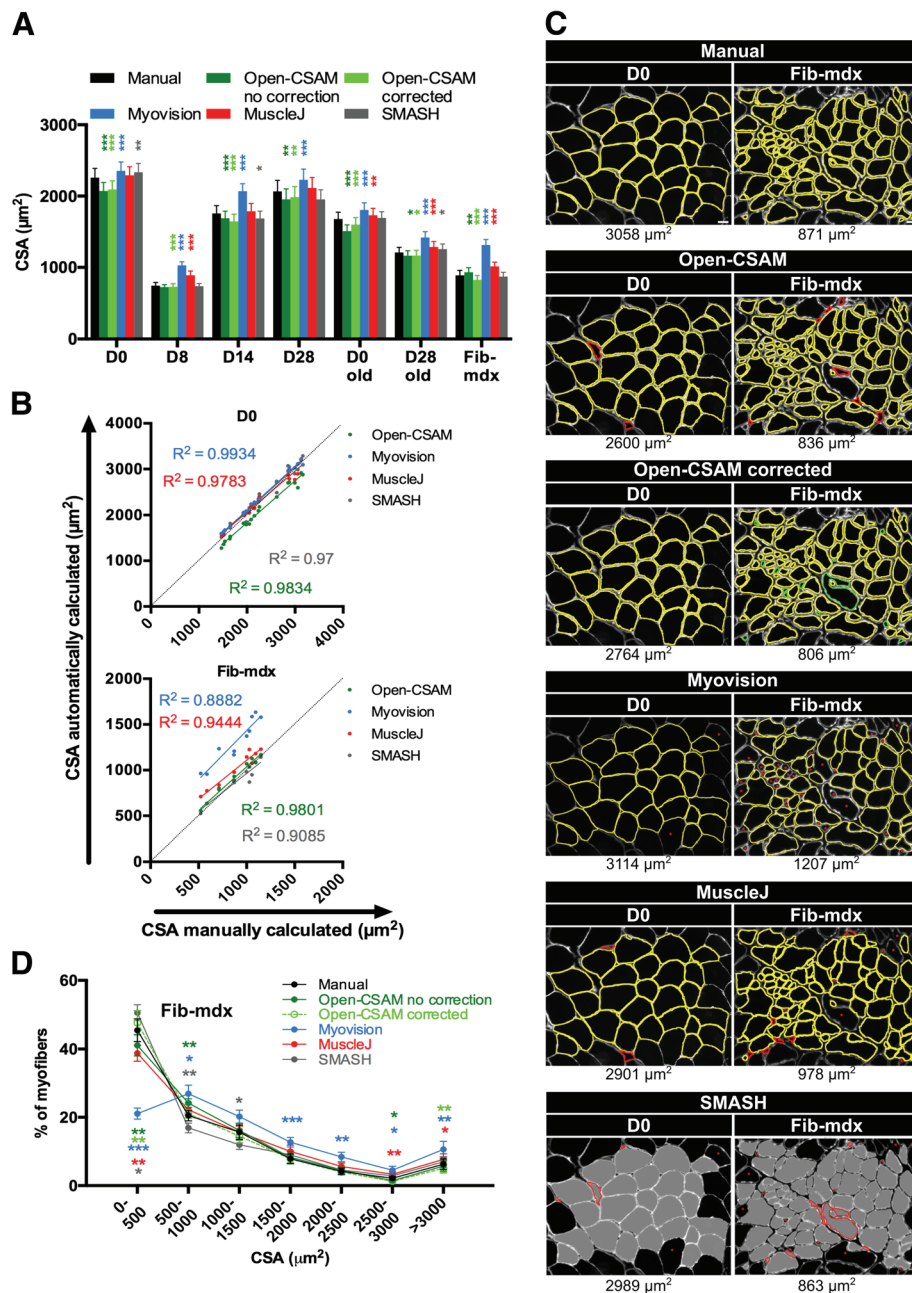


**Fig. 2** Open-CSAM comparison with MyoVision, MuscleJ, and SMASH softwares. The same pictures were analyzed either by manual measurement or using Open-CSAM (with or without manual correction), MyoVision, MuscleJ, or SMASH softwares. **a** Mean cross-section area (CSA) obtained on various *Tibialis Anterior* (TA) muscles. Muscles were isolated from 8- to 12-week-old mice uninjured (D0) or 8 days (D8), 14 days (D14), and 28 days (D28) post-cardiotoxin (CTX) injury, from 2-year-old mice uninjured (D0 old) or 28 days post-CTX injury (D28 old) and from dystrophic fibrotic mice (Fib-mdx). Results are mean  $\pm$  SEM of 10 images from 2 muscles (Fib-mdx), 20 images from 2 muscles (D0 and D0 old), 30 images from 3 muscles (D28 and D28 old), 40 images from 4 muscles (D8), and 45 images from 4 muscles (D14). **b** Correlation between manual measurement (X axis) and Open-CSAM (without manual correction), MyoVision, MuscleJ, or SMASH (Y axis) measurements performed on the same images used in **a**. Each dot represents a picture. The dotted line represents the identity line. **c** Representative images measured manually, by Open-CSAM (before and after correction), MyoVision, MuscleJ, or SMASH softwares. Red fibers were false myofibers identified by the softwares, and green fibers were myofibers not considered by the Open-CSAM software and manually drawn. Lacking myofibers using MyoVision, MuscleJ, or SMASH softwares are shown by red asterisks. **d** Distribution of the CSA obtained with the six methods using the Fib-mdx samples used in **a**. Results are mean  $\pm$  SEM of 10 images from 2 muscles (Fib-mdx). White bar = 25  $\mu\text{m}$ . \* $p < 0.05$ , \*\* $p < 0.01$ , and \*\*\* $p < 0.001$  as compared with manual quantification

### Manual correction is necessary for best accuracy

Figure 2c shows two examples of quantification performed on a single image from an uninjured muscle (left panel) and a dystrophic fibrotic muscle (right panel). In the uninjured muscle picture, Open-CSAM and MuscleJ identified two false myofibers (red lines), which were manually removed with Open-CSAM (Open-CSAM corrected). On the other hand, MyoVision missed two myofibers (red asterisks) while SMASH both identified three false myofibers and missed two myofibers. However, as the myofiber size was quite homogeneous in this picture, this did not really impact the calculated CSA value. In the fibrotic muscle picture (Fig. 2c, right panel), Open-CSAM identified 7 false myofibers (red lines) and missed 16 myofibers that were manually corrected afterwards (green lines). MyoVision missed 33 myofibers (red asterisks) and identified 1 false fiber, which could be excluded by size filter in MyoVision software (red line), inducing a 29% artificial increase in CSA, as compared with manual quantification. Similarly, MuscleJ identified 7 false myofibers (red lines) and missed 14 fibers (red asterisks), leading to a 12.3% increase as compared with manual quantification. Finally, SMASH missed 14 myofibers and misidentified 9 fibers, leading to an 8.2% decrease of mean CSA compared to manual quantification. The distribution of the myofiber CSA in Fib-mdx muscles (same samples as in Fig. 2a) clearly showed that MyoVision and MuscleJ, and to a lower extent, Open-CSAM, preferentially missed the small myofibers ( $< 500 \mu\text{m}^2$ ) (Fig. 2d), thus artificially overestimating the mean CSA. On the contrary, SMASH overestimated the proportion of small myofibers. Taken together, these results show that Open-CSAM accuracy is more consistent as compared with other softwares through various experimental conditions. However, despite its performance, manual correction is necessary for best accuracy. Open-CSAM was designed to enable easy manual correction, allowing the user to directly draw missing fibers and delete the false ones at the same time in ImageJ (Additional file 2: Figure S2). As shown in Additional file 4: Figure S4B, manual correction applied to Open-CSAM improved the measurement accuracy in all conditions ( $R^2 > 0.97$ ) except in old mice 28 days post-injury ( $R^2 = 0.9665$  before and  $0.962$  after correction). In Fib-mdx muscle, this was associated with a convergence of the overall myofiber size distribution towards the distribution obtained with manual quantification (Fig. 2d), notably with a better consideration of small myofibers ( $< 500 \mu\text{m}^2$ ).

### Whole section analysis is necessary for best accuracy

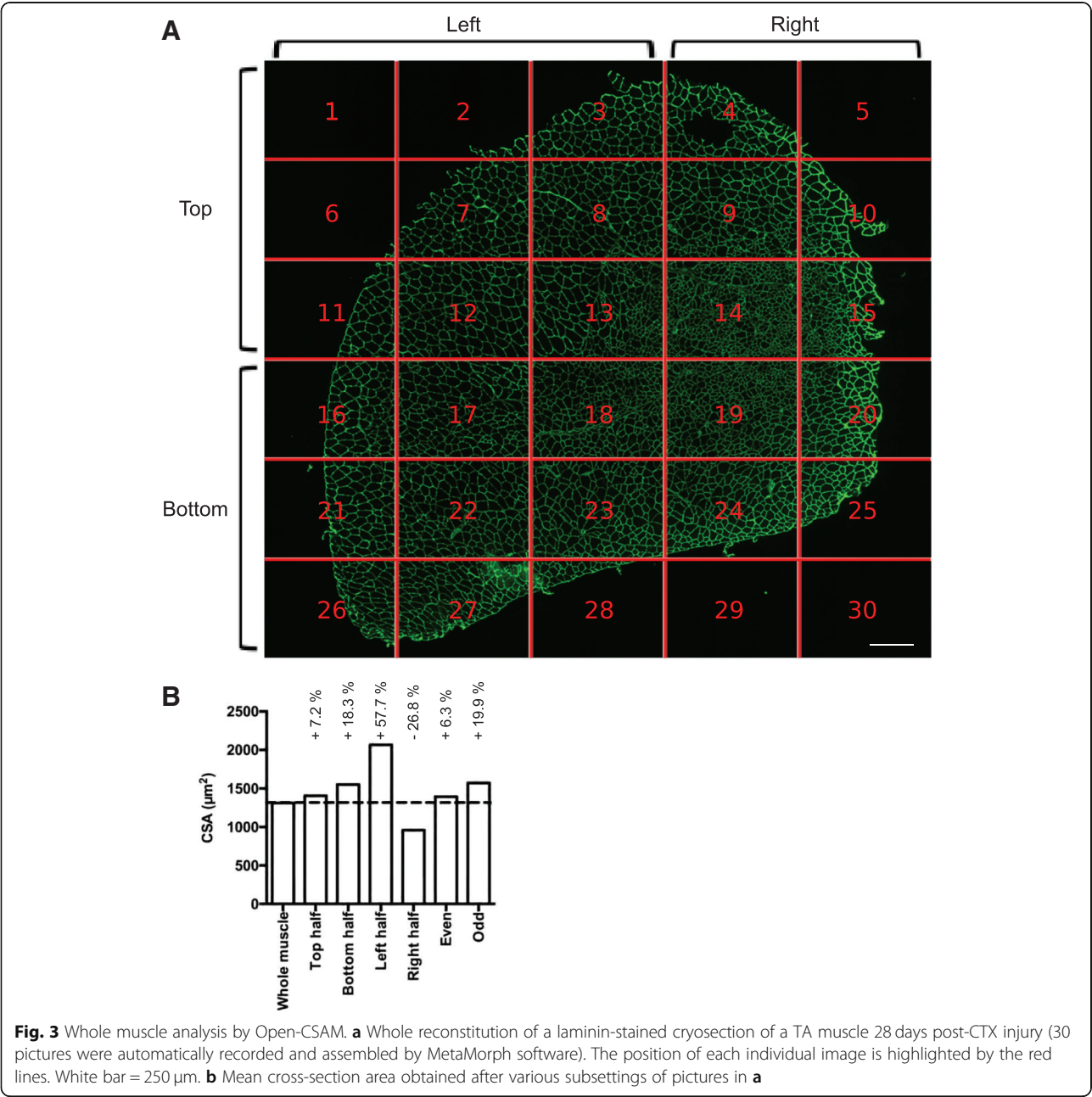
CSA analysis is usually performed on a subset of images randomly taken throughout the muscle section. Depending on the experimenter, the number of images and thus the number of analyzed myofibers can be variable. Moreover,

within the same muscle, myofiber size can be quite heterogeneous and a bias can be introduced depending on the choice of the pictures. Figure 3a shows an example of an entire reconstituted muscle picture. We measured CSA on individual images, calculated the mean CSA on several subsets of images, and compared the results with the CSA obtained on the whole section. When the measurement was made only using a subset of pictures, the myofiber CSA differed from 5 to 28% to that measured on the whole muscle (Fig. 3b). We particularly observed that CSA was overestimated when the left half of the muscle was measured, that corresponded in this example to the peripheral part of the muscle where regeneration is ended. Inversely, measuring the right part of the muscle, here corresponding to smaller regenerating myofibers localized at the center of the muscle, underestimated CSA value. Thus, because TA regeneration after a toxic injury is a centripetal process that ends first at the periphery of the muscle, the whole muscle section should be analyzed when measuring CSA of regenerating muscle in order to obtain an unbiased picture of the process. Moreover, as in diseased muscle, foci of fiber damage or remodeling can occur anywhere, analyzing the whole section also insures an accurate measurement in this context.

### Use of Open-CSAM is robust among users

In a whole muscle section, the number of manual corrections can be variable depending on the quality of the muscle section and of the immunostaining. Considering a high quality of both, we found that the amount of false plus lacking fibers, which needed to be manually removed or re-drawn, ranged from 5% in non-damaged muscles to 10 to 25% in damaged muscles (Fig. 4a). As the manual corrections after Open-CSAM analysis can represent up to 25% of the myofibers, thus potentially introducing variability among users, we tested the robustness of this method. To do so, three independent experimenters analyzed the same image taken from an adult TA muscle 28 days post-CTX injury, where the majority of the muscle has fully regenerated and some central areas are still regenerating (Fig. 4b, c). This muscle was chosen because of the high number of required manual corrections. Using a  $100 \mu\text{m}^2$  size filter and a 0.4 circularity threshold (see Additional file 1: Figure S1 and Table 1), Open-CSAM identified 3757 fibers (Fig. 4c, left images), resulting in a CSA of  $1566.8 \mu\text{m}^2$  (Fig. 4b, left). As shown in Fig. 4c, two areas showed a large number of fibers missed by Open-CSAM. The first area (blue box) was composed of fibers showing a high variability in size where Open-CSAM missed mainly very small fibers. The second area (red box) was composed of medium- to large-sized fibers but with a lower laminin staining intensity. In this area, Open-CSAM failed to identify most of the fibers. Depending on the user, 50 to 145 false fibers were deleted and 860 to 1019 fibers





were manually added (Fig. 4b, right). Despite this variability in the number of manual corrections performed by each user, the corrected CSA reached 1454, 1437, and 1456  $\mu\text{m}^2$ , meaning that variability between users was below 1%. Altogether, these results show that despite the manual corrections required by Open-CSAM, there is no bias introduced by the experimenter.

**Open-CSAM is an accurate tool for whole muscle CSA analysis in regenerating muscle**

As we showed that CSA quantification with Open-CSAM was highly accurate on individual images in various

experimental conditions and that whole muscle analysis was necessary, we tested its performance on several whole muscle images and compared it to fully automated quantification by MyoVision and MuscleJ, as well as to SMASH. We analyzed whole muscle images from young uninjured, 8 days post-injury and 28 days post-injury mice (Fig. 5 and Additional file 5: Figure S5). As we showed for  $\times 20$  individual pictures in uninjured muscle (Fig. 2), MyoVision, MuscleJ, and SMASH modestly overestimated the CSA as compared with corrected Open-CSAM (Fig. 5a, + 11.7%, + 16.5%, and + 13.9%, respectively) (Fig. 5a). On the same muscle, manual correction had negligible impact on

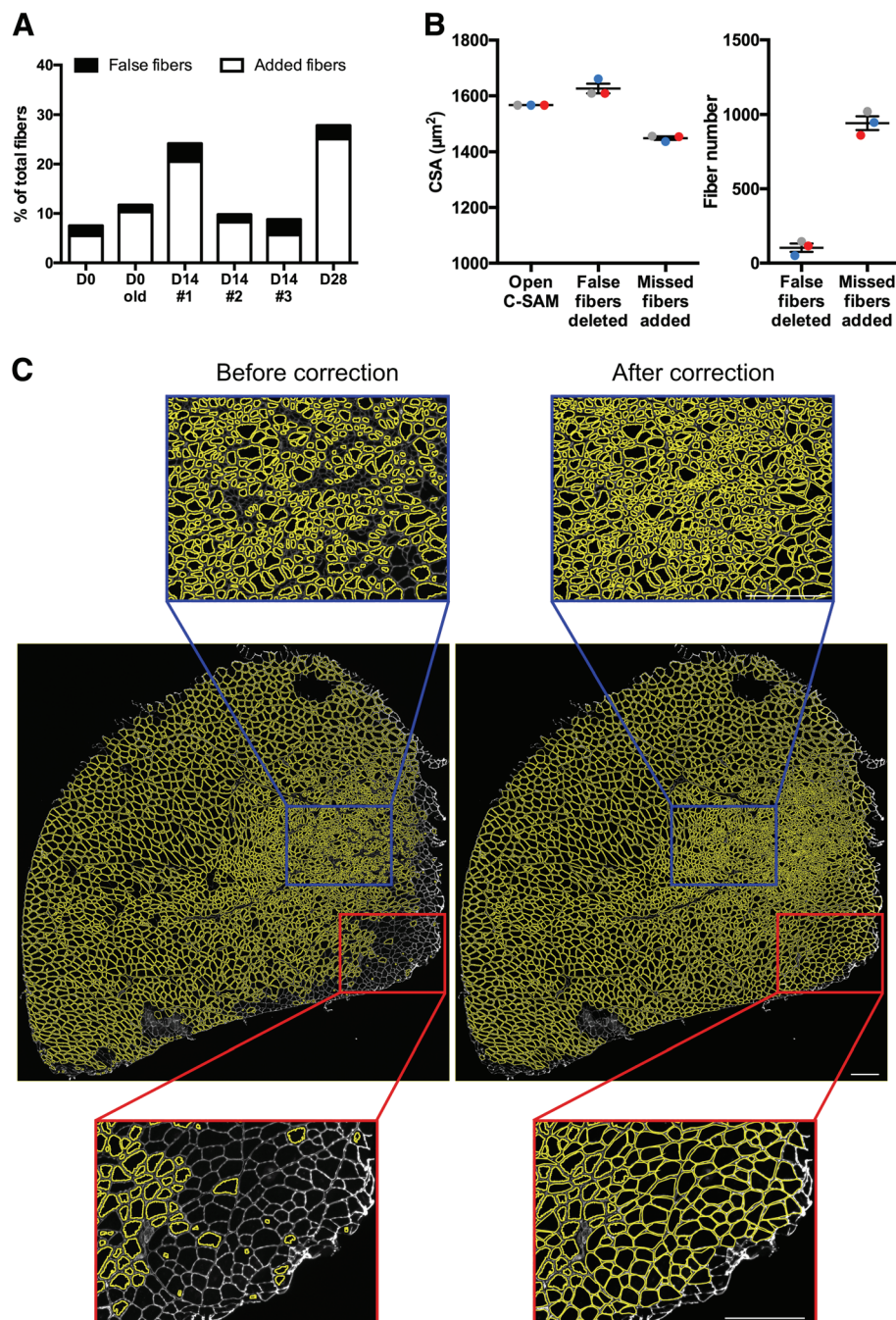


**Fig. 4** Manual corrections after Open-CSAM analysis. **a** Percentage of false myofibers detected (black histograms) and missed myofibers (white histograms) by Open-CSAM that needed manual correction for TA muscles from young and old uninjured mice as well as from 3 muscles analyzed 14 days post-CTX injury. **b, c** Open-CSAM analysis of a TA muscle 28 days post-CTX injury. **b** CSA (left graph) and number of fibers manually corrected (right graph) after analysis by Open-CSAM by three different users (each color represents a single user). **c** Whole image of the TA muscle analyzed in **b** showing myofibers (yellow) detected by Open-CSAM before (left panel) and after (right panel) manual correction. Blue and red boxes represent zoom-in examples of two specific areas that needed extensive manual correction. White bar = 250  $\mu\text{m}$

CSA obtained by Open-CSAM, highlighting its high performance on uninjured whole muscle section (Fig. 5a, -1.1% before correction). Corroborating this observation, CSA distribution was identical for

Open-CSAM before and after correction (Fig. 5d). On the contrary, MyoVision, MuscleJ, and SMASH overlooked small fibers ( $< 1000 \mu\text{m}^2$ ) and overestimated bigger fibers ( $> 3000 \mu\text{m}^2$ ). In the D8

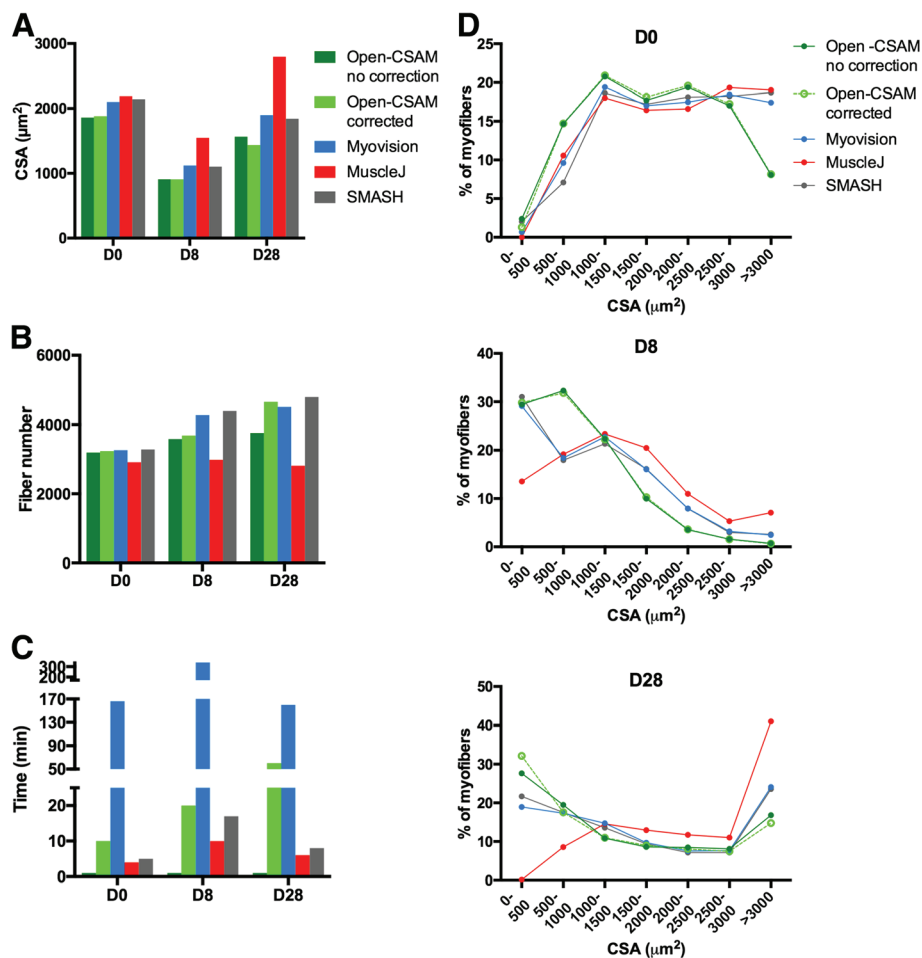


**Fig. 5** Comparison of Open-CSAM, MyoVision, MuscleJ, and SMASH CSA quantification on whole muscle sections. CSA was measured using Open-CSAM (with or without manual correction), MyoVision, MuscleJ, or SMASH on whole TA muscle images obtained from uninjured (D0) or 8 days (D8) and 28 days (D28) post-CTX injury. **a** Mean CSA measured by the different softwares. **b** Number of fibers identified by the softwares. **c** Total analysis time required by the softwares. **d** Distribution of CSA obtained by the five methods on D0 (top graph), D8 (middle graph), and D28 (bottom graph) whole muscles

condition, where small fibers represent an important part of the whole muscle section area and the D28 condition, where small myofibers are still concentrated in specific areas (see Fig. 4), MyoVision (+ 24 and + 32.1%, respectively), MuscleJ (+ 71.2 and + 92.3%, respectively), and SMASH (+ 22 and 26.8%, respectively) accounted for a much higher CSA than Open-CSAM. This is mainly due to the non-detection of the small myofibers (Fig. 5d) and, in the case of MuscleJ, to the merging of several myofibers into one (Additional file 5: Figure S5B, Fig. 5b). Again, correction in Open-CSAM induced a negligible change in CSA measurement on day 8 post-injury muscle (Fig. 5a, + 0.3% before correction). Finally, manual correction of Open-CSAM in day 28 post-injury muscle corrected a slight underestimation of small fibers (Fig. 5d), leading to an artificial increase in CSA (Fig. 5a, + 7.8% before correction).

The main defect of Open-CSAM is the time of experimenter that is required for the complete implementation of CSA measurement. Although running Open-CSAM macro in ImageJ took less than 1 min (even for the whole muscle pictures), which was faster compared to other softwares (4 to 10 min for MuscleJ, 5 to 17 min for SMASH, and 166 to 340 min for MyoVision), the post-automation manual corrections lasted between 10 and 60 min in the examples provided (Fig. 5c, Additional file 5: Figure S5). However, those corrections are required for achieving a full analysis of the whole muscle in order to provide an accurate CSA value. Taken together, these results show that Open-CSAM is a highly accurate tool to measure myofiber CSA on whole muscle section images from different experimental conditions, including regenerating muscle.



## Discussion

Histology is the gold standard technique to assess some characteristics of skeletal muscle. Measurement of myofiber CSA is classically used as a parameter of normal and pathological skeletal muscle regeneration after labeling with anti-laminin or anti-dystrophin antibodies. However, there are various strategies to analyze images and CSA measurement that can give highly heterogeneous results. On the one hand, manual quantification, consisting in manually drawing the myofiber contour to measure the area, is extremely time-consuming and potentially variable between experimenters as it is meticulousness-dependent. According to our experience, it takes about 1 h to draw 1000 fibers. On the other hand, automated programs that were developed to reduce the impact of the experimenter, and to save time, give satisfactory results in uninjured muscle [2–8] but fail to be accurate in regenerating muscle.

Among the recent described softwares are SMASH, MyoVision, and MuscleJ. SMASH is a MATLAB application which is also available as a free Windows program (SMASH Stand Alone). MyoVision is a program operating in Windows environment whereas MuscleJ is a macro working in ImageJ program (Table 2). They were developed to automate, with various levels of flexibility, the quantification of several muscle parameters including fiber number, CSA, myonuclei number and fiber type distribution. As previously described [2], MyoVision showed a significant CSA overestimation as compared with manual quantification. This could be explained by the stronger overlapping of MyoVision outlines with the laminin staining (Fig. 2c), thus integrating a part of the basal lamina into the myofiber area. Despite this overestimation of the mean CSA as compared with manual quantification, MyoVision performed accurately on isolated images from

uninjured muscles. However, regenerating, old and dystrophic muscles are characterized by high myofiber size heterogeneity. In this context, MyoVision measurement was still good at day 14 and 28 after injury, i.e. at time points when regenerating myofibers are already formed. On the contrary, correlation with manual estimation was much lower in muscles at 8 days post-injury in young mice, at 28 days post-injury in old mice and in muscles of dystrophic fibrotic mice. These three conditions are characterized by a lower mean CSA and the presence of high numbers of very small myofibers, which are not considered by MyoVision, thus overestimating the mean CSA. MuscleJ software was efficient in measuring mean CSA in individual  $\times 20$  pictures from uninjured young as well as 14 and 28 days post-injury muscles. However, it measured higher mean CSA values in 8 days post-injury regenerating muscles, old muscles (uninjured and 28 days post-injury) and dystrophic muscles, even though the values were closer to manual quantification than that calculated by MyoVision. Here again, this was due to an oversight of small myofibers. Finally, SMASH showed high accuracy in uninjured young muscles. For the other conditions, even though mean CSA was relatively close to manual quantification, the accuracy was very variable between images, leading to overestimation of small myofibers in Fib-mdx (Fig. 2d) and oversight of these same small fibers in regenerating muscles (Fig. 5d), making it not reliable to analyze and compare various conditions.

In order to provide a tool usable in various biological conditions, we developed Open-CSAM, an ImageJ macro allowing the automatic measurement of CSA with the possibility for the experimenter to apply manual corrections afterwards. CSA values obtained with Open-CSAM were very close to the values obtained manually in all tested conditions. Generally, Open-CSAM omitted only few myofibers in muscles containing small fibers

**Table 2** Comparison of software characteristics

Program	Software base	OS	Minimal configuration tested		Manual correction
			PC	MAC	
Open-CSAM	ImageJ plugin	Mac OS/Windows	Windows 10-Intel core i3 CPU 550 3.2 GHz-4 Go RAM	Mac OS 10.12/Intel core i3-3.2 GHz/12 Go RAM	Yes—during the analysis → Draw/delete ImageJ tools
MyoVision	Windows application	Windows	Windows 10-Intel core i3 CPU 550 3.2 GHz-4 Go RAM (single image analysis)/Windows 7-Intel core i5 vpro 3.1 GHz/16 Go RAM (whole muscle analysis)	Not applicable	No
MuscleJ	ImageJ plugin	Mac OS/Windows	Windows 10-Intel core i3 CPU 550 3.2 GHz-4 Go RAM	Mac OS 10.13/Intel core i5-2.7 GHz/16 Go RAM	Yes—after the analysis → Open picture → Import ROI file on the picture → Draw/delete ImageJ tools
SMASH Stand Alone	Windows application	Windows	Windows 10-Intel core i3 CPU 550 3.2 GHz-4 Go RAM	Not applicable	Yes—during the analysis → Step 1 draw—validate → Step 2 delete—validate (cumbersome: small screen, no back and forth allowed between steps 1 and 2)

(regenerating muscle, old muscle, dystrophic muscles). Then, lacking myofibers are easily manually drawn and incorporated into the analysis using ImageJ, which is not possible using the fully automated softwares. The main drawback of Open-CSAM is that it identifies some false myofibers in the interstitial space between myofibers, notably when this space is large in early regenerating and fibrotic muscles. This issue can be overcome by increasing the size and the circularity thresholds but this also increases the risk of omitting real myofibers. Because it is faster to delete false myofibers than manually drawing lacking myofibers, we recommend to keep thresholds as low as possible to reduce the number of lacking myofibers. We therefore provided starting thresholds for the different conditions we have tested, that have to be adjusted depending on the specific experiment (Table 1). According to our experience, the false fibers identified by Open-CSAM represented less than 5% of the total fibers in all the muscles we have analyzed so far.

CSA measurement is usually performed on a subset of images randomly taken throughout the muscle section. However, myofiber size is quite heterogeneous within the same muscle, and we showed that considering only a part of the muscle section led to the introduction of bias depending on the image selection, potentially hiding a relevant phenotype or artificially creating a non-relevant one. Of note, image acquisition and reconstitution of the whole muscle section is automatically performed, saving time, as compared with manually recording random pictures. Then, Open-CSAM is capable of measuring the myofiber CSA on the whole section in a few seconds. Depending on the size of the image, it may be necessary to split it in two or four parts. This may be also useful when the laminin labeling intensity is not homogenous on the entire section since Open-CSAM may omit faint labeled areas.

When measuring CSA on whole muscle section pictures, using uninjured or 8-day and 28-day regenerating muscles, we found that Open-CSAM (including the manual post-automation corrections) was the most accurate way to measure myofiber CSA. MuscleJ program was efficient at implementing CSA from uninjured muscle (still with overestimated values) but failed to accurately measure myofiber CSA of regenerating muscle, due to failure to detect small fibers and to merging of several myofibers into one. Even though MuscleJ was built as a ready-to-use toolbox to avoid experimenter intervention, post-automation corrections are possible. Indeed, the user may generate a file containing the ROIs analyzed that can be imported back into ImageJ to perform manual corrections in a similar way as Open-CSAM. However, given its poor performance on whole regenerating muscle section as compared with Open-CSAM, the amount of manual corrections and thus the time spent would be not competitive towards Open-CSAM

measurement. SMASH and MyoVision gave similar results, as they moderately overestimated mean CSA in uninjured muscle, an overestimation that was amplified in 8-day and 28-day regenerating muscles which contain a higher proportion of small rounded-shape myofibers. MyoVision was very slow in implementing the analysis of the whole muscle images (between 166 and 340 min), making it not competitive towards manual measurement. Moreover, it does not allow manual correction. SMASH was faster (between 5 and 17 min), and it was designed to allow the user to perform manual corrections during the analysis. However, the correction process has several drawbacks. First, the application cannot be displayed into full screen, which makes inconvenient to easily detect the myofiber delimitations. Second, after the segmentation, the correction process is composed of 2 sequential steps. The first step allows to manually split merged fibers or draw the missed ones. After validation of the drawing, the second step allows manual deletion of the false fibers identified by the program. Unfortunately, at this point, it is not possible anymore to come back to correct merged or missed fibers that would have appeared after the second step. Given this lack of flexibility, performing manual correction in Open-CSAM is much easier and faster.

According to our experience with Open-CSAM, the amount of manual corrections required after the automatic measurement depends on the status of the muscle, the quality of the cryosection, and the quality of the immunolabeling. We recommend performing a new cryosection and/or labeling rather than trying to analyze poor quality images. Typically, if we consider a high-quality image, the analysis of an uninjured TA lasts less than 15 min to process 2000 to 3000 myofibers. In the worst condition we experienced, processing of a regenerating TA can last from 15 min to 1 h for the experimenter to obtain an accurate measurement of myofiber CSA (as compared with 1 h per 1000 fibers in the case of a full manual quantification, thus 2–3 h per muscle). Moreover, we showed that despite the relatively high level of manual correction required for some muscles, the difference in corrected CSA obtained by independent experimenters was negligible (less than 1%), highlighting the robustness of this method.

## Conclusion

The use of Open-CSAM program on whole muscle sections is a powerful strategy to measure myofiber CSA of muscles from various experimental conditions in an easy, highly accurate, and reproducible way, providing values very close to the absolute values. This user-friendly (tutorial in Additional file 2: Figure S2) method is semi-automated and therefore requires the commitment of the experimenter (who is still the best expert to define what a myofiber is), allowing the most accurate CSA measurement of regenerating muscle so far.

## Additional files

**Additional file 1: Figure S1.** Macro to be run for the implementation of Open-CSAM program (left) and related explanations of the functions (right column). (PDF 31.1 kb)

**Additional file 2: Figure S2.** Tutorial for the use of Open-CSAM. (PDF 785 kb)

**Additional file 3: Figure S3.** The same pictures as in Fig. 2 were analyzed either by manual measurement or using MuscleAnalyzer. The mean CSA obtained with the two methods is shown. \*\*\* $p < 0.001$  as compared with manual quantification by two-way ANOVA analysis. (PDF 80 kb)

**Additional file 4: Figure S4.** Mean CSA was measured manually and with Open-CSAM, MyoVision, MuscleJ, or SMASH softwares on the same samples as described in Fig. 2a. Muscles were isolated from 8- to 12-week-old mice 8 days (D8), 14 days (D14), and 28 days (D28) post-CTX injury, from uninjured (D0 old) or 28 days post-CTX injury (D28 old) 2-year-old mice. **A** The correlation between manual measurement (X axis) and Open-CSAM (without manual correction), MyoVision, MuscleJ, or SMASH (Y axis) measurements is presented. **B** Correlation between manual measurement (X axis) and Open-CSAM (Y axis) before and after manual correction. Each dot represents a picture. The dotted line represents the identity line. (PDF 833 kb)

**Additional file 5: Figure S5.** CSA was measured using Open-CSAM, MyoVision, MuscleJ, or SMASH softwares on whole TA muscle images obtained from uninjured (D0) or 8 days (D8) and 28 days (D28) post-CTX injury. **A** Pictures showing the myofibers (yellow shapes except for SMASH which is in gray) detected by Open-CSAM, MyoVision, SMASH, and MuscleJ. The white dotted lines show where the images were split for Open-CSAM and MyoVision analysis. **B** Red boxes represent zoom-in examples of specific areas obtained by MuscleJ. Red asterisks show examples of group of myofibers that are merged. White bar = 250  $\mu\text{m}$ . (PDF 12792 kb)

## Abbreviations

CSA: Cross-sectional area; CTX: Cardiotoxin; Fib-mdx: Fibrotic dystrophic mice; ROI: Region of interest; TA: Tibialis anterior

## Funding

Chazaud Lab is funded by CNRS, INSERM, and UCBL.

## Availability of data and materials

N/A.

## Authors' contributions

RM and BC helped in the conceptualization. TD, SLy, BC, DR, JG, RM, BC, and GJ contributed to the methodology. TD, JG, RM, BC, and GJ helped in the validation and formal analysis. TD, SLi, SLy JB, AK, AT, and GJ carried out the investigation. TD and GJ wrote the original draft and helped in the visualization. TD, SL, AT, DR, JG, RM, BC, and GJ helped in writing the review and editing. BC and GJ supervised the study. All authors read and approved the final manuscript.

## Ethics approval and consent to participate

N/A

## Consent for publication

N/A

## Competing interests

The authors declare that they have no competing interests.

## Publisher's Note

Springer Nature remains neutral with regard to jurisdictional claims in published maps and institutional affiliations.

## Author details

<sup>1</sup>Institut NeuroMyoGène, Univ Lyon, Université Claude Bernard Lyon 1, CNRS UMR 5310, INSERM U1217, 8 Avenue Rockefeller, F-69008 Lyon, France.

<sup>2</sup>CREATIS, Univ Lyon, Université Claude Bernard Lyon 1, CNRS UMR 5220, INSERM U1206, INSA Lyon, 69100 Villeurbanne, France. <sup>3</sup>CIQLE, Lyon Bio Image, Univ Lyon, Université Claude Bernard Lyon 1, Structure Fédérative de Recherche santé Lyon-Est CNRS UMS3453/INSERM US7, 69008 Lyon, France.

Received: 17 September 2018 Accepted: 4 December 2018

Published online: 08 January 2019

## References

1. Yin H, Price F, Rudnicki MA. Satellite cells and the muscle stem cell niche. *Physiol Rev*. 2013;93:23–67.
2. Wen Y, Murach KA, Vechetti IJ Jr, Fry CS, Vickery C, Peterson CA, et al. MyoVision: software for automated high-content analysis of skeletal muscle immunohistochemistry. *J Appl Physiol*. 2018;124:40–51.
3. Miazaki M, Viana MP, Yang Z, Comin CH, Wang Y, Costa L d F, et al. Automated high-content morphological analysis of muscle fiber histology. *Comput Biol Med*. 2015;63:28–35 Elsevier.
4. Liu F, Fry CS, Mula J, Jackson JR, Lee JD, Peterson CA, et al. Automated fiber-type-specific cross-sectional area assessment and myonuclei counting in skeletal muscle. *J Appl Physiol*. 2013;115:1714–24.
5. Kostrominova TY, Reiner DS, Haas RH, Ingemannson R, McDonough PM. Automated methods for the analysis of skeletal muscle fiber size and metabolic type. *Int Rev Cell Mol Biol*. 2013;306:275–332.
6. Kim Y-J, Brox T, Feiden W, Weickert J. Fully automated segmentation and morphometrical analysis of muscle fiber images. *Cytometry*. 2007;71A:8–15.
7. Smith LR, Barton ER. SMASH—semi-automatic muscle analysis using segmentation of histology: a MATLAB application. *Skelet Muscle*. 2014;4:21–16.
8. Mayeuf-Louchart A, Hardy D, Thorel Q, Roux P, Gueniot L, Briand D, et al. Muscle J: a high-content analysis method to study skeletal muscle with a new Fiji tool. *Skelet Muscle*. 2018;8:25.
9. Théret M, Gsaier L, Schaffer B, Juban G, Ben Larbi S, Weiss Gayet M, et al. AMPK $\alpha$ 1-LDH pathway regulates muscle stem cell self-renewal by controlling metabolic homeostasis. *EMBO J*. 2017;36:1946–62.
10. Desguerre I, Arnold L, Vignaud A, Cuvellier S, Yacoub-Youssef H, Gherardi RK, et al. A new model of experimental fibrosis in hindlimb skeletal muscle of adult mdx mouse mimicking muscular dystrophy. *Muscle Nerve*. 2012;45:803–14.
11. Lau YS, Xu L, Gao Y, Han R. Automated muscle histopathology analysis using CellProfiler. *Skelet Muscle*. 2018;8:32.

**Ready to submit your research? Choose BMC and benefit from:**

- fast, convenient online submission
- thorough peer review by experienced researchers in your field
- rapid publication on acceptance
- support for research data, including large and complex data types
- gold Open Access which fosters wider collaboration and increased citations
- maximum visibility for your research: over 100M website views per year

**At BMC, research is always in progress.**

Learn more [biomedcentral.com/submissions](https://biomedcentral.com/submissions)



Functions	Explanations
<pre>// Initialisation roiManager("Reset"); setBackground(0, 0, 0); run("Close All");  if (isOpen("Summary")) {   selectWindow("Summary");   run("Close"); } if (isOpen("Results")) {   selectWindow("Results");   run("Close"); }  // Open muscle section image open(); run("Set Scale...", "distance=1 known=0.645 unit=µm"); original = getImageID(); run("Duplicate...", ""); mask = getImageID();  setAutoThreshold("Huang");  setOption("BlackBackground", false); run("Convert to Mask"); run("Options...", "iterations=2 count=1 do=Open"); run("Fill Holes");  run("Set Measurements...", "area shape feret's area_fraction display add redirect=None decimal=3"); run("Analyze Particles...", "size=100-Infinity circularity=0.4-1.00 show=Masks display exclude summarize add in_situ");  roiManager("Show All"); selectImage(original); run("Enhance Contrast", "saturated=0.35"); roiManager("Show All");</pre>	<p>This function is used for rebooting all the tools used for the measure of myofiber size and for closing all the opened windows (image and others) to avoid interference with the macro during the analysis of a new image.</p> <p>This function allows a new image to open. It also allows to scale the picture. So it is very important to know the pixel camera and to adjust it depending on the microscope-camera used in the following section in bold: run("Set Scale...", "distance=1 known=<b>0.645</b> unit=µm");</p> <p>We use here the threshold filter "Huang". By empiric measures, it appeared to be the most appropriate threshold filter to convert images in a 8-bit binary image that is required for the next steps.</p> <p>These functions allow to close the mask of the myofibers which are not completely closed after the threshold and to eliminate all isolated particles within the myofiber mask.</p> <p>These functions allow to define the analyzed parameters (area is the most important) and the characteristics of particles to be analyzed (size and circularity). The size of the particles must be adjusted depending on the characteristics of the sample (e.g. smaller myofibers are observed at early stages of regeneration than at late stages). Circularity (<math>4\pi \times \text{Area} / \text{Perimeter}^2</math>) defines if the object is a perfect circle (circ=1) or a very elongated polygon (circ close to 0). Circularity is used to exclude the most elongated and polygonal objects (such as very elongated myofibers and non myofiber objects). It also allows to exclude oblique sections. We consider only sections with a mean circularity &gt;0.6.</p> <p>These parameters allow to show all the particles measured in the original image. This function is very useful to check if the measure is accurate, and to do some corrections if necessary (delete fake myofibers and draw the lacking myofibers with the "freehand selections" tool).</p>



## Tutorial

Open-CSAM works with ImageJ or Fiji software.

- 1- Drag the Open-CSAM macro on ImageJ window to open it (Open-CSAM.ijm downloaded from Image J website), or create the macro (copy paste the macro program (in red in Supplemental Figure 1) in the macro-record function of ImageJ).
- 2- Adjust the pixel size depending on the pixel/camera of the microscope used to record pictures:  
*run("Set Scale...", "distance=1 known=**0.645** unit=μm");*  
(in the above example, 0.645 in bold is the pixel camera)

Open-CSAM uses a size and a circularity filter to exclude extra-cellular spaces from the analysis. Depending on the experimental condition, it can be relevant to adjust the size and the circularity of the selected myofibers that have to be analyzed in the following section of the program in bold:

```
run("Analyze Particles...", "size=100-Infinity circularity=0.4-1.00 show=Masks display exclude  
summarize add in_situ");
```

- 3- Run Open-CSAM (*Macros* ➔ *Run macro*).
- 4- A window automatically opens to choose the picture to be analyzed (Open-CSAM can read several formats: TIFF, JPEG, PNG but we preferentially use TIFF format).
- 5- Let Open-CSAM analyzing the picture.
- 6- At the end of the analysis, myofiber shapes analyzed by Open-CSAM are shown in the original picture for a visual check of the analysis.  
If the analysis is perfect, results can be exported into excel.

If corrections are required:

- a- deleting false fibers: select and delete the false fibers directly on the picture (example in blue in the picture), they will be deleted from the ROI Manager.

- b- drawing missing fibers: with the freehand tool, draw missing fibers. When you have finished to draw one fiber, press Command+T (Mac.OS) or CTL+T (Windows) to add the new myofiber to the ROI manager.



- 7- When all the corrections are made, close the previous *Results* window and in the ROI manager, select all the ROIs and click on *Measure* to measure the area of all the fibers/ROI. Results (see a screenshot below) can be exported into excel.



Results									
	Label	Area	Circ.	Feret	%Area	FeretX	FeretY	FeretAngle	MinFeret
1	A16-79 TAD.tif	2792.360	0.596	82.343	100	2248.470	81.270	95.845	48.627
2	A16-79 TAD.tif	2303.946	0.451	78.300	100	2503.245	131.580	11.402	44.272
3	A16-79 TAD.tif	1027.998	0.556	52.002	100	2660.625	118.035	136.005	30.407
4	A16-79 TAD.tif	1735.240	0.457	80.003	100	2636.115	118.680	119.458	35.962
5	A16-79 TAD.tif	1985.271	0.641	65.403	100	2465.190	185.760	84.908	38.329
6	A16-79 TAD.tif	2236.134	0.452	74.161	100	2712.225	133.515	139.939	47.792
7	A16-79 TAD.tif	2694.594	0.663	71.830	100	2254.920	198.015	4.635	54.807
8	A16-79 TAD.tif	2143.777	0.649	65.078	100	2342.640	207.045	50.631	46.751
9	A16-79 TAD.tif	4374.919	0.683	97.256	100	2500.665	157.380	111.801	59.757
10	A16-79 TAD.tif	1374.131	0.571	63.358	100	2792.205	161.250	144.530	35.572



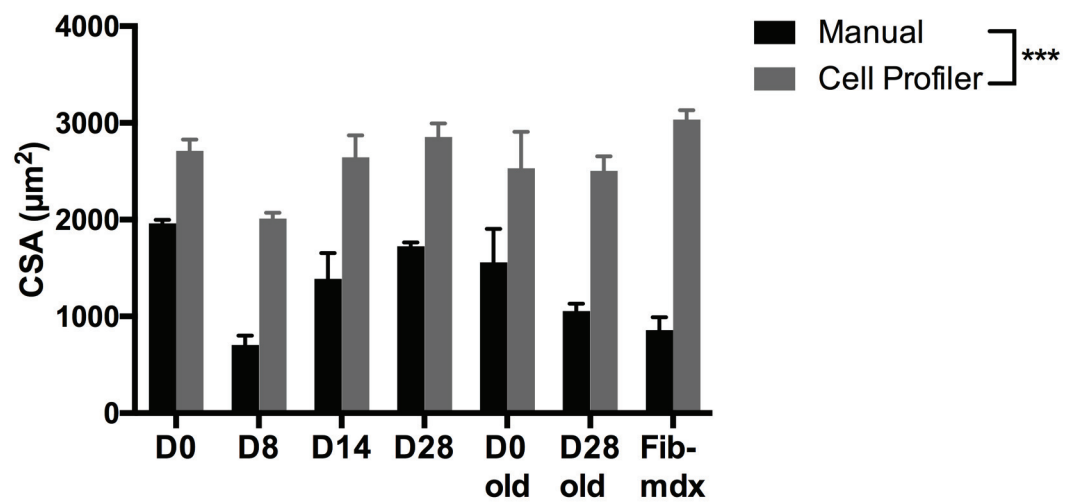
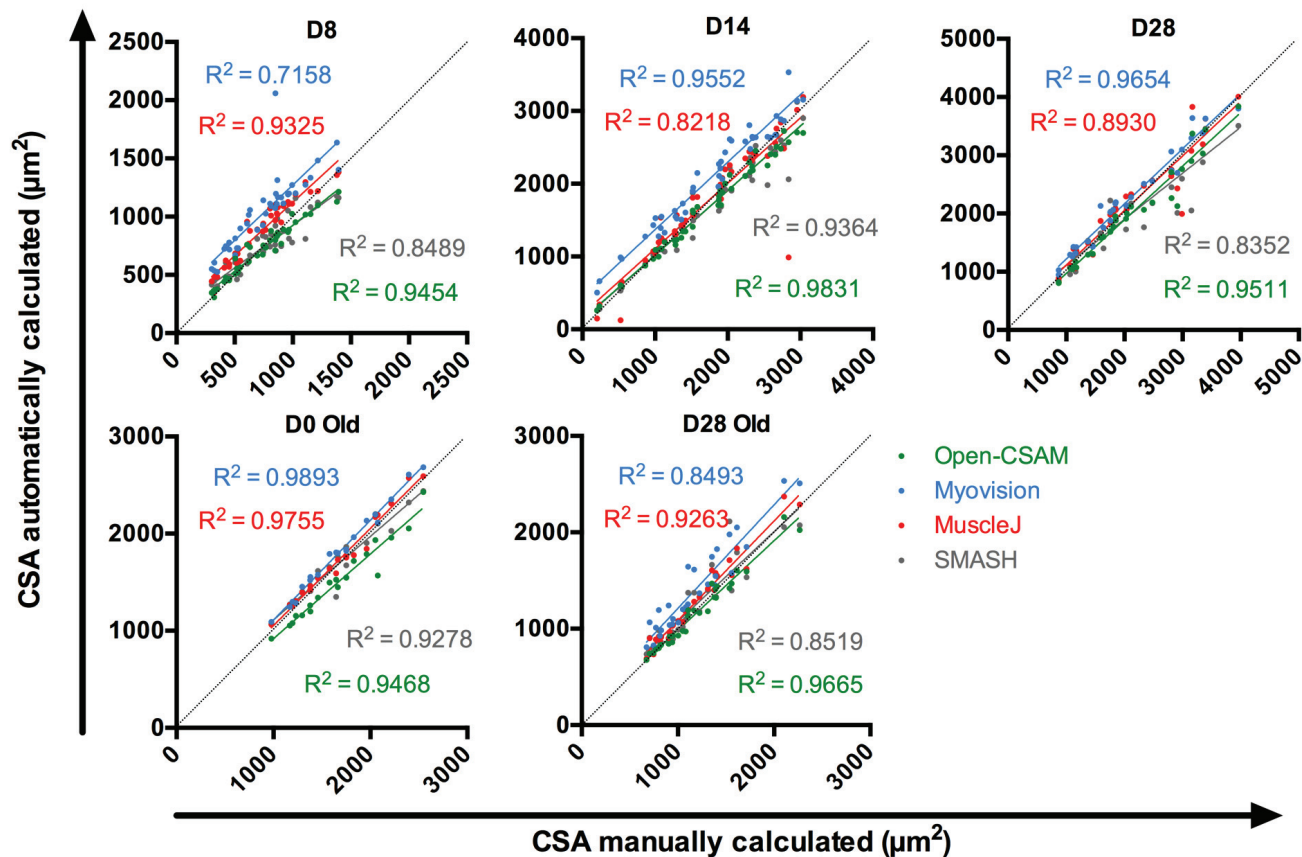


Figure S3

**A**



**B**

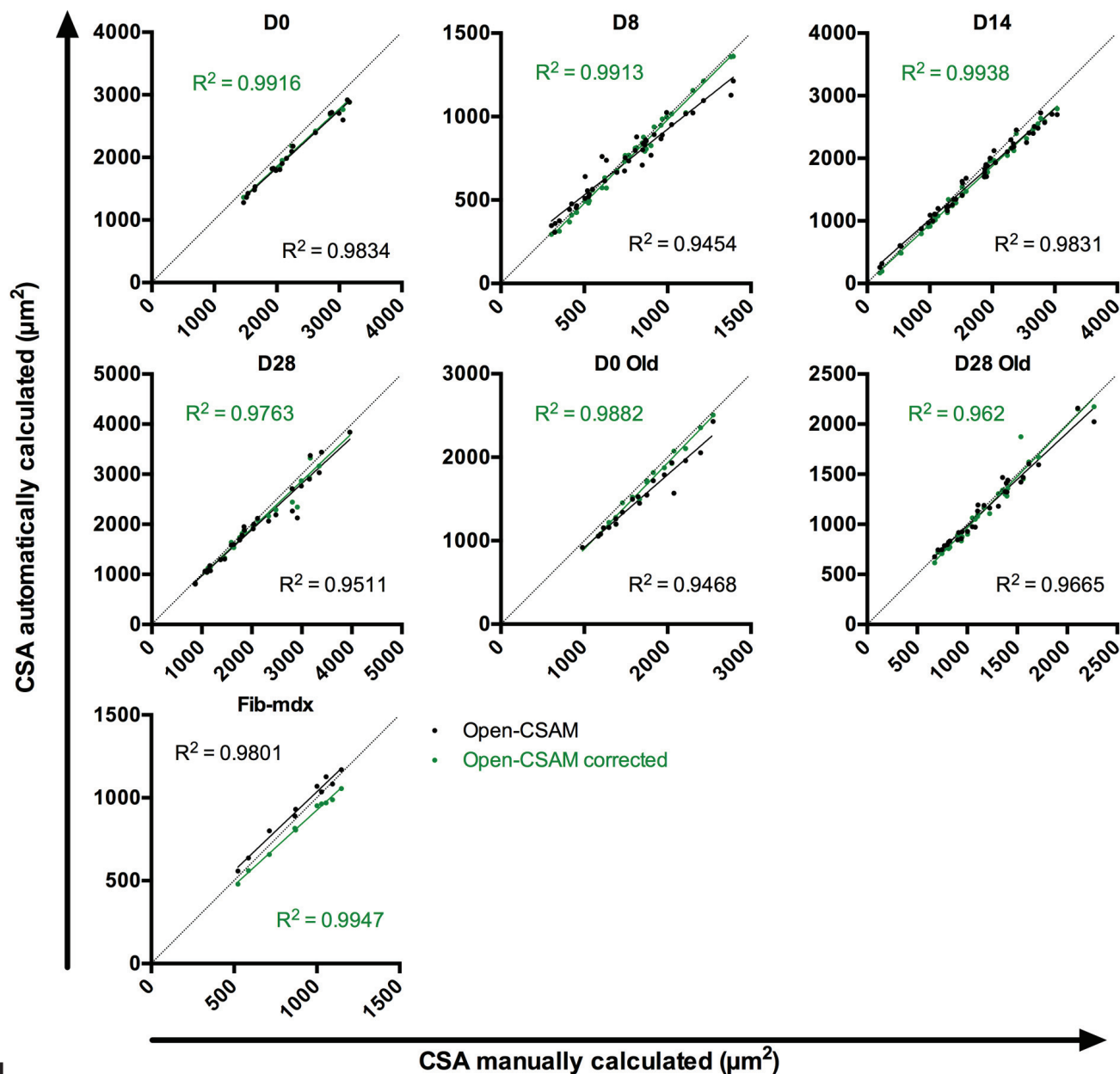


Figure S4



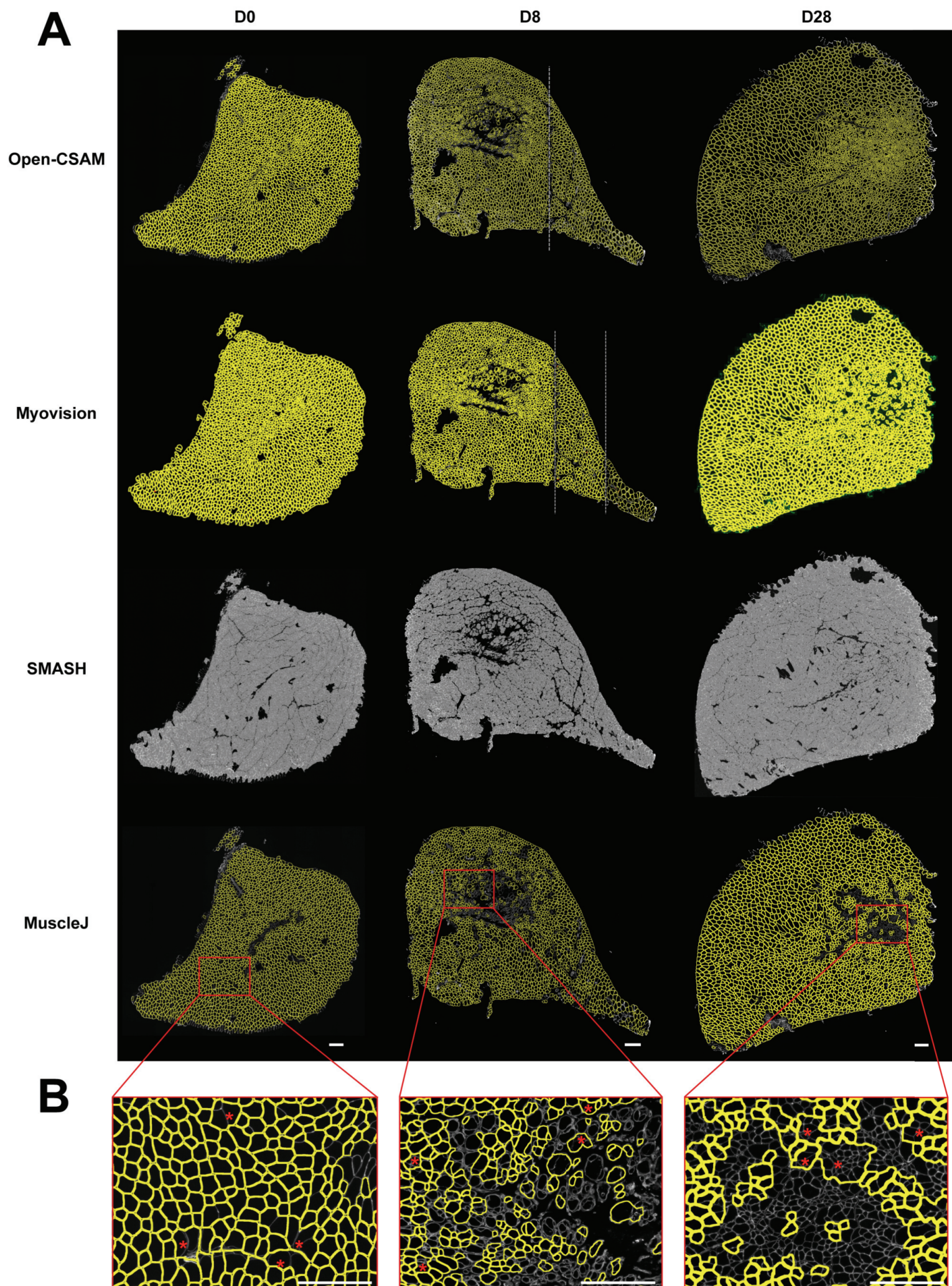


Figure S5

## **PERSPECTIVES**





The results obtained during my PhD program gave evidence of a crosstalk between AMPK and GR. However, the exact mechanism remains to be elucidated.

#### AMPK and GR crosstalk: involvement of other molecular partners?

Interestingly, it was shown in hepatocytes that the transcription factor C/EBP $\beta$  co-regulates at least 60% of the genes regulated by GR (Grontved et al., 2013). C/EBP $\beta$  modulates chromatin accessibility at GR binding sites. When C/EBP $\beta$  cannot bind these sites, GR binding was altered (Grontved et al., 2013). Furthermore, AMPK activation was shown to inhibit the C/EBP $\beta$  protein in cardiomyocytes (Zhang et al., 2018) and in hepatoma cells (Choudhury et al., 2011). In macrophages, AMPK $\alpha$ 1 activation induces the inhibition and the degradation of another C/EBP protein member, C/EBP homologous protein (CHOP) (Dai et al., 2016). Following that logic, the absence of AMPK $\alpha$ 1 in macrophages could lead to active C/EBP $\beta$  protein, that allows chromatin accessibility to GR on DNA after DEX binding. This seems counterintuitive to our results showing that GR requires AMPK activation for shifting macrophage phenotype. Moreover, the mechanism is likely much more complex as C/EBP $\beta$  was shown to induce macrophage phenotype switch (Ruffell et al., 2009), which seems again contradictory with the above described mechanisms.

Beside C/EBP, several molecular links have already been made between AMPK $\alpha$ 1 and GR in other cell systems. AMPK induces the phosphorylation of MAPKinase p38, which induces the phosphorylation of GR in hepatocytes at serine 211 (Nader et al., 2010). Finally, it was recently shown in epithelial cells that AMPK phosphorylation is very dynamic. AMPK activation is oscillatory: the more there are oscillations, the more AMPK is active (Hung et al., 2017). The frequency of AMPK activation seems to be an important parameter that could differently regulate downstream targets. In macrophages, the frequency of AMPK activation could also be important to regulate phenotype switch and GC effect.

Another partner potentially implicated in the interaction between AMPK and GR is annexin A1. Annexin A1 belongs to the family of annexin proteins which are Ca<sup>2+</sup>-dependent phospholipid-binding proteins. The expression of annexin A1 is induced by GCs (annexin A1 gene promoter has a GRE domain) (Perretti and D'Acquisto, 2009). We recently showed (see Study #2) that i) annexin A1 is required for proper skeletal muscle regeneration; ii) annexin A1 induces AMPK $\alpha$ 1 phosphorylation; iii) AMPK $\alpha$ 1 is required for annexin A1-induced anti-

inflammatory profile of macrophages and *in vitro* myogenesis. Thus, annexin A1 seems to be a good candidate for AMPK-GR crosstalk.

In macrophages, all these molecules could interact to each other to induce the phenotype switch of macrophages thereby forming a super network (Figure P1). Because the resolution of inflammation is very important for the maintenance of the tissue homeostasis, is it is likely that several redundant, and may be interconnected, pathways are at work to ensure that shift in macrophages.

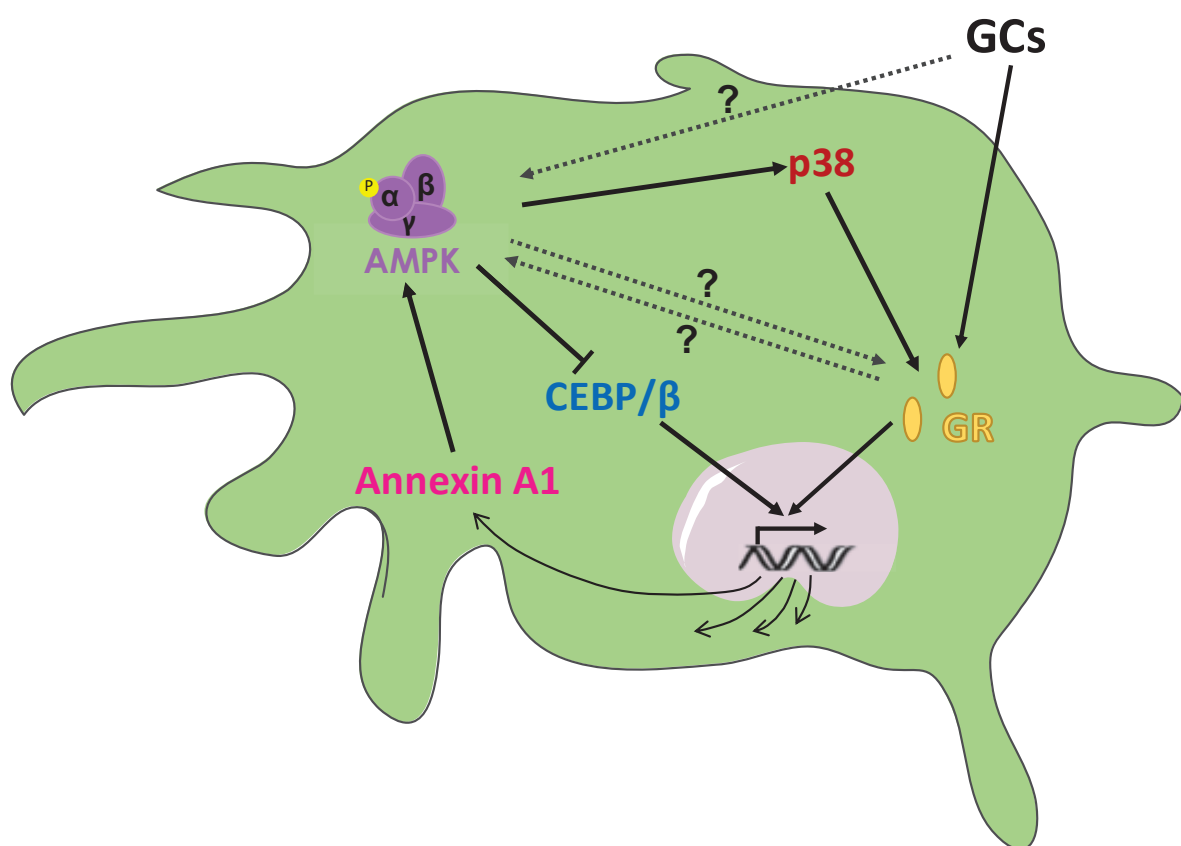


**Figure P1. Signaling pathways that may regulate the phenotype switch of macrophages through AMPK and GR crosstalk.** Glucocorticoids (GCs) induce Glucocorticoid Receptor (GR) translocation into the nucleus, which subsequently regulates gene expression. GR is associated with other transcription factors such as CEBP/β to modulate gene expression (in hepatocyte). GCs also induce AMPK phosphorylation and AMPK inhibits CEBP/β (in cardiomyocyte, hepatoma cells, macrophage) which may modify GR-regulating gene as CEBP/β is not able to associate with GR. Moreover, phosphorylation of GR modulates its transcriptional activity. The MAPK p38 phosphorylates GR at serine 211 that can modulate GR activity (hepatocyte). AMPK also induces p38 phosphorylation thereafter changing GR transcriptional activity. Furthermore, expression of Annexin A1 is induced by GC-GR (Annexin A1 promoter gene has Glucocorticoid Response Element). Annexin A1 induces AMPK phosphorylation (in macrophage).

## AMPK and GC crosstalk: metabolic regulation?

GCs and AMPK both regulate cell metabolism. Moreover, metabolic regulation in macrophages is crucial for their phenotype switch (Juban and Chazaud, 2017). The lab showed that metabolic shift of macrophages precedes the phenotype shift from pro- to anti-inflammatory profile (Varga et al, 2016). Indeed, genes associated with oxidative phosphorylation and TCA cycle are upregulated between day 1 and day 2 after cardiotoxin injury whereas genes associated with glycolysis are downregulated between day 2 and day 4 after injury (Varga et al, 2016). Thus, the investigation of metabolism in macrophages upon DEX and 991 treatment could give clues on how these pathways interact. This work is ongoing in collaboration with the group of Julien Courchet at INMG. We just finished to set up the technique to transfect macrophages with FRET-sensors, which detect several molecules involved in the glycolytic or oxidative/phosphorylation pathways such as lactate, pyruvate, glucose or AMPK activity (Figure P2) (Tsou et al., 2011). By live imaging, we aim to identify what kind of metabolic changes are induced upon AMPK activator and GC treatments and whether these changes are similar in WT and AMPK $\alpha$ 1 deficient macrophages. These experiments will determine whether AMPK and GR interact through metabolic regulations.

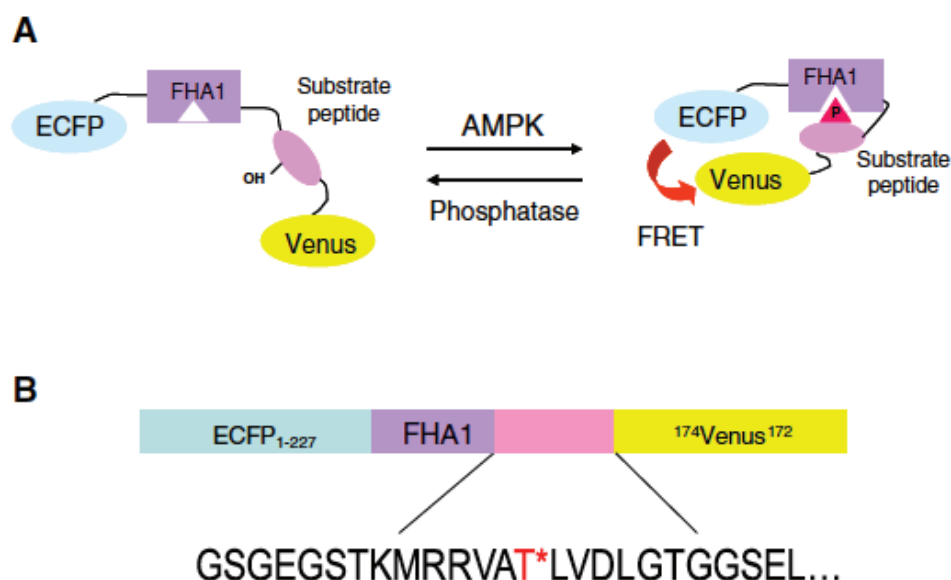


**Figure P2. FRET-sensor for AMPK activity.** The substrate peptide will be phosphorylated by AMPK on a specific threonine (Thr). Then, the phospho-Thr will bind the FHA1 domain (which specifically recognizes phospho-Thr). This binding will change the conformation of the molecules allowing FRET signal (Tsou et al., 2011).



### Regulation of gene expression

Another perspective of our results is to understand how macrophages may regulate myosin expression in myofibers. Regulation of MHCII myosin locus is still not understood. We attempted to model *in vitro* the expression of adult myosin in primary highly differentiated myotube cultures. Myotubes were differentiated between 2 layers of Matrigel for 3 to 14 days in differentiating medium (DMEM F12, 2 % horse serum). Unfortunately, whatever the time point considered, we did not detect MHCI, MHCIIa or MHCIIb expression by immunofluorescence assay in differentiated myotubes in culture, even when contracting. Thus, we were not able to develop an *in vitro* model to study myosin expression and to analyze the impact of macrophages on this phenomenon, which remains a quite puzzling issue.

Finally, as mentioned in the discussion, RNA sequencing experiments from WT and AMPK $\alpha$ 1<sup>-/-</sup> macrophages treated with DEX and 991 are ongoing and should provide a list of genes differentially expressed between WT and AMPK $\alpha$ 1<sup>-/-</sup> cells, to further investigate how AMPK and GR interact in macrophages. Thanks to this experiment, we expect to define more precisely the mechanism involving AMPK and GR in macrophages to submit this work in a high rank journal the next fall. I will be first co-author of this work with Giorgio Caratti, our collaborator in this project who is working in Jan Tuckermann's lab.

### AMPK and GR crosstalk: on the GR side

My PhD project focused on the role of AMPK in GC signaling pathway. Another perspective is to investigate whether GR is required for AMPK signaling in macrophages. Because at the beginning of the project, we did not know how AMPK and GR were linked, we performed *in vitro* experiments to phenotype the inflammatory status of GR deficient macrophages upon AMPK activation. The results showed that the AMPK activator AICAR did not induce the acquisition of the anti-inflammatory profile of macrophages deficient for GR (Figure P3A). We also asked the question if the dimerization of GR is required. GR<sup>dim</sup> mouse model was designed to avoid GR dimerization by a mutation on DNA-Binding Domain of the GR protein (Reichardt et al., 1998). Using GR<sup>dim</sup> bone marrow-derived macrophages, we showed that neither AMPK activator nor DEX induced the phenotype switch of macrophages *in vitro* (Figure P3B). These results show an additional level of complexity of the molecular network for the phenotype shift in macrophages since they suggest that GR dimerization was also required for AMPK induced phenotype switch of macrophages. We started *in vivo* experiments in collaboration with the group of Jan Tuckermann using LysM<sup>cre/+</sup>;GR<sup>fl/fl</sup> mice, that are ongoing.

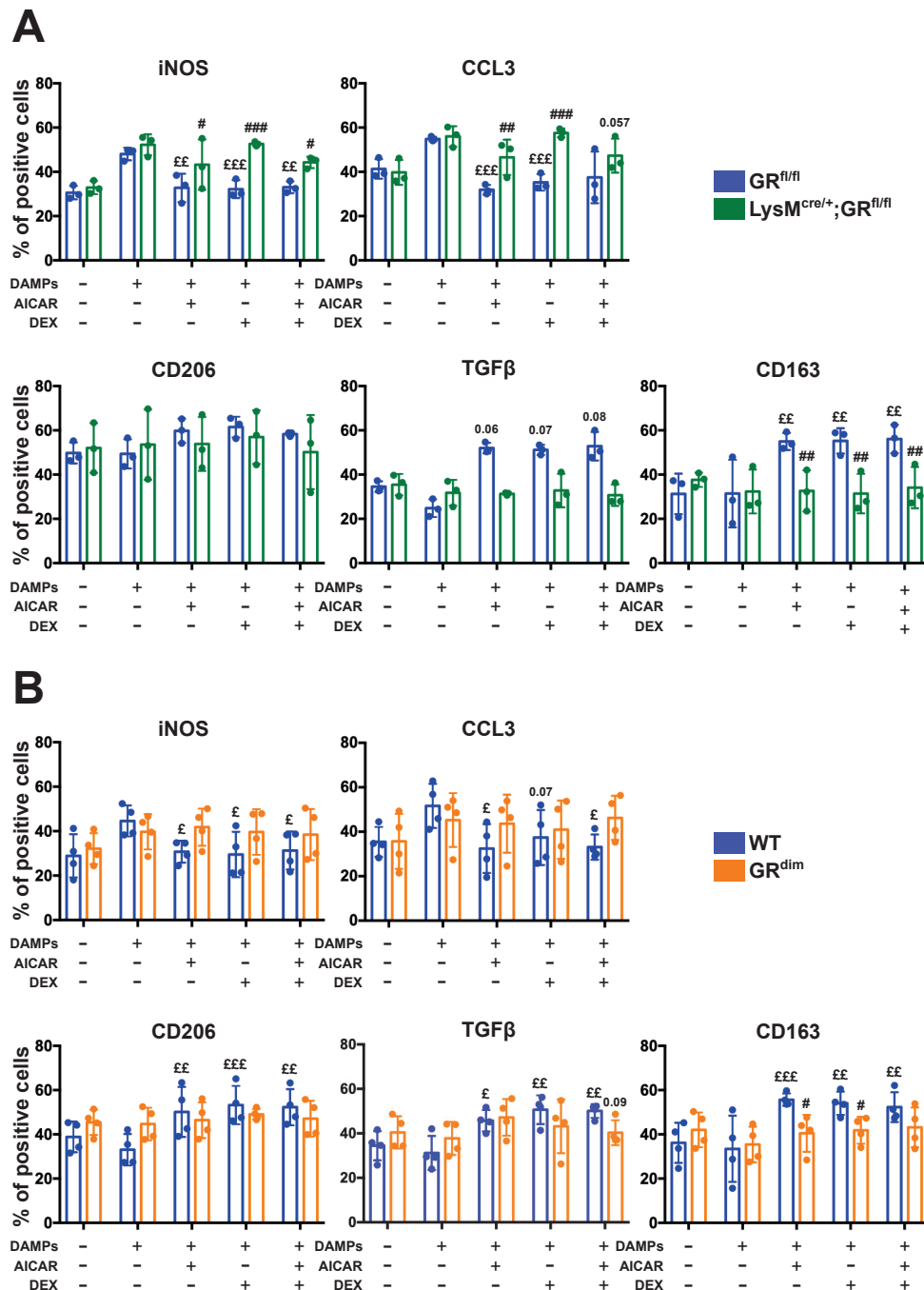


**Figure P3. Acquisition of macrophage anti-inflammatory status induced by AICAR requires GR and its dimerization.** To mimic sterile inflammation, macrophages were first activated by muscle Damaged Associated Molecular Patterns (DAMPs) for 24 h and then treated with AICAR and DEX treatment for 6. **(A)** Immunofluorescence of macrophages deficient for the glucocorticoid receptor (GR) ( $\text{LysM}^{\text{cre/+}};\text{GR}^{\text{fl/fl}}$ ). The percentage of cells expressing the pro-inflammatory markers iNOS and CCL3 or the anti-inflammatory markers CD206, TGF $\beta$  and CD163 was analyzed. Graphs show the number of positive cells. Blue bars represent WT macrophages, green bars represent  $\text{LysM}^{\text{cre/+}};\text{GR}^{\text{fl/fl}}$  macrophages. **(B)** Immunofluorescence of macrophages deficient for the dimerization of the GR ( $\text{GR}^{\text{dim}}$ ). The percentage of cells expressing the pro-inflammatory markers iNOS and CCL3 or the anti-inflammatory markers CD206, TGF $\beta$  and CD163 was analyzed. Graphs show the number of positive cells. Blue bars represent WT macrophages, orange bars represent  $\text{GR}^{\text{dim}}$  macrophages. £  $p<0.05$ , ££  $p<0.01$  and £££  $p<0.010$  versus the DAMPs-treated condition. #  $p<0.05$ , ##  $p<0.01$  and ###  $p<0.001$  versus  $\text{LysM}^{\text{cre/+}};\text{GR}^{\text{fl/fl}}$  or  $\text{GR}^{\text{dim}}$  macrophages in each condition of treatment.



# **SCIENTIFIC PUBLICATIONS AND COMMUNICATIONS**



## Scientific publications

Desgeorges T., Liot S., Lyon S., Bouvière J., Kemmel A., Trignol A., Rousseau D., Chapuis B., Gondin J., Mounier R., Chazaud B. and Juban G. "Open-CSAM, a New Tool for Semi-Automated Analysis of Myofiber Cross-Sectional Area in Regenerating Adult Skeletal Muscle." ***Skeletal Muscle*** 9, no. 1 (January 2019). <https://doi.org/10.1186/s13395-018-0186-6>.

McArthur S., Gobbetti T., Juban G., Desgeorges T., Theret M., Gondin J., Toller-Kawahisa J., Reutelingsperger C., Perretti M., and Mounier R. "Annexin A1 Drives Macrophage Skewing towards a Resolving Phenotype to Accelerate the Regeneration of Muscle Injury through AMPK Activation." ***BioRxiv***, August 29, 2018. <https://doi.org/10.1101/375709>. In revision at *Journal of Clinical Investigation*.

Faes C., Juban G., Aufradet E., Desgeorges T., Charrin E., Connes P., Mury P., Mattè A., De Franceschi L., Martin C. and Pialoux V., "Effects of hypoxia/reoxygenation stimuli on renal redox status and nuclear factor 1 erythroid2-related factor 2 pathway in sickle cell SAD mice." Submitted at British Journal of Haematology

Desgeorges T., Caratti G., Mounier R., Tuckerman J. and Chazaud B. "Glucocorticoids shape macrophage phenotype for tissue repair". Review, submitted at *Frontiers in Immunology*.

## Communications

### Oral communications

Gordon Research Seminar (GRS) (Lucca / Barga, Italy – June 2019) "Crosstalk of Glucocorticoid Receptor and AMP-activated protein kinase in macrophages during skeletal muscle regeneration".

Club metabolism of Lyon (Lyon, France – December 2018) "The role of macrophage AMPK $\alpha$ 1 for anti-inflammatory effects of glucocorticoids during skeletal muscle regeneration."

Days of the French Society of Myology (Brest, France – November 2018) “The role of macrophage AMPK $\alpha$ 1 for anti-inflammatory effects of glucocorticoids during skeletal muscle regeneration.”

Seminar at the Institute of Comparative Molecular Endocrinology (CME) (Ulm, Germany – February 2018) “Crosstalk of Glucocorticoid Receptor and AMP-activated protein Kinase in macrophages during skeletal muscle regeneration.”

PhD School day (Villeurbanne, France – October 2017) “Crosstalk of Glucocorticoid Receptor and AMP-activated protein Kinase in macrophages during skeletal muscle regeneration.”

Internal seminar of the Institut NeuroMyoGène (Lyon, France - December 2016) “Crosstalk of Glucocorticoid Receptor and AMP-activated protein Kinase in macrophages during skeletal muscle regeneration.”

#### Poster communications

Gordon Research Conference (GRC) (Lucca / Barga, Italy – June 2019) “Crosstalk of Glucocorticoid Receptor and AMP-activated protein kinase in macrophages during skeletal muscle regeneration”.

Annual Day of Young Researchers of the Institut NeuroMyoGène (Lyon, France – February 2019) “Crosstalk of Glucocorticoid Receptor and AMP-activated protein Kinase in macrophages during skeletal muscle regeneration.”

3<sup>rd</sup> European workshop on AMPK (Porquerolles, France – September 2017) “Crosstalk of Glucocorticoid Receptor and AMP-activated protein Kinase in macrophages during skeletal muscle regeneration.”



### **Teaching**

During the 3 first years of my PhD, I taught 192 h to 1<sup>st</sup> year Bachelor students in practical courses of Cell Biology.

During the 4<sup>th</sup> year of my PhD, I taught 40 h to 1<sup>st</sup> year of Master degree students in practical courses of cell culture. I also gave lecture for 33.5 h to 1<sup>st</sup> year Bachelor students on Kidney Physiology.

### **Mentoring**

During my PhD, I supervised 2 students:

- A student in 2<sup>nd</sup> year of Bachelor degree for 3 months (Roxane Cuzin)
- A student in 1<sup>st</sup> year of Master degree for 2 months (Emilie Charles)

### **Other activities**

I was vice-treasurer for 1 year and treasurer for 1 year of the association of the young researchers of the institute Neuromyogène (YRIN).



## REFERENCES



Armbrust, T., Kreissig, M., Tron, K., and Ramadori, G. (2004). Modulation of fibronectin gene expression in inflammatory mononuclear phagocytes of rat liver after acute liver injury. *Journal of Hepatology* 40, 638–645.

Arnold, L., Henry, A., Poron, F., Baba-Amer, Y., van Rooijen, N., Plonquet, A., Gherardi, R.K., and Chazaud, B. (2007). Inflammatory monocytes recruited after skeletal muscle injury switch into antiinflammatory macrophages to support myogenesis. *The Journal of Experimental Medicine* 204, 1057–1069.

Auffray, C., Fogg, D., Garfa, M., Elain, G., Join-Lambert, O., Kayal, S., Sarnacki, S., Cumano, A., Lauvau, G., and Geissmann, F. (2007). Monitoring of Blood Vessels and Tissues by a Population of Monocytes with Patrolling Behavior. *Science* 317, 666–670.

Bae, H.-B., Zmijewski, J.W., Deshane, J.S., Tadie, J.-M., Chaplin, D.D., Takashima, S., and Abraham, E. (2011). AMP-activated protein kinase enhances the phagocytic ability of macrophages and neutrophils. *The FASEB Journal* 25, 4358–4368.

Baghdadi, M.B., Castel, D., Machado, L., Fukada, S., Birk, D.E., Relaix, F., Tajbakhsh, S., and Mourikis, P. (2018). Reciprocal signalling by Notch–Collagen V–CALCR retains muscle stem cells in their niche. *Nature* 557, 714–718.

Ballegeer, M., Van Looveren, K., Timmermans, S., Eggermont, M., Vandevyver, S., Thery, F., Dendoncker, K., Souffriau, J., Vandewalle, J., Van Wyngene, L., et al. (2018). Glucocorticoid receptor dimers control intestinal STAT1 and TNF-induced inflammation in mice. *Journal of Clinical Investigation* 128, 3265–3279.

Balow, J.E., and Rosenthal, A.S. (1973). Glucocorticoid suppression of macrophage migration inhibitory factor. *The Journal of Experimental Medicine* 137, 1031–1041.

Barczyk, K., Ehrchen, J., Tenbrock, K., Ahlmann, M., Kneidl, J., Viemann, D., and Roth, J. (2010). Glucocorticoids promote survival of anti-inflammatory macrophages via stimulation of adenosine receptor A3. *Blood* 116, 446–455.

Bar-Shavit, Z., Kahn, A.J., Pegg, L.E., Stone, K.R., and Teitelbaum, S.L. (1984). Glucocorticoids modulate macrophage surface oligosaccharides and their bone binding activity. *The Journal of Clinical Investigation* 73, 1277–1283.

Baschant, U., Frappart, L., Rauchhaus, U., Bruns, L., Reichardt, H.M., Kamradt, T., Brauer, R., and Tuckermann, J.P. (2011). Glucocorticoid therapy of antigen-induced arthritis depends on the dimerized glucocorticoid receptor in T cells. *Proceedings of the National Academy of Sciences* 108, 19317–19322.

Beauchamp, J.R., Heslop, L., Yu, D.S.W., Tajbakhsh, S., Kelly, R.G., Wernig, A., Buckingham, M.E., Partridge, T.A., and Zammit, P.S. (2000). Expression of Cd34 and Myf5 Defines the Majority of Quiescent Adult Skeletal Muscle Satellite Cells. *The Journal of Cell Biology* 151, 1221–1234.

Beg, H., Allmann, D.W., and Gibson, D.M. (1973). MODULATION OF 3-HYDROXY-3-METHYLGLUTARYL COUZYME A REDUCTASCE ACTIVITY WITH cAMP AND WITH PROTEIN FRACTIONS OF RAT LIVER CYTOSOL. *BIOCHEMICAL AND BIOPHYSICAL RESEARCH COMMUNICATIONS* 54, 8.

Bentzinger, C.F., Wang, Y.X., and Rudnicki, M.A. (2012). Building Muscle: Molecular Regulation of Myogenesis. *Cold Spring Harbor Perspectives in Biology* 4, a008342–a008342.

Berrebi, D., Bruscoli, S., Cohen, N., Foussat, A., Migliorati, G., Bouchet-Delbos, L., Maillot, M.C., Portier, A., Couderc, J., Galanaud, P., et al. (2003). Synthesis of glucocorticoid-induced leucine zipper (GILZ) by macrophages: an anti-inflammatory and immunosuppressive mechanism shared by glucocorticoids and IL-10. *Blood* 101, 729–738.

Bischoff, R. (1974). Enzymatic liberation of myogenic cells from adult rat muscle. *The Anatomical Record* 180, 645–661.

Bischoff, R. (1975). Regeneration of single skeletal muscle fibers in vitro. *The Anatomical Record* 182, 215–235.

Bjornson, C.R.R., Cheung, T.H., Liu, L., Tripathi, P.V., Steeper, K.M., and Rando, T.A. (2012). Notch Signaling Is Necessary to Maintain Quiescence in Adult Muscle Stem Cells. *STEM CELLS* 30, 232–242.

Brigitte, M., Schilte, C., Plonquet, A., Baba-Amer, Y., Henri, A., Charlier, C., Tajbakhsh, S., Albert, M., Gherardi, R.K., and Christien, F. (2010). Muscle resident macrophages control the immune cell reaction in a mouse model of notexin-induced myoinjury. *Arthritis & Rheumatism* 62, 268–279.

Burzyn, D., Kuswanto, W., Kolodin, D., Shadrach, J.L., Cerletti, M., Jang, Y., Sefik, E., Tan, T.G., Wagers, A.J., Benoist, C., et al. (2013). A Special Population of Regulatory T Cells Potentiates Muscle Repair. *Cell* 155, 1282–1295.

Caratti, G., Matthews, L., Poolman, T., Kershaw, S., Baxter, M., and Ray, D. (2015). Glucocorticoid receptor function in health and disease. *Clinical Endocrinology* 83, 441–448.

Carlin, L.M., Stamatiades, E.G., Auffray, C., Hanna, R.N., Glover, L., Vizcay-Barrena, G., Hedrick, C.C., Cook, H.T., Diebold, S., and Geissmann, F. (2013). Nr4a1-Dependent Ly6Clow Monocytes Monitor Endothelial Cells and Orchestrate Their Disposal. *Cell* 153, 362–375.

Carling, D., Zammit, V.A., and Hardie, D.G. (1987). A common bicyclic protein kinase cascade inactivates the regulatory enzymes of fatty acid and cholesterol biosynthesis. *FEBS Letters* 223, 217–222.

Carlson, C.A., and Kim, K.H. (1973). Regulation of hepatic acetyl coenzyme A carboxylase by phosphorylation and dephosphorylation. *J. Biol. Chem.* 248, 378–380.

Chapman, M.A., Meza, R., and Lieber, R.L. (2016). Skeletal muscle fibroblasts in health and disease. *Differentiation* 92, 108–115.



Chargé, S.B.P., and Rudnicki, M.A. (2004). Cellular and Molecular Regulation of Muscle Regeneration. *Physiological Reviews* 84, 209–238.

Chatzopoulou, A., Heijmans, J.P., Burgerhout, E., Oskam, N., Spaink, H.P., Meijer, A.H., and Schaaf, M.J. (2016). Glucocorticoid-Induced Attenuation of the Inflammatory Response in Zebrafish. *Endocrinology* 157, 2772–2784.

Chazaud, B. (2016). Inflammation during skeletal muscle regeneration and tissue remodeling: application to exercise-induced muscle damage management. *Immunology and Cell Biology* 94, 140–145.

Chazaud, B., Sonnet, C., Lafuste, P., Bassez, G., Rimaniol, A.-C., Poron, F., Authier, F.-J., Dreyfus, P.A., and Gherardi, R.K. (2003). Satellite cells attract monocytes and use macrophages as a support to escape apoptosis and enhance muscle growth. *The Journal of Cell Biology* 163, 1133–1143.

Chen, X., Guo, Y., Jia, G., Liu, G., Zhao, H., and Huang, Z. (2018). Arginine promotes skeletal muscle fiber type transformation from fast-twitch to slow-twitch via Sirt1/AMPK pathway. *The Journal of Nutritional Biochemistry* 61, 155–162.

Cheng, M., Nguyen, M.-H., Fantuzzi, G., and Koh, T.J. (2008). Endogenous interferon- $\gamma$  is required for efficient skeletal muscle regeneration. *American Journal of Physiology-Cell Physiology* 294, C1183–C1191.

Cheung, P.C.F., Salt, I.P., Davies, S.P., Hardie, D.G., and Carling, D. (2000). Characterization of AMP-activated protein kinase  $\gamma$ -subunit isoforms and their role in AMP binding. *Biochemical Journal* 346, 659–669

Chinenov, Y., Coppo, M., Gupte, R., Sacta, M.A., and Rogatsky, I. (2014). Glucocorticoid receptor coordinates transcription factor-dominated regulatory network in macrophages. *BMC Genomics* 15, 656.

Choudhury, M., Qadri, I., Rahman, S.M., Schroeder-Gloeckler, J., Janssen, R.C., and Friedman, J.E. (2011). C/EBP $\beta$  is AMP kinase sensitive and up-regulates PEPCK in response to ER stress in hepatoma cells. *Molecular and Cellular Endocrinology* 331, 102–108.

Christ-Crain, M., Kola, B., Lolli, F., Fekete, C., Seboek, D., Wittmann, G., Feltrin, D., Igreja, S.C., Ajodha, S., Harvey-White, J., et al. (2008). AMP-activated protein kinase mediates glucocorticoid-induced metabolic changes: a novel mechanism in Cushing's syndrome. *The FASEB Journal* 22, 1672–1683.

Christov, C., Chretien, F., Abou-Khalil, R., Bassez, G., Vallet, G., Bassaglia, Y., Shinin, V., Tajbakhsh, S., Chazaud, B., and Gherardi, R.K. (2007). Muscle Satellite Cells and Endothelial Cells: Close Neighbors and Privileged Partners. *Molecular Biology of the Cell* 18, 13.

Collins, C.A., and Partridge, T.A. (2005). Self-Renewal of the Adult Skeletal Muscle Satellite Cell. *Cell Cycle* 4, 1338–1341.

Conboy, I.M., and Rando, T.A. (2002). The regulation of Notch signaling controls satellite cell activation and cell fate determination in postnatal myogenesis. *Dev. Cell* 3, 397–409.

Conerly, M.L., Yao, Z., Zhong, J.W., Groudine, M., and Tapscott, S.J. (2016). Distinct Activities of Myf5 and MyoD Indicate Separate Roles in Skeletal Muscle Lineage Specification and Differentiation. *Developmental Cell* 36, 375–385.

Coppo, M., Chinenov, Y., Sacta, M.A., and Rogatsky, I. (2016). The transcriptional coregulator GRIP1 controls macrophage polarization and metabolic homeostasis. *Nature Communications* 7, 12254.

Crist, C.G., Montarras, D., and Buckingham, M. (2012). Muscle Satellite Cells Are Primed for Myogenesis but Maintain Quiescence with Sequestration of Myf5 mRNA Targeted by microRNA-31 in mRNP Granules. *Cell Stem Cell* 11, 118–126.

D'Adamio, F., Zollo, O., Moraca, R., Ayroldi, E., Bruscoli, S., Bartoli, A., Cannarile, L., Migliorati, G., and Riccardi, C. (1997). A New Dexamethasone-Induced Gene of the Leucine Zipper Family Protects T Lymphocytes from TCR/CD3-Activated Cell Death. *Immunity* 7, 803–812.

Dai, X., Ding, Y., Liu, Z., Zhang, W., and Zou, M.-H. (2016). Phosphorylation of CHOP (C/EBP Homologous Protein) by the AMP-Activated Protein Kinase Alpha 1 in Macrophages Promotes CHOP Degradation and Reduces Injury-Induced Neointimal Disruption In Vivo. *Circulation Research* 119, 1089–1100.

David, D.S., Grieco, M.H., and Cushman, P. (1970). Adrenal glucocorticoids after twenty years. *Journal of Chronic Diseases* 22, 637–711.

Davies, L.C., Jenkins, S.J., Allen, J.E., and Taylor, P.R. (2013). Tissue-resident macrophages. *Nature Immunology* 14, 986–995.

Davies, S. P., Helps, N. R., Cohen P. T., and Hardie D. G. (1995). 5'-AMP Inhibits Dephosphorylation, as Well as Promoting Phosphorylation, of the AMP-Activated Protein Kinase. Studies Using Bacterially Expressed Human Protein Phosphatase-2C Alpha and Native Bovine Protein Phosphatase-2AC. *FEBS Letters* 377, no. 3, 421–25.

Desgeorges, T., Liot, S., Lyon, S., Bouvière, J., Kemmel, A., Trignol, A., Rousseau, D., Chapuis, B., Gondin, J., Mounier, R., et al. (2019). Open-CSAM, a new tool for semi-automated analysis of myofiber cross-sectional area in regenerating adult skeletal muscle. *Skeletal Muscle* 9.

Dougherty, T.F., and Schneebeli, G.L. (1950). Role of cortisone in regulation of inflammation. *Proc. Soc. Exp. Biol. Med.* 75, 854–859.

Ehrchen, J., Steinmuller, L., Barczyk, K., Tenbrock, K., Nacken, W., Eisenacher, M., Nordhues, U., Sorg, C., Sunderkotter, C., and Roth, J. (2007). Glucocorticoids induce differentiation of a specifically activated, anti-inflammatory subtype of human monocytes. *Blood* 109, 1265–1274.

Evano, B., and Tajbakhsh, S. (2018). Skeletal muscle stem cells in comfort and stress. *Npj Regenerative Medicine* 3.

Fadok, V.A., Bratton, D.L., Konowal, A., Freed, P.W., Westcott, J.Y., and Henson, P.M. (1998). Macrophages that have ingested apoptotic cells in vitro inhibit proinflammatory cytokine production through autocrine/paracrine mechanisms involving TGF-beta, PGE2, and PAF. *Journal of Clinical Investigation*. 101, 890–898.

Fogg, D.K. (2006). A Clonogenic Bone Marrow Progenitor Specific for Macrophages and Dendritic Cells. *Science* 311, 83–87.

Franchimont, D., Martens, H., Hagelstein, M.T., Louis, E., Dewe, W., Chrousos, G.P., Belaiche, J., and Geenen, V. (1999). Tumor necrosis factor alpha decreases, and interleukin-10 increases, the sensitivity of human monocytes to dexamethasone: potential regulation of the glucocorticoid receptor. *The Journal of Clinical Endocrinology and Metabolism* 84, 2834–2839.

Franco, L.M., Gadkari, M., Howe, K.N., Sun, J., Kardava, L., Kumar, P., Kumari, S., Hu, Z., Fraser, I.D.C., Moir, S., et al. (2019). Immune regulation by glucocorticoids can be linked to cell type–dependent transcriptional responses. *The Journal of Experimental Medicine* jem.20180595.

Freire-de-Lima, C.G., Xiao, Y.Q., Gardai, S.J., Bratton, D.L., Schiemann, W.P., and Henson, P.M. (2006). Apoptotic Cells, through Transforming Growth Factor- $\beta$ , Coordinately Induce Anti-inflammatory and Suppress Pro-inflammatory Eicosanoid and NO Synthesis in Murine Macrophages. *Journal of Biological Chemistry* 281, 38376–38384.

Fumagalli, M. (2011). Role of purinergic signalling in neuro-immune cells and adult neural progenitors. *Frontiers in Bioscience* 16, 2326.

van Furth, R. (1968). THE ORIGIN AND KINETICS OF MONONUCLEAR PHAGOCYTES. *Journal of Experimental Medicine* 128, 415–435.

van Furth, R., Cohn, Z.A., Hirsch, J.G., Humphrey, J.H., Spector, W.G., and Langevoort, H.L. (1972). The mononuclear phagocyte system: a new classification of macrophages, monocytes, and their precursor cells. *Bull. World Health Organ.* 46, 845–852.

Galic, S., Fullerton, M.D., Schertzer, J.D., Sikkema, S., Marcinko, K., Walkley, C.R., Izon, D., Honeyman, J., Chen, Z.-P., van Denderen, B.J., et al. (2011). Hematopoietic AMPK  $\beta$ 1 reduces mouse adipose tissue macrophage inflammation and insulin resistance in obesity. *Journal of Clinical Investigation* 121, 4903–4915.

Galuppo, P., Vettorazzi, S., Hovelmann, J., Scholz, C.J., Tuckermann, J.P., Bauersachs, J., and Fraccarollo, D. (2017). The glucocorticoid receptor in monocyte-derived macrophages is critical for cardiac infarct repair and remodeling. *FASEB Journal: Official Publication of the Federation of American Societies for Experimental Biology* 31, 5122–5132.

Garabuczi, É., Sarang, Z., and Szondy, Z. (2015). Glucocorticoids enhance prolonged clearance of apoptotic cells by upregulating liver X receptor, peroxisome proliferator-activated receptor- $\delta$  and UCP2. *Biochimica et Biophysica Acta (BBA) - Molecular Cell Research* 1853, 573–582.

van de Garde, M.D., Martinez, F.O., Melgert, B.N., Hylkema, M.N., Jonkers, R.E., and Hamann, J. (2014). Chronic exposure to glucocorticoids shapes gene expression and modulates innate and adaptive activation pathways in macrophages with distinct changes in leukocyte attraction. *Journal of Immunology (Baltimore, Md. : 1950)* 192, 1196–1208.

Geissmann, F., Manz, M.G., Jung, S., Sieweke, M.H., Merad, M., and Ley, K. (2010). Development of Monocytes, Macrophages, and Dendritic Cells. *Science* 327, 656–661.

Gell, P.G., and Hinde, I.T. (1953). The effect of cortisone on macrophage activity in mice. *Br J Exp Pathol* 34, 273–275.

Gerke, V., Creutz, C.E., and Moss, S.E. (2005). Annexins: linking  $\text{Ca}^{2+}$  signalling to membrane dynamics. *Nature Reviews Molecular Cell Biology* 6, 449–461.

Giles, K.M., Ross, K., Rossi, A.G., Hotchin, N.A., Haslett, C., and Dransfield, I. (2001). Glucocorticoid augmentation of macrophage capacity for phagocytosis of apoptotic cells is associated with reduced p130Cas expression, loss of paxillin/pyk2 phosphorylation, and high levels of active Rac. *Journal of Immunology* (Baltimore, Md. : 1950) *167*, 976–986.

Ginhoux, F., and Guilliams, M. (2016). Tissue-Resident Macrophage Ontogeny and Homeostasis. *Immunity* *44*, 439–449.

van der Goes, A., Hoekstra, K., van den Berg, T.K., and Dijkstra, C.D. (2000). Dexamethasone promotes phagocytosis and bacterial killing by human monocytes/macrophages in vitro. *Journal of Leukocyte Biology* *67*, 801–807.

Gordon, S. (2003). Alternative activation of macrophages. *Nature Reviews Immunology* *3*, 23–35.

Gratchev, A., Guillot, P., Hakiy, N., Politz, O., Orfanos, C.E., Schledzewski, K., and Goerdts, S. (2001). Alternatively activated macrophages differentially express fibronectin and its splice variants and the extracellular matrix protein beta1G-H3. *Scandinavian Journal of Immunology* *53*, 386–392.

Gratchev, A., Kzhyshkowska, J., Utikal, J., and Goerdts, S. (2005). Interleukin-4 and dexamethasone counterregulate extracellular matrix remodelling and phagocytosis in type-2 macrophages. *Scandinavian Journal of Immunology* *61*, 10–17.

Grøntved, L., John, S., Baek, S., Liu, Y., Buckley, J.R., Vinson, C., Aguilera, G., and Hager, G.L. (2013). C/EBP maintains chromatin accessibility in liver and facilitates glucocorticoid receptor recruitment to steroid response elements. *The EMBO Journal* *32*, 1568–1583.

Hardie, D.G. (2008). AMPK: a key regulator of energy balance in the single cell and the whole organism. *International Journal of Obesity* *32*, S7–S12.

Hardie, D.G., Carling, D., Ferrari, S., Guy, P.S., and Aitken, A. (1986). Characterization of the phosphorylation of rat mammary ATP-citrate lyase and acetyl-CoA carboxylase by  $\text{Ca}^{2+}$  and calmodulin-dependent multiprotein kinase and  $\text{Ca}^{2+}$  and phospholipid-dependent protein kinase. *European Journal of Biochemistry* 157, 553–561.

Hardy, D., Besnard, A., Latil, M., Jouvion, G., Briand, D., Thépenier, C., Pascal, Q., Guguin, A., Gayraud-Morel, B., Cavaillon, J.-M., et al. (2016). Comparative Study of Injury Models for Studying Muscle Regeneration in Mice. *PLOS ONE* 11, e0147198.

Hasty, P., Bradley, A., Morris, J.H., Edmondson, D.G., Venuti, J.M., Olson, E.N., and Klein, W.H. (1993). Muscle deficiency and neonatal death in mice with a targeted mutation in the myogenin gene. *Nature* 364, 501–506.

Hawley, S.A., Boudeau, J., Reid, J.L., Mustard, K.J., Udd, L., Mäkelä, T.P., Alessi, D.R., and Hardie, D.G. (2003). Complexes between the LKB1 tumor suppressor, STRAD $\alpha/\beta$  and MO25 $\alpha/\beta$  are upstream kinases in the AMP-activated protein kinase cascade. *Journal of Biology* 16.

Hawley, S.A., Pan, D.A., Mustard, K.J., Ross, L., Bain, J., Edelman, A.M., Frenguelli, B.G., and Hardie, D.G. (2005). Calmodulin-dependent protein kinase kinase- $\beta$  is an alternative upstream kinase for AMP-activated protein kinase. *Cell Metabolism* 2, 9–19.

Heasman, S.J., Giles, K.M., Ward, C., Rossi, A.G., Haslett, C., and Dransfield, I. (2003). Glucocorticoid-mediated regulation of granulocyte apoptosis and macrophage phagocytosis of apoptotic cells: implications for the resolution of inflammation. *The Journal of Endocrinology* 178, 29–36.

Heasman, S.J., Giles, K.M., Rossi, A.G., Allen, J.E., Haslett, C., and Dransfield, I. (2004). Interferon gamma suppresses glucocorticoid augmentation of macrophage clearance of apoptotic cells. *European Journal of Immunology* 34, 1752–1761.

Heideveld, E., Hampton-O'Neil, L.A., Cross, S.J., van Alphen, F.P.J., van den Biggelaar, M., Toye, A.M., and van den Akker, E. (2018). Glucocorticoids induce differentiation of monocytes



towards macrophages that share functional and phenotypical aspects with erythroblastic island macrophages. *Haematologica* 103, 395–405.

Heredia, J.E., Mukundan, L., Chen, F.M., Mueller, A.A., Deo, R.C., Locksley, R.M., Rando, T.A., and Chawla, A. (2013). Type 2 Innate Signals Stimulate Fibro/Adipogenic Progenitors to Facilitate Muscle Regeneration. *Cell* 153, 376–388.

Hollenberg, S.M., Weinberger, C., Ong, E.S., Cerelli, G., Oro, A., Lebo, R., Brad Thompson, E., Rosenfeld, M.G., and Evans, R.M. (1985). Primary structure and expression of a functional human glucocorticoid receptor cDNA. *Nature* 318, 635–641.

Homsher, E., and Kean, C.J. (1978). Skeletal Muscle Energetics and Metabolism. *Annual Review of Physiology* 40, 93–131.

Hong, S.-P., Leiper, F.C., Woods, A., Carling, D., and Carlson, M. (2003). Activation of yeast Snf1 and mammalian AMP-activated protein kinase by upstream kinases. *Proceedings of the National Academy of Sciences* 100, 8839–8843.

Hoppstadter, J., and Kiemer, A.K. (2015). Glucocorticoid-induced leucine zipper (GILZ) in immuno suppression: master regulator or bystander? *Oncotarget* 6, 38446–38457.

Hung, Y.P., Teragawa, C., Kosaisawe, N., Gillies, T.E., Pargett, M., Minguet, M., Distor, K., Rocha-Gregg, B.L., Coloff, J.L., Keibler, M.A., et al. (2017). Akt regulation of glycolysis mediates bioenergetic stability in epithelial cells. *ELife* 6.

Ibraghimov-Beskrovnaya, O., Ervasti, J.M., Leveille, C.J., Slaughter, C.A., Sernett, S.W., and Campbell, K.P. (1992). Primary structure of dystrophin-associated glycoproteins linking dystrophin to the extracellular matrix. *Nature* 355, 696–702.

Iwabuchi, M., Yamauchi, T., Okada-Iwabuchi, M., Sato, K., Nakagawa, T., Funata, M., Yamaguchi, M., Namiki, S., Nakayama, R., Tabata, M., et al. (2010). Adiponectin and AdipoR1 regulate PGC-1 $\alpha$  and mitochondria by Ca<sup>2+</sup> and AMPK/SIRT1. *Nature* 464, 1313–1319.

Jensen, T.E., and Richter, E.A. (2012). Regulation of glucose and glycogen metabolism during and after exercise: Regulation of glucose and glycogen metabolism in exercise. *The Journal of Physiology* 590, 1069–1076.

Jensen, T.E., Sylow, L., Rose, A.J., Madsen, A.B., Angin, Y., Maarbjerg, S.J., and Richter, E.A. (2014). Contraction-stimulated glucose transport in muscle is controlled by AMPK and mechanical stress but not sarcoplasmic reticulum Ca<sup>2+</sup> release. *Molecular Metabolism* 3, 742–753.

Jeong, H.W., Hsu, K.C., Lee, J.-W., Ham, M., Huh, J.Y., Shin, H.J., Kim, W.S., and Kim, J.B. (2009). Berberine suppresses proinflammatory responses through AMPK activation in macrophages. *American Journal of Physiology-Endocrinology and Metabolism* 296, E955–E964.

Joe, A.W.B., Yi, L., Natarajan, A., Le Grand, F., So, L., Wang, J., Rudnicki, M.A., and Rossi, F.M.V. (2010). Muscle injury activates resident fibro/adipogenic progenitors that facilitate myogenesis. *Nature Cell Biology* 12, 153–163.

Juban, G., and Chazaud, B. (2017). Metabolic regulation of macrophages during tissue repair: insights from skeletal muscle regeneration. *FEBS Letters* 591, 3007–3021.

Juban, G., Saclier, M., Yacoub-Youssef, H., Kernou, A., Arnold, L., Boisson, C., Ben Larbi, S., Magnan, M., Cuvellier, S., Théret, M., et al. (2018). AMPK Activation Regulates LTBP4-Dependent TGF- $\beta$ 1 Secretion by Pro-inflammatory Macrophages and Controls Fibrosis in Duchenne Muscular Dystrophy. *Cell Reports* 25, 2163-2176.e6.

Jubb, A.W., Young, R.S., Hume, D.A., and Bickmore, W.A. (2016). Enhancer Turnover Is Associated with a Divergent Transcriptional Response to Glucocorticoid in Mouse and Human Macrophages. *Journal of Immunology (Baltimore, Md.: 1950)* 196, 813–822.

Jubb, A.W., Boyle, S., Hume, D.A., and Bickmore, W.A. (2017). Glucocorticoid Receptor Binding Induces Rapid and Prolonged Large-Scale Chromatin Decompaction at Multiple Target Loci. *Cell Reports* 21, 3022–3031.

Khalil, N., Whitman, C., Zuo, L., Danielpour, D., and Greenberg, A. (1993). Regulation of alveolar macrophage transforming growth factor-beta secretion by corticosteroids in bleomycin-induced pulmonary inflammation in the rat. *Journal of Clinical Investigation* 92, 1812–1818.

Kim, J.H., Ren, Y., Ng, W.P., Li, S., Son, S., Kee, Y.-S., Zhang, S., Zhang, G., Fletcher, D.A., Robinson, D.N., et al. (2015). Mechanical Tension Drives Cell Membrane Fusion. *Developmental Cell* 32, 561–573.

Kino, T. (2018). GR-regulating Serine/Threonine Kinases: New Physiologic and Pathologic Implications. *Trends in Endocrinology & Metabolism* 29, 260–270.

Kleiman, A., Hubner, S., Rodriguez Parkitna, J.M., Neumann, A., Hofer, S., Weigand, M.A., Bauer, M., Schmid, W., Schutz, G., Libert, C., et al. (2012). Glucocorticoid receptor dimerization is required for survival in septic shock via suppression of interleukin-1 in macrophages. *FASEB Journal: Official Publication of the Federation of American Societies for Experimental Biology* 26, 722–729.

Kuang, S., and Rudnicki, M.A. (2008). The emerging biology of satellite cells and their therapeutic potential. *Trends in Molecular Medicine* 14, 82–91.

Kumar, R., and Thompson, E.B. (1999). The structure of the nuclear hormone receptors. *Steroids* 64, 310–319.

LaBarge, M.A., and Blau, H.M. (2002). Biological Progression from Adult Bone Marrow to Mononucleate Muscle Stem Cell to Multinucleate Muscle Fiber in Response to Injury. *Cell* 111, 589–601.

Laker, R.C., Drake, J.C., Wilson, R.J., Lira, V.A., Lewellen, B.M., Ryall, K.A., Fisher, C.C., Zhang, M., Saucerman, J.J., Goodyear, L.J., et al. (2017). Ampk phosphorylation of Ulk1 is required for targeting of mitochondria to lysosomes in exercise-induced mitophagy. *Nature Communications* 8.

Latroche, C., Gitiaux, C., Chrétien, F., Desguerre, I., Mounier, R., and Chazaud, B. (2015). Skeletal Muscle Microvasculature: A Highly Dynamic Lifeline. *Physiology* 30, 417–427.

Latroche, C., Weiss-Gayet, M., Muller, L., Gitiaux, C., Leblanc, P., Liot, S., Ben-Larbi, S., Abou-Khalil, R., Verger, N., Bardot, P., et al. (2017). Coupling between Myogenesis and Angiogenesis during Skeletal Muscle Regeneration Is Stimulated by Restorative Macrophages. *Stem Cell Reports* 9, 2018–2033.

Lemos, D.R., Babaeijandaghi, F., Low, M., Chang, C.-K., Lee, S.T., Fiore, D., Zhang, R.-H., Natarajan, A., Nedospasov, S.A., and Rossi, F.M.V. (2015). Nilotinib reduces muscle fibrosis in chronic muscle injury by promoting TNF-mediated apoptosis of fibro/adipogenic progenitors. *Nature Medicine* 21, 786–794.

Lepper, C., Partridge, T.A., and Fan, C.-M. (2011). An absolute requirement for Pax7-positive satellite cells in acute injury-induced skeletal muscle regeneration. *Development* 138, 3639–3646.

Leung, D.Y.M., Hamid, Q., Vottero, A., Szeffler, S.J., Surs, W., Minshall, E., Chrousos, G.P., and Klemm, D.J. (1997). Association of Glucocorticoid Insensitivity with Increased Expression of Glucocorticoid Receptor. *Journal of Experimental Medicine* 186, 1567–1574.

Lewis-Tuffin, L. J. and Cidlowski, J.A. (2006). The Physiology of Human Glucocorticoid Receptor Beta (HGRbeta) and Glucocorticoid Resistance. *Annals of the New York Academy of Sciences* 1069, 1–9.

Liu, J., Peng, Y., Wang, X., Fan, Y., Qin, C., Shi, L., Tang, Y., Cao, K., Li, H., Long, J., et al. (2016). Mitochondrial Dysfunction Launches Dexamethasone-Induced Skeletal Muscle Atrophy via AMPK/FOXO3 Signaling. *Molecular Pharmaceutics* 13, 73–84.

Liu, L., Song, Z., Jiao, H., and Lin, H. (2014). Glucocorticoids Increase NPY Gene Expression via Hypothalamic AMPK Signaling in Broiler Chicks. *Endocrinology* 155, 2190–2198.

Liu, Y., Cousin, J.M., Hughes, J., Van Damme, J., Seckl, J.R., Haslett, C., Dransfield, I., Savill, J., and Rossi, A.G. (1999). Glucocorticoids promote nonphlogistic phagocytosis of apoptotic leukocytes. *Journal of Immunology* (Baltimore, Md.: 1950) 162, 3639–3646.

Lombardi, L., Forte, N., and Paradisi, F. (1978). Effect of pretreatment with prednisolone on the phagocytic activity of mouse peritoneal macrophages in vitro. *Experientia* 34, 1503–1504.

Luedke, C.E., and Cerami, A. (1990). Interferon-gamma overcomes glucocorticoid suppression of cachectin/tumor necrosis factor biosynthesis by murine macrophages. *The Journal of Clinical Investigation* 86, 1234–1240.

Maderna, P., Yona, S., Perretti, M., and Godson, C. (2005). Modulation of phagocytosis of apoptotic neutrophils by supernatant from dexamethasone-treated macrophages and annexin-derived peptide Ac (2-26). *Journal of Immunology* (Baltimore, Md.: 1950) 174, 3727–3733.

von Maltzahn, J., Jones, A.E., Parks, R.J., and Rudnicki, M.A. (2013). Pax7 is critical for the normal function of satellite cells in adult skeletal muscle. *Proceedings of the National Academy of Sciences* 110, 16474–16479.

Martinez, F.O., Helming, L., and Gordon, S. (2009). Alternative Activation of Macrophages: An Immunologic Functional Perspective. *Annual Review of Immunology* 27, 451–483.

Mauro, A. (1961). SATELLITE CELL OF SKELETAL MUSCLE FIBERS. *The Journal of Cell Biology* 9, 493–495.

McBride, A., Ghilagaber, S., Nikolaev, A., and Hardie, D.G. (2009). The Glycogen-Binding Domain on the AMPK  $\beta$  Subunit Allows the Kinase to Act as a Glycogen Sensor. *Cell Metabolism* 9, 23–34.

McColl, A., Bournazos, S., Franz, S., Perretti, M., Morgan, B.P., Haslett, C., and Dransfield, I. (2009). Glucocorticoids Induce Protein S-Dependent Phagocytosis of Apoptotic Neutrophils by Human Macrophages. *The Journal of Immunology* 183, 2167–2175.

McMaster, A., and Ray, D.W. (2008). Drug Insight: selective agonists and antagonists of the glucocorticoid receptor. *Nature Clinical Practice Endocrinology & Metabolism* 4, 91–101.

Meers, G.K., Bohnenberger, H., Reichardt, H.M., Lühder, F., and Reichardt, S.D. (2018). Impaired resolution of DSS-induced colitis in mice lacking the glucocorticoid receptor in myeloid cells. *PLOS ONE* 13, e0190846.

Michelucci, A., Heurtaux, T., Grandbarbe, L., Morga, E., and Heuschling, P. (2009). Characterization of the microglial phenotype under specific pro-inflammatory and anti-inflammatory conditions: Effects of oligomeric and fibrillar amyloid- $\beta$ . *Journal of Neuroimmunology* 210, 3–12.

Michlewska, S., Dransfield, I., Megson, I.L., and Rossi, A.G. (2009). Macrophage phagocytosis of apoptotic neutrophils is critically regulated by the opposing actions of pro-inflammatory and anti-inflammatory agents: key role for TNF- $\alpha$ . *FASEB Journal: Official Publication of the Federation of American Societies for Experimental Biology* 23, 844–854.

Millay, D.P., O'Rourke, J.R., Sutherland, L.B., Bezprozvannaya, S., Shelton, J.M., Bassel-Duby, R., and Olson, E.N. (2013). Myomaker is a membrane activator of myoblast fusion and muscle formation. *Nature* 499, 301–305.

Miller, S.C., and Melnykovich, G. (1982). Inhibition by glucocorticoids of endocytosis in a macrophage-like cell line. *Journal of Cellular Biochemistry* 18, 423–431.

Miller, R.A., Chu, Q., Le Lay, J., Scherer, P.E., Ahima, R.S., Kaestner, K.H., Foretz, M., Viollet, B., and Birnbaum, M.J. (2011). Adiponectin suppresses gluconeogenic gene expression in mouse hepatocytes independent of LKB1-AMPK signaling. *Journal of Clinical Investigation* 121, 2518–2528.

Miner, J.N., and Yamamoto, K.R. (1992). The basic region of AP-1 specifies glucocorticoid receptor activity at a composite response element. *Genes Dev.* 6, 2491–2501.

Montarras, D. (2005). Direct Isolation of Satellite Cells for Skeletal Muscle Regeneration. *Science* 309, 2064–2067.

Mosser, D.M., and Edwards, J.P. (2008). Exploring the full spectrum of macrophage activation. *Nature Reviews Immunology* 8, 958–969.

Mounier, R., Lantier, L., Leclerc, J., Sotiropoulos, A., Pende, M., Daegelen, D., Sakamoto, K., Foretz, M., and Viollet, B. (2009). Important role for AMPK $\alpha$ 1 in limiting skeletal muscle cell hypertrophy. *The FASEB Journal* 23, 2264–2273.

Mounier, R., Chrétien, F., and Chazaud, B. (2011). Blood Vessels and the Satellite Cell Niche. In *Current Topics in Developmental Biology*, (Elsevier), pp. 121–138.

Mounier, R., Théret, M., Arnold, L., Cuvellier, S., Bultot, L., Göransson, O., Sanz, N., Ferry, A., Sakamoto, K., Foretz, M., et al. (2013). AMPK $\alpha$ 1 Regulates Macrophage Skewing at the Time of Resolution of Inflammation during Skeletal Muscle Regeneration. *Cell Metabolism* 18, 251–264.

Mounier, R., Théret, M., Lantier, L., Foretz, M., and Viollet, B. (2015). Expanding roles for AMPK in skeletal muscle plasticity. *Trends in Endocrinology & Metabolism* 26, 275–286.

Mourikis, P., Sambasivan, R., Castel, D., Rocheteau, P., Bizzarro, V., and Tajbakhsh, S. (2012). A Critical Requirement for Notch Signaling in Maintenance of the Quiescent Skeletal Muscle Stem Cell State. *STEM CELLS* 30, 243–252.

Murphy, M.M., Lawson, J.A., Mathew, S.J., Hutcheson, D.A., and Kardon, G. (2011). Satellite cells, connective tissue fibroblasts and their interactions are crucial for muscle regeneration. *Development* *138*, 3625–3637.

Murray, P.J., Allen, J.E., Biswas, S.K., Fisher, E.A., Gilroy, D.W., Goerdts, S., Gordon, S., Hamilton, J.A., Ivashkiv, L.B., Lawrence, T., et al. (2014). Macrophage Activation and Polarization: Nomenclature and Experimental Guidelines. *Immunity* *41*, 14–20.

Nader, N., Ng, S.S.M., Lambrou, G.I., Pervanidou, P., Wang, Y., Chrousos, G.P., and Kino, T. (2010). AMPK Regulates Metabolic Actions of Glucocorticoids by Phosphorylating the Glucocorticoid Receptor through p38 MAPK. *Molecular Endocrinology* *24*, 1748–1764.

Nahrendorf, M., Pittet, M.J., and Swirski, F.K. (2010). Monocytes: Protagonists of Infarct Inflammation and Repair After Myocardial Infarction. *Circulation* *121*, 2437–2445.

Neumann, D. (2018). Is TAK1 a Direct Upstream Kinase of AMPK? *International Journal of Molecular Sciences* *19*, 2412.

Nicolaides, N.C., Galata, Z., Kino, T., Chrousos, G.P., and Charmandari, E. (2010). The human glucocorticoid receptor: Molecular basis of biologic function. *Steroids* *75*, 1–12.

Noirez, P., Torres, S., Cebrian, J., Agbulut, O., Peltzer, J., Butler-Browne, G., Daegelen, D., Martelly, I., Keller, A., and Ferry, A. (2006). TGF-beta1 favors the development of fast type identity during soleus muscle regeneration. *Journal of Muscle Research and Cell Motility* *27*, 1–8.

Norton, J.M., and Munck, A. (1980). In vitro actions of glucocorticoids on murine macrophages: effects on glucose transport and metabolism, growth in culture, and protein synthesis. *Journal of Immunology (Baltimore, Md. : 1950)* *125*, 259–266.



Ochoa, O., Sun, D., Reyes-Reyna, S.M., Waite, L.L., Michalek, J.E., McManus, L.M., and Shireman, P.K. (2007). Delayed angiogenesis and VEGF production in CCR2<sup>-/-</sup> mice during impaired skeletal muscle regeneration. *American Journal of Physiology-Regulatory, Integrative and Comparative Physiology* 293, R651–R661.

Oh, K.-S., Patel, H., Gottschalk, R.A., Lee, W.S., Baek, S., Fraser, I.D.C., Hager, G.L., and Sung, M.-H. (2017). Anti-Inflammatory Chromatinscape Suggests Alternative Mechanisms of Glucocorticoid Receptor Action. *Immunity* 47, 298-309.e5.

Olguin, H.C., Yang, Z., Tapscott, S.J., and Olwin, B.B. (2007). Reciprocal inhibition between Pax7 and muscle regulatory factors modulates myogenic cell fate determination. *The Journal of Cell Biology* 177, 769–779.

Orkin, S.H., and Zon, L.I. (2008). Hematopoiesis: An Evolving Paradigm for Stem Cell Biology. *Cell* 132, 631–644.

Otrocka-Domagala, I., Paździor-Czapula, K., and Gesek, M. (2019). Dexamethasone-induced impairment of post-injury skeletal muscle regeneration. *BMC Veterinary Research* 15.

Panettieri, R.A., Schaafsma, D., Amrani, Y., Koziol-White, C., Ostrom, R., and Tliba, O. (2019). Non-genomic Effects of Glucocorticoids: An Updated View. *Trends in Pharmacological Sciences* 40, 38–49.

Parsons, M.J., Campos, I., Hirst, E.M.A., and Stemple, D.L. (2002). Removal of dystroglycan causes severe muscular dystrophy in zebrafish embryos. *Development* 129, 3505–3512.

Pasut, A., Jones, A.E., and Rudnicki, M.A. (2013). Isolation and Culture of Individual Myofibers and their Satellite Cells from Adult Skeletal Muscle. *Journal of Visualized Experiments*.

Pellicoro, A., Ramachandran, P., Iredale, J.P., and Fallowfield, J.A. (2014). Liver fibrosis and repair: immune regulation of wound healing in a solid organ. *Nature Reviews Immunology* 14, 181–194.

Pemmari, A., Paukkeri, E.-L., Hämäläinen, M., Leppänen, T., Korhonen, R., and Moilanen, E. (2018). MKP-1 promotes anti-inflammatory M(IL-4/IL-13) macrophage phenotype and mediates the anti-inflammatory effects of glucocorticoids. *Basic & Clinical Pharmacology & Toxicology*.

Perdiguerro, E., Sousa-Victor, P., Ruiz-Bonilla, V., Jardí, M., Caelles, C., Serrano, A.L., and Muñoz-Cánoves, P. (2011). p38/MKP-1-regulated AKT coordinates macrophage transitions and resolution of inflammation during tissue repair. *The Journal of Cell Biology* *195*, 307–322.

Perretti, M., and D'Acquisto, F. (2009). Annexin A1 and glucocorticoids as effectors of the resolution of inflammation. *Nature Reviews Immunology* *9*, 62–70.

Prokic, L.M., and Vilic, I.M. (1983). Effect of prednisolone in vitro on the migration ability of peritoneal macrophages in rats. *Experientia* *39*, 1133–1134.

Quattrocelli, M., Salamone, I.M., Page, P.G., Warner, J.L., Demonbreun, A.R., and McNally, E.M. (2017). Intermittent Glucocorticoid Dosing Improves Muscle Repair and Function in Mice with Limb-Girdle Muscular Dystrophy. *The American Journal of Pathology* *187*, 2520–2535.

Ray, A., and Prefontaine, K.E. (1994). Physical association and functional antagonism between the p65 subunit of transcription factor NF- $\kappa$ B and the glucocorticoid receptor. *Proc. Natl. Acad. Sci. USA* *5*.

Reichardt, H.M., Kaestner, K.H., Tuckermann, J., Kretz, O., Wessely, O., Bock, R., Gass, P., Schmid, W., Herrlich, P., Angel, P., et al. (1998). DNA Binding of the Glucocorticoid Receptor Is Not Essential for Survival. *Cell* *93*, 531–541.

Ricardo, S.D., van Goor, H., and Eddy, A.A. (2008). Macrophage diversity in renal injury and repair. *Journal of Clinical Investigation* *118*, 3522–3530.

Rieger, M.A., and Schroeder, T. (2012). Hematopoiesis. *Cold Spring Harbor Perspectives in Biology* 4, a008250–a008250.

Rodgers, J.T., King, K.Y., Brett, J.O., Cromie, M.J., Charville, G.W., Maguire, K.K., Brunson, C., Mastey, N., Liu, L., Tsai, C.-R., et al. (2014). mTORC1 controls the adaptive transition of quiescent stem cells from G0 to GAlert. *Nature* 510, 393–396.

Rogers, N.M., Ferenbach, D.A., Isenberg, J.S., Thomson, A.W., and Hughes, J. (2014). Dendritic cells and macrophages in the kidney: a spectrum of good and evil. *Nature Reviews Nephrology* 10, 625–643.

Rollins, D.A., Kharlyngdoh, J.B., Coppo, M., Tharmalingam, B., Mimouna, S., Guo, Z., Sacta, M.A., Pufall, M.A., Fisher, R.P., Hu, X., et al. (2017). Glucocorticoid-induced phosphorylation by CDK9 modulates the coactivator functions of transcriptional cofactor GRIP1 in macrophages. *Nature Communications* 8, 1739.

Roszer, T. (2017). Transcriptional control of apoptotic cell clearance by macrophage nuclear receptors. *Apoptosis : An International Journal on Programmed Cell Death* 22, 284–294.

Ruffell, D., Mourkioti, F., Gambardella, A., Kirstetter, P., Lopez, R.G., Rosenthal, N., and Nerlov, C. (2009). A CREB-C/EBP cascade induces M2 macrophage-specific gene expression and promotes muscle injury repair. *Proceedings of the National Academy of Sciences* 106, 17475–17480.

Sacco, A., Doyonnas, R., Kraft, P., Vitorovic, S., and Blau, H.M. (2008). Self-renewal and expansion of single transplanted muscle stem cells. *Nature* 456, 502–506.

Sacrier, M., Cuvellier, S., Magnan, M., Mounier, R., and Chazaud, B. (2013a). Monocyte/macrophage interactions with myogenic precursor cells during skeletal muscle regeneration. *FEBS Journal* 280, 4118–4130.

Saclier, M., Yacoub-Youssef, H., Mackey, A.L., Arnold, L., Ardjoune, H., Magnan, M., Sailhan, F., Chelly, J., Pavlath, G.K., Mounier, R., et al. (2013b). Differentially Activated Macrophages Orchestrate Myogenic Precursor Cell Fate During Human Skeletal Muscle Regeneration. *STEM CELLS* 31, 384–396.

Sacta, M.A., Tharmalingam, B., Coppo, M., Rollins, D.A., Deochand, D.K., Benjamin, B., Yu, L., Zhang, B., Hu, X., Li, R., et al. (2018). Gene-specific mechanisms direct glucocorticoid-receptor-driven repression of inflammatory response genes in macrophages. *ELife* 7.

Sag, D., Carling, D., Stout, R.D., and Suttles, J. (2008). Adenosine 5'-Monophosphate-Activated Protein Kinase Promotes Macrophage Polarization to an Anti-Inflammatory Functional Phenotype. *The Journal of Immunology* 181, 8633–8641.

Sakai, Y. (1977). EXPERIMENTAL STUDIES ON THE ROLE OF SATELLITE CELLS IN REGENERATION OF RAT SKELETAL MUSCLE FIBERS. *Pathology International* 27, 305–320.

Sambasivan, R., Yao, R., Kissenpfennig, A., Van Wittenberghe, L., Paldi, A., Gayraud-Morel, B., Guenou, H., Malissen, B., Tajbakhsh, S., and Galy, A. (2011). Pax7-expressing satellite cells are indispensable for adult skeletal muscle regeneration. *Development* 138, 3647–3656.

Sampath, S.C., Sampath, S.C., and Millay, D.P. (2018). Myoblast fusion confusion: the resolution begins. *Skeletal Muscle* 8.

Schaer, D.J., Boretti, F.S., Schoedon, G., and Schaffner, A. (2002). Induction of the CD163-dependent haemoglobin uptake by macrophages as a novel anti-inflammatory action of glucocorticoids. *British Journal of Haematology* 119, 239–243.

Schakman, O., Kalista, S., Barbé, C., Loumaye, A., and Thissen, J.P. (2013). Glucocorticoid-induced skeletal muscle atrophy. *The International Journal of Biochemistry & Cell Biology* 45, 2163–2172.

Scheschowitsch, K., Leite, J.A., and Assreuy, J. (2017). New Insights in Glucocorticoid Receptor Signaling-More Than Just a Ligand-Binding Receptor. *Frontiers in Endocrinology* 8, 16.

Schiaffino, S. (2018). Muscle fiber type diversity revealed by anti-myosin heavy chain antibodies. *The FEBS Journal*.

Schiaffino, S., and Reggiani, C. (2011). Fiber types in mammalian skeletal muscles. *Physiological Reviews* 91, 1447–1531.

Schwander, M., Leu, M., Stumm, M., Dorchies, O.M., Ruegg, U.T., Schittny, J., and Müller, U. (2003). Beta1 integrins regulate myoblast fusion and sarcomere assembly. *Dev. Cell* 4, 673–685.

Seale, P., Sabourin, L.A., Girgis-Gabardo, A., Mansouri, A., Gruss, P., and Rudnicki, M.A. (2000). Pax7 Is Required for the Specification of Myogenic Satellite Cells. *Cell* 102, 777–786.

Shaw, R.J., Kosmatka, M., Bardeesy, N., Hurley, R.L., Witters, L.A., DePinho, R.A., and Cantley, L.C. (2004). The tumor suppressor LKB1 kinase directly activates AMP-activated kinase and regulates apoptosis in response to energy stress. *Proceedings of the National Academy of Sciences* 101, 3329–3335.

Shepherd, V.L., Konish, M.G., and Stahl, P. (1985). Dexamethasone increases expression of mannose receptors and decreases extracellular lysosomal enzyme accumulation in macrophages. *The Journal of Biological Chemistry* 260, 160–164.

Shezen, E., Shirman, M., and Goldman, R. (1985). Opposing effects of dexamethasone on the clonal growth of granulocyte and macrophage progenitor cells and on the phagocytic capability of mononuclear phagocytes at different stages of differentiation. *Journal of Cellular Physiology* 124, 545–553.

Shimizu, H., Arima, H., Watanabe, M., Goto, M., Banno, R., Sato, I., Ozaki, N., Nagasaki, H., and Oiso, Y. (2008). Glucocorticoids Increase Neuropeptide Y and Agouti-Related Peptide Gene

Expression via Adenosine Monophosphate-Activated Protein Kinase Signaling in the Arcuate Nucleus of Rats. *Endocrinology* 149, 4544–4553.

Shireman, P.K., Contreras-Shannon, V., Ochoa, O., Karia, B.P., Michalek, J.E., and McManus, L.M. (2007). MCP-1 deficiency causes altered inflammation with impaired skeletal muscle regeneration. *Journal of Leukocyte Biology* 81, 775–785.

Sica, A., and Mantovani, A. (2012). Macrophage plasticity and polarization: in vivo veritas. *Journal of Clinical Investigation* 122, 787–795.

Sonnet, C., Lafuste, P., Arnold, L., Brigitte, M., Poron, F., Authier, J.-F., Chrétien, F., Gherardi, R.K., and Chazaud, B. (2006). Human macrophages rescue myoblasts and myotubes from apoptosis through a set of adhesion molecular systems. *Journal of Cell Science* 119, 2497–2507.

Spadaro, L., Privitera, G., Fede, G., Meli, G., and Purrello, F. (2017). Cortisol as Biomarkers in Cirrhosis. In *Biomarkers in Liver Disease*, V.B. Patel, and V.R. Preedy, eds. (Dordrecht: Springer Netherlands), pp. 387–406.

Spain, D.M., Molomut, N., and Haber, A. (1950). Biological Studies on Cortisone in Mice. *Science* 112, 335–337.

Su, Z., Zhang, P., Yu, Y., Lu, H., Liu, Y., Ni, P., Su, X., Wang, D., Liu, Y., Wang, J., et al. (2016). HMGB1 Facilitated Macrophage Reprogramming towards a Proinflammatory M1-like Phenotype in Experimental Autoimmune Myocarditis Development. *Scientific Reports* 6.

Sun, D., Martinez, C.O., Ochoa, O., Ruiz-Willhite, L., Bonilla, J.R., Centonze, V.E., Waite, L.L., Michalek, J.E., McManus, L.M., and Shireman, P.K. (2009). Bone marrow-derived cell regulation of skeletal muscle regeneration. *The FASEB Journal* 23, 382–395.

Suter, M., Riek, U., Tuerk, R., Schlattner, U., Wallimann, T., and Neumann, D. (2006). Dissecting the Role of 5'-AMP for Allosteric Stimulation, Activation, and Deactivation of AMP-activated Protein Kinase. *Journal of Biological Chemistry* 281, 32207–32216.

Tajbakhsh, S. (2009). Skeletal muscle stem cells in developmental versus regenerative myogenesis. *Journal of Internal Medicine* 266, 372–389.

Tedesco, F.S., Dellavalle, A., Diaz-Manera, J., Messina, G., and Cossu, G. (2010). Repairing skeletal muscle: regenerative potential of skeletal muscle stem cells. *Journal of Clinical Investigation* 120, 11–19.

Teitelbaum, S.L., Malone, J.D., and Kahn, A.J. (1981). Glucocorticoid enhancement of bone resorption by rat peritoneal macrophages in vitro. *Endocrinology* 108, 795–799.

Theret, M., Gsaier L., Schaffer B., Juban G., Ben Larbi S., Weiss-Gayet M., Bultot L., Collodet C., Foretz M., Desplanches D., Sanz P., Zang Z., Yang Y., Vial G., Viollet B., Sakamoto K., Brunet A., Chazaud B. and Mounier R. (2017). AMPK $\alpha$ 1-LDH Pathway Regulates Muscle Stem Cell Self-renewal by Controlling Metabolic Homeostasis. *The EMBO Journal* 36, no. 13: 1946–62.

Tliba, O., Cidlowski, J.A., and Amrani, Y. (2006). CD38 Expression Is Insensitive to Steroid Action in Cells Treated with Tumor Necrosis Factor-Alpha and Interferon-Gamma by a Mechanism Involving the up-Regulation of the Glucocorticoid Receptor Beta Isoform. *Molecular Pharmacology* 69, 588–96.

Tomlinson, J.E., Žygelytė, E., Grenier, J.K., Edwards, M.G., and Cheetham, J. (2018). Temporal changes in macrophage phenotype after peripheral nerve injury. *Journal of Neuroinflammation* 15.

Townley, R., and Shapiro, L. (2007). Crystal Structures of the Adenylate Sensor from Fission Yeast AMP-Activated Protein Kinase. *Science* 315, 1726–1729.

Tsou, P., Zheng, B., Hsu, C.-H., Sasaki, A.T., and Cantley, L.C. (2011). A Fluorescent Reporter of AMPK Activity and Cellular Energy Stress. *Cell Metabolism* 13, 476–486.

Tuckermann, J.P., Kleiman, A., Moriggl, R., Spanbroek, R., Neumann, A., Illing, A., Clausen, B.E., Stride, B., Forster, I., Habenicht, A.J., et al. (2007). Macrophages and neutrophils are the targets for immune suppression by glucocorticoids in contact allergy. *The Journal of Clinical Investigation* 117, 1381–1390.

Uhlenhaut, N.H., Barish, G.D., Yu, R.T., Downes, M., Karunasiri, M., Liddle, C., Schwalie, P., Hubner, N., and Evans, R.M. (2013). Insights into negative regulation by the glucocorticoid receptor from genome-wide profiling of inflammatory cistromes. *Molecular Cell* 49, 158–171.

Ustanina, S., Carvajal, J., Rigby, P., and Braun, T. (2007). The Myogenic Factor Myf5 Supports Efficient Skeletal Muscle Regeneration by Enabling Transient Myoblast Amplification. *Stem Cells* 25, 2006–2016.

Vaibhav, K., Braun, M., Khan, M.B., Fatima, S., Saad, N., Shankar, A., Khan, Z.T., Harris, R.B.S., Yang, Q., Huo, Y., et al. (2018). Remote ischemic post-conditioning promotes hematoma resolution via AMPK-dependent immune regulation. *The Journal of Experimental Medicine* 215, 2636–2654.

Van Dyke, J.M., Smit-Ostad, I.M., Macrander, C., Krakora, D., Meyer, M.G., and Suzuki, M. (2016). Macrophage-mediated inflammation and glial response in the skeletal muscle of a rat model of familial amyotrophic lateral sclerosis (ALS). *Experimental Neurology* 277, 275–282.

Varga, T., Mounier, R., Gogolak, P., Poliska, S., Chazaud, B., and Nagy, L. (2013). Tissue LyC6-Macrophages Are Generated in the Absence of Circulating LyC6- Monocytes and Nur77 in a Model of Muscle Regeneration. *The Journal of Immunology* 191, 5695–5701.

Varga, T., Mounier, R., Horvath, A., Cuvellier, S., Dumont, F., Poliska, S., Ardjoune, H., Juban, G., Nagy, L., and Chazaud, B. (2016). Highly Dynamic Transcriptional Signature of Distinct Macrophage Subsets during Sterile Inflammation, Resolution, and Tissue Repair. *The Journal of Immunology* 196, 4771–4782.



Vazquez-Tello, A., Halwani R., Hamid, Q., and Al-Muhsen, S. (2013). Glucocorticoid Receptor-Beta Up-Regulation and Steroid Resistance Induction by IL-17 and IL-23 Cytokine Stimulation in Peripheral Mononuclear Cells. *Journal of Clinical Immunology* 33, 466–78.

Weigert, A. (2006). Apoptotic cells promote macrophage survival by releasing the antiapoptotic mediator sphingosine-1-phosphate. *Blood* 108, 1635–1642.

Werb, Z. (1978). Biochemical actions of glucocorticoids on macrophages in culture. Specific inhibition of elastase, collagenase, and plasminogen activator secretion and effects on other metabolic functions. *Journal of Experimental Medicine* 147, 1695–1712.

Werb, Z., Foley, R., and Munck, A. (1978). Glucocorticoid receptors and glucocorticoid-sensitive secretion of neutral proteinases in a macrophage line. *Journal of Immunology (Baltimore, Md. : 1950)* 121, 115–121.

Whirlledge, S., and DeFranco, D.B. (2018). Glucocorticoid Signaling in Health and Disease: Insights From Tissue-Specific GR Knockout Mice. *Endocrinology* 159, 46–64.

Wood, W.M., Etemad, S., Yamamoto, M., and Goldhamer, D.J. (2013). MyoD-expressing progenitors are essential for skeletal myogenesis and satellite cell development. *Developmental Biology* 384, 114–127.

Woods, A., Johnstone, S.R., Dickerson, K., Leiper, F.C., Fryer, L.G.D., Neumann, D., Schlattner, U., Wallimann, T., Carlson, M., and Carling, D. (2003). LKB1 Is the Upstream Kinase in the AMP-Activated Protein Kinase Cascade. *Current Biology* 13, 2004–2008.

Woods, A., Dickerson, K., Heath, R., Hong, S.-P., Momcilovic, M., Johnstone, S.R., Carlson, M., and Carling, D. (2005). Ca<sup>2+</sup>/calmodulin-dependent protein kinase kinase- $\beta$  acts upstream of AMP-activated protein kinase in mammalian cells. *Cell Metabolism* 2, 21–33.

Wright, W.E., Sassoon, D.A., and Lin, V.K. (1989). Myogenin, a factor regulating myogenesis, has a domain homologous to MyoD. *Cell* 56, 607–617.

Xavier, A.M., Anunciato, A.K.O., Rosenstock, T.R., and Glezer, I. (2016). Gene Expression Control by Glucocorticoid Receptors during Innate Immune Responses. *Frontiers in Endocrinology* 7.

Xue, J., Schmidt, S.V., Sander, J., Draffehn, A., Krebs, W., Quester, I., De Nardo, D., Gohel, T.D., Emde, M., Schmidleithner, L., et al. (2014). Transcriptome-Based Network Analysis Reveals a Spectrum Model of Human Macrophage Activation. *Immunity* 40, 274–288.

Yablonka-Reuveni, Z., Rudnicki, M.A., Rivera, A.J., Primig, M., Anderson, J.E., and Natanson, P. (1999). The Transition from Proliferation to Differentiation Is Delayed in Satellite Cells from Mice Lacking MyoD. *Developmental Biology* 210, 440–455.

Yamamoto, M., Legendre, N.P., Biswas, A.A., Lawton, A., Yamamoto, S., Tajbakhsh, S., Kardon, G., and Goldhamer, D.J. (2018). Loss of MyoD and Myf5 in Skeletal Muscle Stem Cells Results in Altered Myogenic Programming and Failed Regeneration. *Stem Cell Reports* 10, 956–969.

Yang, Y.H., Aeberli, D., Dacumos, A., Xue, J.R., and Morand, E.F. (2009). Annexin-1 regulates macrophage IL-6 and TNF via glucocorticoid-induced leucine zipper. *Journal of Immunology* (Baltimore, Md.: 1950) 183, 1435–1445.

Yin, H., Price, F., and Rudnicki, M.A. (2013). Satellite Cells and the Muscle Stem Cell Niche. *Physiological Reviews* 93, 23–67.

Zahuczky, G., Kristof, E., Majai, G., and Fesus, L. (2011). Differentiation and glucocorticoid regulated apopto-phagocytic gene expression patterns in human macrophages. Role of Mertk in enhanced phagocytosis. *PloS One* 6, e21349.

Zhang, Y., Liu, X., Zhang, L., Li, X., Zhou, Z., Jiao, L., Shao, Y., Li, M., Leng, B., Zhou, Y., et al. (2018). Metformin Protects against H<sub>2</sub>O<sub>2</sub>-Induced Cardiomyocyte Injury by Inhibiting the miR-1a-3p/GRP94 Pathway. *Molecular Therapy - Nucleic Acids* 13, 189–197.

